National Institute of Materials Physics

ANNUAL REPORT 2016

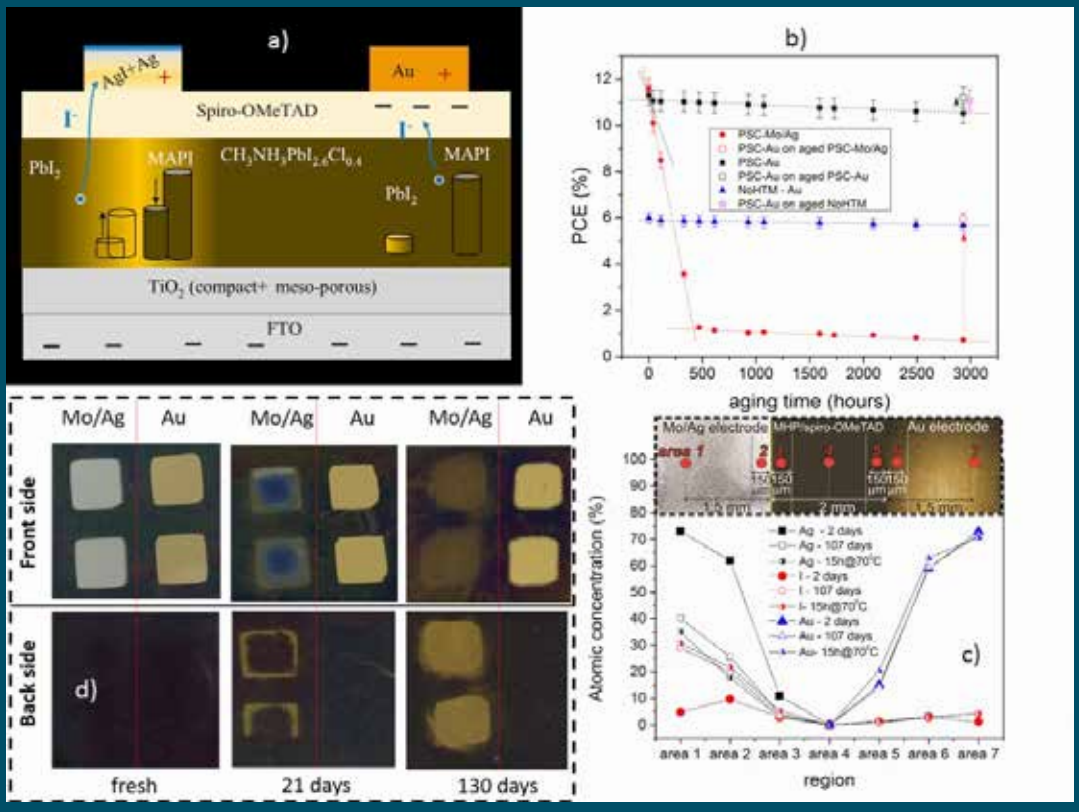

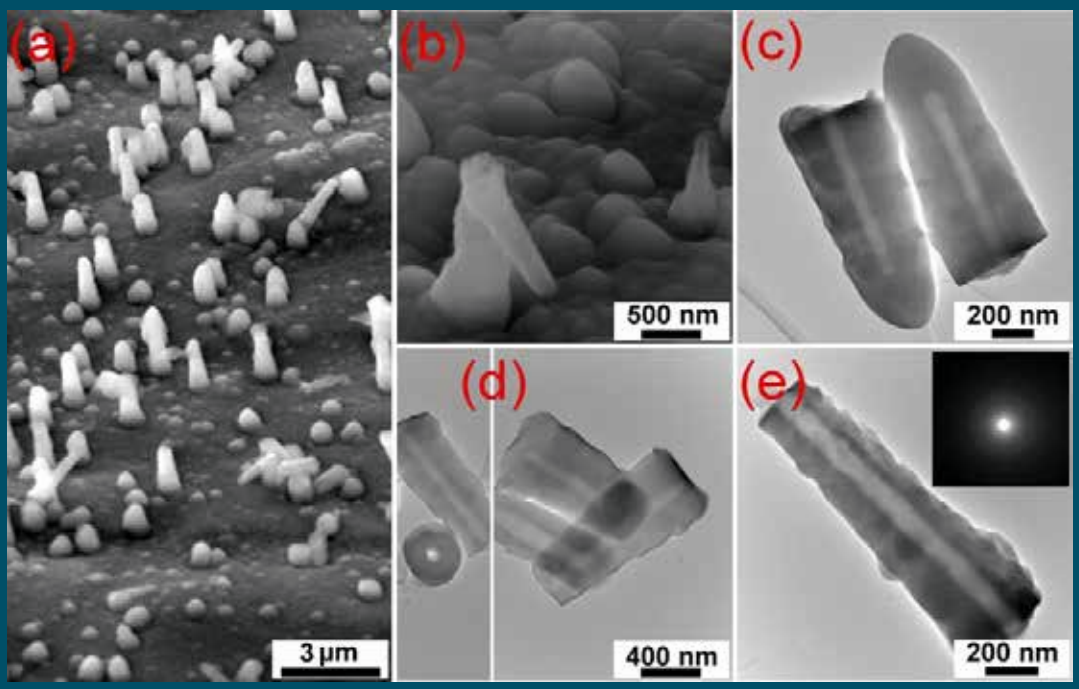

COVER IMAGE

Upper line: [1]

a) Schematic of the perovskite solar cell showing iodine migration when Ag contacts are used;

b) graph showing the degradation of PCE in time for differente variants of perovskite solar cells;

c) I, Ag and Au content on the contacts and between the contacts as determined from XPS investigations;

d) photographs of the front and backside of a PSC sample with both type of electrodes atdifferent aging times at 24 °C, in N_2 atmosphere, dark, humidity below 10%. The deposited area of the electrodes is 3x3 mm².

Lower line: [2]

(a, b) SEM and (c–e) TEM images of (a) arrays and (b–e) individual BG submicrometer cones grown by radio-frequency magnetron sputtering at a working pressure of 0.4 Pa argon onto Ti substrates. Inset (e): Typical SAED pattern of a BG cone.

[1]C. Besleaga, L. E. Abramiuc, V. Stancu, A. G. Tomulescu, M. Sima, L. Trinca, N. Plugaru, L. Pintilie, G. A. Nemnes, M. Iliescu, H. G. Svavarsson, A. Manolescu, and I. Pintilie, J. Phys. Chem. Lett. 7, 5168-5175 (2016)

[2]A.C. Popa, G.E. Stan, C. Besleaga, L. Ion, V.A. Maraloiu, D.U. Tulyaganov, and J.M.F. Ferreira, ACS Appl. Mater. Interfaces 8, 4357–4367 (2016).

Directorate

General Director: **Dr. Ionuț Marius ENCULESCU**

Scientific Director: **Dr. Lucian PINTILIE**

Economic Director: **Ec. Gabriela IVĂNUȘ**

National Institute of Materials Physics
405A Atomistilor Street, PO BOX MG-7, Măgurele, România

Phone: + 4 021 369 01 85
Fax: + 4 021 369 01 77

Email

Dr. I. ENCULESCU: director@infim.ro
Dr. L. PINTILIE: pintilie@infim.ro

Website

www.infim.ro

Contents

FOREWORD 06

LABORATORIES 10

PERSONNEL 16

- List of Personnel 17
- Visiting Guests 25
- Ph. D. Theses 29
- Awards 30
- Honorary Membership 32

PUBLICATIONS AND PRESENTATIONS 35

- Book Chapters 36
- Journals 37
- Contributed Presentations 54
- Invited Lectures 73

SELECTED RESULTS 77

- Condensed Matter Physics at Mesoscale 77
- Nanoscale Physics 104
- Potential Applications 121

PATENTS AND PATENT REQUESTS 150

EVENTS 153

INTERNATIONAL COOPERATION 162

FUNDING 170

FOREWORD

NIMP is a highly appreciated research and development organization having national and international reputation and visibility. This report contains examples of NIMP's applied expertise in the materials physics along with notable facts and figures from the past year. The scientific output of NIMP over the last 10 years is reflected in the capture below, taken from Web of Science.

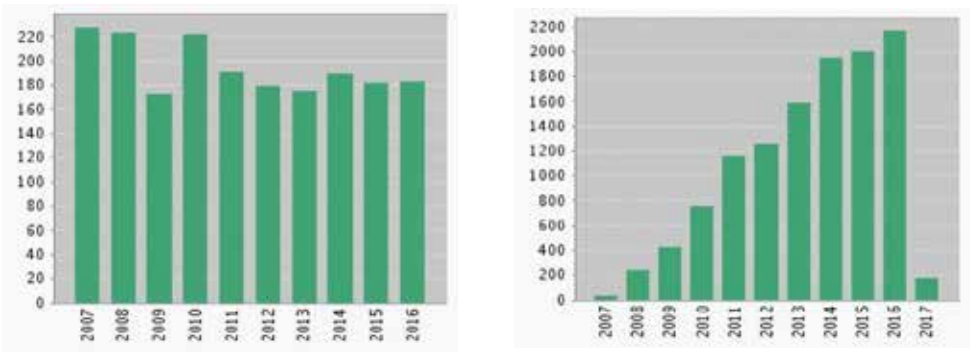

Fig.1: The scientific output of NIMP in the last 10 years: articles (left); citations (right).

One can see that the number of published articles in international journals or conference proceedings was relatively stable, with about 180 publications per year. Also, one can see that the number of citations has steadily increased, reaching a value of about 2200 in 2016 (to mention that the citations are only for the articles published in the last 10 years).

However, one has to underline that the quality of the journals where NIMP has published its research results has steadily increased in the last 10 years, as reflected in the figure below, showing the number of publications in journals having impact factor equal or larger than 4.

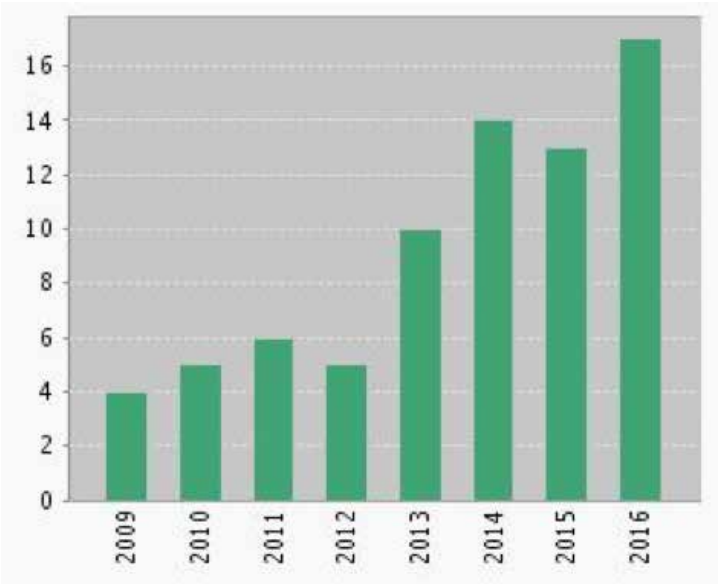

Fig. 2: The number of articles published in journals having the impact factor larger than 4.

One can see that, before 2009 there were no articles published in journals with impact factor larger than 4 while in 2016 are more than 16 articles published in journals like Scientific Reports, ACS Nano, ACS Photonics, Nano Research, ACS Applied Materials and Interfaces and others.

Another important aspect is that 2016 was the final year for a large number of projects implemented under the rules of the National Program for Research, Development and Innovation 2 (project won at competitions organized in the period 2007-2014). On the other hand new competitions were organized under the rules of the National Program for Research, Development and Innovation 3. NIMP has already won 6 PED-type projects (manufacturing experimental demonstrators) and has good chances to win at least 7 PCE-type projects (projects for exploratory research). Other projects were won in 2016 in the frame of various programs such as IFA-CEA, ELI-NP, EURATOM, FAIR, M-ERA NET, etc.

An important success in 2016 was the signing of contracts for 4 projects funded from structural funds: 2 projects type E (attracting reputed scientists from abroad to come and work in the institute), one lead by Dr. Victor Diculescu (coming from Portugal) and the other lead by Dr. Adrian Crisan (coming from UK); 2 project type G (transferring knowledge towards the private sector), one lead by Dr. Mihaela Baibarac (for the health sector) and the other lead by Dr. Lucian Pintilie (for high-tech industry).

The international visibility of NIMP has been promoted by participation to international conferences and by organizing scientific events. One important moment was the organization of the first edition of the International Workshop on Materials Physics. IWMP was held at NIMP premises between 23 and 25 of May 2016. A list of the invited participants (20 from abroad and 6 from Romania) is presented in the next table.

#	NAME	AFFILIATION
01	**Prof. Rodrigo MARTINS**	Head of Materials Science Department - FCT/UNL Director of Centre of Excellence in Micro and Optoelectronic Processes Institute of New technologies, CEMOP/UNINOVA Immediate Past President of the European Materials Research Society President of E-MRS Senate Member of Advisory Board of Horizon 2020 (Advanced Materials, Nanotechnology, Biotechnology) Universidade Nova de Lisboa, Portugal
02	**Prof. Elvira Maria Correia FORTUNATO**	Universidade Nova de Lisboa, Portugal Deputy Chair of the High Level Group of Scientific Advisors of the EC Scientific Advice Mechanism
03	**Prof. dr. ing. A.J.H.M. RIJNDERS**	University of Twente, Netherland
04	**Dr. Jana KOLAR**	Executive Director of C-ERIC, Trieste, Italy
05	**Dr. Tanja MEYER**	IPA Fraunhofer Institute, Stuttgart, Germany
06	**Dr. Udo GOMMEL**	IPA Fraunhofer Institute, Stuttgart, Germany
07	**Dr. Mangala SRINIVAS**	Radboud Institute for Molecular Life Sciences (RIMLS) Nijmegen, Netherlands
08	**Dr. Silvano LIZZIT**	Elettra-Sincrotrone Trieste S.C.p.A. di interesse nazionale

#	NAME	AFFILIATION
09	**Prof. Marin ALEXE**	Department of Physics, University of Warwick, Coventry, CV4 7AL, UK
10	**Prof. Magdalena TITIRICI**	Queen Mary University London, UK
11	**Prof. Steve DUNN**	Queen Mary University London, UK
12	**Dr. Russel BINIONS**	Queen Mary University London, UK
13	**Dr. Nick BARRETT**	Service de Physique et Chimie des Surfaces et des Interfaces CEA, France
14	**Dr. Carlo RIZZUTO**	Elettra-Sincrotrone Trieste S.C.p.A. di interesse nazionale
15	**Dr. Thomas RATH**	University of Graz, Austria
16	**Prof. Vladimir MATOLIN**	Charles University in Prague Czech Republic
17	**Prof. dr hab. Marek STANKIEWICZ**	Uniwersytet Jagielloński, Krakaw, Poland
18	**Dr. Primoz SKET**	Slovenian NMR Centre National Institute of Chemistry, Ljubljana, Slovenia
19	**Dr. Angelo AGOSTINO**	Department of Chemistry - University of Turin
20	**Dr. Augusto MARCELLI**	INFN - Laboratori Nazionali di Frascati, Via E. Fermi 40, 00044 Frascati, Italy
21	**Dr. Nicoleta LUPU**	Technical Physics Institute, Iassy, Romania
22	**Prof. Mihai GARTU**	Ovidius University, Constanta, Romania
23	**Prof. Daniel VIZMAN**	West University, Timisoara, Romania
24	**Prof. Viorel POP**	Babes-Boliay University, Cluj-Napoca Romania
25	**Conf. Alexandru NEMNES**	Bucharest University, Romania
26	**Dr. Mircea DRAGOMAN**	Institute of Microtechnolgy, Bucharest, Romania

Professor Fortunato presenting at the first edition of IWMP.

NIMP has been co-organizer to other 2 events:

- 11 April 2016: "ALD for Novel Sensors and Biosensors" workshop
- 04 April 2016: "Interdisciplinary vocation of Life, Physics and Space Sciences" workshop

In 2016 the team of NIMP has made a significant effort to submit an application for the H2020 Teaming program, having as partners the University of Twente (Netherlands), IPA Fraunhofer Stuttgart (Germany), C-ERIC (Italy), and Shumann Associates (Belgium). The project is aiming to create a center for excellence in research and technological transfer in the field of advanced functional materials (acronym RO-FUNMAT).
The research infrastructure from NIMP is now visible for potential partners not only on the institute's site (www.infim.ro), but also on ERRIS (www.erris.gov.ro search for National Institute of materials Physics).

NIMP is present in some of the rankings for research institutions. For example, on http://research.webometrics.info/ the institute can be found on the third position in Romania for Research Centers (see the table below).

Romania

ranking	World Rank	Institute	Size	Visibility	Rich Files	scholar
1	758	(1) Academia Româna	1926	1479	914	425
2	906	Horia Hulubei National Institute of Physics and Nuclear Engineering	2463	2052	688	386
3	1129	National Institute of Materials Physics	2504	2573	1320	403
4	1286	Institute of Mathematics Academia Romana	1999	2589	1175	657
5	1810	National Institute for Earth Physics	1566	777	4525	3186
6	2063	Institutul de Cercetari Pentru Inteligenta Artificiala Academia Romana	3497	3388	2485	1059
7	2085	Institutul National de Cercetari Aerospatiale Elie Carafoli Bucuresti	4507	4058	1616	755
8	2166	National Institute for Research and Development of Isotopic and Molecular Technologies	2283	4169	2513	1013
9	2453	Institutul de Prognoza Economica Academia Romana	4554	5275	1796	620
10	2466	National Institute for Laser, Plasma and Radiation Physics	2815	3337	1673	2155

Another important milestone in 2016 was the starting of a new Core Program for 2016 and 2017. In conclusion, 2016 was a transition year in terms of funding sources, with new Core program and new competitions launched in the frame of National Program for Research, Development and Innovation 3.

Dr. Ionuț Marius ENCULESCU
General Director

LABORATORIES

10. Laboratory of Multifunctional Materials and Structures

The laboratory is divided into two research groups:

- The group of functional nanostructures, which includes teams with research interests in the field of preparation and characterization of different nano-objects (nanoparticles, nanotubes, nanowires or nano-strips) with potential applications in micro- and nano-optoelectronics (field effect transistors, hybrid LED or photodiodes), advanced sensors (with a focus on bio- sensors), renewable energy and medicine (biocompatible and / or biofunctional materials).
- The group of complex heterostructures and perovskite oxides, which includes teams working with research interests in the preparation and characterization of oxide materials with dielectric, ferroelectric, multiferroic properties or semiconductors for applications in micro- and nano-electronics (non-volatile memories, transparent electronics), telecommunications and security (devices for emitting-receiving of microwaves), advanced sensors (pyroelectric sensing and photoconductor), solar cells (based on the photovoltaic effect in ferroelectrics or other perovskites), medicine (2D and 3D coatings with biocompatible / biofunctional oxides).

Teams working in the laboratory carry out both fundamental research related to identifying and explaining the physical and chemical phenomena that occur in the obtained materials and structures (in particular size effect, interfaces, doping/stoichiometry) , as well as development activities of various applications such as sensors, field effect transistors, photovoltaic cells, apparatus for processing materials. Research topics are generally multidisciplinary, requiring collaboration between physicists, chemists and engineers.

The human resources of the laboratory consist of 8 CS1, 4 CS2, 8 CS3, 4 CS, 14 ACS, two sub- engineers, five technicians and two workers. The laboratory infrastructure includes modern equipment for preparing and characterizing including: systems of pulsed laser deposition (PLD and MAPLE); sputter deposition systems in magnetron (RF and DC); scanning electron microscope (SEM); microfluorescence microscope; cryoprobes with vertical and horizontal magnetic fields and illumination facilities with UV radiation; vector analyzer for networks up to 325 GHz ; THz spectrometer (up to 7 THz); spectroscopic ellipsometer; FTIR spectrometers and UV-Vis; fluorescence spectrometer; magnetic circular dichroism spectrometer.

20. Laboratory of Magnetism and Superconductivity

The laboratory is devoted to research in the field of materials with magnetic or superconducting properties. The research process covers all stages from preparation (bulk materials, thin films and nanostructures) to structural and electronic characterization, completed by thorough analysis of magnetic and superconducting properties. The research is focused mainly on the study of nanostructures, especially nanoparticle systems and multilayer magnetic materials for colossal magnetoresistance (CMR), giant magnetoresistance (GMR) and tunneling magnetoresistance (TMR), soft and hard magnetic materials, magnetic diluted semiconductors, but also on materials working under extreme conditions. In the case of superconducting materials, superconductors of high critical temperatures are especially targeted, as thin films with nanometric inclusions for pinning, MgB2 (bulk and strip), superconductors in the class of Fe-based pnictides (FeSmAsFxO1-x), new superconducting materials, etc.

Among the most important research equipment, targeting both the infrastructure of preparation and characterization, we mention the following: spark plasma sintering equipment, microwave sintering installation, melt spinning installation, system for preparing nanoparticles by hydrothermal/solvothermal synthesis in autoclave and centrifugation for separation by size, laser ablation deposition (PLD) system, magnetic multilayer deposition system by RF and DC sputtering with 4 sources and vacuum based in the 10- 9 mbar domain, radiofrequency thermal transfer facility to determine SAR in magnetic nanoparticles systems, systems for thermo-gravimetric determination, Vibrating Sample Magnetometer systems (VSM) for up to 9 Tesla magnetic fields, Mossbauer systems with various accessories to carry out measurements at variable temperatures (4.5 K - 1000 K) also in applied fields by detection of radiation gamma / X-ray /conversion electrons, a complex system of measuring the physical properties (PPMS) with magnetic fields up to 14 Tesla, a SQUID type magnetometer system (Superconducting Quantum Interference Device) and a liquid He production unit (18 l / 24 h).

For the high temperatures field, the laboratory has a Laser Flash Analyzer system which enables the defining of thermal diffusivity, specific heat and thermal conductivity of the bulk or multi-layer (3-layer, including liquids) materials in the range of 25-1100 C, a dilatometer (Netzsch C 402, 2015) for determining the coefficients of thermal expansion (25-1600 C) and an equipment (Netzsch, Nemesis 2015) for determining electrical conductivity and the Seebeck coefficient (25-800 C).

Spark Plasma Sintering

30. Laboratory of Nanoscale Condensed Matter

The subjects of experimental investigation are directed towards the properties and the specific processes of the low dimensional systems, supplemented by modeling of the morphology, structure and composition, electric transport and phototransport, of the ferroic properties, chemical activity and surface/interface processes, as well as the phenomena of capture and storage of charge carriers for memory effects. Various types of nanostructured materials (e.g. nanostructures and nanocomposites, surfaces and interfaces with different features, especially magnetic, ferroelectric and catalytic properties) are prepared through advanced cleaning and deposition by physical methods (evaporation, sputtering).

An important part of the research that is done in the laboratory is aimed at applications in micro- and nanoelectronics, optoelectronics, spintronics, advanced sensors, photocatalysis and heterogeneous catalysis.

Theoretical investigations are largely motivated by recent results and aim at: the spectral properties of the Lieb optical networks and of the topological insulators, charge transport of the bidimensional materials (e.g. graphene, phosphorene), the dynamics of excitons in optically active quantum dots including magnetic impurities, artificial nanomagnets.

In the laboratory there are two "clusters" dedicated to the study of in-situ surfaces, which operate in ultra-vacuum (UHV 10^{-10} – 10^{-11} mbar). Each system is comprised of a preparation chamber by molecular beam epitaxy (MBE), a photoelectron spectroscopy characterization (XPS, UPS) chamber and a characterization by scanning tunneling microscopy (STM) chamber. In MBE systems there also the following in-situ characterization processes: fast and slow electron diffraction RHEED, LEED, thermal desorption by mass spectrometry studies, Auger electron spectroscopy. The XPS-UPS chambers permit spectroscopy measurements with angular resolution (photoelectron diffraction, dispersion laws in the valence band) and, in the case of one of the two clusters, also spin. Thus one can determine the atomic composition, the nature of chemical bonds, the structure at a nanoscopic scale, band structure.

Currently, one of the two clusters is located at Elettra synchrotron in Trieste. The LEEM-PEEM microscope (Low-Energy Electron Microscopy- Photoelectron Electron Microscopy) allows the investigation of samples with nanometer resolution using slow electrons (hence ideal for sensitive or insulating samples) as well as photoelectron spectroscopy studies with spatial resolution in the order of 20 nm. A third XPS automatic equipment allows investigation of several samples simultaneously and XPS analysis with spatial resolution in the order of 200 m, coupled with the possibility of in situ thermal treatment at high values of pressure (4 bar) and temperature (1000° C). The magnetron sputtering equipment (10-8 torr high vacuum) for deposition of thin films and multi-layer structures is equipped with in situ analysis techniques consisting of Auger electron surface spectroscopy and diffraction low-energy electron diffraction – LEED, as well as real time in situ ellipsometric monitoring. For thermal processing under controlled conditions, there is a rapid heat treatment equipment (RTA) in inert gas, oxidation - RTO and nitriding RTN.

Lab 30 carries out also complex experimental studies of the surfaces, interfaces (ferromagnetism, ferroelectrics, catalysis) of certain thin layers and multi- layer structures based on nanocrystals from the GeSiSn system (correlated with modeling studies), and studies of certain 2D semiconductor materials based on chalcogenides of (2D-TMD) transition metals.

For experimental studies, the laboratory is equipped with three chains for electrical and photoelectric, Hall effect and magnetoresistance measurements.

40. Laboratory of Optical Process in Nanostructured Materials

This laboratory is almost entirely dedicated to optical investigative methods applied to materials and focusing on nanostructures and nanocomposites. Other research topics are related to : the preparation and characterization of nanoscale semiconducting polymers with special properties, electrochemistry and production and characterization of chalcogenide glasses.

The main equipment used for optical characterization of investigated materials are: UV-Vis-NIR and FTIR absorption spectrophotometry, FTIR imaging microscope, FTRaman equipped with a YAG: Nd laser, confocal Raman spectrophotometer equipped with Ar and Kr lasers, SNOM (Scanning Near Field Optical Microscope) coupled with AFM (Atomic Force Microscope), systems for photoluminescence in VIS and NIR and thermoluminescence, and experimental setups for solar simulator and photoconductivity.

Other equipment used in the characterization and / or preparation of the studied materials are: broadband dielectric spectroscopy system, drop shape analysis for estimation of contact angle, equipment for deposition by vacuum evaporation of organic materials, Langmuir-Blodgett film deposition systems and potentiostats/galvanostats for the synthesis of composite materials and their testing as electrode materials in battery and supercapacitors.

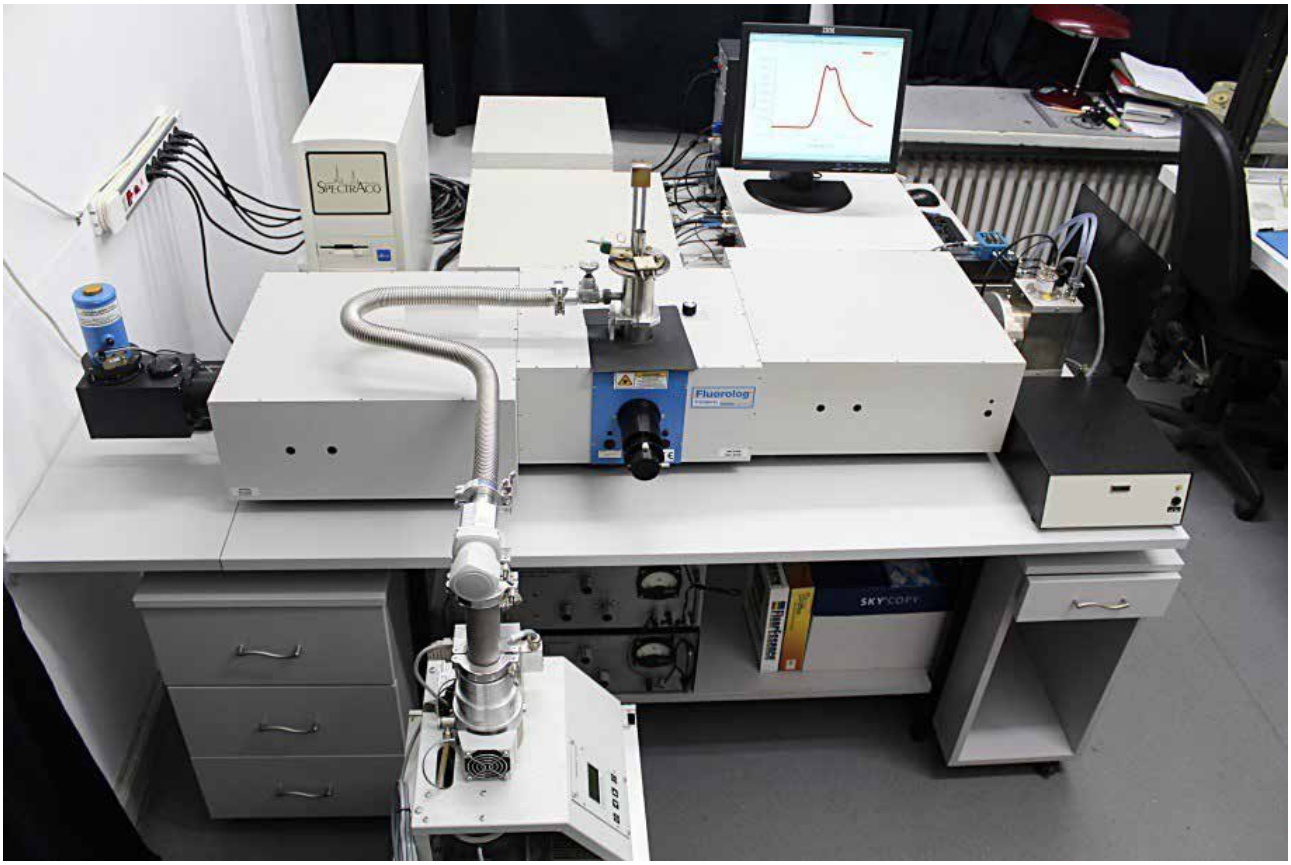

Fluorolog-3, model FL3-22, Horiba Jobin Yvon

50. Laboratory of Atomic Structures and Defects in Advanced Materials

This laboratory is mainly committed to structural investigations by advanced characterization methods such as analytical transmission electron microscopy (TEM) and scanning electron microscopy (SEM), electron paramagnetic resonance (EPR), Mössbauer spectroscopy, evaluation of physical properties in controlled environments (gas sensors, photocatalysis). The research activity includes, also, synthesis of nanostructured materials by the hydrothermal or co-precipitation methods. Among the important research equipment we mention: an aberration-corrected analytical HRTEM/STEM; a high-resolution analytical electron microscope for electron tomography and in-situ heating/cooling experiments; a conventional transmission electron microscopy; preparation equipment of TEM/SEM specimens; a SEM-FIB dual analytical system; five EPR spectrometers operating in several microwave bands and working modes in continuous wave or in pulsed regime, down to liquid He temperature; He liquefaction station; three Mössbauer spectrometers in the temperature range 4-1000 K; XRD diffractometers for powders and thin films; gas mixing station and associated electrical measurements equipments for materials testing under controlled atmosphere; specialized equipment for hydrothermal and co-precipitation synthesis.

The high resolution electron microscope is provided with probe Cs corrector of the spherical aberration and EDS and EELS microanalytical facilities, allowing a spatial resolution under 1 A and atomic elemental mapping. The SEM-FIB dual system is used for morphostructural and microanalytical investigations (SEM, EDS, EBSD) and for the processing of advanced materials at micro and nanometric scale by means of a Ga+ ion beam and nanomanipulators. The HRTEM and EPR spectroscopy facilities are included in the European network of research infrastructures C-ERIC (http://www.c-eric.eu/).

The research activity of the scientists working in this laboratory is focused on the physical properties of advanced materials (structure, optical), resulting either as size effects (nanostructures, thin films) or as structural defect engineering. The scientific concerns are mainly directed towards the discovery, investigation and manipulation of physical properties at nanometric and atomic scale for the development and characterization of functional materials to be used in various applications.

a. High resolution analytical transmission electron microscope (0.08 nm in mode STEM HAADF);

b. Analytical SEM-FIB dual system;

c. RES spectrometer in X band (9.7 GHz) in pulsed regime with accessories ENDOR;

d. Mossbauer spectrometer with cryostate for high magnetic fields (7 T) and cryogenic temperatures

e. Setup for electrical measurements in controlled atmosphere gas mixing station.

PERSONNEL

LIST OF PERSONNEL

Lab. 10 – Laboratory of Multifunctional Materials and Structures	
HEAD: Dr. Silviu POLOSAN	**E-mail:** silv@infim.ro **Phone:** (+4) 021.369.01.85 **Fax:** (+4) 021.369.01.77

#	NAME	POSITION
01	Dr. Marian Gabriel BANCIU	Senior Researcher I
02	Dr. Maria Monica ENCULESCU	Senior Researcher I
03	Dr. Aurelian Catalin GALCA	Senior Researcher I
04	Dr. Corneliu Florin MICLEA	Senior Researcher I
05	Dr. Cornel MICLEA	Senior Researcher I
06	Dr. Ioana PINTILIE	Senior Researcher I
07	Dr. Daniela PREDOI	Senior Researcher I
08	Dr. Elena MATEI	Senior Researcher II
09	Dr. Liviu NEDELCU	Senior Researcher II
10	Dr. Nicoleta Roxana PREDA	Senior Researcher II
11	Dr. George STAN	Senior Researcher II
12	Dr. Luminita AMARANDE	Senior Researcher III
13	Dr. Cristina BESLEAGA STAN	Senior Researcher III
14	Dr. Andra-Georgia BONI	Senior Researcher III
15	Dr. Florentina Cristina CHIRILA	Senior Researcher III
16	Dr. Steluta Carmen CIOBANU	Senior Researcher III
17	Dr. Victor-Constantin DICULESCU	Senior Researcher III
18	Dr. Lucian-Dragos FILIP	Senior Researcher III
19	Dr. Luminita Mirela HRIB	Senior Researcher III
20	Dr. Alin IUGA	Senior Researcher III
21	Dr. Lucia LEONAT	Senior Researcher III
22	Dr. Iuliana PASUK	Senior Researcher III
23	Dr. Roxana RADU	Senior Researcher III

#	NAME	POSITION
24	Dr. Viorica STANCU	Senior Researcher III
25	Dr. Lucian TRUPINA	Senior Researcher III
26	Dr. Ioana-Mihaela BOTEA	Senior Researcher
27	Dr. Marius CIOANGHER	Senior Researcher
28	Dr. Iulia Corina CIOBOTARU	Senior Researcher
29	Dr. Liliana Andreea COSTAS	Senior Researcher
30	Dr. Camelia-Florina FLORICA	Senior Researcher
31	Mihaela BEREGOI	Assistant Researcher
32	Dr. Constantin Claudiu CIOBOTARU	Assistant Researcher
33	Daniela Emilia DOGARU	Assistant Researcher
34	Alexandru-Ionut EVANGHELIDIS	Assistant Researcher
35	Irina Sorina GHITA	Assistant Researcher
36	Simona-Liliana ICONARU	Assistant Researcher
37	Marian Cosmin ISTRATE	Assistant Researcher
38	Cristina MOZACEANU	Assistant Researcher
39	Melania Loredana ONEA	Assistant Researcher
40	Alexandra Maria PALICI	Assistant Researcher
41	Cristina-Liana POPA	Assistant Researcher
42	Dr. Adrian Claudiu POPA	Assistant Researcher
43	Cristian RADU	Assistant Researcher
44	Dorin RUSU	Assistant Researcher
45	Andrei-Gabriel TOMULESCU	Assistant Researcher
46	Liliana-Marinela TRINCA	Assistant Researcher
47	Alexandru GAVRILA	Assistant Engineer
48	Vasilica TOMA	Assistant Engineer

Lab. 20 – Laboratory of Magnetism and Superconductivity	
HEAD: Dr. Victor Eugen KUNCSER	**E-mail:** kuncser@infim.ro **Phone:** (+4) 021.369.01.85 **Fax:** (+4) 021.369.01.77

#	NAME	POSITION
01	Dr. Gheorghe ALDICA	Senior Researcher I
02	Dr. Petre BADICA	Senior Researcher I
03	Dr. Ioan Adrian CRISAN	Senior Researcher I
04	Dr. Ovidiu Alexandru CRISAN	Senior Researcher I
05	Dr. George FILOTI	Senior Researcher I (associate collaborator)
06	Dr. Andrei GALATANU	Senior Researcher I
07	Dr. Lucica MIU	Senior Researcher I
08	Dr. Neculai PLUGARU	Senior Researcher I
09	Dr. Viorel Constantin SANDU	Senior Researcher I
10	Dr. Mihaela VALEANU	Senior Researcher I
11	Dr. Petru PALADE	Senior Researcher II
12	Dr. Gabriel-Alexandru SCHINTEIE	Senior Researcher II
13	Dr. Cristina BARTHA	Senior Researcher III
14	Dr. Ancuta BIRSAN	Senior Researcher III
15	Dr. Daniela-Alina CRISAN	Senior Researcher III
16	Dr. Valentina MIHALACHE	Senior Researcher III
17	Dr. Felicia TOLEA	Senior Researcher III
18	Dr. Simona-Gabriela GRECULEASA	Senior Researcher
19	Dr. Ion IVAN	Senior Researcher
20	Dr. Bogdan Vasilica POPESCU	Senior Researcher
21	Dr. Mihaela SOFRONIE	Senior Researcher
22	Mihail BURDUSEL	Assistant Researcher
23	Andrei CATRINA	Assistant Researcher
24	Dr. Cezar Catalin COMANESCU	Assistant Researcher
25	Magdalena GALATANU	Assistant Researcher
26	Mihai-Alexandru GRIGOROSCUTA	Assistant Researcher

#	NAME	POSITION
27	**Marinela Alina IONESCU**	Assistant Researcher
28	**Anda Elena STANCIU**	Assistant Researcher
29	**Dr. Carmen PLAPCIANU**	Chemist
30	**Aurel LECA**	Engineer
31	**Dr. Adrian Daniel Ion JIANU**[1]	Senior Researcher I
32	**Dr. Marilena Tatiana TOMUT**[2]	Senior Researcher III

[1]Institute for Pulsed Power and Microwave Technology, Forschungszentrum Karlsruhe.
[2]GSI / KP2 Nuclear Structure and Nuclear Chemistry, Darmstadt.

Lab. 30 – Laboratory of Nanoscale Condensed Matter	
HEAD: Dr. Valeriu MOLDOVEANU	**E-mail:** valim@infim.ro **Phone:** (+4) 021.369.01.85 **Fax:** (+4) 021.369.01.77

#	NAME	POSITION
01	Dr. Alexandru Emil ALDEA	Senior Researcher I
02	Dr. Lidia Magdalena CIUREA	Senior Researcher I
03	Dr. Sorina LAZANU	Senior Researcher I
04	Dr. Mihail Florin LAZARESCU	Senior Researcher I
05	Dr. Dan MACOVEI	Senior Researcher I
06	Dr. Stefan Adrian MANEA	Senior Researcher I
07	Dr. Nicolae POPA	Senior Researcher I
08	Dr. Toma STOICA	Senior Researcher I
09	Dr. Cristian Mihail TEODORESCU	Senior Researcher I
10	Dr. Rodica GHITA	Senior Researcher II
11	Dr. Gheorghe IORDACHE	Senior Researcher II
12	Dr. Nicoleta Georgiana APOSTOL	Senior Researcher III
13	Dr. Bogdana-Lenuta BORCA	Senior Researcher III
14	Dr. Maria-Ruxandra COSTESCU	Senior Researcher III
15	Dr. Ion Viorel DINU	Senior Researcher III
16	Dr. Marius Adrian HUSANU	Senior Researcher III
17	Dr. Ana Maria LEPADATU	Senior Researcher III
18	Dr. Constantin LOGOFATU	Senior Researcher III
19	Dr. George Adrian LUNGU	Senior Researcher III
20	Dr. Stefan NEATU	Senior Researcher III
21	Dr. Constantin Catalin NEGRILA	Senior Researcher III
22	Dr. Marian NITA	Senior Researcher III
23	Dr. Dana-Georgeta POPESCU	Senior Researcher III
24	Dr. Adrian SLAV	Senior Researcher III
25	Dr. Ionel STAVARACHE	Senior Researcher III
26	Dr. Mugurel TOLEA	Senior Researcher III

#	NAME	POSITION
27	**Dr. Elena-Laura ABRAMIUC**	Senior Researcher
28	**Dr. Bogdan OSTAHIE**	Senior Researcher
29	**Dr. Catalin PALADE**	Senior Researcher
30	**Dr. Mihaela STEGARESCU**	Senior Researcher
31	**Dr. Liviu Cristian TANASE**	Senior Researcher
32	**Amelia-Elena BOCIRNEA**	Assistant Researcher
33	**Dr. Costel COTIRLAN SIMIONIUC**	Assistant Researcher
34	**Radu DRAGOMIR**	Assistant Researcher
35	**Stefan STANCIU**	Assistant Researcher
36	**Ioana Cristina BUCUR**	Engineer
37	**Cristian TACHE**	Engineer
38	**Dr. Nicolae BIRSAN[1]**	Senior Researcher I
39	**Dr. Andrei MANOLESCU[2]**	Senior Researcher I

[1]Institute of Physical and Theoretical Chemistry, University of Tübingen.
[2]School of Science and Engineering, Reykjavik, Iceland.

Lab. 40 – Laboratory of Optical Processes in Nanostructured Materials	
HEAD: Dr. Mihaela BAIBARAC	**E-mail:** barac@infim.ro **Phone:** (+4) 021.369.01.85 **Fax:** (+4) 021.369.01.77

#	NAME	POSITION
01	Dr. Ioan BALTOG	Senior Researcher I
02	Dr. Ligia FRUNZA	Senior Researcher I
03	Dr. Stefan FRUNZA	Senior Researcher I
04	Dr. Mihai POPESCU	Senior Researcher I
05	Dr. Mihail SECU	Senior Researcher I
06	Dr. Marian SIMA	Senior Researcher II
07	Dr. Anca-Ioana STANCULESCU	Senior Researcher II
08	Dr. Constantin Paul GANEA	Senior Researcher III
09	Dr. Adam LORINCZI	Senior Researcher III
10	Dr. Oana RASOGA	Senior Researcher III
11	Dr. Florinel SAVA	Senior Researcher III
12	Dr. Elisabeta Corina SECU	Senior Researcher III
13	Dr. Mariana SIMA	Senior Researcher III
14	Dr. Marcela SOCOL	Senior Researcher III
15	Dr. Alin VELEA	Senior Researcher III
16	Dr. Irina Ionela ZGURA	Senior Researcher III
17	Carmen Steliana BREAZU	Assistant Researcher
18	Monica Alexandra DAESCU	Assistant Researcher
19	Mirela ILIE	Assistant Researcher
20	Adelina MATEA	Assistant Researcher
21	Dr. Oana-Claudia MIHAI	Assistant Researcher
22	Andreea Alexandra NILA	Assistant Researcher
23	Dr. Iosif Daniel SIMANDAN	Assistant Researcher
24	Ion SMARANDA	Assistant Researcher
25	Dr. Malvina Simona STROE	Assistant Researcher
26	Dr. Valeriu-Florin COTOROBAI	Physicist

Lab. 50 – Laboratory of Atomic Structures and Defects in Advanced Materials	
HEAD: Dr. Corneliu GHICA	**E-mail:** cghica@infim.ro **Phone:** (+4) 021.369.01.85 **Fax:** (+4) 021.369.01.77

#	NAME	POSITION
01	Dr. Lucian DIAMANDESCU	Senior Researcher I
02	Dr. Sergiu Vasile NISTOR	Senior Researcher I
03	Dr. Leona Cristina NISTOR	Senior Researcher I
04	Dr. Valentin Serban TEODORESCU	Senior Researcher I
05	Dr. Florin Dan VASILIU	Senior Researcher I
06	Dr. Marin CERNEA	Senior Researcher II
07	Dr. Adelina STANOIU	Senior Researcher II
08	Dr. Mariana STEFAN	Senior Researcher II
09	Dr. Alina BANUTA	Senior Researcher III
10	Dr. Daniela GHICA	Senior Researcher III
11	Dr. Adrian Valentin MARALOIU	Senior Researcher III
12	Dr. Traian POPESCU	Senior Researcher III
13	Dr. Cristian SIMION	Senior Researcher III
14	Dr. Aurel Mihai VLAICU	Senior Researcher III
15	Dr. Andrei Cristian KUNCSER	Senior Researcher
16	Dr. Ionel MERCIONIU	Senior Researcher
17	Dr. Raluca Florentina NEGREA	Senior Researcher
18	Dr. Ioana-Dorina VLAICU	Senior Researcher
19	Alexandra-Camelia JOITA	Assistant Researcher
20	Dr. Manuela STIR	Assistant Researcher
21	Dr. Marcel FEDER	Chemist
22	Stefan BULAT	Engineer
23	Ovidiu Gabriel FLOREA	Engineer
24	Gheorghe STERIAN	Assistant Engineer

VISITING GUESTS

Dr. Halldor Gudfinnur SVAVARSSON Associate Professor, School of Science and Engineering, Reykjavik University, Iceland "Large arrays of ultra-high aspect ratio periodic silicon nanowires obtained via top–down route"	**27.03.2016**
Prof. Dr. Andreas ROODT Department of Chemistry, University of the Free State, South Africa "Small molecule structure/ reactivity relationships as important probes in applied chemistry processes"	**02.06.2016**
Dr. Markus ETZKORN Max Planck Institute for Solid State Research Stuttgart, Germany "Josephson Scanning Tunneling Microscopy"	**21.06.2016**
Dr. Uta SCHLICKUM Max Planck Institute for Solid State Research Stuttgart, Germany "Single molecule optoelectronic devices"	**21.06.2016**
Prof. Yoshihiko TAKANO National Institute for Materials Science (NIMS), Tsukuba, Japan "Recipes to Improve the Performance of Iron Chalcogenide Superconductors"	**27.06.2016**
Dr. Raul ARENAL Laboratorio de Microscopias Avanzadas (LMA) at the Instituto de Nanociencia de Aragon (INA), Zaragoza University, Spain "Structural and Local Spectroscopic Studies on Hybrid/Hetero Nanomaterials by TEM"	**24.06.2016**
Dr. Ovidiu Cristian ANDRONESI Harvard University, USA "Advanced high field MR imaging of human brain to study neurological diseases"	**19.08.2016**
Prof. Mark C. HERSAM Northwestern University, USA "Fundamentals and Applications of Low-Dimensional Nanoelectronic Heterostructures"	**16.09.2016**
Prof. Fabrice CHARRA CEA-Sarclay, Paris, France "Graphene-based supramolecular architectures for photonics	**20.09.2016**

Dr. Markus MEYER International Sales Manager, Netzsch, Germany “Advanced Thermal Analysis and Applications”	**29.09.2016**
Prof. Ovidiu ERSEN Strasbourg University, Institut de Physique et Chimie des Matériaux de Strasbourg (IPCMS), France "Advanced TEM techniques: 3D and operando views of the materials at the nanoscale"	**10.11.2016**
Dr. Adrian BALAN CNRS-Thales, France "Emerging electronic states in 2D materials: Introducing Phosphorene"	**21.12.2016**
Prof. Ioan OPRIS University of Miami Miller School of Medicine Miami, USA “The executive control of movement: from prefrontal cortex to striatum and brainstem”	**02.11.2016**
WORKING STAGES	
Dr. Alberto NALDONI CNR - ISTM - Consiglio Nazionale delle Ricerche - Istituto Scienze e Tecnologie Molecolari, Italy Enhancing the solubility of silicon in hematite nanostructures for solar water splitting: interplay among morphology, crystallographic, magnetic and electronic properties Consortium C-ERIC, Lab. 50 EPR spectroscopy group (invitation Dr. M. Stefan)	**29-30.03.2016**
Dr. Giovanni De GIUDICI Università degli Studi di Cagliari - Dipartimento di Scienze della Terra, Italy Characterization of biomineralization processes, biopolymers, trace element speciation and microbial carbonation Consortium C-ERIC, Lab. 50 EPR spectroscopy group (invitation Dr. M. Stefan)	**29-30.03.2016**
Dr. Nalini SUNDARAM Poornaprajna Institute of Scientific Research, India Evaluation of Micro structure and Phase Composition of Bi2-xGdxWO6(x = 0.2 to 1) Mixed phase Nano Photocatalysts. Consortium C-ERIC, Lab. 50 electron microscopy group (invitation Dr. C. Ghica)	**29-30.03.2016**
Dr. Venkatesan DHANASEKARAN SOLEIL - Société Civile Synchrotron SOLEIL, France Structural and morphological analysis of mono/bi metallic nanostructures for CO oxidation. Consortium C-ERIC, Lab. 50 electron microscopy group (invitation Dr. C. Ghica)	**11-15.04.2016**

Dr. Cinzia Anna VENTURA Università degli Studi di Messina - Dipartimento di Scienze del Farmaco e dei Prodotti per la Salute (SCIFAR), Italy Spatial disposition of hyaluronic acid in chitosan-hyaluronan nanoparticles for drug delivery: a combined UV resonant Raman and microscopy study. Consortium C-ERIC, Lab. 50 electron microscopy group (invitation Dr. C. Ghica)	**26-27.04.2016**
Dr. Rubina SHAHEEN PINSTECH, Electronic and Magnetic Materials Group, NPD Pakistan Anomalous Structures, Microstructure and Temperature Induced Phase Transitions in Rare Doubly Ordered Perovskites NaLaMgBO6 (B=Te, W). Consortium C-ERIC, Lab. 50 electron microscopy group (invitation Dr. C. Ghica)	**11-17.05.2016**
Dr. Marko KARLUSIC Ruder Boskovic Institute, Croatia Swift heavy ion track formation in GaN: role of defects. Consortium C-ERIC, Lab. 50 electron microscopy group (invitation Dr. C. Ghica)	**02-03.06.2016**
Dr. Charlotte COCHARD Ecole Centrale Paris - Laboratoire SPMS UMR 8580, France Relationship between local orders and global properties. Consortium C-ERIC, Lab. 50 electron microscopy group (invitation Dr. C. Ghica)	**06-10.06.2016**
Dr. Jose SILVA Departamento de Fisica Universidade do Minho, Portugalia ((1-x)Ba(Zr0.2Ti0.8)O3-x(Ba0.7Ca0.3)TiO3/ZnO heterostructures for resistive random access memories. Consortium C-ERIC, Lab. 50 electron microscopy group (invitation Dr. C. Ghica)	**27.06-01.07.2016**
Dr. Sara BAGHERIFARD I.N.F.M. - c/o Politecnico di Milano, Italy Surface nanocrystallization of Mg alloy for Improved Spinal Fusion. Consortium C-ERIC, , Lab. 50 electron microscopy group (invitation Dr. C. Ghica)	**19-23.09.2016**
Dr. Claudio FERRARI C.N.R. - Ist. MASPEC, Italy The origin of compressive strain in surface damaged materials. Consortium C-ERIC, Lab. 50 electron microscopy group (invitation Dr. C. Ghica)	**03-07.10.2016**

Dr. Elisabetta COMINI Università di Brescia, Italy Electronic, chemical, microstructural interface properties of metal oxide nanowires and heterojunctions for gas sensing applications. Consortium C-ERIC, Lab. 50 electron microscopy group (invitation Dr. C. Ghica)	**07-11.11.2016**
Dr. Alberto NALDONI CNR - ISTM - Consiglio Nazionale delle Ricerche - Istituto Scienze e Tecnologie Molecolari, Italy Enhancing the solubility of silicon in hematite nanostructures for solar water splitting: interplay among morphology, crystallographic, magnetic and electronic properties. Consortium C-ERIC, Lab. 50 electron microscopy group (invitation Dr. C. Ghica)	**14-18.11.2016**
Dr. Giovanni DE GIUDICI I.N.F.M. - c/o Politecnico di Milano, Italy Characterization of biomineralization processes, biopolymers, trace element speciation and microbial carbonation. Consortium C-ERIC, Lab. 50 electron microscopy group (invitation Dr. C. Ghica)	**24-28.11.2016**
Dr. Mohamed AL-HADA ICTP - International Centre for Theoretical Physics Abdus Salam (CIFT - Centro Internazionale di Fisica Teorica Abdus Salam), Italy Inner and final state effects contributing to the XPS binding energy in supported mass selected Ag-clusters on free standing and supported Gr. Consortium C-ERIC, Lab. 50 electron microscopy group (invitation Dr. C. Ghica)	**28-29.11.2016**

Ph. D. THESES

M. BIRZU (part-time at NIMP)
Hydrphobic processes in textile materials: physical-chemical characteristics and statistical-mathematical modeling
2016

Liliana TRINCA
ZnO based heterostructures with applications in electronics
October 2016

Simona Liliana ICONARU
Iron oxide nanoparticles and hydroxyapatite: reactivity and influence on the environment.
March 2016

Radu DRAGOMIR
Transport phenomena and exciton dynamics in optically activated quantum dots
September 2016

Catalin PALADE
Electric and photoelectric properties of layers formed of Ge nanoparticles embedded in oxidic matrix
Octomber 2016

AWARDS

AWARDS AT INTERNATIONAL FAIRS AND EXHIBITIONS
XIV International Inventics Salon PRO INVENT, Cluj-Napoca
L. PINTILIE, G. STAN, I. PINTILIE, M. BOTEA, A. IUGA, A. GAVRILA, G. DOBRESCU, M. CIOCA, L. CULEA, P. SOARE Pyroelectric detector with optical amplification for operating at high temperature **GOLD MEDAL and Diploma of Excellence**
M. GALATANU, G. RUIU, S. CRETU, M. ENCULESCU, A. GALATANU Multi-metal, multi-ceramic stratified composite **GOLD MEDAL and Diploma of Excellence**
G. ALDICA, M. BURDUSEL, P. BADICA Mechanical workable superconductor material and magnetic field concentrator **GOLD MEDAL and Diploma of Excellence**
I. PINTILIE, C. BESLEAGA-STAN, V. STANCU, A. TOMULESCU, M. SIMA, M. MIHALCEA, L. PINTILIE Hybrid solar cell **BRONZ MEDAL and Diploma of Excellence**
L. PINTILIE, I. PINTILIE, M. BOTEA, A. IUGA, M. CIOCA, L. CULEA, P. SOARE, G. DOBRESCU, A. GAVRILA Pyroelectric detector from bulk ceramic with concentration gradient **Diploma of Excellence**
GAVRILA-FLORESCU CL, POPOVICI E, MORJAN I, **DIAMANDESCU LC**, RADITOIU V, RADITOIU A, WAGNER LE, BADOI AD, MIRON D Method of nano titanium dioxide synthesis by laser pyrolysis targeting photocatalytic applications **DIPLOME OF EXCELLENCE and GOLD MEDAL with SPECIAL MENTION**
European Exhibition of Creativity and Innovation EUROINVENT, IASI, MAI 2016
L. PINTILIE, I. PINTILIE, M. BOTEA, A. IUGA, M. CIOCA, L. CULEA, P. SOARE, G. DOBRESCU, A. GAVRILA Pyroelectric detector from bulk ceramic with concentration gradient **GOLD MEDAL**
I. PINTILIE, C. BESLEAGA-STAN, V. STANCU, A. TOMULESCU, M. SIMA, M. MIHALCEA, L. PINTILIE Hybrid solar cell **GOLD MEDAL**
C. COTIRLAN-SIMIONUC, A. RIZEA, D. V. URSU Optoelectronic Device with Electrically Configurable Metasurface for Controlling the Polarization of Light and Getting the Optical Resolution Below the Classic Diffraction Limit **SILVER MEDAL**

L. PINTILIE, G. STAN, I. PINTILIE, M. BOTEA, A. IUGA, A. GAVRILA, G. DOBRESCU, M. CIOCA, L. CULEA, P. SOARE
Pyroelectric detector with optical amplification for operating at high temperature
SILVER MEDAL

G. ALDICA, M. BURDUSEL, P. BADICA
Mechanical workable superconductor material and magnetic field concentrator
BRONZ MEDAL

M. GALATANU, G. RUIU, S. CRETU, M. ENCULESCU, A. GALATANU
Multi-metal, multi-ceramic stratified composite
BRONZ MEDAL

HONORARY MEMBERSHIP

NIMP is present in following databases:

- The **CEEC IST NET** portal (www.eu-istcommunity.net) – is a support instrument for partners search and consortia creation in the field of research and innovation concerning the information society technologies
- **Europartners Search** (www.europartnersearch.net)
- **Resource Guide to Nanotechnology and Nanomaterials Services** (named **NanoPerspective**) - This guide includes a list of more 1000 organizations active in the field of Nanotehnology and Nanomaterials.
- http://wikimapia.org/19116027/INCDFM-National-RD-Institute-of-Materials-Physics-NIMP
- http://cercetare.ccib.ro/intranetHTML/infoFILES/infoHTML/File/2012_03_22_prezentare INCDFM.pdf
- http://www.research.gov.ro/ro/articol/1320/sistemul-de-cercetare-incd-institute-nationale-de-cercetare-dezvoltare-institute-nationale-de-cercetare-dezvoltarehttp://www.infocercetare.ro/ro/Listeaza-Institutie/Ilfov-84_Localitate_Magurele- 86_Institutie_INCD-pentru-Fizica-Materialelor-INCDFM-253
- http://ro-ro.facebook.com/pages/INCDFM/122100527823931
- http://site.roinno.ro/data/pdf/ca/369.pdf

NIMP is member of C-ERIC (Central European Research Infrastructure Consortium, http://www.ceric-eric.eu/). a distributed research facility, set up as an ERIC, by **Austria, Czech Republic, Italy, Romania, Croatia, Polonia, Slovenia, Serbia,** and **Hungary** and open to other interested countries.

The specific scope of this ERIC concerns the offer as an integrated service provided to external researchers who can thus accede to synchrotron light and other microscopic probes for analytical and processing techniques notably for materials preparation and characterization, structural investigations and imaging in Life Sciences, Nanoscience and Nanotechnology, Cultural Heritage, Enviroment and Materials Sciences and to their various technological and industrial outcomes ranging from energy to biomedical and of interest to most manufacturing industries.

CERIC's mission is to bring the integrated service to world-level quality thus contributing to the attractiveness of the European Research Area and stimulating a beneficial impact on the scientific and economic development of the entire region, also helping to introduce a strong interchange between scientists and technicians and attraction of scientists from other regions.

Membership in Other International Organizations, Evaluators and Members in Comissions of Trust

ALDICA Gheorghe: member of European Applied Superconductivity Society; expert evaluator UEFISCDI

BADICA Petre: member of American Chemical Society, German Physical Society, European Applied Superconductivity Society; expert evaluator UEFISCDI; expert evaluator for ICC-IMR Japan and for NATO Science for Peace projects

BANCIU Marian Gabriel: member of IEEE: Microwave Theory and Techniques Society, Antennas and Propagation Society; founding member of Romanian Society for Non-Ionizing Radiation Safety (SRPRNI); evaluator expert UEFISCDI

BARTHA Cristina: member of EcerS

BURDUSEL Mihai: member of European Applied Superconductivity Society

CIUREA Magdalena Lidia: member of European Physical Society, expert evaluator UEFISCDI

COSTAS Liliana Andreea: member of European Physical Society; member of European Microscopy Society; member of Romanian Society of Electron Microscopy

CRISAN Ovidiu: member of Institute of Nanotechnology, UK; member of Materials Research Society; expert evaluator of EC, program H2020, calls H2020-ECSEL-2016-2-IA (innovation actions) and H2020-ECSEL-2016-1-RIA (research and innovation actions); expert evaluator EC, Executive Agency of Research REA, program H2020, FET Open, Vice-Chair, supervising evaluators for calls H2020-FETOPEN-2015/2-RIA, H2020-FETOPEN-2016-RIA-1; monitor for EC of the project DENECOR of ENIAC JU Grant Agreement nr. 324257; expert evaluator of CFCA (Central Finance and Contracting Agency) Letonia, for call Industry-Driven Research of the operational program Growth & Development - EU Structural and Cohesion Fund; expert evaluator PN III, calls Eureka PN-III-P3-3.5-EUK-2016, Romania-Moldova PN-III-P3-3.1-PM-RO-MD-2016, Bridge Grant PN-III-P2-2.1-BG-2016 and Transfer to Economic Partner PN-III-P2-2.1-PTE-2016; expert evaluator structural funds POC AXE 1 RESEARCH call A P.4

CRISAN Alina: expert evaluator UEFISCDI

DIAMANDESCU Lucian: member of "American Nano Science"; Romanian Representative in International Board on the Applications of Mössbauer Effect - IBAME (2011-2017); member in Editorial Board of "ISRN Nanomaterials" (SUA); expert evaluator UEFISCDI

FRUNZA Ligia: member of American Chemical Society and of Romanian Society of Catalysis

GHICA Corneliu: member of European Materials Research Society; member of European Microscopy Society; member in Directory Council of Romanian Society of Electron Microscopy

GHICA Daniela: member of European Materials Research Society

KUNCSER Andrei Cristian: member of European Microscopy Society; member of Romanian Society of Electron Microscopy

KUNCSER Victor: expert evaluator UEFISCDI; member in commission for associate professor position at the Department of Theoretical Physics, Faculty of Physics Bucharest

LEPADATU Ana Maria: member of European Physical Society

MARALOIU Valentin Adrian: member of Société Française des Microscopies; member of Romanian Society of Electron Microscopy

MERCIONIU Ionel Florinel: member of European Microscopy Society; member of Romanian Society of Electron Microscopy

NEGREA Raluca Florentina: member of European Microscopy Society; member of Romanian Society of Electron Microscopy
NISTOR Leona Cristina: member of European Microscopy Society; vicepresident of Romanian Society of Electron Microscopy
NISTOR Sergiu Vasile: member of American Physical Society
PINTILIE Lucian: member of European Physical Society; honorary member of Romanian Society of Electron Microscopy; member in Task Force Characterization for Research Directorate of EC; evaluator expert UEFISCDI
PLUGARU Neculai: member in commission for assistant professor position at the Department of Electricity, Solid State Physics and Biophysics, Faculty of Physics, Bucharest
POLOSAN Silviu: evaluator expert UEFISCDI
POPESCU Mihai: member of NACNOG (North Atlantic Consortium on Non-Oxide Glasses, 19 countries from Europe, Canada și SUA)
- member of VIP (Virtual Institute of Physics): http://www.infim.ro/~inst
PREDOI Daniela: member of Romanian Society of Catalysis
SANDU Viorel: member of American Physical Society and Material Research Society Singapore
SARBU Corneliu: member of Microscopical Society of America; member of Romanian Society of Electron Microscopy
SOCOL Marcela: member of International Organization on Crystal Growth
STANCULESCU Anca: member of International Organization on Crystal Growth
- member of SPIE
TEODORESCU Valentin Șerban: member of European Microscopy Society; general secretary of Romanian Society of Electron Microscopy
TEODORESCU Cristian Mihail: expert evaluator UEFISCDI
VALEANU Mihaela: expert evaluator UEFISCDI
VASILIU Florin: member of European Microscopy Society; member of Romanian Society of Electron Microscopy
VLAICU Aurel Mihai: member of European Microscopy Society; member of Romanian Society of Electron Microscopy
VLAICU Dorina Ioana: member of Romanian Society of Chemistry; member of Royal Society of Chemistry

PUBLICATIONS AND PRESENTATIONS

BOOK CHAPTERS

Miculescu, F; Maidaniuc, A; **Stan, GE**; Miculescu, M; Voicu, SI; Cimpean, A; Mitran, V; Batalu, D, Tuning hydroxyapatite particles' characteristics for solid freeform fabrication of bone scaffolds; pp. 321–397;
In: Advanced Composite Materials; Eds. A. Tiwari, M.R. Alenezi, and S.C. Jun; Publisher: John Wiley & Sons, 2016; ISBN: 978-1-119-24253-6 (DOI: 10.1002/9781119242666.ch7).

Ligia Frunza, Irina Zgura, Valeriu Florin Cotorobai, Constantin Paul Ganea, Stefan Frunza
Chapter 10 "Microdroplets of laser irradiated drug solutions: surface tension and contact angle" pp1-32, (www.benthamscience.com/ebooks) 2016

Plugaru R.; Mihalache I.; Gavrila R.; Boldeiu G.; Nedelcu O.; **Plugaru N.; Maraloiu V.A.; Ghica D.; Stefan M.; Nistor S. V.**; "Zinc oxide thin films for radiation hardeneed devices by materials engineering",
In: "Nanomaterials, Nanoparticles, Nanodevices", M. Zaharescu, H. Chiriac, D. Dascalu (Eds.), Publishing House of the Romanian Academy, pp.185-208, 2016. Book chapter.

Kuncser V.; Palade P.; Schinteie G.; Dumitrache F.; Fleaca C.; Scarisoareanu M.; Morjan I.; **Filoti G.**; Transition Metal/Carbon nanocomposites
In: Carbon Nanomaterials Sourcebook, Vol. II, CRC Press Taylor & Francis Group, LLC (2016) ed. Klaus D. Sattler, International Standard Book Number 13: 978-1-4822-5271-2

Baibarac M.; Baltog I.; Szunerits S.; "Raman and FTIR spectroscopy as valuable tools for the characterization of graphene-based materials"
In: "Graphene Science Handbook: Size-dependent properties", vol.5, Mahmood Aliofkhazraei, Nasar Ali, William I. Milne, Cengiz S. Ozkan, Stanislaw Mitura, Juana L. Gervasoni (Eds.), CRC Press, Taylor &Francis Group, pp. 235-253, 2016, ISBN: 13-978-4665-9136-3.

Cheran L-E, Cheran A, Lupu A-R, **Popescu T**, Nano and microtechnology for monitoring stem cell differentiation,
In: „Stem Cells Between Regeneration and Tumorigenesis", C Tanase and Neagu M (Ed), Bentham Science, ISBN: 978-1-68108-332-2, eISBN : 978-1-68108-331-5, 2016

JOURNALS

Papers in ISI Ranked Journals (with Impact Factor and AIS)

01. **Aldica, G**; **Burdusel, M**; **Popa, S**; Hayasaka, Y; **Badica, P**;
Graphene addition to MgB_2 superconductor obtained by ex-situ spark plasma sintering technique
MATERIALS RESEARCH BULLETIN, (2016), **77**, pp.205-211, **2.435**, **0.441**

02. **Amarande, L**; **Miclea, C**; **Cioangher, M**; **Grecu, MN**; **Pasuk, I**;
Effects of vanadium doping on sintering conditions and functional properties of Nb-Li co-doped PZT ceramics. Comments on Li location
JOURNAL OF ALLOYS AND COMPOUNDS, (2016), **685**, pp.159-166, **3.014**, **0.558**

03. **Apostol, NG**; **Lungu, GA**; **Bucur, IC**; **Tache, CA**; **Hrib, L**; **Pintilie, L**; **Macovei, D**; **Teodorescu, CM**;
Non-interacting, sp(2) carbon on a ferroelectric lead zirco-titanate: towards graphene synthesis on ferroelectrics in ultrahigh vacuum
RSC ADVANCES, (2016), **6**, pp.67883-67887, **3.289**, **0.628**

04. Avotina, L; Marcu, A; Porosnicu, C; Lungu, M; Stancalie, A; Ilie, AG; **Ganea, PC**; Savastru, D; Kalnacs, J; Lungu, CP; Kizane, G; Antohe, S;
MULTI-WAVELENGTH LASER IRRADIATION OF Be-C-W COATINGS
DIGEST JOURNAL OF NANOMATERIALS AND BIOSTRUCTURES, (2016), **11**, pp.293-302, **0.756**, **0.139**

05. **Badica, P**; **Burdusel, M**; **Popa, S**; **Pasuk, I**; **Ivan, I**; Borodianska, H; Vasylkiv, O; **Kuncser, A**; **Ionescu, AM**; **Miu, L**; **Aldica, G**;
Reactive spark plasma sintering of MgB_2 in nitrogen atmosphere for the enhancement of the high-field critical current density
SUPERCONDUCTOR SCIENCE & TECHNOLOGY, (2016), **29**, 105020, **2.717**, **0.835**

06. **Baibarac, M**; **Baltog, I**; **Daescu, M**; Lefrant, S; Chirita, P;
Optical evidence for chemical interaction of the polyaniline/fullerene composites with N-methyl-2-pyrrolidinone
JOURNAL OF MOLECULAR STRUCTURE, (2016), **1125**, pp.340-349, **1.78**, **0.29**

07. **Baibarac, M**; **Baltog, I**; **Ilie, M**; Humbert, B; Lefrant, S; **Negrila, C**;
Influence of Single-Walled Carbon Nanotubes Enriched in Semiconducting and Metallic Tubes on the Vibrational and Photoluminescence Properties of Poly(para-phenylenevinylene)
JOURNAL OF PHYSICAL CHEMISTRY C, (2016), **120**, pp.5694-5705, **4.509**, **1.171**

08. **Baibarac, M**; **Nila, A**; **Baltog, I**;
Exciton-phonon interaction in CdS of different morphological forms manifested as stimulated Raman scattering
OPTICAL MATERIALS EXPRESS, (2016), **6**, pp.1881-1895, **2.657**, **0.87**

09. **Baibarac, M**; **Nila, A**; **Baltog, I**;
Polarized Raman spectra of phosphorene in edge and top view measuring configurations
RSC ADVANCES, (2016), **6**, pp.58003-58009, **3.289**, **0.628**

10. **Baltog, I**; **Baibarac, M**; **Smaranda, I**; **Matea, A**; **Ilie, M**; Mevellec, JY; Lefrant, S;
Optical properties of single-walled carbon nanotubes functionalized with copolymer poly(3,4-ethylenedioxythiophene-co-pyrene)
OPTICAL MATERIALS, (2016), **62**, pp.604-611, **2.183**, **0.461**

11. Barca, ES; Filipescu, M; Luculescu, C; Birjega, R; Ion, V; Dumitru, M; **Nistor, LC**; Stanciu, G; Abrudeanu, M; Munteanu, C; Dinescu, M;
Pyramidal growth of ceria nanostructures by pulsed laser deposition
APPLIED SURFACE SCIENCE, (2016), **363**, pp.245-251, **3.15**, **0.574**

12. **Bartha, C**; **Plapcianu, C**; **Crisan, A**; **Enculescu, M**; **Leca, A**;
STRUCTURAL AND MAGNETIC PROPERTIES OF Sr_2FeMoO_6 OBTAINED AT LOW TEMPERATURES
DIGEST JOURNAL OF NANOMATERIALS AND BIOSTRUCTURES, (2016), **11**, pp.773-780, **0.756**, **0.139**

13. **Bartha, C**; **Secu, CE**; **Secu, M**;
Non-isothermal crystallization kinetics growth of $LiYF_4$(Yb,Er) nanoparticles
CERAMICS INTERNATIONAL, (2016), **42**, pp.18732-18736, **2.758**, **0.465**

14. Batalu, D; **Aldica, G**; **Badica, P**;
$Ge_2C_6H_{10}O_7$- Added MgB_2 Superconductor Obtained by Ex-Situ Spark Plasma Sintering
IEEE TRANSACTIONS ON APPLIED SUPERCONDUCTIVITY, (2016), **26**, **1.092**, **0.229**

15. Batalu, D; Paun, A; Ferbinteanu, M; **Aldica, G**; **Vlaicu, AM**; **Teodorescu, VS**; **Badica, P**;
Thermal analysis of repa-germanium (Ge-132)
THERMOCHIMICA ACTA, (2016), **644**, pp.20-27, **1.938**, **0.533**

16. **Beregoi, M**; **Busuioc, C**; **Evanghelidis, A**; **Matei, E**; Iordache, F; Radu, M; Dinischiotu, A; **Enculescu, I**;
Electrochromic properties of polyaniline-coated fiber webs for tissue engineering applications
INTERNATIONAL JOURNAL OF PHARMACEUTICS, (2016), **510**, pp.465-473, **3.994**, **0.797**

17. **Besleaga, C**; **Abramiuc, LE**; **Stancu, V**; **Tomulescu, AG**; **Sima, M**; **Trinca, L**; **Plugaru, N**; **Pintilie, L**; Nemnes, GA; Iliescu, M; Svavarsson, HG; Manolescu, A; **Pintilie, I**;
Iodine Migration and Degradation of Perovskite Solar Cells Enhanced by Metallic Electrodes
JOURNAL OF PHYSICAL CHEMISTRY LETTERS, (2016), **7**, pp.5168-5175, **8.539**, **2.482**

18. **Besleaga, C**; **Stan, GE**; **Pintilie, I**; Barquinha, P; Fortunato, E; Martins, R;
Transparent field-effect transistors based on AlN-gate dielectric and IGZO-channel semiconductor
APPLIED SURFACE SCIENCE, (2016), **379**, pp.270-276, **3.15**, **0.574**

19. **Bibicu, I**; **Constantinescu, S**; **Tarabasanu-Mihaila, D**; **Grecu, MN**;
CEMS MEASUREMENTS ON LOW Fe-57 DOPED ANATASE NANOPARTICLES
ROMANIAN REPORTS IN PHYSICS, (2016), **68**, pp.1506-1512, **1.367**, **0.184**

20. **Birsan, A**; **Kuncser, V**;
First principle investigations of the structural, electronic and magnetic properties of predicted new zirconium based full-Heusler compounds, Zr(2)MnZ (Z=Al, Ga and In)
JOURNAL OF MAGNETISM AND MAGNETIC MATERIALS, (2016), **406**, pp.282-288, **2.357**, **0.47**

21. Bita, AI; **Stan, GE**; Niculescu, M; Ciuca, I; Vasile, E; Antoniac, I;
Adhesion evaluation of different bioceramic coatings on Mg-Ca alloys for biomedical applications
JOURNAL OF ADHESION SCIENCE AND TECHNOLOGY, (2016), **30**, pp.1968-1983, **0.863**, **0.26**

22. Bjelajac, A; Petrovic, R; Socol, G; Mihailescu, IN; **Enculescu, M**; Grurriezescu, V; Pavlovic, V; Janackovic, D;
CdS quantum dots sensitized TiO_2 nanotubes by matrix assisted pulsed laser evaporation method
CERAMICS INTERNATIONAL, (2016), **42**, pp.9011-9017, **2.758**, **0.465**

23. **Busuioc, C**; **Evanghelidis, A**; **Galatanu, A**; **Enculescu, I**;
Direct and contactless electrical control of temperature of paper and textile foldable substrates using electrospun metallic-web transparent electrodes
SCIENTIFIC REPORTS, (2016), **6**, 34584, **5.228**, **1.865**

24. Calenic, B; Greabu, M; Caruntu, C; Nicolescu, MI; Moraru, L; Surdu-Bob, CC; Badulescu, M; Anghel, A; **Logofatu, C**; Boda, D;
Oral keratinocyte stem cells behavior on diamond like carbon films
ROMANIAN BIOTECHNOLOGICAL LETTERS, (2016), **21**, pp.11914-11922, **0.381**, **0.087**

25. Catrangiu, AS; **Beregoi, M**; Cojocaru, A; Anicai, L; Cotarta, A; Visan, T;
ELECTROCHEMICAL DEPOSITION OF ZINC TELLURIDE THIN FILMS FROM ETHALINE IONIC LIQUID
CHALCOGENIDE LETTERS, (2016), **13**, pp.187-199, **0.676**, **0.155**

26. **Cernea, M**; Galizia, P; Ciuchi, I; **Aldica, G**; **Mihalache, V**; **Diamandescu, L**; Galassi, C;
$CoFe_2O_4$ magnetic ceramic derived from gel and densified by spark plasma sintering
JOURNAL OF ALLOYS AND COMPOUNDS, (2016), **656**, pp.854-862, **3.014**, **0.558**

27. **Cernea, M**; **Negrea, RF**; Ciuchi, IV; Baldisserri, C; Trusca, R; Galassi, C;
Dielectric characterization of $Ba_xSr_{1-x}Fe_{12}O_{19}$ (x=0.05-0.35) ceramics
CERAMICS INTERNATIONAL, (2016), **42**, pp.1050-1056, **2.758**, **0.465**

28. **Cernea, M**; Vasilescu, CA; **Secu, M**; **Aldica, G**; Surdu, A; **Ganea, P**;
Dielectric and photoluminescence properties of Nd and Ga codoped-$BaTiO_3$, prepared by sol-gel method
JOURNAL OF MATERIALS SCIENCE-MATERIALS IN ELECTRONICS, (2016), **27**, pp.11371-11378, **1.798**, **0.234**

29. **Ciobanu, CS**; **Popa, CL**; **Predoi, D**;
Cerium-doped hydroxyapatite nanoparticles synthesized by the co-precipitation method
JOURNAL OF THE SERBIAN CHEMICAL SOCIETY, (2016), **81**, pp.433-446, **0.97**, **0.207**

30. Cirstea, CD; **Tolea, F**; Leonat, L; Lungu, M; Cucos, A; Cirstea, V; Tsakiris, V;
Characterization of TiNi shape memory alloys obtained by spark plasma sintering process
JOURNAL OF OPTOELECTRONICS AND ADVANCED MATERIALS, (2016), **18**, pp.857-862, **0.383**, **0.078**

31. Constanda, S; Stan, MS; **Ciobanu, CS**; Motelica-Heino, M; Guegan, R; Lafdi, K; Dinischiotu, A; **Predoi, D**;
Carbon Nanotubes-Hydroxyapatite Nanocomposites for an Improved Osteoblast Cell Response
JOURNAL OF NANOMATERIALS, (2016), 3941501, **1.758**, **0.411**

32. Constantinescu, C; Vizireanu, S; Ion, V; **Aldica, G**; Stoica, SD; Lazea-Stoyanova, A; Alloncle, AP; Delaporte, P; Dinescu, G;
Laser-induced forward transfer of carbon nanowalls for soft electrodes fabrication
APPLIED SURFACE SCIENCE, (2016), **374**, pp.49-55, **3.15**, **0.574**

33. **Cotirlan, C**; **Ghita, RV**; **Negrila, CC**; **Logofatu, C**; **Frumosu, F**; **Lungu, GA**;
Aspects of native oxides etching on n-GaSb(100) surface
APPLIED SURFACE SCIENCE, (2016), **363**, pp.83-90, **3.15**, **0.574**

34. **Cotirlan-Simiontuc, C**; **Logofatu, C**; **Iordache, G**; Rizea, A; Ursu, DV;
FTDT investigations for fabrication of sub-wavelength metal wire-grid polarizes and quarter waveplate
JOURNAL OF OPTOELECTRONICS AND ADVANCED MATERIALS, (2016), **18**, pp.922-927, **0.383**, **0.078**

35. **Cotorobai, VF**; **Zgura, I**; Birzu, M; **Frunza, S**; **Frunza, L**;
Wicking behavior of fabrics described by simultaneous acquiring the images of the wet region and monitoring the liquid weight
COLLOIDS AND SURFACES A-PHYSICOCHEMICAL AND ENGINEERING ASPECTS, (2016), **497**, pp.146-153, **2.76**, **0.592**

36. Craciun, D; Socol, G; Le Caer, S; **Trinca, LM**; **Galca, AC**; Pantelica, D; Ionescu, P; Craciun, V;
Gamma irradiation effects on the properties of indium zinc oxide thin films
THIN SOLID FILMS, (2016), **614**, pp.2-6, **1.761**, **0.426**

37. Craciun, F; **Cernea, M**; Fruth, V; Zaharescu, M; Atkinson, I; Stanica, N; **Tanase, LC**; **Diamandescu, L**; **Iuga, A**; Galassi, C;
Novel multiferroic (Pb-1 (-) Nd-3x/2(x))(Ti-0.98 (-) yFeyMn0.02)O-3 ceramics with coexisting ferroelectricity and ferromagnetism at ambient temperature
MATERIALS & DESIGN, (2016), **110**, pp.693-704, **3.997**, **0.928**

38. Craciun, V; Craciun, D; Socol, G; Behdad, S; Boesl, B; Himcinschi, C; Makino, H; **Socol, M**; Simeone, D;
Investigations of Ar ion irradiation effects on nanocrystalline SiC thin films
APPLIED SURFACE SCIENCE, (2016), **374**, pp.339-345, **3.15**, **0.574**

39. **Crisan, O**; **Crisan, AD**; **Enculescu, M**;
Interfacial mechanisms of novel laser-irradiated L1(0)-based nanocomposite magnets
APPLIED PHYSICS A-MATERIALS SCIENCE & PROCESSING, (2016), **122**, 411, **1.444**, **0.39**

40. **Crisan, O**; **Crisan, AD**; **Mercioniu, I**; Nicula, R; **Vasiliu, F**;
Development and structural characterization of exchange-spring-like nanomagnets in (Fe,Co)-Pt bulk nanocrystalline alloys
JOURNAL OF MAGNETISM AND MAGNETIC MATERIALS, (2016), **401**, pp.711-715, **2.357**, **0.47**

41. **Crisan, O**; **Vasiliu, F**; **Palade, P**; **Mercioniu, I**;
Nitriding-induced texture, ordering and coercivity enhancement in FePtAgB nanocomposite magnets
JOURNAL OF MAGNETISM AND MAGNETIC MATERIALS, (2016), **401**, pp.965-968, **2.357**, **0.47**

42. del Pino, AP; Gyorgy, E; Cotet, C; Baia, L; **Logofatu, C**;
Laser-induced chemical transformation of free-standing graphene oxide membranes in liquid and gas ammonia environments
RSC ADVANCES, (2016), **6**, pp.50034-50042, **3.289**, **0.628**

43. Dinischiotu, A; Nica, CI; Stan, MS; Dumitrescu, I; **Diamandescu, L**;
New-developed TiO_2-based photocatalytic nano particles exhibit biocompatibility on MRC-5 lung fibroblasts after short-term exposure
JOURNAL OF BIOTECHNOLOGY, (2016), **231**, pp.S66-S67, **2.667**, **0.776**

44. Duinea, MI; **Costas, A**; **Baibarac, M**; Chirita, P;
Mechanism of the cathodic process coupled to the oxidation of iron monosulfide by dissolved oxygen
JOURNAL OF COLLOID AND INTERFACE SCIENCE, (2016), **467**, pp.51-59, **3.782**, **0.805**

45. Duta, L; **Stan, GE**; **Popa, AC**; **Husanu, MA**; Moga, S; **Socol, M**; **Zgura, I**; Miculescu, F; Urzica, I; Popescu, AC; Mihailescu, IN;
Thickness Influence on In Vitro Biocompatibility of Titanium Nitride Thin Films Synthesized by Pulsed Laser Deposition
MATERIALS, (2016), **9**, UNSP 38, **2.728**, **0.77**

46. Duta, L; **Stan, GE**; Stroescu, H; Gartner, M; Anastasescu, M; Fogarassy, Z; Mihailescu, N; Szekeres, A; Bakalova, S; Mihailescu, IN;
Multi-stage pulsed laser deposition of aluminum nitride at different temperatures
APPLIED SURFACE SCIENCE, (2016), **374**, pp.143-150, **3.15**, **0.574**

47. Duta, M; Simeonov, S; **Teodorescu, V**; Predoana, L; Preda, S; Nicolescu, M; Marin, A; Spasov, D; Gartner, M; Zaharescu, M; Szekeres, A;
Structural and electrical properties of Nb doped TiO_2 films prepared by the sol-gel layer-by-layer technique
MATERIALS RESEARCH BULLETIN, (2016), **74**, pp.15-20, **2.435**, **0.441**

48. **Enculescu, M**; **Matei, E**;
Influence of metallic and semiconducting nanostructures on the optical properties of dye-doped polymer thin films
THIN SOLID FILMS, (2016), **614**, pp.31-35, **1.761**, **0.426**

49. Endo, K; Arisawa, S; Kaneko, T; Tsuyumoto, I; Tateno, Y; **Badica, P**;
Characterization by X-Ray Diffraction of Non-c-Axis Epitaxial $Bi_2Sr_2CaCu_2O_8$+delta Thin Films
IEEE TRANSACTIONS ON APPLIED SUPERCONDUCTIVITY, (2016), **26**, 7500104, **1.092**, **0.229**

50. **Filip, LD**; **Pintilie, L**;
Metal-ferroelectric-metal current-voltage characteristics: A charge flow balance through interfaces approach
EUROPEAN PHYSICAL JOURNAL B, (2016), **89**, 44, **1.223**, **0.456**

51. Florea, NM; Lungu, A; Balanuca, B; **Badica, P**; Craciun, L; Damian, CM; **Enculescu, M**; Ionescu, C; Tihan, G; Iovu, H;
Effect of polyhedral oligomeric silsesquioxane nanoreinforcement on the properties of epoxy resin/monoglycidylether-terminated poly(dimethylsiloxane) nanocomposites
HIGH PERFORMANCE POLYMERS, (2016), **28**, pp.724-734, **1.045**, **0.198**

52. **Florica, C**; **Costas, A**; **Kuncser, A**; **Preda, N**; **Enculescu, I**;
High performance FETs based on ZnO nanowires synthesized by low cost methods
NANOTECHNOLOGY, (2016), **27**, 475303, **3.573**, **0.961**

53. **Florica, C**; **Preda, N**; **Costas, A**; **Zgura, I**; **Enculescu, I**;
ZnO nanowires grown directly on zinc foils by thermal oxidation in air: Wetting and water adhesion properties
MATERIALS LETTERS, (2016), **170**, pp.156-159, **2.437**, **0.453**

54. Fort, CI; Cotet, LC; **Vasiliu, F**; Marginean, P; Danciu, V; Popescu, IC;
Methanol oxidation at carbon paste electrodes modified with (Pt-Ru)/carbon aerogels nanocomposites
MATERIALS CHEMISTRY AND PHYSICS, (2016), **172**, pp.179-188, **2.101**, **0.479**

55. **Frunza, S**; **Frunza, L**; **Ganea, CP**; **Zgura, I**; Bras, AR; Schonhals, A;
Rod-like cyanophenyl probe molecules nanoconfined to oxide particles: Density of adsorbed surface species
EUROPEAN PHYSICAL JOURNAL PLUS, (2016), **131**, 27, **1.521**, **0.398**

56. **Ganea, CP**;
Modeling the charge transfer at the electrode-ionic liquid interface in dielectric spectroscopy measurements
JOURNAL OF MOLECULAR LIQUIDS, (2016), **221**, pp.422-433, **2.74**, **0.456**

57. **Ganea, CP**; Mindru, C; Vineticu, N; Alexandru, HV;
Dielectric spectroscopy in para-ferro transition of TGS
FERROELECTRICS, (2016), **493**, pp.165-171, **0.491**, **0.129**

58. **Gartner, P**; Halati, CM;
Laser transition in the thermodynamic limit for identical emitters in a cavity
PHYSICAL REVIEW A, (2016), **93**, 13817, **2.765**, **0.898**

59. Ghalem, A; Huitema, L; Crunteanu, A; Rammal, M; **Trupina, L**; **Nedelcu, L**; **Banciu, MG**; Dutheil, P; Constantinescu, C; Marchet, P; Dumas-Bouchiat, F; Champeaux, C;
Electrical transport properties and modelling of electrostrictive resonance phenomena in $Ba_2/3Sr_1/3TiO_3$ thin films
JOURNAL OF APPLIED PHYSICS, (2016), **120**, 184101, **2.101**, **0.637**

60. Ghalem, A; Rammal, M; Huitema, L; Crunteanu, A; Madrangeas, V; Dutheil, P; Dumas-Bouchiat, F; Marchet, P; Champeaux, C; **Trupina, L**; **Nedelcu, L**; **Banciu, MG**;
Ultra-High Tunability of Ba(2/3)Sr(1/3) TiO3-Based Capacitors Under Low Electric Fields
IEEE MICROWAVE AND WIRELESS COMPONENTS LETTERS, (2016), **26**, pp.504-506, **1.599**, **0.811**

61. Gheorghe, C; Lupei, A; Hau, S; Voicu, F; Gheorghe, L; **Vlaicu, AM**;
Compositional dependence of optical properties of Sm3+-doped Y3ScxAl5-xO12 polycrystalline ceramics
JOURNAL OF ALLOYS AND COMPOUNDS, (2016), **683**, pp.547-553, **3.014**, **0.558**

62. **Ghica, D**; **Vlaicu, ID**; **Stefan, M**; **Nistor, LC**; **Nistor, SV**;
On the agent role of Mn^{2+} in redirecting the synthesis of $Zn(OH)(_2)$ towards nano-ZnO with variable morphology
RSC ADVANCES, (2016), **6**, pp.106732-106741, **3.289**, **0.628**

63. **Greculeasa, SG**; **Palade, P**; **Schinteie, G**; **Lungu, GA**; Porosnicu, C; Jepu, I; Lungu, CP; **Kuncser, V**;
Be/W and W/Be bilayers deposited on Si substrates with hydrogenated Fe-Cr and Fe-Cr-Al interlayers for plasma facing components
JOURNAL OF NUCLEAR MATERIALS, (2016), **481**, pp.73-80, **2.199**, **0.592**

64. **Greculeasa, SG**; **Schinteie, G**; **Palade, P**; **Filoti, G**; **Ghita, IS**; **Kuncser, V**;
MAGNETIC AND MOSSBAUER SPECTROSCOPY STUDY OF Fe-Cr-Al THIN FILMS SPUTTERED ON Si SUBSTRATES
ROMANIAN REPORTS IN PHYSICS, (2016), **68**, pp.249-258, **1.367**, **0.184**

65. Groza, A; **Ciobanu, CS**; **Popa, CL**; **Iconaru, SL**; Chapon, P; Luculescu, C; Ganciu, M; **Predoi, D**;
Structural Properties and Antifungal Activity against Candida albicans Biofilm of Different Composite Layers Based on Ag/Zn Doped Hydroxyapatite-Polydimethylsiloxanes
POLYMERS, (2016), **8**, 131, **2.944**, **0.9**

66. Groza, A; Surmeian, A; Diplasu, C; **Negrila, C**; Mihalcea, B; Ganciu, M;
INFRARED AND X-RAY PHOTOELECTRON SPECTROSCOPY IN SURFACE CHARACTERIZATION OF POLYDIMETHYLSILOXANE THIN FILMS GENERATED ON METALLIC SUBSTRATES IN MULTIPOINTS TO PLANE CORONA DISCHARGES
ROMANIAN JOURNAL OF PHYSICS, (2016), **61**, pp.648-656, **1.398**, **0.173**

67. Gyorgy, E; del Pino, AP; Datcu, A; Duta, L; **Logofatu, C**; Iordache, I; Duta, A;
Titanium oxide - reduced graphene oxide - silver composite layers synthesized by laser technique: Wetting and electrical properties
CERAMICS INTERNATIONAL, (2016), **42**, pp.16191-16197, **2.758**, **0.465**

68. Huitema, L; **Cernea, M**; Crunteanu, A; **Trupina, L**; **Nedelcu, L**; **Banciu, MG**; Ghalem, A; Rammal, M; Madrangeas, V; Passerieux, D; Dutheil, P; Dumas-Bouchiat, F; Marchet, P; Champeaux, C;
Microwave dielectric properties of BNT-$BT_{0.08}$ thin films prepared by sol-gel technique
JOURNAL OF APPLIED PHYSICS, (2016), **119**, 144103, **2.101**, **0.637**

69. Huyen, PT; Krivec, M; Kocevar, M; **Bucur, IC**; Rizescu, C; Parvulescu, VI;
Hydrogenation of Condensed Aromatic Compounds over Mesoporous Bifunctional Catalysts Following a Diels-Alder Adduct Pathway
CHEMCATCHEM, (2016), **8**, pp.1146-1156, **4.724**, **1.212**

70. Iacob, N; **Schinteie, G**; **Bartha, C**; **Palade, P**; Vekas, L; **Kuncser, V**;
Effects of magnetic dipolar interactions on the specific time constant in superparamagnetic nanoparticle systems
JOURNAL OF PHYSICS D-APPLIED PHYSICS, (2016), **49**, 295001, **2.772**, **0.838**

71. Ianculescu, A; **Pintilie, I**; Vasilescu, CA; **Botea, M**; **Iuga, A**; Melinescu, A; Dragan, N; **Pintilie, L**;
Intrinsic pyroelectric properties of thick, coarse grained $Ba_{1-x}Sr_xTiO_3$ ceramics
CERAMICS INTERNATIONAL, (2016), **42**, pp.10338-10348, **2.758**, **0.465**

72. Ianculescu, AC; Vasilescu, CA; **Trupina, L**; Vasile, BS; Trusca, R; **Cernea, M**; **Pintilie, L**; Nicoara, A;
Characteristics of Ce^{3+}-doped barium titanate nanoshell tubes prepared by template-mediated colloidal chemistry
JOURNAL OF THE EUROPEAN CERAMIC SOCIETY, (2016), **36**, pp.1633-1642, **2.933**, **0.674**

73. **Iconaru, SL**; Guegan, R; **Popa, CL**; Motelica-Heino, M; **Ciobanu, CS**; **Predoi, D**;
Magnetite (Fe_3O_4) nanoparticles as adsorbents for As and Cu removal
APPLIED CLAY SCIENCE, (2016), **134**, pp.128-135, **2.586**, **0.589**

74. **Iconaru, SL**; Prodan, AM; Turculet, CS; Beuran, M; **Ghita, RV**; Costescu, A; Groza, A; Chifiriuc, MC; Chapon, P; Gaiaschi, S; Hristu, R; Stanciu, GA; Trusca, R; Ganciu, M; Raita, SM; Vineticu, N; **Ciobanu, CS**;
Enamel Based Composite Layers Deposited on Titanium Substrate with Antifungal Activity
JOURNAL OF SPECTROSCOPY, (2016), 4361051, **0.814**, **0.181**

75. **Iconaru, SL**; Turculet, C; Le Coustumer, P; Bleotu, C; Chifiriuc, MC; Lazar, V; Surugiu, A; Badea, M; Iordache, FM; Soare, M; Prodan, AM;
BIOLOGICAL STUDIES ON DEXTRIN COATED IRON OXIDE NANOPARTICLES
ROMANIAN REPORTS IN PHYSICS, (2016), **68**, pp.1536-1544, **1.367**, **0.184**

76. **Ivan, I**; **Sandu, V**; **Enculescu, M**; **Aldica, G**; **Ionescu, AM**;
Physical Properties of Polycrystalline $CuGeO_3$ Prepared by Field-assisted Sintering Technique
JOURNAL OF SUPERCONDUCTIVITY AND NOVEL MAGNETISM, (2016), **29**, pp.775-780, **1.1**, **0.182**

77. **Ionescu, AM**; **Aldica, G**; **Popa, S**; **Enculescu, M**; **Sandu, V**; **Pasuk, I**; **Kuncser, A**; **Miu, L**; **Badica, P**;
Spark plasma sintered MgB_2 co-added with c-BN and C-60
MATERIALS CHEMISTRY AND PHYSICS, (2016), **170**, pp.201-209, **2.101**, **0.479**

78. Ionita, MD; Vizireanu, S; Stoica, SD; Ionita, M; Pandele, AM; Cucu, A; Stamatin, I; **Nistor, LC**; Dinescu, G;
Functionalization of carbon nanowalls by plasma jet in liquid treatment
EUROPEAN PHYSICAL JOURNAL D, (2016), **70**, 31, **1.208**, **0.429**

79. **Ivan, I**; **Ionescu, AM**; Miu, D; Mele, P; **Miu, L**;
Vortex activation energy in the AC magnetic response of superconducting $YBa_2Cu_3O_7$ thin films with complex pinning structures
SUPERCONDUCTOR SCIENCE & TECHNOLOGY, (2016), **29**, 95013, **2.717**, **0.835**

80. Jin, JH; **Stoica, T**; Trellenkamp, S; Chen, Y; Anttu, N; Migunov, V; Kawabata, RMS; Buenconsejo, PJS; Lam, YM; Haas, F; Hardtdegen, H; Grutzmacher, D; Kardynal, BE;
Dense, Regular GaAs Nanowire Arrays by Catalyst-Free Vapor Phase Epitaxy for Light Harvesting
ACS APPLIED MATERIALS & INTERFACES, (2016), **8**, pp.22484-22492, **7.145**, **1.462**

81. Klimczyk, P; Cura, ME; **Vlaicu, AM**; **Mercioniu, I**; Wyzga, P; Jaworska, L; Hannula, SP;
Al_2O_3-cBN composites sintered by SPS and HPHT methods
JOURNAL OF THE EUROPEAN CERAMIC SOCIETY, (2016), **36**, pp.1783-1789, **2.933**, **0.674**

82. Knoll, L; **Teodorescu, V**; Minamisawa, RA;
Ultra-Thin Epitaxial Tungsten Carbide Schottky Contacts in 4H-SiC
IEEE ELECTRON DEVICE LETTERS, (2016), **37**, pp.1318-1320, **2.528**, **0.846**

83. Komur, B; Lohse, T; Can, HM; Khalilova, G; Gecimli, ZN; Aydogdu, MO; Kalkandelen, C; **Stan, GE**; Sahin, YM; Sengil, AZ; Suleymanoglu, M; Kuruca, SE; Oktar, FN; Salman, S; Ekren, N; Ficai, A; Gunduz, O;
Fabrication of naturel pumice/hydroxyapatite composite for biomedical engineering
BIOMEDICAL ENGINEERING ONLINE, (2016), **15**, 81, **1.382**, **0.496**

84. Larciprete, R; Colonna, S; Ronci, F; Flammini, R; Lacovig, P; **Apostol, N**; Politano, A; Feulner, P; Menzel, D; Lizzit, S;
Self-Assembly of Graphene Nanoblisters Sealed to a Bare Metal Surface
NANO LETTERS, (2016), **16**, pp.1808-1817, **13.779**, **4.869**

85. Lazanu, I; **Lazanu, S**;
Contribution of the electron-phonon interaction to Lindhard energy partition at low energy in Ge and Si detectors for astroparticle physics applications
ASTROPARTICLE PHYSICS, (2016), **75**, pp.44-54, **3.425**, **1.164**

86. **Lazanu, S**; Lazanu, I;
MODIFICATION OF LINDHARD ENERGY PARTITION FOR LOW ENERGY RECOILS IN GERMANIUM AND SILICON FOR DETECTORS DUE TO ELECTRON PHONON COUPLING
ROMANIAN REPORTS IN PHYSICS, (2016), **68**, pp.594-603, **1.367**, **0.184**

87. **Lazanu, S**; Lazanu, I;
MODEL OF ENERGY EXCHANGE THROUGH ELECTRON-PHONON COUPLING DURING TRANSIENT PHENOMENA IN MATERIALS FOR DETECTORS
ROMANIAN REPORTS IN PHYSICS, (2016), **68**, pp.1015-1023, **1.367**, **0.184**

88. **Lorinczi, A**; **Sava, F**; **Simandan, ID**; **Velea, A**; **Popescu, M**;
Photoexpansion in amorphous As_2S_3: A new explanation
JOURNAL OF NON-CRYSTALLINE SOLIDS, (2016), **447**, pp.123-125, **1.825**, **0.428**

89. **Maraloiu, VA**; Appaix, F; Broisat, A; Le Guellec, D; **Teodorescu, VS**; Ghezzi, C; van der Sanden, B; Blanchin, MG;
Multiscale investigation of USPIO nanoparticles in atherosclerotic plaques and their catabolism and storage in vivo
NANOMEDICINE-NANOTECHNOLOGY BIOLOGY AND MEDICINE, (2016), **12**, pp.191-200, **5.671**, **1.492**

90. **Matei, E**; **Costas, A**; **Florica, C**; **Enculescu, M**; **Pintilie, I**; **Pintilie, L**; **Enculescu, I**;
Electrical properties of templateless electrodeposited ZnO nanowires
MATERIALS SCIENCE IN SEMICONDUCTOR PROCESSING, (2016), **42**, pp.364-372, **2.264**, **0.354**

91. Mihailescu, IN; Bociaga, D; Socol, G; **Stan, GE**; Chifiriuc, MC; Bleotu, C; **Husanu, MA**; Popescu-Pelin, G; Duta, L; Luculescu, CR; Negut, I; Hapenciuc, C; **Besleaga, C**; **Zgura, I**; Miculescu, F;
Fabrication of antimicrobial silver-doped carbon structures by combinatorial pulsed laser deposition
INTERNATIONAL JOURNAL OF PHARMACEUTICS, (2016), **515**, pp.592-606, **3.994**, **0.797**

92. Mihailescu, N; **Stan, GE**; Duta, L; Chifiriuc, MC; Bleotu, C; Sopronyi, M; Luculescu, C; Oktar, FN; Mihailescu, IN;
Structural, compositional, mechanical characterization and biological assessment of bovine-derived hydroxyapatite coatings reinforced with MgF_2 or MgO for implants functionalization
MATERIALS SCIENCE & ENGINEERING C-MATERIALS FOR BIOLOGICAL APPLICATIONS, (2016), **59**, pp.863-874, **3.42**, **0.625**

93. **Mihalache, V**;
Thermal analysis of ball-milled Fe-14Cr-3W-0.4Ti-0.25Y(2)O(3) ferritic steel powder Evidence for contamination from the air
JOURNAL OF THERMAL ANALYSIS AND CALORIMETRY, (2016), **124**, pp.1179-1192, **1.781**, **0.247**

94. Minamisawa, RA; Mihaila, A; Farkas, I; **Teodorescu, VS**; Afanas'ev, VV; Hsu, CW; Janzen, E; Rahimo, M;
Characterization of a n+3C/n-4H SiC heterojunction diode
APPLIED PHYSICS LETTERS, (2016), **108**, 143502, **3.142**, **1.045**

95. Mitran, RA; Radulescu, MC; Buhalteanu, L; **Tanase, LC**; Dumitrescu, DG; Matei, C;
Formation of pure-phase W2C nanoparticles through carbothermal reduction in the presence of Pd(0) nanoparticles
JOURNAL OF ALLOYS AND COMPOUNDS, (2016), **682**, pp.679-685, **3.014**, **0.558**

96. Mitsa, V; Holomb, R; Marton, A; Veres, M; Toth, S; Himics, L; **Lorinczi, A**; **Popescu, M**;
Investigation of atmospheric corrosion by photon energy dependent luminescence and Raman spectroscopy in aged and freshly fractured g-,c-As_2S_3 with photosensitive realgar inclusions
JOURNAL OF NON-CRYSTALLINE SOLIDS, (2016), **453**, pp.23-27, **1.825**, **0.428**

97. **Miu, L**; **Ivan, I**; **Ionescu, AM**; Miu, D;
AC magnetic response of superconducting $YBa_2Cu_3O_7/PrBa_2Cu_3O_7$ superlattices
AIP ADVANCES, (2016), **6**, 65027, **1.444**, **0.48**

98. **Moldoveanu, V**; **Dinu, IV**; **Dragomir, R**; Tanatar, B;
Light-hole exciton mixing and dynamics in Mn-doped quantum dots
PHYSICAL REVIEW B, (2016), **93**, 165421, **3.718**, **1.229**

99. Mun, E; Weickert, F; Kim, J; Scott, BL; **Miclea, CF**; Movshovich, R; Wilcox, J; Manson, J; Zapf, VS;
Partially disordered antiferromagnetism and multiferroic behavior in a frustrated Ising system $CoCl_2$-$2SC(NH_2)(_2)$
PHYSICAL REVIEW B, (2016), **9**3, 104407, **3.718**, **1.229**

100. **Negrila, CC**; **Lazarescu, MF**; **Logofatu, C**; **Cotirlan, C**; **Ghita, RV**; **Frumosu, F**; **Trupina, L**;
XPS Analysis of AuGeNi/Cleaved GaAs(110) Interface
JOURNAL OF NANOMATERIALS, (2016), 7574526, **1.758**, **0.411**

101. Nica, IC; Stan, MS; Dinischiotu, A; Popa, M; Chifiriuc, MC; Lazar, V; Pircalabioru, GG; Bezirtzoglou, E; Iordache, OG; Varzaru, E; Dumitrescu, I; **Feder, M**; **Vasiliu, F**; **Mercioniu, I**; **Diamandescu, L**;
Innovative Self-Cleaning and Biocompatible Polyester Textiles Nano-Decorated with Fe-N-Doped Titanium Dioxide
NANOMATERIALS, (2016), **6**, 214, **2.69**, **0.687**

102. Nistor, M; **Mihut, L**; Millon, E; Cachoncinlle, C; Hebert, C; Perriere, J;
Tailored electric and optical properties of Nd doped ZnO: from transparent conducting oxide to photon down-shifting thin films
RSC ADVANCES, (2016), **6**, pp.41465-41472, **3.289**, **0.628**

103. **Nistor, SV**; **Stefan, M**; **Nistor, LC**; **Ghica, D**; **Vlaicu, ID**;
Distribution and interaction of Mn^{2+} ions incorporated in cubic ZnS quantum dots over a broad concentration range
JOURNAL OF ALLOYS AND COMPOUNDS, (2016), **662**, pp.193-199, **3.014**, **0.558**

104. **Nistor, SV**; **Stefan, M**; **Nistor, LC**; **Kuncser, V**; **Ghica, D**; **Vlaicu, ID**;
Aggregates of Mn^{2+} Ions in Mesoporous Self-Assembled Cubic ZnS:Mn Quantum Dots: Composition, Localization, Structure, and Magnetic Properties
JOURNAL OF PHYSICAL CHEMISTRY C, (2016), **120**, pp.14454-14466, **4.509**, **1.171**

105. Opris, C; Cojocaru, B; **Gheorghe, N**; Tudorache, M; Coman, SM; Parvulescu, VI; Duraki, B; Krumeich, F; van Bokhoven, JA;
Lignin fragmentation over magnetically recyclable composite $Co@Nb_2O_5@Fe_3O_4$ catalysts
JOURNAL OF CATALYSIS, (2016), **339**, pp.209-227, **7.354**, **1.587**

106. **Ostahie, B**; **Aldea, A**;
Phosphorene confined systems in magnetic field, quantum transport, and superradiance in the quasiflat band
PHYSICAL REVIEW B, (2016), **93**, 75408, **3.718**, **1.229**

107. **Ostahie, B**; **Nita, M**; **Aldea, A**;
Non-Hermitian approach of edge states and quantum transport in a magnetic field
PHYSICAL REVIEW B, (2016), **94**, 195431, **3.718**, **1.229**

108. Oumezzine, M; **Galca, AC**; **Pasuk, I**; **Chirila, CF**; **Leca, A**; **Kuncser, V**; **Tanase, LC**; **Kuncser, A**; **Ghica, C**; Oumezzine, M;
Structural, magnetic and magnetocaloric effects in epitaxial $La_{0.67}Ba_{0.33}Ti_{0.02}Mn_{0.98}O_3$ ferromagnetic thin films grown on 001-oriented $SrTiO_3$ substrates
DALTON TRANSACTIONS, (2016), **45**, pp.15034-15040, **4.177**, **0.8**

109. **Palade, C**; **Lepadatu, AM**; **Slav, A**; **Ciurea, ML**; **Lazanu, S**;
Correlation between strain and defects in Bi implanted Si
JOURNAL OF PHYSICS AND CHEMISTRY OF SOLIDS, (2016), **93**, pp.27-32, **2.048**, **0.416**

110. **Palade, P**; **Plapcianu, C**; **Mercioniu, I**; **Comanescu, CC**; **Schinteie, G**;
MOSSBAUER AND MAGNETIC INVESTIGATION OF IRON NITRIDE WITH MARTENSITE STRUCTURE SYNTHESISED FROM OXY-HYDROXIDE TYPE PRECURSOR
DIGEST JOURNAL OF NANOMATERIALS AND BIOSTRUCTURES, (2016), **11**, pp.53-63, **0.756**, **0.139**

111. Pana, A; Ilis, M; Staicu, T; **Pasuk, I**; Circu, V;
Columnar bis(pyridinium) ionic liquid crystals derived from 4-hydroxypyridine: synthesis, mesomorphism and emission properties
LIQUID CRYSTALS, (2016), **43**, pp.381-392, **2.244**, **0.281**

112. Pana, A; **Pasuk, I**; Micutz, M; Circu, V;
Nematic ionic liquid crystals based on pyridinium salts derived from 4-hydroxypyridine
CRYSTENGCOMM, (2016), **18**, pp.5066-5069, **3.849**, **0.67**

113. Pantelica, D; Ionescu, P; Petrascu, H; Dracea, MD; Statescu, M; **Matei, E**; **Rasoga, O**; Stancu, C; Marascu, V; Ion, V; Acsente, T; Dinescu, G;
Characterization of hydrogenated and deuterated silicon carbide films codeposited by magnetron sputtering
NUCLEAR INSTRUMENTS & METHODS IN PHYSICS RESEARCH SECTION B-BEAM INTERACTIONS WITH **MATERIALS AND ATOMS**, (2016), **371**, pp.322-326, **1.389**, **0.426**

114. Petrea, N; Petre, R; Epure, G; Somoghi, V; **Tanase, LC**; **Teodorescu, CM**; **Neatu, S**;
The combined action of methanolysis and heterogeneous photocatalysis in the decomposition of chemical warfare agents
CHEMICAL COMMUNICATIONS, (2016), **52**, pp.12956-12959, **6.567**, **1.538**

115. Plugaru, R; **Plugaru, N**;
Assessment of structural, optical and conduction properties of ZnO thin films in the presence of acceptor impurities
JOURNAL OF PHYSICS-CONDENSED MATTER, (2016), **28**, 224008, **2.209**, **0.857**

116. Politano, A; Cattelan, M; Boukhvalov, DW; Campi, D; Cupolillo, A; Agnoli, S; **Apostol, NG**; Lacovig, P; Lizzit, S; Farias, D; Chiarello, G; Granozzi, G; Larcipretev, R;
Unveiling the Mechanisms Leading to H-2 Production Promoted by Water Decomposition on Epitaxial Graphene at Room Temperature
ACS NANO, (2016), **10**, pp.4543-4549, **13.334**, **4.112**

117. **Polosan, S**; **Secu, M**; **Enculescu, M**;
STRUCTURAL AND MORPHOLOGICAL EVOLUTIONS INDUCED BY THE ANNEALING OF CaF_2 NANOCRYSTALLINE POWDERS BY USING Eu^{3+} ION PROBE LUMINESCENCE
DIGEST JOURNAL OF NANOMATERIALS AND BIOSTRUCTURES, (2016), **11**, pp.615-624, **0.756**, **0.139**

118. **Popa, AC**; **Stan, GE**; **Besleaga, C**; Ion, L; **Maraloiu, VA**; Tulyaganov, DU; Ferreira, JMF;
Submicrometer Hollow Bioglass Cones Deposited by Radio Frequency Magnetron Sputtering: Formation Mechanism, Properties, and Prospective Biomedical Applications
ACS APPLIED MATERIALS & INTERFACES, (2016), **8**, pp.4357-4367, **7.145**, **1.462**

119. **Popa, CL**; Albu, M; **Bartha, C**; Costescu, A; Luculescu, C; Trusca, R; Antohe, S;
STRUCTURAL CHARACTERIZATION AND OPTICAL PROPERTIES OF HYDROXYAPATITE/COLLAGEN MATRIX
ROMANIAN REPORTS IN PHYSICS, (2016), **68**, pp.1149-1158, **1.367**, **0.184**

120. **Popa, CL**; **Ciobanu, CS**;
SYNTHESIS AND CHARACTERIZATION OF FLUORESCENT HYDROXYAPATITE
ROMANIAN REPORTS IN PHYSICS, (2016), **68**, pp.1170-1177, **1.367**, **0.184**

121. **Popa, CL**; Deniaud, A; Michaud-Soret, I; Guegan, R; Motelica-Heino, M; **Predoi, D**;
Structural and Biological Assessment of Zinc Doped Hydroxyapatite Nanoparticles
JOURNAL OF NANOMATERIALS, (2016), 1062878, **1.758**, **0.411**

122. **Popa, CL**; Prodan, AM; **Ciobanu, CS**; **Predoi, D**;
The tolerability of dextran-coated iron oxide nanoparticles during in vivo observation of the rats
GENERAL PHYSIOLOGY AND BIOPHYSICS, (2016), **35**, pp.299-310, **0.892**, **0.268**

123. Popescu, C; Dorcioman, G; Bita, B; **Besleaga, C**; **Zgura, I**; Himcinschi, C; Popescu, AC;
Fabrication of periodical surface structures by picosecond laser irradiation of carbon thin films: transformation of amorphous carbon in nanographite
APPLIED SURFACE SCIENCE, (2016), **390**, pp.236-243, **3.15**, **0.574**

124. **Popescu, DG**;
Theoretical investigation of a Ge 2D photonic crystal by optical reflectivity correlated with band distributions
JOURNAL OF OPTOELECTRONICS AND ADVANCED MATERIALS, (2016), **18**, pp.769-774, **0.383**, **0.078**

125. **Popescu, M**; **Sava, F**; **Lorinczi, A**; **Velea, A**; **Simandan, ID**; **Galca, AC**; **Matei, E**; Socol, G; Gherendi, F; Savastru, D; Miclos, S;
Amorphous thin films in the gallium-chalcogen system
PHYSICA STATUS SOLIDI B-BASIC SOLID STATE PHYSICS, (2016), **253**, pp.1033-1037, **1.522**, **0.466**

126. Preda, L; Anastasescu, M; Dobrescu, G; **Negrila, C**; Lazarescu, V;
Role of the dithiolate backbone on the passivation of p-GaAs(111)B surface
JOURNAL OF ELECTROANALYTICAL CHEMISTRY, (2016), **771**, pp.56-63, **2.822**, **0.544**

127. **Predoi, D**; **Popa, CL**; Chapon, P; Groza, A; **Iconaru, SL**;
Evaluation of the Antimicrobial Activity of Different Antibiotics Enhanced with Silver-Doped Hydroxyapatite Thin Films
MATERIALS, (2016), **9**, 778, **2.728**, **0.77**

128. Rusen, E; Diacon, A; Mocanu, A; Gavrila, R; **Nistor, LC**; Dinescu, A;
CdSe (quantum dots)-graphene oxide system for thiophene polymerization: a new strategy, a new material
RSC ADVANCES, (2016), **6**, pp.25577-25583, **3.289**, **0.628**

129. Rusen, E; Diacon, A; Mocanu, A; **Nistor, LC**;
Novel facile method for obtaining CdSe/polyaniline/C-60 composite materials
SCIENTIFIC REPORTS, (2016), **6**, 32237, **5.228**, **1.865**

130. **Sandu, V**; **Aldica, G**; **Popa, S**; **Enculescu, M**; **Badica, P**;
Tellurium addition as a solution to improve compactness of ex-situ processed MgB_2-SiC superconducting tapes
SUPERCONDUCTOR SCIENCE & TECHNOLOGY, (2016), **29**, 65012, **2.717**, **0.835**

131. **Sandu, V**; Craciun, L; **Ionescu, AM**; **Aldica, G**; **Miu, L**; **Kuncser, A**;
Superconductivity in MgB_2 irradiated with energetic protons
PHYSICA C-SUPERCONDUCTIVITY AND ITS APPLICATIONS, (2016), **528**, pp.27-34, **0.835**, **0.23**

132. **Sandu, V**; Suo, HL; **Aldica, G**; **Ionescu, AM**; Suo, C; Liu, ZY;
Possible Enhancement of Spin Fluctuations by Ag addition to $SmFeAsO_{1-x}$ F ($_x$)
JOURNAL OF SUPERCONDUCTIVITY AND NOVEL MAGNETISM, (2016), **29**, pp.303-308, **1.1**, **0.182**

133. Scarisoreanu, ND; Craciun, F; Birjega, R; Ion, V; **Teodorescu, VS**; **Ghica, C**; **Negrea, R**; Dinescu, M;
Joining Chemical Pressure and Epitaxial Strain to Yield Y-doped $BiFeO_3$ Thin Films with High Dielectric Response
SCIENTIFIC REPORTS, (2016), **6**, 25535, **5.228**, **1.865**

134. **Secu, CE**; **Matei, E**;
SOL-GEL TEMPLATE ASSISTED SYNTHESIS AND UP-CONVERSION PROPERTIES OF (Yb-Er) DOPED SiO_2-$LiYF_4$ GLASS CERAMIC RODS
DIGEST JOURNAL OF NANOMATERIALS AND BIOSTRUCTURES, (2016),11, pp.489-494, **0.756**, **0.139**

135. **Secu, M**; **Secu, CE**;
Up-conversion luminescence of $BaCl_2:Er^{3+}$ nanocrystals embedded in oxychloride nano-glass ceramic
JOURNAL OF THE EUROPEAN CERAMIC SOCIETY, (2016), **36**, pp.1699-1703, **2.933**, **0.674**

136. **Secu, M**; **Secu, CE**; **Bartha, C**;
Crystallization and luminescence properties of a new Eu^{3+}-doped LaOCl nano-glass-ceramic
JOURNAL OF THE EUROPEAN CERAMIC SOCIETY, (2016), **36**, pp.203-207, **2.933**, **0.674**

137. Shakir, AJ; Florea, M; Culita, DC; Ionita, G; **Ghica, C**; Stavarache, C; Hanganu, A; Ionita, P;
Exploring porous nanosilica-TEMPO as heterogeneous aerobic oxidation catalyst: the influence of supported gold clusters
JOURNAL OF POROUS MATERIALS, (2016), **23**, pp.247-254, **1.385**, **0.279**

138. **Simion, CE**; **Stanoiu, A**; **Teodorescu, VS**; Rusti, CF; Piticescu, RM; Vasile, E; Vasile, E; Tudor, IA;
AMMONIA SENSING WITH 5 MOL% LANTHANUM DOPED BARIUM STRONTIUM TITANATE UNDER HUMID AIR BACKGROUND
REVUE ROUMAINE DE CHIMIE, (2016), **61**, pp.97-+, **0.25**, **0.065**

139. **Slav, A**; **Palade, C**; **Lepadatu, AM**; **Ciurea, ML**; **Teodorescu, VS**; **Lazanu, S**; **Maraloiu, AV**; **Logofatu, C**; Braic, M; Kiss, A;
How morphology determines the charge storage properties of Ge nanocrystals in HfO_2
SCRIPTA MATERIALIA, (2016), **113**, pp.135-138, **3.305**, **1.23**

140. **Socol, M**; **Preda, N**; **Rasoga, O**; **Breazu, C**; **Stavarache, I**; Stanculescu, F; Socol, G; Gherendi, F; Grumezescu, V; Popescu-Pelin, G; Girtan, M; Stefan, N;
Flexible heterostructures based on metal phthalocyanines thin films obtained by MAPLE
APPLIED SURFACE SCIENCE, (2016), **374**, pp.403-410, **3.15**, **0.574**

141. Stan, MS; Nica, IC; Dinischiotu, A; Varzaru, E; Iordache, OG; Dumitrescu, I; Popa, M; Chifiriuc, MC; Pircalabioru, GG; Lazar, V; Bezirtzoglou, E; **Feder, M**; **Diamandescu, L**;
Photocatalytic, Antimicrobial and Biocompatibility Features of Cotton Knit Coated with Fe-N-Doped Titanium Dioxide Nanoparticles
MATERIALS, (2016), **9**, 789, **2.728**, **0.77**

142. **Stanculescu, A**; Socol, G; Vacareanu, L; **Socol, M**; **Rasoga, O**; **Breazu, C**; Girtan, M; Stanculescu, F;
MAPLE preparation and characterization of mixed arylenevinylene based oligomers:C-60 layers
APPLIED SURFACE SCIENCE, (2016), **374**, pp.278-289, **3.15**, **0.574**

143. Stanculescu, F; **Stanculescu, A**;
Polycarbonate-Based Blends for Optical Non-linear Applications
NANOSCALE RESEARCH LETTERS, (2016), **11**, 87, **2.584**, **0.644**

144. Stange, D; von den Driesch, N; Rainko, D; Schulte-Braucks, C; Wirths, S; Mussler, G; Tiedemann, AT; **Stoica, T**; Hartmann, JM; Ikonic, Z; Mantl, S; Grutzmacher, D; Buca, D;
Study of GeSn based heterostructures: towards optimized group IV MQW LEDs
OPTICS EXPRESS, (2016), **24**, pp.1358-1367, **3.148**, **0.967**

145. Stange, D; Wirths, S; Geiger, R; Schulte-Braucks, C; Marzban, B; von den Driesch, N; Mussler, G; Zabel, T; **Stoica, T**; Hartmann, JM; Mantl, S; Ikonic, Z; Gruetzmacher, D; Sigg, H; Witzens, J; Buca, D;
Optically Pumped GeSn Microdisk Lasers on Si
ACS PHOTONICS, (2016), **3**, pp.1279-1285, **5.404**, **2.196**

146. **Stanoiu, A**; Somacescu, S; Calderon-Moreno, JM; **Teodorescu, VS**; **Florea, OG**; Sackmann, A; **Simion, CE**;
Low level NO_2 detection under humid background and associated sensing mechanism for mesoporous SnO_2
SENSORS AND ACTUATORS B-CHEMICAL, (2016), **231**, pp.166-174, **4.758**, **0.773**

147. **Stavarache, I**; **Maraloiu, VA**; Prepelita, P; **Iordache, G**;
Nanostructured germanium deposited on heated substrates with enhanced photoelectric properties
BEILSTEIN JOURNAL OF NANOTECHNOLOGY, (2016), **7**, pp.1492-1500, **2.778**, **0.789**

148. **Stoica, T**; Stoica, M; Duchamp, M; Tiedemann, A; Mantl, S; Grutzmacher, D; Buca, D; Kardynal, BE;
Vapor transport growth of MoS_2 nucleated on SiO_2 patterns and graphene flakes
NANO RESEARCH, (2016), **9**, pp.3504-3514, **8.893**, **2.235**

149. Sych, O; Gunduz, O; Pinchuk, N; **Stan, GE**; Oktar, FN;
Tissue Engineering Scaffolds from La_2O_3 - Hydroxyapatite\Boron Glass Composites
JOURNAL OF THE AUSTRALIAN CERAMIC SOCIETY, (2016), **52**, pp.103-110, **0.96**, **0.142**

150. Tamion, A; Hillenkamp, M; Hillion, A; **Maraloiu, VA**; **Vlaicu, ID**; **Stefan, M**; **Ghica, D**; Rositi, H; Chauveau, F; Blanchin, MG; Wiart, M; Dupuis, V;
Ferritin surplus in mouse spleen 14 months after intravenous injection of iron oxide nanoparticles at clinical dose
NANO RESEARCH, (2016), **9**, pp.2398-2410, **8.893**, **2.235**

151. **Tanase, LC**; **Apostol, NG**; **Abramiuc, LE**; **Tache, CA**; **Hrib, L**; **Trupina, L**; **Pintilie, L**; **Teodorescu, CM**;
Ferroelectric triggering of carbon monoxide adsorption on lead zirco-titanate (001) surfaces
SCIENTIFIC REPORTS, (2016), **6**, 35301, **5.228**, **1.865**

152. **Tanase, LC**; **Bocirnea, AE**; Serban, AB; **Abramiuc, LE**; **Bucur, IC**; **Lungu, GA**; **Costescu, RM**; **Teodorescu, CM**;
Growth mechanisms and band bending in Cu and Pt on Ge(001) investigated by LEED and photoelectron spectroscopy
SURFACE SCIENCE, (2016), **653**, pp.97-106, **1.931**, **0.534**

153. **Teodorescu, VS**; **Maraloiu, AV**; **Negrea, RF**; **Ghica, D**; Scarisoreanu, ND; Dinescu, M; Gartner, M; Blanchin, MG;
High atomic diffusivity during pulsed laser irradiation of TiON quasi-amorphous films
APPLIED SURFACE SCIENCE, (2016), **374**, pp.248-251, **3.15**, **0.574**

154. **Tolea, M**; **Nita, M**;
Ground state spin and excitation energies in half-filled Lieb lattices
PHYSICAL REVIEW B, (2016), **94**, 165103, **3.718**, **1.229**

155. Trandafir, MM; Pop, L; Hadade, ND; Florea, M; Neatu, F; **Teodorescu, CM**; Duraki, B; van Bokhoven, JA; Grosu, I; Parvulescu, VI; Garcia, H;
An adamantane-based COF: stability, adsorption capability, and behaviour as a catalyst and support for Pd and Au for the hydrogenation of nitrostyrene
Catalysis Science & Technology, (2016), **6**, pp.8344-8354, **5.287**, **1.16**

156. **Trinca, LM**; **Galca, AC**; **Aldica, G**; **Radu, R**; **Mercioniu, I**; **Pintilie, L**;
On the growth of conductive aluminum doped zinc oxide on 001 strontium titanate single crystals
APPLIED SURFACE SCIENCE, (2016), **364**, pp.365-370, **3.15**, **0.574**

157. Ungureanu, BS; **Teodorescu, CM**; Saftoiu, A;
Magnetic Nanoparticles for Hepatocellular Carcinoma Diagnosis and Therapy
JOURNAL OF GASTROINTESTINAL AND LIVER DISEASES, (2016), **25**, pp.375-383, **1.891**, **0.585**

158. Ungureanu, C; Dumitriu, C; Popescu, S; **Enculescu, M**; Tofan, V; **Popescu, M**; Pirvu, C;
Enhancing antimicrobial activity of TiO_2/Ti by torularhodin bioinspired surface modification
BIOELECTROCHEMISTRY, (2016), **107**, pp.14-24, **3.556**, **0.79**

159. **Valeanu, M**; **Sofronie, M**; **Galca, AC**; **Tolea, F**; Elisa, M; Sava, B; Boroica, L; **Kuncser, V**;
The relationship between magnetism and magneto-optical effects in rare earth doped aluminophosphate glasses
JOURNAL OF PHYSICS D-APPLIED PHYSICS, (2016), **49**, 75001, **2.772**, **0.838**

160. Vasilache, D; Cismaru, A; Dragoman, M; **Stavarache, I**; **Palade, C**; **Lepadatu, AM**; **Ciurea, ML**;
Non-volatile memory devices based on Ge nanocrystals
PHYSICA STATUS SOLIDI A-APPLICATIONS AND MATERIALS SCIENCE, (2016), **213**, pp.255-259, **1.648**, **0.404**

161. Vasylkiv, O; Demirskyi, D; **Badica, P**; Nishimura, T; Tok, AIY; Sakka, Y; Borodianska, H;
Room and high temperature flexural failure of spark plasma sintered boron carbide
CERAMICS INTERNATIONAL, (2016), **42**, pp.7001-7013, **2.758**, **0.465**

162. Vasylkiv, O; Demirskyi, D; Borodianska, H; Sakka, Y; **Badica, P**;
High temperature flexural strength in monolithic boron carbide ceramic obtained from two different raw powders by spark plasma sintering
JOURNAL OF THE CERAMIC SOCIETY OF JAPAN, (2016), **124**, pp.587-592, **0.828**, **0.183**

163. Visan, A; **Stan, GE**; Ristoscu, C; Popescu-Pelin, G; Sopronyi, M; **Besleaga, C**; Luculescu, C; Chifiriuc, MC; Hussien, MD; Marsan, O; Kergourlay, E; Grossin, D; Brouillet, F; Mihailescu, IN;
Combinatorial MAPLE deposition of antimicrobial orthopedic maps fabricated from chitosan and biomimetic apatite powders
INTERNATIONAL JOURNAL OF PHARMACEUTICS, (2016), **511**, pp.505-515, **3.994**, **0.797**

164. **Zgura, I**; **Frunza, S**; **Frunza, L**; **Enculescu, M**; **Florica, C**; **Cotorobai, VF**; **Ganea, CP**;
POLYESTER FABRICS COVERED WITH AMORPHOUS TITANIUM DIOXIDE LAYERS: COMBINING WETTABILITY MEASUREMENTS AND PHOTOINDUCED HYDROPHILICITY TO ASSESS THEIR SURFACE PROPERTIES
ROMANIAN REPORTS IN PHYSICS, (2016), **68**, pp.259-269, **1.367**, **0.184**

Articles in non-ISI Journals or Conference Proceedings

01. Mihailescu, N; **Stan, GE**; Ristoscu, C; Sopronyi, M; Mihailescu, IN
Bioactive glass thin films synthesized by advanced pulsed laser techniques
JOURNAL OF PHYSICS–CONFERENCE SERIES, (2016), **764**, 012020. DOI: 10.1088/1742-6596/764/1/012020.

02. Antonova, K; Szekeres, A, Duta L, **Stan, GE**; Mihailescu, N; Mihailescu, IN
Orientation of the nanocrystallites in AlN thin film determined by FTIR spectroscopy
JOURNAL OF PHYSICS–CONFERENCE SERIES, (2016), **682**, 012024. DOI: 10.1088/1742-6596/682/1/012024.

03. **Palade C**, **Slav A**, **Lepadatu AM**, **Maraloiu AV**, **Lazanu S**, **Logofatu C**, **Teodorescu VS**, **Ciurea ML**
Non-volatile memory structures with Ge NCs-HfO_2 intermediate layer
CAS 2016 Proceedings IEEE (2016 International Semiconductor Conference, October 10-12, Sinaia, Romania), pages 163–166, IEEE, New York (2016)

04. Dumitrescu I, Iordache OG, **Diamandescu L** and Popa M
Photocatalytic Efficiency and Antifungal Effects of Cotton Treated with TiO_2 Nanoparticles
Journal of Fashion Technology & Textile Engineering (2016) S2, pp 1-8.

05. **Maraloiu VA**, Appaix F, Broisat A, LeGuellec D, **Teodorescu VS**, Ghezzi C, van der Sanden B, Blanchin M-G
Multiscale investigation of USPIO nanoparticles in atherosclerotic plaques amd their catabolism and storage in vivo
Proceedings European Microscopy Congress- EMC2016, ed:Wiley 2016 Vol.2.1, Materials Science, pp.147-148

06. **Palade C**, **Slav A**, **Lepadatu A-M**, **Maraloiu AV**, **Lazanu S**, **Logofatu C**, **Teodorescu VS**, **Ciurea ML**
Non-volatile memory structures with GeNCs-HfO_2 intermediate layer
Proceedings CAS 2016, pp 163-166

07. **Popescu T**, Cremer L, Tudor M, Lupu A-R,
ROS-mediated Cytotoxicity and Macrophage Activation Induced by TiO_2 Nanoparticles with Different in vitro Non-Cellular Photocatalytic Activities
South-East European Journal of Immunology, 2016, 1-8

08. **Simion CE**, **Stanoiu A**, **Teodorescu VS**, Rusti CF, Piticescu RM, Vasile E, Tudor IA
Ammonia sensing with 5 mol% lanthanum doped barium strontium titanate under humid air background
Revue Roumaine de Chimie 61, 97-103 (2016)

09. Sorescu M, **Diamandescu L**, DiGnazio J, Xu T
Europium Oxide-Hematite Magnetic Ceramic Nanoparticles
MRS ADVANCES, Volume 1, Issue 3 (Nanomaterials and Synthesis) 2016, pp. 215-220.

10. **Teodorescu VS**, **Ghica C**, **Maraloiu AV**, **Kuncser AC**, **Lepadatu AM**, **Stavarache I**, **Ciurea ML**, Scarisoreanu ND, Dinescu M
Fast atomic diffusion in amorphous films induced by laser pulse annealing
Proceedings CAS 2016, pp 155-158.

11. **Teodorescu VS**, **Maraloiu AV**, **Kuncser A**, **Ghica C**, **Ciurea ML**, **Lepadatu A-M**, **Stavarache I**, Scarisoreanu DN, Dinescu M, Blanchin M-G
XTEM observations revealing high diffusivity and Ge segregation in UV laser pulse annealed SiGeO and GeTiO amorphous films
Proceedings European Microscopy Congress- EMC2016, ed:Wiley 2016 Vol.2.1, Materials Science, pp.155-156

12. **Teodorescu VS**, **Nistor LC**, Preda S, Zaharescu M, Blanchin M-G
Details on the TiO_2 nanotubes wall structure revealed by HRETM
Proceedings European Microscopy Congress- EMC2016, ed:Wiley 2016 Vol.2.1, Materials Science, pp.472-473

13. **Vasiliu F**
Public politics in nowadays Romanian research
Revue of politics of science and scientometry 5(2) (2016) 115 - 119

14. E.I. Ionete, M. Vijulie, A. Soare, A. Rizoiu, B. Monea, I. Spiridon, L. Stefan, I. Ana-Maria, I. Stamatin, **A. Leca,** A. Stanciu
Cryogenic temperature nanosensor
Refrigeration Science and Technology 22-25 (2016) 149-156

15. D. Batalu, A. Semenescu, M. I. Mates, D. O. Negoita, L. V. Purcarea, **P. Badica**,
Computer assisted design and finite element analysis of contact lenses
Romanian Journal of Ophtalmology 60 (2016) 132-137

16. A. Semenescu, F. Radu-Ionita, M. I. Mates, **P. Badica**, D. Batalu, D. O Negoita, L. V. Purcarea
Finite element analysis of a medical implant
Romanian Journal of Ophtalmology 60 (2016) 116-119

17. A. Semenescu, F. Radu-Ionita, M. I. Mates, **P. Badica**, D. Batalu,
Finite element analysis of modified short hip endoprosthesis
Romanian J. Military Medicine, CXIX (2016) 27-32

18. **F. Tolea, M. Sofronie, A. D. Crisan, B. Popescu, M. Tolea, M. Valeanu**,
Effect of thermal treatments in Ni-Fe-Ga with Co substitutions and Ni-Mn-Ga melt spun ribbons
Procedia Structural Integrity 2 (2016) 1473 – 1480

19. **M. Sofronie, F. Tolea, A.D. Crisan, B. Popescu, M. Valeanu**
Magnetoelastic properties in polycrystalline ferromagnetic shape memory Heusler alloys
Procedia Structural Integrity 2 (2016) 1530-1537

CONTRIBUTED PRESENTATIONS

01. **Aldica Gh V, Burdusel M, Pasuk I, Badica P**
Controlled processing of MgB_2 superconductor using spark plasma sintering
8th International Conference on Materials Science and Condensed Matter Physics (MSCPM), Chisinau, Moldavia
11-14.09.2016 - Poster

02. **Apostol NG**
Chemistry of carbon and carbon monoxide on $Pb(Zr,Ti)O_3(001)$ surfaces
International Workshop of Materials Physics, Măgurele, Romania
23-25.05.2016 - Oral presentation

03. **Banciu MG, Nedelcu L, Trupina L, Pasuk I, Chirila C, Hrib L, Trinca LM**
Terahertz time-domain spectrometric investigations on barium strontium titanate films
Electroceramics XV, Limoges, France
27-29.06.2016 - Oral presentation

04. **Banciu MG, Nedelcu L**
Terahertz propertires of BST bulk and film samples
9th International Conference on Broadband Dielectric Spectroscopy and its Applications- BDS 2016, Pisa, Italy
11-16.09.2016 - Poster

05. Batalu D, Nakamura T, **Aldica G, Badica P**
A comparative study of Ge-based organometallics additions to MgB_2
1st Asian ICMC and CSSJ 50th Anniversary Conference, Kanazawa, Japan
07-10.11.2016 - Poster

06. Batalu D, Nastase F, Militaru M, Gherghiceanu M, **Badica P**
In vivo assessment of TiNi coated with oxide and polymer films
Science and Applications of Thin Films, Conference & Exhibition (SATF 2016), Cesme, Turkey
19-23.09.2016 - Oral presentation

07. Becherescu N, Mihailescu IN, Socol G, Luculescu C, Tiron V, Stan GE, Udrea M
Comparison between HiPIMS and PLD Deposition of ZnO and TiO_2 thin films
10th International Conference on Photoexcited Processes and Applications (ICPEPA-10), Brasov, Romania
29.08–02.09.2016 - Poster

08. Berger K, Batalu D, **Aldica G, Badica P**
Trapped Magnetic Field Over 5 T in Doped Bulk MgB_2 Obtained by ex-situ Spark Plasma Sintering
5th International Conference on Superconductivity and Magnetism (ICSM 2016), Fethiye, Turkey
24-30.04.2016 - Poster

09. **Besleaga C, Stan GE, Radu R, Trinca LM, Galca AC, Pintilie I**
Transparent Field Effect Transistors based on IGZO and AlN
The 8th International Conference on Materials Science and Condensed Matter Physics, Chisinau, Moldavia
12–16.09.2016 - Oral presentation

10. **Besleaga C, Stan GE, Radu R, Trinca LM, Galca AC, Pintilie I**
Annealing influence on amorphous IGZO and AlN based TFTs
The 8th International Conference on Materials Science and Condensed Matter Physics, Chisinau, Moldavia
12–16.09.2016 - Poster

11. **Birzu M, Cotorobai VF, Frunza S, Zgura I, Ganea CP, Frunza L**
Using dye solutions for studying the wicking in monocomponent textile fabrics
International Conference of Physical Chemistry ROMPHYSCHEM 16, Galati, Romania
21-24.09.2016 - Poster

12. **Birzu M, Cotorobai F, Frunza S, Ganea CP, Diamandescu L, Zgura I, Frunza L**
Complex characterization of the wool fabrics deposited by ZnO nanoparticles
A XXXIV-a Conferinta Nationala de Chimie, Calimanesti-Caciulata, Romania
04-07.10.2016 - Poster

13. **Bocirnea A, Costescu R, Lungu A, Pasuk I, Macovei D, Teodorescu C**
Structural and magnetic properties of Ni nanofilms grown by molecular beam epitaxy on heated Ge(001) substrates
11th International Conference on Physics of Advanced Materials (ICPAM-11), Cluj-Napoca, Romania
08–14.09.2016 - Oral presentation

14. **Bocirnea AE, Costescu MR, Tanase LC, Apostol NG, Teodorescu CM**
Growth mechanisms and band bending effects in Ni on Ge(001) investigated by XPS and LEED
11th International Conference on Physics of Advanced Materials (ICPAM-11), Cluj-Napoca, Romania
08–14.09.2016 - Oral presentation

15. **Boni AG, Chirila C, Hrib L, Negrea R, Pasuk I, Ghica C, Filip L, Pintilie I, Pintilie L**
The influence of the interlayer type on ferroelectric/dielectric characteristics of multilayered structures
ELECTROCERAMICS XV, Limoges, France
27-29.06.2016 - Oral presentation

16. **Breazu C, Socol M, Preda N, Stanculescu A**, Stanculescu F, Gartan M, Socol G, **Rasoga O**
Effect of nano-patterning on the properties of the organic heterostructures prepared on Si substrate
EMRS Spring Meeting, Lille, France
02–06.05.2016 - Poster

17. **Breazu C, Socol M, Preda N**, Mallet R, **Stanculescu A**, Stanculescu F, Girtan M, **Rasoga O**
On the properties of organic heterostructures prepared on nano-patterned electrode
ICPAM, Cluj, Romania
08-11.09.2016. Poster.

18. **Breazu C, Rasoga O, Socol M**, Stanculescu F, Socol G, Grumezescu V, **Stanculescu A**
Effect of carbon allotropes thin films on beta-amyloid aggregation
EMRS Spring meeting, Lille, France
02–06.05.2016 - Poster

19. **Bucur C, Abramiuc L, Lungu A, Tanase L, Tache C, Teodorescu C**
Band bending at Pt/PZT interfaces investigated by XPS spectroscopy
European Conference on Surface Science (ECOSS 32), Grenoble, France
28.08–02.09.2016 - Oral presentation

20. Capat C, **Frunza L**, Olaru EA, Papa F, Crini G, Euvrard E, Negrila C, Munteanu C, Bradu C
Pd-Cu catalysts supported on anion exchange resins for the selective reduction of nitrate from water
The 11th International Symposium of the Romanian Catalysis Society, Timisoara, Romania
06-08.06.2016 - Poster

21. **Cernea M, Nedelcu L, Trupina L, Banciu MG**, Huitema L., Crunteanu A, Ghalem A, Rammal M, Madrangeas V, Passerieux D, Dutheil P, Dumas-Bouchiat F, Marchet P, Champeaux C
BNT-$BT_{0.08}$ thin films for electrically-controlled microwave devices
Electroceramics XV, Limoges, France
27-29.06.2016 - Poster

22. **Ciobotaru C. C., Polosan S.**
Energy transfer in a thin film of CBP polymer doped with IrQ$(ppy)_2$ phosphorescent molecules
IBWAP 2016, Constanta, Romania
07-09.07.2016 - Oral presentation

23. **Cotirlan-Simioniuc C, Logofatu C, Negrila CC, Manea AS**
Characterization of plasmonic metasurfaces for optical components able to manipulate the light beyond the fundamental diffraction limit
The 16th International Balkan Conference on Applied Physics (IBWAP 2016), Constanța, Romania
07-09.07.2016 - Poster

24. Craciun D, Socol G, Behdad S, Boesl B, Lambers E, Pantelica D, Ionescu P, Vasile B, Makino H, T**rinca LM, Galca AC**, Simeone D, Craciun V
Radiation effects in nanostructured thin films
11th International Conference on Physics of Advanced Materials (ICPAM), Cluj-Napoca, Romania
08-14.09.2016 - Oral presentation

25. **Crisan A, Crisan O, Stanciu A, Kuncser A, Filoti G, Kuncser V, G. Schinteie**
Magnetic behavior and interfacial coupling in transition metal based multilayers with soft and hard magnetic properties
The XXth International Conference on Solid Compounds of Transition Elements, Zaragoza, Spain
11-15.04.2016 - Poster

26. **Crisan A, Ivan I, Ionescu AM, Miu L**, Dang VS, Mele P, Mosquira J
High critical current density and pinning potential in YBCO films with sysnergetic pinning centres
Int. conf. on Nano confined superconductors and their applications, Garmish-Partenkirchen, Germany
03-07.09.2016 - Poster

27. **Crisan A**, Tanaka Y
Old experiments in multicomponent superconductors
11th Int. Conf. on New Theories, Discoveries, Applications of Superconductors and Related Materials, Bled, Slovenia
11-16.09. 2016 - Oral presentation

28. **Crisan A, Ivan I, Ionescu AM, Miu L**, Dang VS, Mele P, Mosqueira J
High critical current density and pinning potential in YBCO films with synergetic pinning centres, International Superconductivity Symposium (ISS29), Tokyo, Japan
13-15.12.2016 - Oral presentation

29. **Crisan AD**
Mn-induced spin reorientation mechanism in L10-based nanocomposite magnets
Global Nanotechnology Congress, Nanotech, Dubai, United Arab Emirates
21-23.04.2016 - Poster

30. **Crisan O**
Mechanisms of spin reversal induced by Mn in L10-based melt spun ribbons,
7th International Conference Magnetism and Metallurgy WMM '16, Roma, Italy
12-16.06.2016 - Oral presentation

31. **Crisan O**
Texturing, coercivity enhancement and RKKY-type interlayer exchange coupling in FePt-based nanocomposite magnets
13th International Conference on Nanostructured Materials NANO2016, Quebec City, Canada
07-13.08.2016 - Oral presentation

32. **Crisan O**
Nanoindentation studies of advanced hard coatings of MAX ternary phases obtained by ion-assisted deposition
15th European Mechanics of Materials Conference EMMC15, Bruxelles, Belgium
04-09.09.2016 - Poster

33. Nemnes GA, Nicolaev A, Mitran TL, **Plugaru N**, Manolescu A, Antohe S
Band alignment in perovskite solar cells with Cu_2O as hole transport material
E-MRS 2016 Fall Meeting, Symposium-L "Carbon and materials for energy applications", Warsaw, Poland
19-22.09.2016 - Oral presentation

34. **Diculescu V.C.,** Jesus C.S.H., Popa O.M., Enache T.A.
Electrochemical sensing of enzymes catalytic activities for screening compounds with potential medical applications
XI Symposium of the Romanian Catalysis Society, Timisoara, Romania
06-08.6.2016 - Oral presentation

35. **Diculescu V.C.**, Oliveira-Brett A.M.
In situ electrochemical evaluation of DNA interaction with the anticancer drug danusertib
XIII Encuentro de Química Analítica, Valdivia, Chile
18-21.10.2016 - Oral presentation

36. Dinischiotu A, Nica CI, Stan MS, Dumitrescu I, **Diamandescu L**
New-developed TiO_2-based photocatalytic nano particles exhibit biocompatibility on MRC-5 lung fibroblasts after short-termexposure
European Biotechnology Congress, Riga, Lithuania
05–07.05.2016 - Poster

37. **Dogaru D, Besleaga C, Stancu V, Tomulescu AG, Sima M, Pintilie L, Pintilie I**
Hybrid halide perovskite based solar cells
11th International Conference on Physics of Advanced Materials (ICPAM), Cluj-Napoca, Romania
08-14.09.2016 - Poster

38. Dorcioman G, Craciun D, Fufa O, Socol G, Ticos C, **Trinca LM, Socol M, Galca AC**, Swart H, Martin C, Craciun V
Investigations of radiation effects in amorphous and transparent indium zinc oxide films
11th International Conference on Physics of Advanced Materials (ICPAM), Cluj-Napoca, Romania
08-14.09.2016 - Poster

39. **Dragomir R**
Selective exchange effects in single-Mn doped quantum dots
International Workshop of Materials Physics, Magurele, Romania
23-25.05.2016 - Oral presentation

40. Dumitrescu I, Varzaru E, Mitran CE, Iordache OG, Pircalabioru G, **Diamandescu L**, Trasnea V
Influenta TiO_2 –Fe(1%)-N +2% GO asupra proprietatilor tricoturilor de bumbac,
9th Forum for Innovation Bucharest, TIB Romexpo, Bucharest, Romania
13-15.10.2016 - Poster

41. Duta L, **Stan GE, Popa AC**, Popescu AC
Functionalization of ultra-high molecular weight polyethylene acetabular cups with bioactive glass coatings synthesized by pulsed laser deposition
EMRS spring meeting, Lille, France
02–06.05.2016. Poster

42. Duta L, **Stan GE**, Grumezescu V, Popescu C
Comparative study between biological and synthetic hydroxyapatite thin films obtained by Pulsed Laser Deposition for a new generation of implants
EMRS spring meeting, Lille, France
02–06.05.2016 - Poster

43. Duta L, **Stan GE**, Popescu-Pelin G, Oktar FN
Highly adherent biological hydroxyapatite thin films reinforced with various oxides and metals for implantology applications
EMRS spring meeting, Lille, France
02–06.05.2016 - Poster

44. Duta L, **Stan GE, Popa AC**, Popescu AC
The influence of thickness upon the biocompatibility of Titanium Nitride thin films synthesized by pulsed laser deposition
EMRS spring meeting, Lille, France
02–06.05.2016 - Poster

45. Duta L, Lungu J, **Stan GE**, Popescu AC, Popescu-Pelin G, Ristoscu C, Oktar FN, Mihailescu IN
Pulsed Laser Deposition of simple and reinforced biological Hydroxyapatites for medical applications
16th International Balkan Workshop on Applied Physics and Materials Science, Constanta, Romania
07–09.07.2016 - Poster

46. Duta L, Popescu AC, **Stan GE**, Popescu-Pelin G, Mihailescu IN, Florian PE, Sima LE, Roseanu A, Oktar FN
In vitro assessment of reinforced biological hydroxyapatite thin films for implantology applications
10th International Conference on Photoexcited Processes and Applications (ICPEPA-10), Brasov, Romania
29.08–2.09.2016 - Poster

47. **Enculescu M.**
Luminescent Principles and Applications to Organic Semiconductors
Summer School of Organic Electronics & Applications, ELBYSIER
18-22.04.2016 - Oral presentation

48. **Enculescu M., Evanghelidis A., Enculescu I.**
Optical properties of nanofibers produced by electrospinning
16th International Balkan Workshop on Applied Physics and Materials Science, Constanta, Romania
07-09.07.2016 - Oral presentation

49. Endo K, Arisawa S, Tateno Y, Kawai S, Wada M, Kaneko T, Tsuyumoto I, **Badica P**
MOCVD Growth and Characterization by X-ray Diffraction of Epitaxial $Bi_2Sr_2CaCu_2O_8$ Thin Films,
1st Asian ICMC and CSSJ 50th Anniversary Conference, Kanazawa, Japan
07 – 10.11.2016 - Poster

50. **Filip LD, Pintilie L**
Thin film metal-ferroelectric-metal current voltage characteristics: An electron tunnelling approach
Electroceramics XV, Limoges, France
27-29.06.2016 - Oral presentation

51. **Filip LD, Pintilie L**, Tam W-S, Kok C-W
Leakage current for thin film metal-ferroelectric-metal devices
5th International Symposium on Next-Generation Electronics (ISNE 2016), Hsinchu, Taiwan
03-06.05.2016 - Poster

52. **Florica C., Costas A., Matei E. , Enculescu M., Enculescu I.**
Single nanowire field effect transistor,
11th International Conference on Surfaces, Coatings and Nanostructured Materials, Aveiro, Portugalia
06-09.09.2016 - Oral presentation

53. **Frunza L, Diamandescu L, Zgura I, Ganea CP, Frunza S, Negrila CC, Birzu M**
Photocatalytic activity of some low temperature TiO_2 deposited fabrics: Methylene blue degradation as a test reaction
The 11th International Symposium of the Romanian Catalysis Society, Timisoara, Romania
06-08.06.2016 - Oral presentation

54. **Frunza L, Frunza S, Ganea CP, Zgura I**, Schönhals A
Molecular mobility properties of cyanophenyl alkylbenzoates with 2,3 and 7 carbon atoms in the alkyl tail
5th International Colloquium 'Physics of Materials' - PM-5, Bucuresti, Romania
10-11.11.2016 - Oral presentation

55. **Galatanu M, Enculescu M, Galatanu A**
Thermal properties of micro- and nano- structured W-Cu functional gradient materials
The 25th Symposium on Thermal Analysis and Calorimetry–Eugen SEGAL, Bucharest, Romania
15.04.2016 - Oral presentation.

56. **Galatanu A, Galatanu M**, Jianu A, Weisenburger A,
Heat Transfer Analysis for Metal-Liquid Lead Interface
Nuclear 2016 – Annual International Conference on Sustainable Development through Nuclear Research and Education, Pitesti, Romania
18-20.05.2016 - Oral presentation

57. **Galatanu M, Enculescu M, Galatanu A**
Tungsten based composite materials obtained by Spark Plasma Sintering as possible armour materials for fusion reactors
IBWAP 2016, Constantza, Romania.
07-09.07.2016 - Poster

58. **Galatanu M, Enculescu M, Ruiu G, Popescu B, Galatanu A**
Cu-based composites as thermal barrier materials in DEMO divertor components
SOFT 2016, 29th Symposium on Fusion Technology, Prague, Czech Republic
05-09.09.2016 - Poster

59. **Galatanu A, Galatanu M, Enculescu M Ruiu G**, Stancu C
FAST brazing technology for W multi-metal laminates,
SOFT 2016, 29th Symposium on Fusion Technology, Prague, Czech Republic
05-09.09.2016 - Poster

60. **Galatanu M, Enculescu M, Cretu S, Galatanu A**
Morphology and thermo-physical properties of SPS-ed SiC ceramics and composites
Annual Intenational Conference ROMPHYSCHEM 2016, Galati, Romania
21-24.09.2016 - Oral presentation

61. **Galatanu M**
FA-Thermo-physical properties of metal-ceramic composites
Advanced Thermal Analysis and Applications, Bucharest-Magurele, Romania
13.10.2016 - Oral presentation

62. **Ganea CP, Banciu MG**
Boundary conditions at electrode - ionic liquid interface for dielectric spectroscopy measurements
9th International Conference on Broadband Dielectric Spectroscopy and its Applications, Pisa, Italy
11–16.09.2016 - Poster

63. Gavrila-Florescu L, Popovici E, Morjan I, Dutu E, Badoi AD, Demian G, Demian M, Iliescu M, Stanciu EM, **Diamandescu LC**, Raditoiu V, Raditoiu A, Wagner LE
Method of nano titanium dioxide synthesis by laser pyrolysis targeting photocatalytic applications
10th International Conference on Photoexcited Processes and Applications, ICPEPA-10, Brasov, Romania
29.08–02.09.2016 - Poster

64. **Galca AC, Trinca LM**, Socol G, Craciun V
Synthesis and characterization of transparent amorphous oxide thin films
The 8th International Conference on Materials Science and Condensed Matter Physics, Chisinau, Moldavia
12-16.09.2016 - Oral presentation

65. **Ghica C, Negrea RF, Teodorescu VS, Chirila CF**, Scarisoreanu ND
On the evolution of the residual strain in thin epitaxial films by HRTEM quantification and nanoscale mapping
8th International Conference on Nanomaterials - Research & Application, NANOCON 2016, Brno, Czech Republic
19-21.10.2016 - Oral presentation

66. **Ghica C, Negrea RF, Teodorescu VS, Chirila CF, Pintilie L**
QHRTEM investigation on growth evolution of the residual strain in epitaxial films
6th International Conference on Nanostructures and Nanomaterials Self-Assembly NanoSEA 2016, Giardini-Naxos (Sicilia), Italy
03-08.07.2016 - Poster

67. **Ghica D, Stefan M, Ghica C, Stan GE**
Mn^{2+} ions distribution in RF-sputtered nano-ZnO:Mn films
8th International Conference on Nanomaterials - Research & Application, NANOCON 2016, Brno, Czech Republic
19-21.10.2016 - Oral presentation

68. **Ghica D, Stefan M, Nistor SV, Maraloiu AV**, Plugaru R
Localisation and distribution of the Mn^{2+} dopant ions in nanostructured ZnO films
International Conference on Defects in Insulating Materials, Lyon, France
10-15.07.2016 - Poster

69. **Ghica D, Stefan M, Ghica C, Negrea RF, Stan GE**
Evaluation of the paramagnetic impurities distribution in nanostructured ZnO:Mn films
6th International Conference on NANOstructructures and nanomaterials Self-Assembly, Giardini Naxos, Italy
03–08.07.2016 - Poster

70. Ghinea A, Batalu D, **Aldica G, Badica P**
Finite element analysis of the temperature distribution during spark plasma sintering
4th International Workshop on Numerical Modelling in Aerospace Sciences, Bucharest, Romania
11-12.05.2016 - Oral presentation

71. **Greculeasa S, Schinteie G**, Kumar L, Kumar P, Kumar S, Sahoo B, Kar M, **Kuncser V**
Investigations of cation occupancy and spin canting in nanocrystalline ferrites
SSFUB Annual Meeting, Magurele, Romania
17.06.2016 - Oral presentation

72. **Grigoroscuta M, Ionescu AM, Burdusel M, Aldica G, Badica P**
Pinning force related parameters of the spark plasma sintered MgB_2 obtained for different dwell time,
Nano confined superconductors and their application, Garmisch-Partenkirchen, Germany
03–07.09.2016 - Poster

73. Hapenciuc C, Mihailescu IN, Bociaga D, Socol G, **Stan GE**, Chifiriuc MC, Bleotu C, **Husanu MA**, Luculescu C, Popescu-Pelin G, Duta L, Negut I, **Besleaga C, Zgura I**, Miculescu F
Selection of antimicrobial Silver-doped Carbon structures by combinatorial pulsed laser deposition
10th International Conference on Photoexcited Processes and Applications (ICPEPA-10), Brasov, Romania
29.08–02.09.2016 - Poster

74. **Husanu MA, Popescu DG**, Strocov V, Schmitt T
Interface states with momentum resolution in $BaTiO_3/La_{1-x}Sr_xMnO_3$ ferroelectric-ferromagnetic heterostructure
39th International conference on Vacuum Ultraviolet and X-ray Physics, Zurich, Switzerland
03 – 08.07.2016 - Poster

75. **Ionescu AM, Ivan I, Enculescu M, Grigoroscuta M**, Miu D, **Valeanu M, Badica P, Miu L**
From an anomalous peak effect to a second magnetization peak in Nb-rich Nb-Ti alloys
5th International Conference on Superconductivity and Magnetism, Fethiye, Turkey
24-30.04.2016 - Poster

76. **Ionescu AM, Ivan I, Enculescu M, Grigoroscuta M**, Miu D, **Crisan A, Miu L**
Magnetic hysteresis curves of thermo-mecanically processed Nb-rich Nb-Ti alloys
Int. conf. on Nano confined superconductors and their applications, Garmish-Partenkirchen, Germany
03-07.09.2016 - Poster

77. **Ionescu AM, Ivan I, Enculescu M, Grigoroscuta M**, Miu D, **Valeanu M, Crisan A**, Antohe S, **Miu L**
Peak effect on the DC magnetization curvers of Nb-rich Nb-Ti alloys
International Conference of Physics Students, Msida, Malta
11-18.09.2016 - Poster

78. **Ivan I, Crisan A**, Mele P, Miu D, **Miu L**
AC magnetic response of YBCO thin films with complex pinning structures
Int. conf. on Nano confined superconductors and their applications, Garmish-Partenkirchen, Germany
03-07.09.2016 - Poster

79. **Joita AC, Nistor SV, Pintilie I**
Paramagnetic defects produced by high-radiation doses in silicon detector material
19th International Conference on Defects in Insulating Materials ICDIM 2016, Lyon, Franta
10-15.07.2016 - Poster

80. Kawai S, Tsuchiya T, Arisawa S, Tateno Y, Tsuyumoto I, **Badica P**, Endo K
Bi-based HTS thin films as potential materials to be used at 300-570 K in power electronics applications
1st Asian ICMC and CSSJ 50th Anniversary Conference, Kanazawa, Japan
07–10.11.2016 - Poster

81. **Kuncser V, Schinteie G**, Iacob N, **Kuncser A, Palade P, Leca A, Filoti G**
Functionalized transition metal oxide nanoparticles for bio-medical applications
The XXth International Conference on Solid Compounds of Transition Elements, Zaragoza, Spain
11-15.04.2016 - Oral presentation

82. **Leca A, Kuncser A,** Scarisoreanu M, Morjan I, **Kuncser V, Filoti, G**
Relevant new magnetic features evidenced in particulate TiO_2 obtained by laser pyrolysis
The XXth International Conference on Solid Compounds of Transition Elements, Zaragoza, Spain
11-15.04.2016 - Oral presentation

83. **Leca A**, Schiopu P, **Stanciu A E, Schinteie G, Kuncser V**
Novel methodology for anisotropy magnetoresistance measurements in perpendicular geometry,
Advanced Topics in Optoelectronics Microelectronics and Nanotechnologies, Constantza, Romania
2016 - Oral presentation

84. **Lepadatu AM, Palade C, Slav A, Maraloiu AV, Teodorescu VS, Logofatu C, Ciurea ML**
Improving the performance of Ge NCs-based nonvolatile memory capacitors by manipulating/ controlling the lateral separation between NCs
Workshop "ALD for Novel Sensors and Biosensors", Bucharest, Romania
11-12.05.2016 - Oral presentation

85. **Lepadatu AM, Palade C, Slav A, Maraloiu AV, Teodorescu VS, Logofatu C, Ciurea ML**
Morphology-driven charge storage properties of trilayer structures with Ge nanocrystals in HfO_2
International Workshop of Materials Physics, Magurele
23-25.05.2016 - Oral presentation

86. **Lepadatu AM, Slav A, Palade C, Lazanu S, Enculescu M, Teodorescu VS, Stoica T, Ciurea ML**, Manolescu A, Svavarsson HG,
Ge quantum dots embedded in TiO_2 for VIS-NIR photodetectors
The fifth edition of the International Colloquium 'Physics of Materials, PM-5 2016, Bucharest, Romania
10-11.11.2016 - Oral presentation

87. **Maraloiu VA**, Appaix F, Broisat A, Le Guellec D, **Teodorescu VS**, Ghezzi C, van der Sanden B, Blanchin MG
Using Two Photon Laser Scanning Microscopy to reveal the fate of USPIO nanoparticles in an atherotic murine model
International Conference on Defects in Insulating Materials, ICDIM 2016, Lyon, France
10-15.07.2016 - Oral presentation

88. **Maraloiu VA**, Appaix F, Broisat A, Le Guellec D, **Teodorescu VS**, Ghezzi C, van der Sanden B, Blanchin MG
Multiscale investigation of USPIO nanoparticles in atherosclerotic plaques and their catabolism and storage in vivo
16th European Microscopy Congress, Lyon, France
28.08–02.09.2016 - Poster

89. **Maraloiu VA, Ghica D, Stefan M, Nistor SV**, Plugaru R
TEM and EPR investigations of the localisation and distribution of Mn^{2+} dopant ions in nanostructured ZnO films
8th International Conference on Nanomaterials - Research & Application, NANOCON 2016, Brno, Czech Republic
19-21.10.2016 - Poster

90. **Matei E, Diamandescu L, Enculescu M, Zgura I, Enculescu I**
Electrodeposited ZnO Nanostructures Onto Transparent Metallic Web Electrodes for Photocatalytic Applications
PRiME Pacific RIM Meeting, Honolulu, Hawai, SUA
02-07.10.2016 - Oral presentation

91. **Matei E, Florica , Costas A, Enculescu M, Enculescu I**
Self assembled field effect transistor with ZnO nanowire channel,
11th International Conference on Surfaces, Coatings and Nanostructured Materials (NANOSMAT 2016)", Aveiro, Portugalia
06-09.09.2016 - Oral presentation

92. **Matei E. , Florica C., Costas A., Enculescu M., Enculescu I.**
Self Assembled ZnO Nanowire Field Effect Transistors,
PRiME 2016, Honolulu, Hawaii, SUA
02-07.10.2016 - Oral presentation

93. **Mihalache V, Secu M, Cioanger M, Cernea M**
Ferromagnetism in un-doped cerium oxide (CeO_2) prepared by sol-gel route and annealed in different conditions
The 8th International Conference on Materials Science and Condensed Matter Physics, Chișinău, Moldavia
11-17.09.2016 - Poster

94. Mihailescu N, **Stan GE**, Ristoscu C, Sopronyi M, Mihailescu IN
Nanostructured bioactive glass thin films synthesized by pulsed laser deposition onto biodegradable metallic implants
INERA Conference, Velingrad, Bulgaria
05–09.07.2016 - Poster

95. Mindru I, Gingasu D, Patron L, Marinescu G, Calderon-Moreno JM, Preda S, Stanica N, Oprea O, **Diamandescu L**
New precursor method for $CoFe_2$–xCr_xO_4 spinel oxides
16th International Conference of Physical Chemistry ROMPHYSCHEM-16, Galați, Romania
21-24.09.2016 - Poster

96. **Moldoveanu V**
Geometrical effects on exciton dynamics in magnetic quantum dots
32nd International Physics Congress of the Turkish Physical Society" (TPS-32), Bodrum, Turcia
06-09.09.2016 - Oral presentation

97. Nadaud K, Borderon C, Renoud R, Gundel H, Ghalem A, Crunteanu A, Huitema L, Dumas-Bouchiat F, Dutheil P, Champeaux C, Marchet P, **Nedelcu L, Trupina L, Banciu G**
Étude des mouvements de parois de domaines sur $BaSrTiO_3$ dans la gamme des fréquences microondes
14èmes Journées de Caractérisation Microondes et Matériaux (JCMM2016), Calais, France
23-25.03.2016 - Oral presentation

98. **Nedelcu L, Trupina L, Cernea M, Banciu M**G, Huitema L, Crunteanu A, Ghalem A, Rammal M, Madrangeas V, Passerieux D, Dutheil P, Dumas-Bouchiat F, Marchet P, Champeaux C
Ferroelectric thin film varactors for compact tunable antennas
16th International Balkan Workshop on Applied Physics, IBWAP 2016, Constanta, Romania
07-09.07.2016 - Poster

99. **Nedelcu L, Trupina L, Ganea CP, Geambasu CD, Banciu MG**
Intrinsic and extrinsic contributions in $(Ba,Sr)TiO_3$ ferroelectric ceramics studied by broad-band dielectric spectroscopy
9th International Conference on Broadband Dielectric Spectroscopy and its Applications, BDS 2016, Pisa, Italy
11-16.09.2016 - Poster

100. **Negrea RF, Ghica C, Chirila CF**
Atomic scale STEM and EELS characterization of ferroelectric heterostructures based on $BaTiO_3$
6th International Conference on Nanostructures and Nanomaterials Self-Assembly NanoSEA 2016, Giardini-Naxos (Sicilia), Italy
03-08.07.2016 - Poster

101. Nica C, Stan MS, Dumitrescu I, **Diamandescu L**, Dinischiotu A
In vitro biocompatibility studies of polyester fabrics coated with photocatalytic titanium dioxide nanoparticles,
3rd International Conference on Occupational & Environmental Toxicology ICOETOX, Porto, Portugalia
21-23.06.2016 - Poster

102. **Nistor LC, Nistor SV, Vlaicu ID, Stefan M, Ghica D**
Aggregation of Mn^{2+} ions in a separate phase in the pores of heavily doped cZnS:Mn nanocrystals self-assembled in a mesoporous structure.
6th International Conference on Nanostructures and Nanomaterials Self-Assembly NanoSEA 2016, Giardini-Naxos (Sicilia), Italy
03-08.07.2016 - Poster

103. **Nistor LC, Nistor SV, Stefan M, Vlaicu ID**
Structure and localization of aggregated Mn^{2+} ions as a separate phase in the mesoporous assembly of cZnS:Mn QDs
19th International Conference on Defects in Insulating Materials ICDIM 2016, Lyon, France
10-15.07.2016 - Poster

104. **Nistor SV, Joița AC, Radu R, Pintilie I**
ESR of point defects in pure and doped $^{17}O/^{13}C$ doped Si-FZ irradiated with 3.5 MeV and 27 MeV electrons. Corelation with TSC data.
28th RD50 workshop – Radiation Hard Semiconductor Devices for Very High Luminosity Colliders, Torino, Italy
06-08.06.2016 - Oral presentation

105. **Nistor SV, Stefan M, Nistor LC, Ghica D, Vlaicu ID**
The main role of extended lattice defects in the localization and interaction of Mn^{2+} ions in cubic ZnS quantum dots.
19th International Conference on Defects in Insulating Materials ICDIM 2016, Lyon, France
10-15.07.2016. Oral presentation.

106. **Nistor LC, Pintilie I**
HRTEM investigations of different clusters produced in Si by electron and neutron irradiation
28th RD50-CERN Workshop, Torino, Italy
06-08.06.2016 - Oral presentation

107. **Nistor SV, Joita AC, Radu R, Pintilie I**
EPR of point defects in pure and $^{17}O/^{13}C$ doped Si-FZ irradiated with 3.5 and 27 MeV electrons. Correlation with TSC data
28th RD50-CERN Workshop, Torino, Italy
06-08.06.2016 - Oral presentation

108. **Palade C, Slav A, Lepadatu AM, Maraloiu AV, Lazanu S, Logofatu C, Teodorescu VS, Ciurea ML**
Non-volatile memory structures with Ge NCs -HfO_2 intermediate layer
IEEE International Semiconductor Conference, CAS 2016, Sinaia, Romania
10-12.10.2016 - Oral presentation

109. **Palade C, Slav A, Lepadatu AM, Maraloiu AV, Teodorescu VS, Logofatu C, Ciurea ML**,
High performance nonvolatile memory capacitors with Ge nanocrystals controlled morphology
EMRS Spring Meeting, Lille, France
02-06.05.2016 - Oral presentation

110. **Popescu DG, Husanu MA, Tanase LC, Stoflea LE**
Band bending in Au/$BaTiO_3$ and Cu/ $BaTiO_3$ investigated by X-ray photoelectron spectroscopy
5th Portuguese Young Chemists Meeting (5th PYCheM) - 1st European Young Chemists Meeting, Guimaraes, Portugal
26 – 29.05.2016 - Oral presentation

111. **Popescu DG, Abramiuc LE**
Photoelectron spectromicroscopy of $Pb(Zr,Ti)O_3$(001) and (111) surfaces
International Workshop of Materials Physics, Măgurele, Romania,
23–25.05.2016 - Oral presentation

112. **Popescu DG, Husanu MA**
Interface electronic structure in $BaTiO_3/La_{1-x}Sr_xMnO_3$ ferroelectric-ferromagnetic system,
The 16th International Balkan Conference on Applied Physics (IBWAP 2016), Constanta, Romania
07–09.07.2016 - Poster

113. **Popescu DG, Husanu MA**
Optimization of geometry parameters for a 2D photonic crystal for optimal light manipulation,
International Colloquium 'Physics of Materials' – PM-5, Bucharest, Romania
10–11.11.2016 - Poster

114. Popescu-Pelin G, **Stan GE**, Popescu AC, Grumezescu V, **Enculescu M, Besleaga C, Zgura I**, Florian PE, Sima LE, Roseanu A, Oktar FN, Mihailescu IN, Duta L
In vitro investigations of highly adherent biological hydroxyapatite thin films for a new generation of implants
International Symposium on Priorities of Chemistry for a Sustainable Development, Bucharest, Romania
27-28.10.2016 - Poster

115. Popescu-Pelin G, Sima F, Socol G, Mihailescu CN, **Socol M**, Luculescu C, Sima L, Iordache I, Ristoscu C, Mihailescu I N
Improved osteoblast adhesion on hydroxyapatite thin films capped with fibronectin,
EMRS Spring meeting, Lille, France
02-06.05.2016 - Poster

116. **Popescu B, Crisan AD, Valeanu M, Sofronie M, Tolea F, Galatanu A**
Synthesis and characterization of $CeCoAl_4Si_2$,
Joint European Magnetic Symposia (JEMS 2016) Glasgow, Great Britain
21–27.08.2016 - Poster

117. Rammal M, Ghalem A, Huitema L, Crunteanu A, Passerieux D, Cros D, Monediere T, Madrangeas V, Dutheil P, Dumas-Bouchiat F, Marchet P, Champeaux C, **Nedelcu L, Trupina L, Banciu G**
Dispositifs à base de couches minces ferroelectriques hautement accordables sous champ faible
14èmes Journées de Caractérisation Microondes et Matériaux (JCMM2016), Calais, France
23-25.03.2016 - Oral presentation

118. **Rasoga O, Stanculescu A**, Socol G, Catargiu AM, Grigoras M, **Breazu C, Socol M, Matei E**, Stanculescu F, Girtan M,
Effect of aluminum electrode nano-patterning on the properties of the laser prepared arylenevinylene polymer based mixed layer
ICPEPA Brasov, Romania
30.08.-03.09.2016 - Poster

119. **Rusu D, Pintilie L**
A model for the current-voltage characteristics of a thin film Metal-ferroelectric-metal structure
11th International Conference on Physics of Advanced Materials (ICPAM), Cluj-Napoca, Romania
08-14.09.2016 - Poster

120. Sander A, Garcia V, Strocov V, Bisti F, **Husanu MA**, Rault J, Bertran F, Lefevre P, Arora A, Valencia S, Yamada H, Carretero C, Barthelemy A, Bibes M
Electron-doped manganite films as channels in ferroelectric Mott Transistors,
MRS Spring Meeting & Exibit, Phoenix, Arizona, USA
28.03–01.04.2016 - Oral presentation

121. **Sandu V**
Layering and Defect Formation in Proton Irradiation MgB_2
International MultiSuper Workshop "Novel Quantum Phenomena in Ultra Thin Superconductors", Camerino, Italy
07-08.04.2016 - Oral presentation

122. **Schinteie G**
Cercetare, inovare si formare profesionala prin colaborare internationala
Diaspora and its friends, West University, Timisoara, Romania
25-29.04.2016 - Oral presentation

123. Schiopu P, **Stanciu AE, Leca A, Catrina A**
Unusual magneto-resistive sensors for high field applications
Smart Applications & Technologies for Electronic Engineering, SATEE 2016, Alba Iulia, Romania
13-16.10.2016 - Oral presentation

124. Sima F, Axente E, Sima LE, Chiritoiu M, Visan A, Dorcioman G, Milovanovic D, Luculescu C, **Socol M, Zgura I**, Socol G,
Small-scale areas of titanium modified by laser irradiation for tissue engineering and cellular spreading control,
EMRS Spring meeting, Lille, France
02-06.05.2016 - Poster

125. **Simion CE, Stanoiu A**, Piticescu RM
Transducing Mechanism of Ammonia Detection using $BaSrTiO_3$
International Workshop of Material Physics, Bucharest, Romania
23-25.05.2016 - Oral presentation

126. Socol G, Dorcioman G, Craciun D, Garoi P, Fufa O, **Galca AC, Socol M**, Negut D, Craciun V
Investigations of radiation effects in transparent and conductive oxides
EMRS spring meeting, Lille, France
02-06.05.2016 - Oral presentation

127. Socol G, **Socol M, Preda N**, **Stanculescu A, Breazu C**, Stanculescu F, Iftimie S, Girtan M,
Organic heterostructures deposited by MAPLE on AZO substrate,
ICPEPA 2016, Brasov, Romania
30.08-03.09.2016 - Poster

128. Socol G, **Zgura I, Preda N, Frunza L, Diamandescu L, Enculescu M, Nedelcu L, Ganea CP, Frunza S**
Wet chemical synthesis of ZnO-CdS composites with enhanced photocatalytic activity
10th International Conference on Photo-Excited Processes and Applications ICPEPA-10, Brasov, Romania
30.08-03.09.2016 - Poster

129. **Socol M**, Socol G, **Breazu C, Preda N, Florica C, Rasoga O, Stanculescu A**, Stanculescu F, Girtan M, Swart FH
The properties of organic heterostructures deposited on nanostructured metallic substrates for optoelectronic applications
ICPAM 2016, Cluj, Romania
08-11.09.2016 - Poster

130. **Sofronie MI, Ţolea F, Crisan AD, Popescu B, Valeanu MC**
Effect of rapid solidification and thermal treatment on the magnetoelastic properties in polycrystalline ferromagnetic shape memory Heusler alloys
European Conference on Fracture ECF 21, Catania, Italy
20-22.06.2016 - Poster

131. **Sofronie M, Tolea F, Crisan AD, Popescu B, Valeanu M**
Effect of rapid solidification and thermal treatment on the magnetoelastic properties in polycrystalline ferromagnetic shape memory Heusler alloys,
The European Magnetic Sensors and Actuators (EMSA 2016), Torino, Italy
11-16.07.2016 - Poster

132. **Sofronie M, Tolea F, Crisan AD, Popescu B, Enculescu M, Valeanu M**
Magnetoelastic properties in melt spun Ni-Fe-Ga(Cu) ribbons,
Joint European Magnetic Symposia (JEMS 2016) Glasgow, Great Britain
21–27.08.2016 - Poster

133. **Sofronie M, Galca AC, Tolea F**, Elisa M, **Kuncser V, Valeanu M**
Magneto-optical properties of doped aluminophosphate glasses,
Joint European Magnetic Symposia (JEMS 2016) Glasgow, Great Britain
21–27.08.2016 - Poster

134. **Stan GE, Popa AC, Besleaga C**, Ion L, **Maraloiu VA**, Tulyaganov DU, Ferreira JMF
Formation of bioglass hollow sub-micron cones by magnetron sputtering and their prospective biomedical applications
ALD for Novel Sensors and Biosensors Workshop, Magurele, Romania
11–12.05.2016 - Oral presentation

135. **Stan GE, Popa AC, Husanu MA, Enculescu M, Tanase C**, Ferreira JMF
Dental implant fixtures bio-functionalized with mechanically resistant and cytocompatible bioglass coatings by magnetron sputtering technique
International Workshop of Materials Physics, Magurele, Romania
23–25.05.2016 - Oral presentation

136. **Stan GE, Popa AC**, Marques VMF, **Galca AC, Husanu MA, Enculescu M, Tanase C**, Tulyaganov DU, Ferreira JMF
Mechanical and in vitro biological performance of bioglass coatings deposited by magnetron sputtering on dental implant fixtures
10th International Conference on Photoexcited Processes and Applications (ICPEPA-10), Brasov, Romania
29.08–02.09.2016 - Poster

137. Stan MS, Nica CI, Dumitrescu I, **Diamandescu L**, Dinischiotu A
Cytotoxicity assessment on cotton fabrics coated with photocatalytic titanium dioxide nanoparticles
3rd International Conference on Occupational & Environmental Toxicology ICOETOX, Porto, Portugal
21-23.06.2016 - Poster

138. **Stanciu AE, Greculeasa SG, Schinteie G, Palade P, Kuncser A, Leca A, Kuncser V**
Interplay of structural, magnetic and magneto-transport properties of Fe-Au thin films
International Balkan Workshop on Applied Physics, Constanta, Romania
07-09.07.2016 - Oral presentation

139. **Stanciu AE, Greculeasa SG, Bartha C, Schinteie G, Palade P, Kuncser A, Leca A, Filoti G, Kuncser V**
Local configurations and specific properties of metastable Fe-Cr and Fe-Mo ribbons under thermal treatments in different atmospheres,
SSFUB Annual Meeting, Magurele, Romania
17.06.2016 - Oral presentation

140. **Stancu V, Tomulescu AG, Sima M, Besleaga C, Stoflea LE, Pintilie L, Pintilie I**, Nemnes A, Manolescu A
Aging Effects in Hybrid Perovskite Solar Cells
5th International Conference from Nanoparticles and Nanomaterials to Nanodevices and Nanosystems (IC4N), Porto Heli, Peloponnese, Greece
26-30.06.2016 - Poster

141. **Stanculescu A, Socol M**, Stanculescu F
Effect of heavy ions irradiation on the properties of benyil crystals,
ICPSCG 10, Zakopane Poland
16-21.10.2016 - Oral presentation

142. **Stanculescu A, Rasoga O, Socol M**, Vacareanu L, Grigoras M, Socol G, Stanculescu F, Girtan M, **Breazu C, Preda N**
MAPLE prepared oligoazomethine: fullerene derivative mixed layer for photovoltaic applications
EMRS Spring meeting, Lille, France
02-06.05.2016 - Poster

143. **Stanculescu A, Socol M, Rasoga O**, Vacareanu L, Grigoras M, Socol G, Stanculescu F, **Breazu C**, Girtan M,
MAPLE prepared heterostructures with oligoazomethine: fullerene derivative mixed layer for photovoltaic applications
ICPEPA 2016, Brasov, Romania
30.08.-03.09.2016 - Poster

144. **Stefan M, Nistor SV, Nistor LC, Kuncser V, Vlaicu ID**
Collective magnetism from aggregated Mn2+ activating ions in self-assembled cZnS quantum dots at higher doping levels.
19th International Conference on Defects in Insulating Materials ICDIM 2016, Lyon, France
10-15.07.2016 - Oral presentation

145. Tateno Y, **Badica P**, Arisawa S, Endo K,
Growth of Practical $SrTiO_3$ Single Crystals with a Diameter of 32 mm and Long Length up to 60 mm,
1st Asian ICMC and CSSJ 50th Anniversary Conference, Kanazawa, Japan
07–10.11.2016 - Poster

146. Tateno Y, **Badica P**, Arisawa S, Endo K,
Some optimization aspects of the $SrTiO_3$ single crystal growth by Veneuil method,
26th Annual Meeting of MRS-J, Yokohama, Japan
19-22.12.2016 - Poster

147. **Tănase LC, Abramiuc LE, Apostol NG, Lungu GA, Bucur IC, Popescu DG, Hușanu MA, Hrib L, Trupină L, Pintilie L, Teodorescu CM**
Surface reactions on ferroelectrics single crystal films,
The 11th International Symposium of the Romanian Catalysis Society (RomCat 2016), Timișoara, Romania
06–08.06.2016 - Oral presentation

148. **Teodorescu VS, Maraloiu AV, Kuncser AC, Ghica C, Ciurea ML, Lepadatu AM, Stavarache I**,
Scarisoreanu DN, Dinescu M, Blanchin M-G
Nanoscale segregation of Ge nanoparticles in GeSiO and GeTiO amorphous films by RTA and UV laser pulse annealing
International Conference on Defects in Insulating Materials, ICDIM 2016, Lyon, France
10-15.07.2016 - Oral presentation

149. **Teodorescu VS, Ghica C, Maraloiu AV, Kuncser AC, Lepadatu AM, Stavarache I, Ciurea ML**,
Scarisoreanu ND, Dinescu M
Fast atomic diffusion in amorphous films induced by laser pulse annealing
39th International Semiconductor Conference CAS 2016, Sinaia, Romania
10-12-10.2016 - Oral presentation

150. **Teodorescu VS, Maraloiu AV, Kuncser A, Ghica C, Ciurea ML, Lepadatu A-M, Stavarache I**,
Scarisoreanu DN, Dinescu M, Blanchin M-G
XTEM observations revealing high diffusivity and Ge segregation in UV laser pulse annealed SiGeO and GeTiO amorphous films,
16th European Microscopy Congress- EMC2016, Lyon, France
28.08-02.09.2016 - Poster

151. **Teodorescu VS, Nistor LC**, Preda S, Zaharescu M, Blanchin M-G
Details on the TiO_2 nanotubes wall structure revealed by HRETM,
16th European Microscopy Congress- EMC2016, Lyon, France
28.08-02.09.2016 - Poster

152. **Trinca LM, Galca AC, Iuga AR, Boni AG, Radu R, Chirila C, Besleaga C, Pintilie L**
Zinc oxide based epitaxial, polycrystalline and amorphous multilayers for transparent electronics
16th International Balkan Workshop on Applied Physics and Materials Science, Constanta, Romania
07-09.07.2016 - Oral presentation

153. **Trinca LM, Boni AG, Radu R, Iuga AR, Galca AC, Pintilie L**
Investigation on dielectric/ferroelectric properties of lithium doped zinc oxide
2016 Annual Scientific Meeting of Faculty of Physics, University of Bucharest, Magurele, Romania
17.06.2016 - Oral presentation

154. **Trupina L, Nedelcu L, Banciu MG, Negrila CC**, Champeaux C, Dumas-Bouchiat F, Marchet P, Huitema L, Madrangeas V, Cruntenau A, Passerieux D, Cros D, Monediere T
Iridium bottom electrodes for tunable microwave components
Electroceramics XV, Limoges, France
27-29.06.2016 - Poster

155. **Trupina L, Nedelcu L, Radu R, Banciu MG**, Champeaux C, Dumas-Bouchiat F, Marchet P, Huitema L, Madrangeas V, Cruntenau A, Passerieux D
$(Ba,Sr)TiO_3$ thin films for tunable microwave devices
16th International Balkan Workshop on Applied Physics, IBWAP 2016, Constanta, Romania
07-09.07.2016 - Poster

156. **Tolea F, Sofronie M, Crisan AD, Popescu B, Tolea M, Valeanu M**
Effect of thermal treatments on the structural and magnetic transitions in melt-spun Ni-Fe-Ga-(Co) ribbons
The 25th Symposium on Thermal Analysis and Calorimetry–Eugen SEGAL, Bucharest, Romania
15.04.2016 - Oral presentation

157. **Tolea F, Sofronie M, Crisan AD, Popescu B, Tolea M, Valeanu M**
Effect of thermal treatments in Ni-Fe-Ga with Co substitutions and Ni-Mn-Ga melt spun ribbons
European Conference on Fracture ECF 21 Catania, Italy
20-22.06.2016 - Oral presentation

158. **Tolea F, Tolea M, Sofronie M, Popescu B, Crisan A, Leca A, Valeanu M**
Specific changes in the magnetoresistance of Ni-Fe-Ga Heusler alloys induced by Cu, Co and Al substitutions
The European Magnetic Sensors and Actuators (EMSA 2016), Torino, Italy
11-16.07.2016 - Oral presentation

159. **Tolea F, Sofronie M, Popescu B, Crisan A, Leca A, Valeanu M**
Magnetorezistive effects in NiFeGaCu and NiMnGaCu Heusler compounds
Joint European Magnetic Symposia (JEMS 2016) Glasgow, Great Britain
21–27.08.2016 - Oral presentation

160. **Ţolea F, Ţolea M, Sofronie M, Văleanu M**
Temperature memory effect in Ni-Fe-Ga alloys
Advanced Thermal Analysis and Applications, Bucharest-Magurele, Romania
13.10.2016 - Oral presentation

161. Visan A, Stefan N, Miroiu M, Nita C, Dorcioman G, **Rasoga O, Zgura I, Breazu C**, Iordache I, **Stanculescu A**, Cristescu R, Chifiriuc MC, Sima L, Mihailescu IN, Socol G,
Lysozyme embedded into degradable polymers blends for antimicrobial applications,
EMRS Spring meeting, Lille, France
02-06.05.2016 - Poster

162. **Vlaicu ID, Ghica D, Nistor LC, Nistor SV, Stefan M**
The agent role of Mn^{2+} in redirecting the synthesis of $Zn(OH)_2$ towards ZnO
6th International Conference on Nanostructures and Nanomaterials Self-Assembly NanoSEA 2016, Giardini-Naxos (Sicilia), Italy
03-08.07.2016 - Oral presentation

163. **Vlaicu ID, Ghica D, Stefan M, Nistor LC, Nistor SV**
Manganese ions effect in redirecting the synthesis of micro-$Zn(OH)_2$ towards nano-ZnO
8th International Conference on Nanomaterials - Research & Application, NANOCON 2016, Brno, Czech Republic
19-21.10.2016 - Poster

164. **Zgura I, Ganea CP, Cotorobai VF,** Sorescu AA, Nuta A, **Frunza L**
Coordination polymers of zinc ions obtained from ligands containing parts with two carboxylic groups and with aromatic amides: synthesis and physical properties -Poster
5th International Colloquium 'Physics of Materials' - PM-5, Bucharest, Romania
10-11.11.2016 - Poster

INVITED LECTURES

01. **Badica P**
Spark plasma sintered MgB_2 superconductor, Energy,
Materials Nanotechnology (EMN Prague Meeting) 2016 Prague, Czech Republic
21-24.06.2016 - Invited

02. **Badica P, Aldica G, Popa S, Enculescu M, Pasuk I, Burdusel M, Grigoroscuta M, Ionescu AM**
Recent progress in spark plasma sintered MgB_2
1st Asian ICMC and CSSJ 50th Anniversary Conference, Kanazawa, Japan
07–10.11.2016 - Invited

03. **Badica P**
Research and Development of MgB_2 superconductor at National Institute of Materials Physics
IWSRFM 2016 Tsukuba, Japan
20-22.12.2016 - Invited

04. **Boni AG, Chirila C, Hrib L, Negrea R, Ghica C, Trupina L, Pasuk I, Pintilie I, Pintilie L**
Electrical properties of epitaxial ferroelectric heterostructures
EMN meeting on epitaxy, Budapesta, Hungary
03-09.09.2016 - Invited

05. **Chirila C, Boni A, Hrib L, Trupina L, Pasuk I, Negrea R, Ghica C, Pintilie I, Pintilie L**
Epitaxial ferroelectric thin films grown by pulsed laser deposition (PLD)
EMN meeting on epitaxy, Budapesta, Hungary
03-09.09.2016 - Invited

06. **Ciurea ML, Slav A, Lepadatu AM, Palade C, Stavarache I, Lazanu S, Logofatu C, Teodorescu VS**
Engineering memory properties of trilayers with Ge nanocrystals embedded in oxides
The fifth edition of the International Colloquium 'Physics of Materials, PM-5 2016, University Politehnica of Bucharest, Bucharest, Romania
10-11.11.2016 - Invited

07. Craciun D, Socol G, Behdad S, Boesl B, Lambers E, Pantelica D, Ionescu P, Vasile B, Makino H, **Trinca LM, Galca AC**, Simeone D, Craciun V
Investigations of radiation effects in amorphous and nanostructured thin films
5th International Conference from Nanoparticles and Nanomaterials to Nanodevices and Nanosystems (IC4N), Porto Heli, Peloponnese, Greece
26-30.06.2016 - Invited

08. **Crisan A**, Dong VS, Mikheenko P, Paturi P, Huhtinen H
Critical current and its dependence on field orientation in $YBa_2Cu_3O_7$ multi-layered films with synergetic pinning centres,
5th International Conference on Superconductivity and Magnetism, Fethiye, Turkey
24-30.04.2016 - Invited

09. **Crisan A**

Critical current and pinning potential in YBCO films with nanoengineered pinning centres with various architectures
Intern. Workshop (COST action) Probing superconductivity at the nanoscale: recent advances, Saas-Fee, Switzerland
12-15.04.2016 - Invited

10. **Crisan O**

Novel nano-magnetic logic (NML) concept made of core-shell nanoparticles into hybrid architectured systems
Global Nanotechnology Congress, Nanotech-2016, Dubai, Emiratele Arabe Unite
21-23.04.2016 - Invited

11. **Galca AC**

The road map from XRD raw data to the true lattice constants: A case study on the errors caused by the ubiquitous radial z-displacement of the investigated samples with respect to the diffractometer geometry
The 5th Tunisian Crystallographic Meeting and International Conference, Hammamet, Tunisia
18-25.03.2016 - Invited

12. **Galca AC, Trinca LM, Pintilie L**

Heteroepitaxy between Wurtzite and Cubic Structures: Case Study on the Growth of Zinc Oxide based Thin Layers and Multilayers on 001 Strontium Titanate Single Crystals
EMN meeting on epitaxy, Budapesta, Hungary
03-09.09.2016 - Invited

13. **Galca AC, Trinca LM**, Socol G, Craciun V

Transparent amorphous oxide semiconductor thin films: synthesis, characterization and functionality
11th International Conference on Physics of Advanced Materials (ICPAM), Cluj-Napoca, Romania
08-14.09.2016 - Invited

14. **Kuncser V**

Magnetic relaxation and inter-particle interactions in Fe oxide nanoparticles for bio-medical applications
2nd Mediterranean Conference on the Applications of the Mössbauer Effect, Kavtat, Croatia
31.05-03.06.2016 - Invited

15. **Kuncser V**

Magnetic Nanostructures for (bio-medical) sensing applications; A general perspective and some achivments at NIMP
Seminar at Vinca Institute, Belgrad, Serbia
26.10.2016 - Invited

16. **Miu L, Ionescu AM, Ivan I**, Miu D, Adachi T, Omori K, Koike Y

Behaviour of the second magnetization peak in self-nanostructured $La_{2-x}Sr_xCuO_4$ single crystals
5th International Conference on Superconductivity and Magnetism, Fethiye, Turkey
24-30.04.2016 - Invited

17. **Nistor SV, Nistor LC, Stefan M, Ghica D, Vlaicu ID**

A new perspective on incorporation, localization and interaction of Mn^{2+} ions in self-assembled cubic ZnS:Mn quantum dots and their influence on the optical and magnetic properties.
6th International Conference on Nanostructures and Nanomaterials Self-Assembly NanoSEA 2016, Giardini-Naxos (Sicilia), Italy
03-08.07.2016 - Keynote presentation

18. **Palade C, Slav A, Lepadatu AM, Stavarache I, Lazanu S, Logofatu C, Teodorescu VS**, Kiss A, Braic M, Vasilache D, Dragoman M, **Ciurea ML**,
Morphology management of structures based on Ge nanocrystals in oxide and effect on memory device performance
16th International Balkan Workshop on Applied Physics and Materials Science, IBWAP 2016, Ovidius University of Constanta, Constanta, Romania
07-09.07.2016 - Invited

19. **Pintilie I**
Halide perovskite based solar cells – challenges and perspectives
International Conference on Semiconductor Ferroelectrics and Photoferroelectrics (SEFERR16), Berlin, Germany
12-13.09.2016 - Invited

20. **Pintilie I**
Experimental techniques for defect characterization of highly irradiated materials and structures
25th International Workshop on Vertex Detectors (VERTEX2016), La Biodola, Isola d'Elba, Italy
25.09-1.10.2016 - Invited

21. **Pintilie L**
Feroelectrics: interfaces, microstructure and material constants
IC4N, Porto Heli, Greece
26-30.06.2016 - Invited

22. **Pintilie L**
Polarization and interfaces driven effects in ferroelectric/multiferroic heterostructures
ICTAM-AMF10, New Delhi, India
07-11.11.2016 - Invited

23. **Stan GE**
Comparative in vitro behavior of bioglass coatings in simulated body fluid media with improved biomimicry
University of Nottingham, Faculty of Engineering, Nottingham, UK
29.07.2016 - Invited

24. **Stoica T, Stavarache I, Aldica G**, Stoica M, Buca D, Kardinal B,
Engineering memory properties of trilayers with Ge nanocrystals embedded in oxides
The fifth edition of the International Colloquium 'Physics of Materials, PM-5 2016, University POLITEHNICA of Bucharest, Bucharest, Romania
10-11.11.2016 - Invited

25. **Tache CA**, Pressel F, Lacovig P, Lizzit S, Baraldi A
Different strategies for the growth of epitaxial graphene monolayers,
Conferința Diaspora în Cercetarea Științifică și Invățământul Superior din România, Timișoara, Romania,
25–28.04.2016 - Invited

26. Tateno Y, **Badica P**, Arisawa S, Endo K,
Growth of $SrTiO_3$ Single Crystals for the Thin Films Substrates,
Science and Applications of Thin Films, Conference & Exhibition (SATF 2016), Cesme, Turkey
19-23.09.2016 - Invited

27. **Teodorescu CM**

Graphene-like layers grown on ferroelectrics,

The 16th International Balkan Conference on Applied Physics (IBWAP 2016), Constanța, Romania,

07–09.07.2016 - Invited

28. **Teodorescu CM**

Chimie și cataliză la suprafețe feroelectrice, WE: Perspective în sinteza, investigarea și aplicațiile materialelor,

Conferința Diaspora în Cercetarea Științifică și Invățământul Superior din România, Timișoara, Romania,

25–28.04.2016 - Invited

29. **Teodorescu CM**

CoSMoS: prima facilitate românească instalată pe o sursă de radiație de sincrotron, WE: Colaborarea internațională în cercetarea din fizică,

Conferința Diaspora în Cercetarea Științifică și Invățământul Superior din România, Timișoara, Romania,

25–28.04.2016 - Invited

30. **Velea A**

The interplay between material and device properties in Ge-Te and Si-Te binary systems as a guide for material selection in selector applications

European symposium on Phase-Change and Ovonic Sciences - EPCOS2016, Trinity College, Cambridge, Anglia

04-06.09.2016 - Invited

CONDENSED MATTER PHYSICS AT MESOSCALE

SELECTED RESULTS

Graphene-like carbon layers grown on ferroelectric $Pb(Zr,Ti)O_3(001)$

N.G. Apostol, G.A. Lungu, I.C. Bucur, C.A. Tache, L. Hrib, L. Pintilie, D. Macovei, C.M. Teodorescu
National Institute of Materials Physics

Graphene is a perfect semimetal with large carrier mobility, promoting structures involving graphene conduction channels suitable candidates for ultrahigh frequency field effect transistors. The opening of a gap in graphene was reported when an electric field is applied perpendicular to bilayer graphene [1]. Also, it has been proven that graphene field effect transistors prepared on high-quality single crystal lead zirco-titanate $Pb(Zr,Ti)O_3$ (PZT) substrates exhibit a considerable increase in mobility (in the range of 10^5 $cm^2V^{-1}s^{-1}$) when compared to SiO_2–gated graphene devices [2].

A resistance hysteresis of graphene layers synthesized on ferroelectric substrates is induced via the screening by the graphene layers of the depolarization field [3, 4]. For intrinsic graphene, the conduction character changes when the polarization of the substrate is switched. The source-drain resistance will then exhibit peaks when the polarization of the substrate is switched following a gate voltage (V_G) application. Accordingly, the dependence of the resistance on the gate voltage $R(V_G)$ will show a hysteresis. When the graphene is pre-doped, two stable states with different resistances will exist, for the two polarization orientations of the ferroelectric substrate. This yields to the possibility of synthesizing easy accessible non-volatile memory elements with high readability rates.

The first measurements using transferred graphene layers have shown a behaviour where the sense of the hysteresis is inverted [5, 6]. A “normal” hysteresis was observed only at low temperatures, below 80–100 K [3]. The “anormal” (or inverted) hysteresis is connected with the presence of contaminating molecules adsorbed on graphene or trapped between the graphene and the ferroelectric. Therefore, the aim of this study was to achieve the synthesis of carbon monolayers with structure as close as possible to the graphene, on single-crystal ferroelectric substrates with well defined crystal structure and out-of-plane polarization, and in absence of any contaminants.

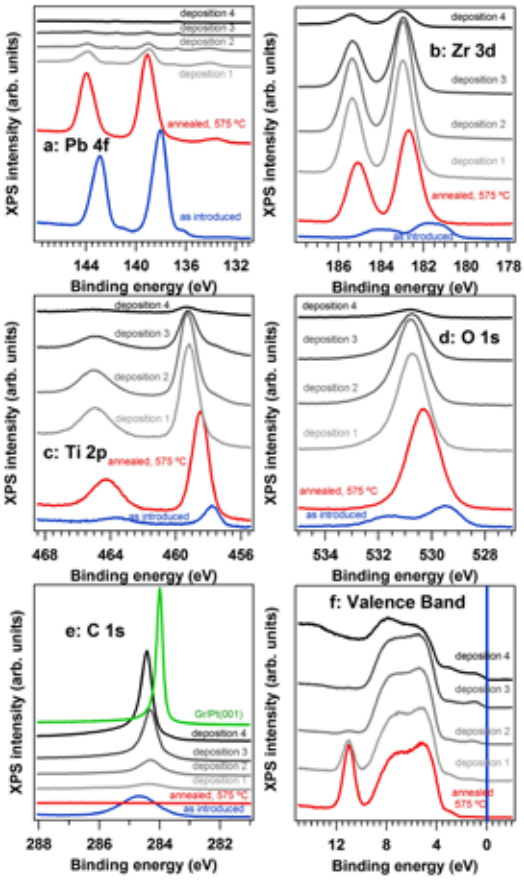

Fig. 1: X-ray photoelectron spectroscopy of as introduced PZT/Pt(001) (blue), cleaned by thermal treatments (red and after carbon depositions (grey): (a) Pb 4f, photon energy hν = 260 eV; (b) Zr 3d, hν = 260 eV; (c) Ti 2p, hν = 600 eV; (d) O 1s, hν = 600 eV; (e) C 1s, hν = 400 eV, including a spectrum of graphene on Pt(001) (green curve). (f) valence band spectra, hν = 120 eV. Adapted from [7].

PZT films were grown on Pt (001) by pulsed laser deposition, then cleaned in ultrahigh vacuum by annealing in a few mPa of O_2. Carbon was deposited at 510 °C, the maximum temperature where carbon is still adsorbed. The resulting heterostructures are characterized by X-ray photoelectron spectroscopy, XPS (Figs. 1, 2) and by near-edge absorption fine structure NEXAFS (Fig. 3). From the core levels of the substrate (Pb 4f, Zr 3d, Ti 2p, O 1s) one finds that the clean PZT (001) is in a state with polarization oriented outwards (Fig. 1) [7]. This polarization state does not change with carbon deposition. The C 1s spectra (Fig. 2) are fit with Doniac–Šunjić profiles whose asymmetry

parameter is close to that of graphene (α = 0.18). Also, from both the C 1s spectra and from the core levels of the substrate no chemical interaction or substrate disruption is detected (e.g. no peaks which might be attributed to the formation of carbonates).

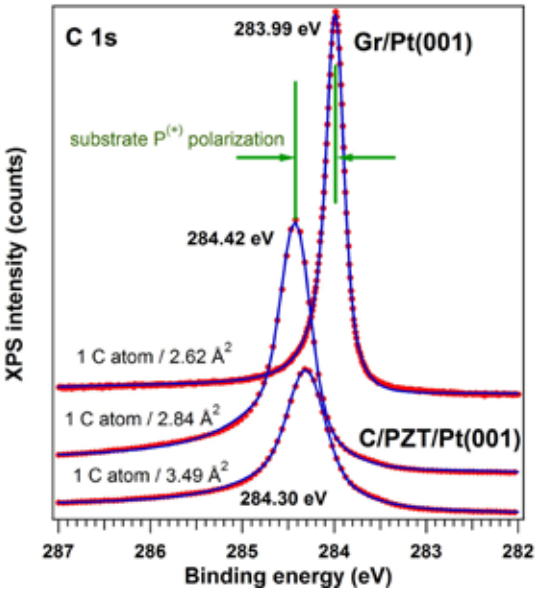

Fig. 2; X-ray photoelectron spectroscopy of graphene-like layers grown on PZT(001) and directly on Pt(001) by MBE. Adapted from [7].

C 1s NEXAFS spectra are recorded as function of the angle between the linear polarization of soft X-rays and the surface normal, probing unoccupied C 2p orbitals parallel or perpendicular to the surface. The 1s → 2pσ transitions prevail when the polarization is parallel to the surface, and the 1s → 2pπ transitions are more prominent when the beam is at grazing incidence on the sample. The difference between the two NEXAFS spectra may be used to derive the percentage of carbon arranged in two-dimensional (2D) structures, which is found to range between 50 and 75 % for carbon coverages from 75 % and 92 % from the carbon surface density of graphene [7]. Consequently, carbon layers which are majoritary 2D were synthesized on ferroelectric PZT(001) with weak chemical interaction with the substrate, without affecting its polarization.

This work was funded by the Romanian Ministry of Research and Innovation through UEFISCDI Contracts Nos. PN-II-ID-PCCE-2011-2-0006 and PN-II-RU-TE-2014-4-0456.

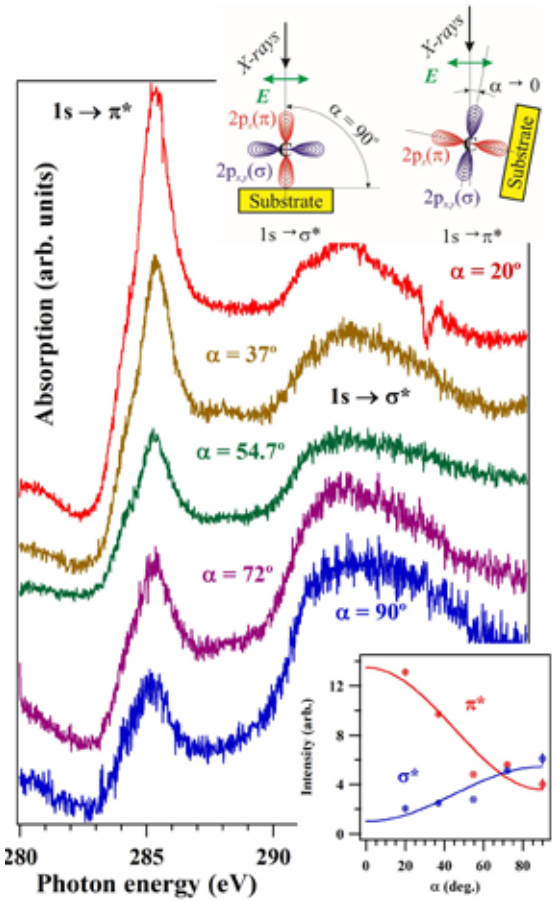

Fig. 3: Near-edge absorption fine structure at the C K-edge vs. the incidence angle for coverage 1 C atom / 3.49 Å² of PZT. Adapted from [7].

References

[1] F. Schwierz, Nat. Nanotechnol. 5, 487–496 (2010).

[2] X. Hong, A. Posadas, K. Zou, C. H. Ahn, J. Zhu, Phys. Rev. Lett. 102, 136808 (2009).

[3] A. Rajapitamahuni, J. Hoffman, C. H. Ahn and X. Hong, Nano Lett., 13, 4374–4379 (2013).

[4] L. Pintilie, M. Alexe, J. Appl. Phys. 98, 124103(1-8) (2005).

[5] X. Hong, J. Hoffman, A. Posadas, K. Zou, C. H. Ahn and J. Zhu, Appl. Phys. Lett. 97, 033114 (2010).

[6] E. B. Song, B. Lian, S. M. Kim, S. J. Lee, T.-K. Chung, M. S. Wang, C. F. Zeng, G. Y. Xu, K. Wong, Y. Zhou, H. I. Rasool, D. H. Seo, H.-J. Chung, J. S. Heo, S. N. Seo and K. L. Wang, Appl. Phys. Lett. 99, 042109 (2011).

[7] N.G. Apostol, G.A. Lungu, I.C. Bucur, C.A. Tache, L. Hrib, L. Pintilie, D. Macovei, C.M. Teodorescu, RSC Adv. 6, 67883-67887 (2016).

Influence of single-walled carbon nanotubes enriched in semiconducting and metallic tubes on the vibrational and photoluminescence properties of poly(para-phenylenevinylene)

M. Baibarac, I. Baltog, M. Ilie, C. Negrila

National Institute of Materials Physics

in collaboration with B. Humbert and S. Lefrant, Institut des Materiaux Jean Rouxel, Nantes, France

The electrochemical reduction of α,α,α′,α′-tetrabromo-p-xylene (TBPX) in the presence of single-walled carbon nanotubes (SWNTs), as mixutes of semiconducting and metallic tubes (M+S) as well as highly separated metallic (M, 98%) and semiconducting (S, 99%) entities, is used to obtain composites of carbon nanotubes (CNTs) functionalized with poly(para-phenylene vinylene) (PPV) (Fig. 1).

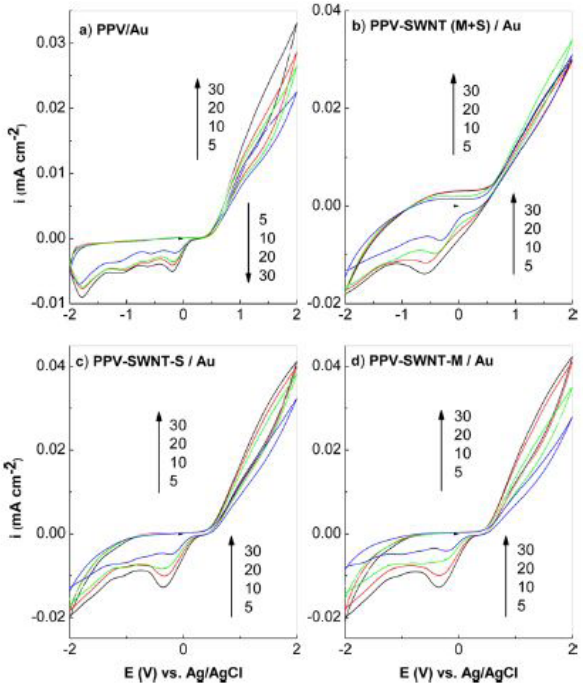

Fig. 1: Cyclic voltammograms recorded onto the blank Au electrode (a) and on the rough Au supports covered with films of M+S (b), S (c) and M (d), when working electrodes were immersed into a solution of 0.02 M TBPX and 0.1 M tetrabuthyl ammoniul bromide (TBAB) in dimethylformamide (DMF). Blank, red, green and blue curves correspond to the 5th, 10th, 20th and 30th cycles, respectively. [1]

As observed in Figs. 2 and 3, an enhancement of the Raman line peaked at 1174 cm^{-1} is observed in the case of PPV synthesized in the presence of M+S, in comparison with PPV synthesized in the presence of S. This behaviour is induced by the surface plasmons (SPs) generated at the PPV/metallic CNTs interface. Variations of the Raman spectra in the spectral range of the RBM and TM bands indicate that the electroreduction of TBPX in the presence CNTs leads to a shielding effect of S and an isolation of the metallic individual tubes from M bundles.

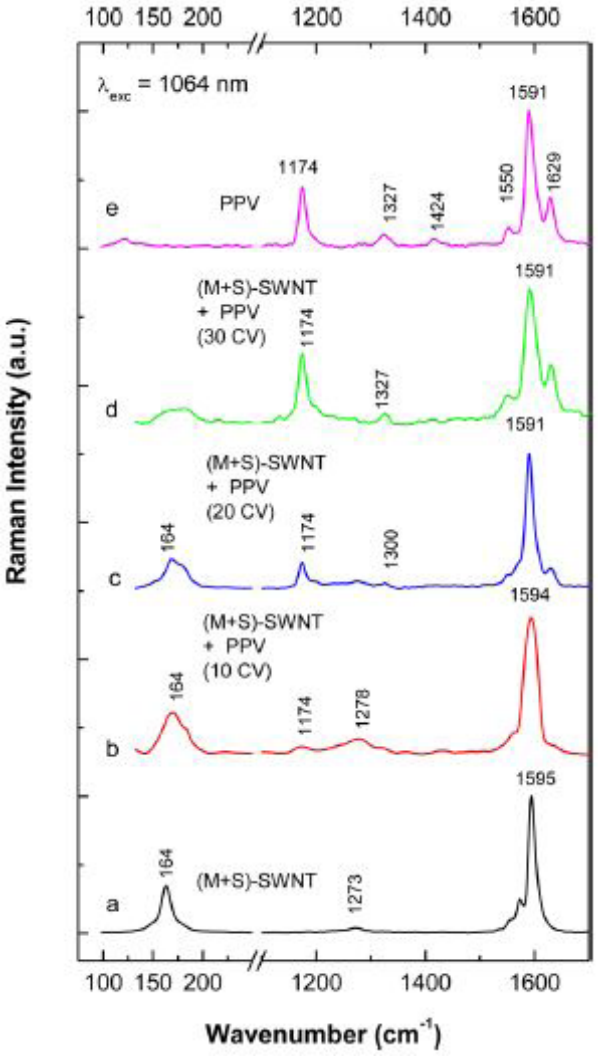

Fig. 2: Raman spectra, recorded at λ_{exc} = 1064 nm, of M+S (a) and its composites obtained by performing 10 (b), 20 (c), and 30 (d) cyclic voltammograms in the presence M+S. The solution consists in 0.02 M TBPX and 0.1 M TBAB in DMF. Panel e corresponds to the Raman spectrum of the PPV film. [1]

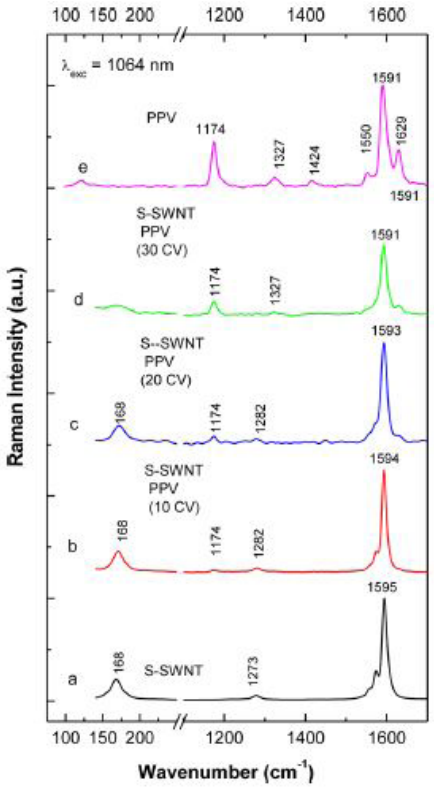

Fig. 3: Raman spectra, recorded at λ_{exc} = 1064 nm, of S (a) and its composites obtained by performing 10 (b), 20 (c), and 30 (d) cyclic voltammograms in the presence S. The solution consists in 0.02 M TBPX and 0.1 M TBAB in DMF. Panel e corresponds to the Raman spectrum of the PPV film. [1]

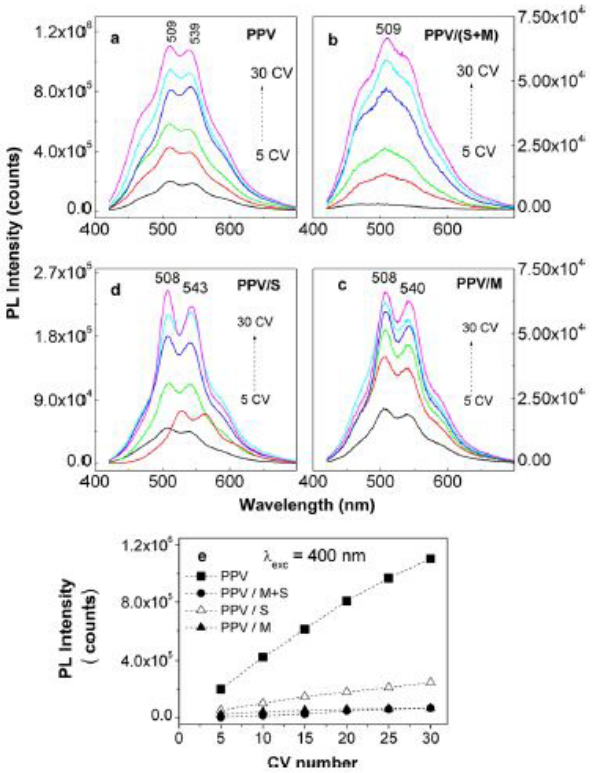

Fig. 4: PL spectra of PPV synthesized onto the blank Au support (a) and in the presence of M+S (b), M (c), and S (d) by carrying out 5 (black curves), 10 (red curves), 15 (green curves), 20 (blue curves), 25 (cyan curves), and 30 (magenta curves) cyclic voltammograms. Panel e shows PL intensity of PPV electrosynthesized onto the blank Au support (black squares) and in the presence of M+S (black circles), M (black triangles) and S (open triangles) as a function of cyclic voltammograms number. [1]

The photoluminescence (PL) spectrum of PPV electrosynthesized onto a blank Au support shows four emission bands that peaked at 2.66, 2.44, 2.28, and 2.1 eV; the first three are assigned to the electronic emission transitions of macromolecular chains (MCs) that have lengths of 4, 5, and 7–10 repeating units (RUs), the last of which corresponds to the vibronic replica of the first order of the PL band at 2.44 eV. [2] The electroreduction of TBPX in the presence of M+S, M, or S induces a reduction of the formation of PPV MCs with lengths of 7–10 RU of ~36% without a change in the weight of the PPV MCs that have a length of 5 RU; a decrease of nearly twice the probability of forming PPV MCs that have lengths of 4 RU is also reported in the presence of M or S.

Funding from the CNCS-UEFISCDI, Module III Bilateral Cooperation, Humbert Curien-Brancusi Project, 1027/ 26.06.2014.

References

[1] M. Baibarac, I. Baltog, M. Ilie, B. Humbert, s. Lefrant, C. Negrila, Influence of single-walled carbon nanotubes enriched in semiconducting and metallic tubes on the vibrational and photoluminescence properties of poly(para-phenylenevinylene). J. Phys. Chem. C 120, 50941 (2016).

[2] J. Wery et al., Photoexcitation in composites of poly(paraphenylene vinylene) and single-walled carbon nanotubes, Phys. Rev. B 67, 115202 (2003).

Exciton-phonon interaction in CdS of different morphological forms manifested as stimulated Raman scattering

M. Baibarac, A. Nila, I. Baltog

National Institute of Materials Physics

Raman studies performed on CdS samples with different morphologies indicate an exciton-phonon interaction (EPI) that manifests by different enhancements in intensity of the Raman spectra in the Stokes (S) and anti-Stokes (aS) branches. This effect, interpreted as stimulated Raman effect (SRS), is conditioned of the degree of overlap of the excitation light with the photoluminescence (PL) band [1]. In this context, Fig. 1 shows different overlapping areas of the Stokes and anti-Stokes Raman branches over the PL band of CdS.

Considering only the Stokes branch, it becomes immediately apparent that under excitation light situated at wavelengths less than the PL maximum, as in the case of laser light of 458 and 476 nm, the area associated with the Stokes branch is higher than in the case where the laser light is situated at higher wavelengths of 488, 496 and 514 nm, for which the ratio I(300 cm^{-1})/I(Ω cm^{-1}) at 88 K decreases exponentially toward the Raman lines of high order.

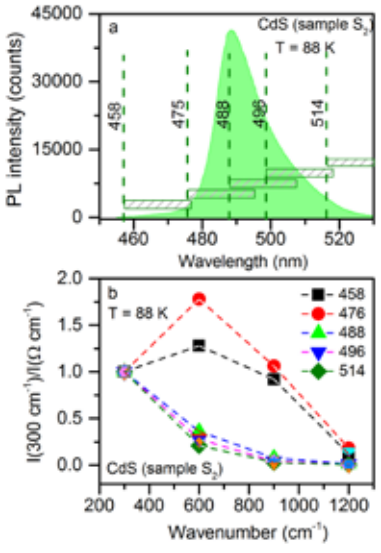

Fig. 1: (a) PL band profile at 88 K of CdS over which are shown the laser excitation lines accompanied by Stokes Raman spectrum related fields (hatched area); (b) Raman intensity ratio I (300 cm^{-1})/I(Ω cm^{1}) of CdS at 88K under different excitation laser lights. Ω indicates the CdS Raman lines situated at 305, 610, 915, and 1220 cm^{-1}.[1]

In condition of resonance, $\sigma(\alpha\Omega)_{aS} \neq \sigma(\alpha\Omega)_{S}$ so that the deviations of the I_{aS}/I_{S} ratio from the Boltzmann law may reveal the occurrence of a nonlinear optical process [2]. In this context, Fig. 2(a) becomes very suggestive, showing how the Raman branches associated with different laser lines cut out unequal areas from the PL band, which is visualized by the different enhancements of the Raman lines in the S and aS branches. In the case of the excitation wavelength of 488 nm, Fig. 2(b), the calculated aS Raman spectrum is more intense than the recorded Raman spectrum, the fact which can be explained by a higher enhancement in the originating S branch due to the larger area of the PL band located in the S and aS ranges. As observed in Fig. 2(c), for the excitation wavelength of 514 nm, the situation is reversed: the anti-Stokes emission is more intense than the calculated Raman spectrum, which means that the PL area located in the aS range is greater than the PL area located in the S range.

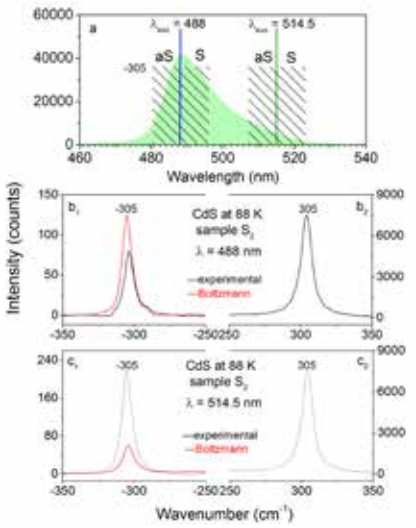

Fig. 2: (a) PL band over which are marked the laser light at 514 and 488 nm, flanked by hatched areas associated with the S and aS Raman branches. (b_1;c_1 and b_2;c_2) Raman line at 305 cm^{-1} in aS and S branch under laser light at 488 and 514.5 nm. Black and red curves show the recorded and calculated Raman spectra with the Boltzmann formulae applied to the S branch.[1]

In the above conditions, the EPI appears as an optical phenomenon resulting from the mixing

of the two optical fields, namely the excitonic photoluminescence and the exciting laser light.

A priori, the achievement of such a process must depend on the effectiveness of overlapping of the two optical fields, which can be performed energetically and geometrically, that is, under a coincidence of the laser excitation light with the PL excitonic band and a superposition of the two light fields, which is more efficient in highly diffusive media. Based on this reasoning, the studies are done on three types of samples: S_1 (single crystal) S_2 (micrometric crystalline powder) and S_3 (this film), the first being characterized by a very low light scattering power and the last by a very small quantity of material submitted to optical excitation. The expectations are confirmed by the following results shown in Fig. 3:

(**a**). Due to the lack of defects the single crystal S1 sample shows an intense and narrow excitonic emission band that results from the dominant contribution to the radiative recombination of free excitons and is less scattered in the volume of the sample. In Figs. 3(b) and 3(c), the contribution of bound excitons and the size of the optically excited CdS particles found in samples S_2 and S_3 is illustrated by a widening towards the low-energy side of the excitonic PL band, which in turn determines a different enhancement along the S Raman spectrum, clearly highlighted in the case of the S_2 and S_3 samples;

(**b**). In a strongly diffusive medium, such as sample S_2, each particle is subjected simultaneously to the laser exciting light and PL excitonic light originating from a neighboring particle, which can mix together. In this context, the scattering of light in all directions extends the optical path length inside the material so that the probability of the light interacting with the matter increases. Therefore, a nonlinear optical effect such as SRS revealed by an enhancement of Raman intensity as a signature of EPI becomes a very tempting mechanism to invoke.

(**c**). Greater width of PL spectrum of S_3 sample is a consequence of granular structure formed by nanometric or micrometric size particles that induce a larger amount of defects which are involved in an up-shifted bound excitonic PL whose emission is less coherent. This, together with the nanometric thickness of the film of CdS, makes another reason for achieving a constructive mixing of the two optical fields for which the enhancement of Raman intensity is approximately 60 times less than the other two samples (Fig. 3(c)).

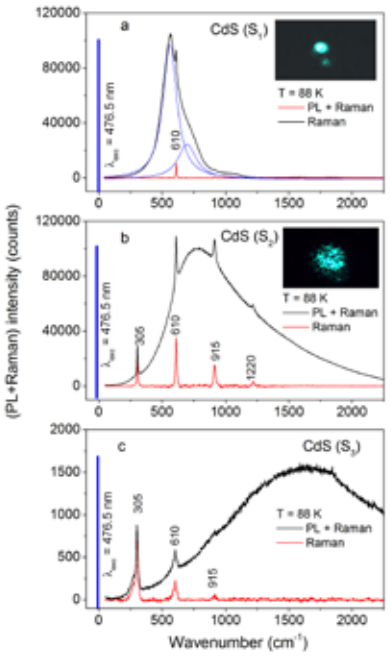

Fig. 3: Influence of the sample morphology on the EPI that manifests in an enhancement of Raman intensity for the CdS samples (S_1 (a), S_2 (b) and S_3 (c)). Black curves show the emission spectra at 88 K, over which the Raman contribution is superposed. Red curves are the Raman spectra obtained by subtraction of the PL band. Blue curves indicate two components in the PL band of S1. [1]

Considering the different enhancement of the Raman lines in the S and aS branches, as long as the dependence of the Raman intensities on the sample morphology, it is tempting to propose the SRS effect for explaining the strength of EPI, which result from the mixing of two coherent optical fields: the laser pump light and PL light, which plays the role of S and aS Raman shift.

Funding from the Romanian National Authority for Scientific Research, CNCSUEFISCDI, project PN-IIIDPCE-2011-3-0619

References

[1] M. Baibarac, A. Nila, I. Baltog, Exciton-phonon interaction in CdS of different morphological forms manifested as stimulated Raman scattering, Opt. Mat. Express 6, 1881 (2016).

Polarized Raman spectra of phosphorene in edge and top view measuring configurations

M. Baibarac, A. Nila, I. Baltog

National Institute of Materials Physics

Phosphorene (P), a new 2D layered crystalline material, can exceed the performance of crystal graphene layers in terms of interesting anisotropic vibrational optical properties [1]. Raman scattering can be successfully used to study dependent vibrational modes (A_{1g}, B_{2g} and A_{2g}) in the edge and top view configurations as a function of two orthogonal polarizations of incident light. A comprehensive study regarding the strongly anisotropic character of P in both edge and top view configurations is conducted.

The crystal structure orientation in the edge view of multi-layer P is shown in Fig. 1a (left), where the L polarized light is along the X axis, which coincides with the armchair direction, and the T polarized light is oriented along the Z axis.

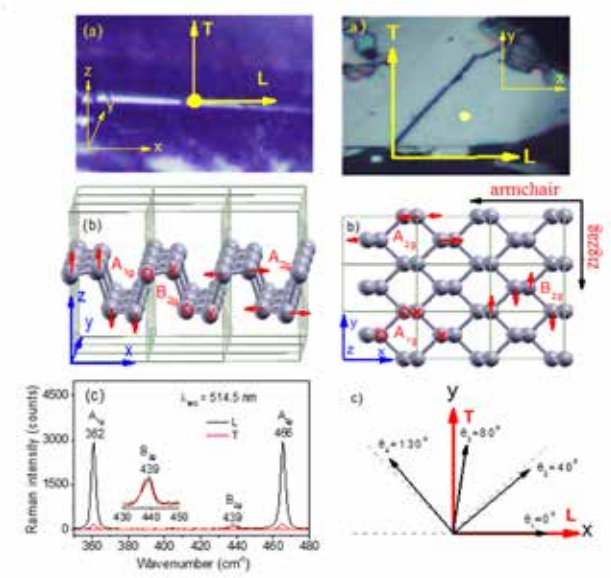

Fig. 1: (a) Edge (left) and top (right) configurations of P. In (b), the edge (left) and top (right) configurations of P and the three ideal Raman modes directions are outlined. In (c)-left, the Raman spectra at room temperature (RT) is showed for the edge configuration under an incident light of 514.5 nm, with L-polarized light along the X-axis (black curves) and T-polarized light parallel to the Z-axis (red curves). In (c)-right, the sample rotation angle at θ_1=0°, 40°, 80° and 130° relative to the orientation of the L and T electric field directions is showed. [2]

The typical Raman modes under two orthogonal polarizations L and T of the incident laser light of 514.5 nm, considering the armchair edge view configuration of P, are outlined in Fig. 1c (left). As can be seen, the A_{2g} mode is activated in edge view configuration only by the optical electric field direction of L polarized laser light (black curve from Fig. 1c (left)). Evaluating the intensity ratio $I_{A2g(L)}/I_{A2g(T)}$, one observes that the A_{2g} mode is ~ 15 times more enhanced in the case of excitation light polarized along the layers (black curve) than in the transverse direction (red curve), which is consistent with the orientation of the crystalline structure of P relative to the optical electric field direction. The layer-to-layer arrangement of the P structure determines stacking faults effects with a strong influence on the A_{1g} out-of-plane mode, when unexpected behavior in both polarizations is observed [2]. The natural changes of the periodic atomic planar layers relative to one another due to the increase of entropy from strain induced is a general issue of the layered structures, which concerns central force potentials with a distortion impact on the natural behavior of the Raman modes.

The oscillation of the B_{2g} mode corresponds to the Y direction. For this reason, in the armchair edge configuration (Fig. 1b (left)), B_{2g} mode is almost inactive in both L and T configurations.

Fig. 1 (right) reveals a plate sample chosen in an XY plane view, which was rotated around the yellow dot that denotes also the spot of the incident laser light propagating along the Z-axis. In this context, we reveal Raman studies under an excitation laser light of 514.5 nm in the top view configuration, performed under L and T polarization of excitation light, for the same sample as in the case of the edge view, but rotated counter clockwise at different angles (0°, 40°, 80°, 130°, denoted as Q_1, Q_2, Q_3 and Q_4) relative to the L and T directions, which are kept in the same initial position every time. Therefore, to explore the different signatures

of the combined armchair and zigzag crystalline directions, Fig. 2 reveals Raman studies in the top view of P.

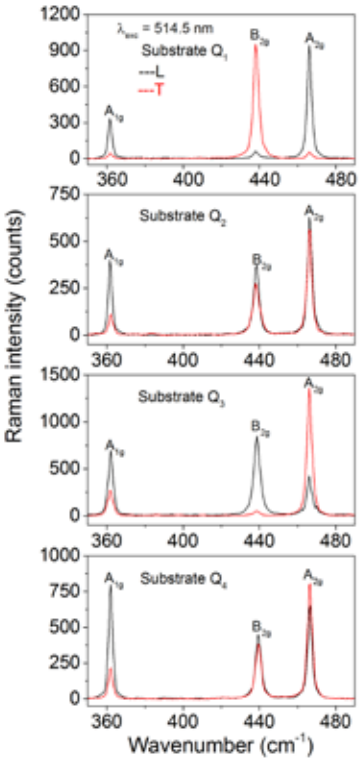

Fig. 2: Raman spectra in the top view of P under the excitation light of 514.5 nm, at different in plane angles of rotation of the sample: θ_1=0° (Q_1), θ_2=40° (Q_2), θ_3=80° (Q_3) and θ_4=130° (Q_4) in two experimental configurations of the polarized light, L (black curve) and T (red curve). [2]

The unusual behaviour of the Raman scattering depicted by the A_{1g} vibrational mode in both the L and T polarizations is also shown in the top view configuration due to the stacking faults effects. At θ_1=0° (Q_1), where the L and T polarizations are oriented along the armchair and zigzag directions, Fig. 2a indicates a higher intensity of A_{2g} and B_{2g} for L and T, respectively, due to the condition of orthogonality established between the two Raman modes. In Fig. 2b and 2d, i.e., the Raman spectra at θ_2=40° and 130° (Q_2 and Q_4), mixing signals collected from both the armchair and zigzag directions are shown, where the intensities in the L and T electric field directions manifest approximately equally in both A_{2g} and B_{2g}. The sample rotated at θ_3=80° gives the Raman spectra in Fig. 2c, where the intensities of the A_{2g} and B_{2g} lines are increased again but in an opposite manner compared with the case of Q_1. A summary of the above result is displayed in Fig. 3, which highlights that the A_{2g} and B_{2g} Raman modes show a quadratic dependence on the sample rotation angle with an inverse parabola depending on L and T polarization configurations.

The A_{1g} mode highlights an increase in intensity due to the change in L and T polarizations of excitation light and should be explained by the coupled out-of-plane and in-plane oscillations, with a larger component signal in the L polarized direction, which depends on the local stacking faults of the material, as was described in detail earlier.

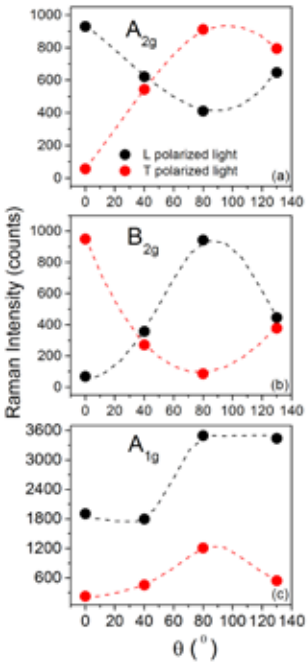

Fig. 3: Raman intensity dependence of sample rotation angle in the three Raman modes: a) A_{2g}; b) B_{2g}; c) A_{1g} in both polarized light configurations under an excitation laser light of 514.5 nm. [2]

Funding from the Romanian National Agency for Scientific Research and Innovation, project no. PN 10N/2016.

References

[1] H. Liu, et al., Phosphorene: an unexploed 2D semiconductor with a high hole mobility, ACS Nano 8, 4033 (2014).

[2] M. Baibarac, A. Nila, I. Baltog, Polarized Raman spectra of phosphorene in edge and top view measuring configurations, RSC Advances 6, 58003-58009 (2016).

$La_{.67}Ba_{.33}Ti_{.02}Mn_{.98}O_3$ epitaxial thin films grown on 001-oriented $SrTiO_3$: Structure, Magnetic properties and Magnetocaloric effect

A.C. Galca, I. Pasuk, C.F. Chirila, A. Leca, V. Kuncser, L.C. Tanase, A. Kuncser, C. Ghica

National Institute of Materials Physics

in collaboration with Ma. Oumezzine, Mo. Oumezzine, University of Monastir, Tunisia

There has been an extensive search for the materials exhibiting magetocaloric effect (MCE), which can be used for efficient magnetic cooling near room temperature. Although that most of current research in this field is limited to bulk perovskite-type manganese oxide materials, the thin films are also of interest for functional micro/ nano scale devices for magnetic refrigeration.

The epitaxial thin films, with thicknesses close to 100 nm were grown on (001) $SrTiO_3$ substrates by ablating a $La_{.67}Ba_{.33}Ti_{.02}Mn_{.98}O_3$ (LBTMO) ceramic target. The stoichiometry of the LBTMO film surface has been determined by X-ray photoelectron spectroscopy (XPS),this being $La_{.69}Ba_{.31}Ti_{.03}Mn^{3+}_{.80}Mn^{4+}_{.17}O_x$.

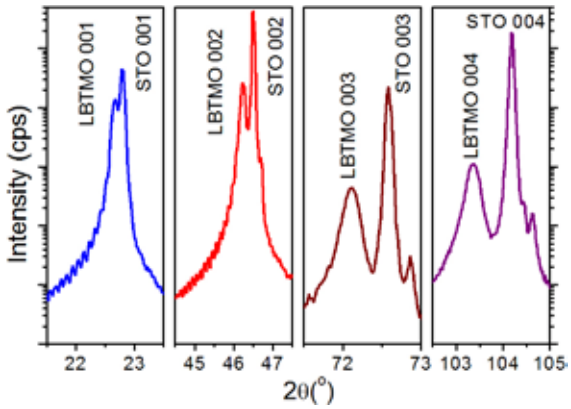

Fig. 1: a) Typical 2θ–ω scans of LBTMO thin film deposited on STO (001);

The X-ray diffraction pattern acquired in coplanar geometry is shown in Fig. 1. The film has a strong out-of plane texture, reflecting only from the (*00l*) crystallographic planes, the ordering being strengthened also by rocking curves [1]. The Bulk LBTMO target is a distorted perovskite with a pseudo cubic lattice parameter of 3.913 Å. The STO substrate (a_{STO} = 3.905 Å) should impose an in-plane compressive stress on LBTMO owing to the small lattice mismatch of ~ +0.2%, which is reflected in a larger c lattice parameter (3.928 Å). Around the 001 and 002 reflections, the Pendellosung fringes are clearly visible, and they indicate the high crystalline quality of the LBMTO layer and the atomic level smoothness of the corresponding interfaces. The epitaxial nature of the film is further confirmed by azimuth scans (ϕ-scans) on the skew planes [1]. From the reciprocal space mapping comprising the -103 nodes, it was found that $a_{LBTMO} = a_{STO}$ = 3.905 Å, with no evidence of strain relaxation toward the film surface.

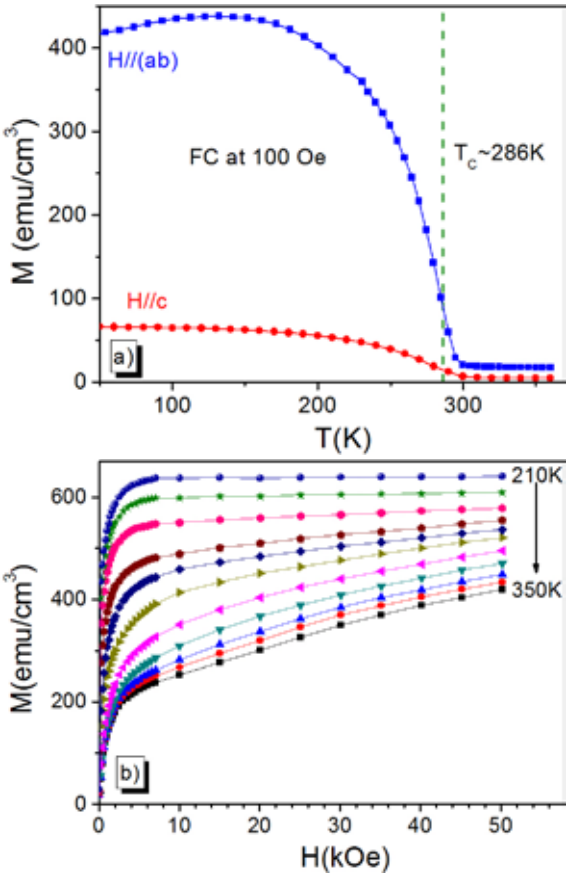

Fig. 2: a) Plots of FC magnetization of LBTMO thin film, measured under a magnetic field of 0.01 T along the (ab) plane and c direction. b) Magnetization vs. applied magnetic field measured at different temperatures.

As inferred from Fig.2a, LBTMO film grown on STO substrate exhibits a sharp para-to-ferrromagnetic (PM-FM) phase transition, while a transition temperature is estimated (T_C=286K).

Isothermal magnetization (M(H)) is recorded and shown in Fig. 2b. The magnetization increases rapidly at low fields and saturates at higher field

values, typical for a ferromagnetic behaviour.

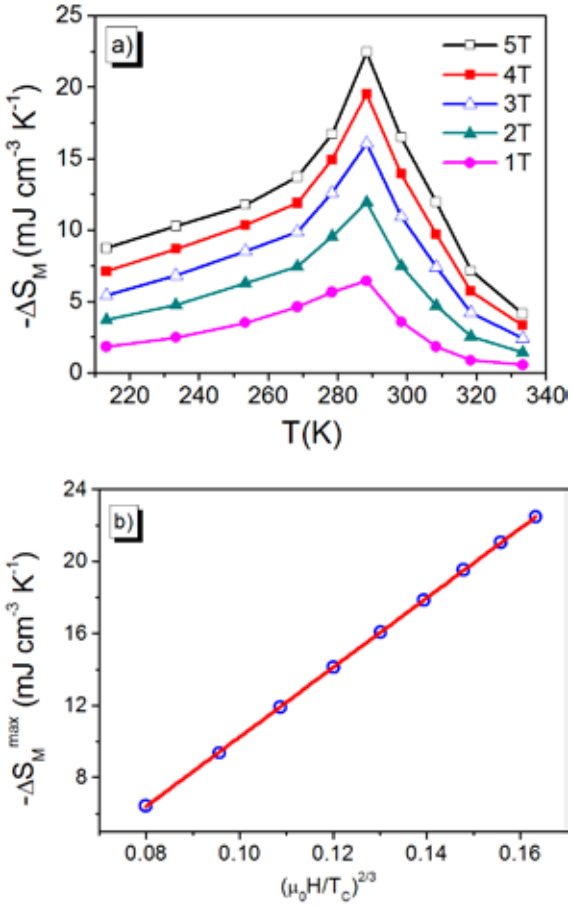

Fig. 3: a) The temperature dependence of the magnetic entropy change around the Curie temperature under different applied magnetic fields. b) Dependence of the magnetic entropy change on the parameter $(\ _0H/T_C)^{2/3}$. The solid line represents a linear fit of the data.

It is observed from Fig.3a that the peak of magnetic entropy change ($-\Delta S_M$) is close to the magnetic transition temperature. The peak value increases by increasing the field and attains a maximum value of 22.45 mJ/(cm^3 K) (3.35 J/(Kg K)) for a field change of 50 kOe, being about one third of the value for bulk Gd (the prototype magnetic refrigerant material). This value is slightly higher than those reported for $La_{.67}Ba_{.33}MnO_3$, $La_{.67}Sr_{.33}MnO_3$ and $La_{.67}Ca_{.33}MnO_3$ thin-films.

The magnetic cooling efficiency of a material is evaluated by considering the Relative Cooling Power (RCP), which is defined as the product of ΔS_M^{max} and the corresponding Full width at Half Maximum (FWHM) of the ΔS_M versus T. From the viewpoint of applications, it is very beneficial to obtain a large magnetic entropy change and a high RCP. At a ΔH of 50 kOe, the RCP of presented LBMTO thin film is 220J/Kg, which is about 55% of the RCP for pure Gd under similar conditions. The obtained value is higher than the observed and reported in manganite thin films, such as $La_{.56}Sr_{.44}MnO_3$, $La_{.67}Sr_{.33}MnO_3$, or $La_{.7}Sr_3MnO_3$ on $SrRuO_3$ superlattices, and $Gd_5(Si,Ge)_4$ thin films. On the other hand, in comparison with the bulk counterpart, LBTMO thin film presents a lower RCP and a smaller T_C, most probably due to strain effects and small stoichiometry differences.

In Fig.3b is shown the dependence of the magnetic entropy change on $(\ _0H/T_C)^{2/3}$. The mean-field theory predicts that in the vicinity of second-order phase transitions, ΔS_M^{max} is proportional to $(\ _0H/T_C)^{2/3}$. The linear fit of the data in figure 4 (b) clearly demonstrates that the relationship $\Delta S_M^{max} \infty (\ _0H/T_C)^{2/3}$ is valid, in agreement with the conclusion that the magnetic interaction between Mn^{3+} and Mn^{4+} in epitaxial LBMTO film is governed by long-range ordering interactions.

Funding from Romanian Ministry of Education (PN-II-ID-PCCE-2011-2-0006 project and core program PN-III-16-480102) and the Tunisian Ministry of Higher Education and Scientific Research.

References

[1] Ma. Oumezzine, A.C. Galca, I. Pasuk, C.F. Chirila, A. Leca, V. Kuncser, L.C. Tanase, A. Kuncser, C. Ghica, Mo. Oumezzine, Dalton Trans., 45, 15034-15040, 2016.

Multilayer thin film structures for studying re-deposition effects on plasma facing components

S.G Greculeasa, G. Schinteie, P. Palade, G. Lungu, I.S. Ghita, G. Filoti, V. Kuncser

National Institute of Materials Physics

in cooperation with C.P. Lungu, C. Porosnicu, and I. Jepu, National Institute for Laser, Plasma and Radiation Physics, 77125, Magurele, Romania

Plasma facing components (PFCs) [1] are complex materials envisioned for operation in extreme temperature and irradiation conditions in nuclear fusion reactors. Tungsten-based materials, presenting low sputtering yields under ion bombardment, high melting point, good thermal conductivity, low tritium retention, are good candidates for PFCs. However, their impact on the plasma core is significant. On the other hand, light elements such as Be, present low influence on the plasma core but have high sputtering yields.

Therefore, a viable approach for the top structure of the PFCs would be a heterostructure composed of these two materials with very distinct behavior. The mechanical properties of the top layers, which are greatly affected by high temperatures can be improved by using special reduced-activation ferritic-martensitic (RAFM) steels (e.g., Eurofer), as underlayers [2].

In order to give more insight into redeposition processes possible to occur in PFCs, investigations of atomic intermixing in specifically designed thin films and multilayers represent a suitable approach. In this respect, thin Fe and Fe-rich alloys (Fe-Cr and Fe-Cr-Al) thin films were sputtered on Si substrates [3] and subsequently subjected to a hydrogenation treatment. Be/W and W/Be bilayers were subsequently deposited by TVA on the Fe-based films [4]. Complex characterizations were made by grazing incidence XRD, XRR, XPS, MOKE and Mössbauer spectroscopy (CEMS).

The as deposited Fe-based films present magnetic texture, in accordance to Stoner-Wohlfarth model, due to an island type grow mechanism (Volmer-Webber), contrary to the hydrogenated films (see Fig.1 left and middle). Well crystallized bcc Fe films are evidenced in the CEM spectra (Fig.1 right) after hydrogenation. The reduction of the Cr content after hydrogenation treatments was also evidenced by X-ray photoelectron spectroscopy in one of our previous studies on binary Fe0.89Cr0.11 thin films [5]. The weak central doublet assigned to a superparamagnetic Fe oxide decreases its relative contribution to only 14% in the case of the Si/Fe hydrogenated sample and 7% in the Si/Fe-Cr-Al sample.

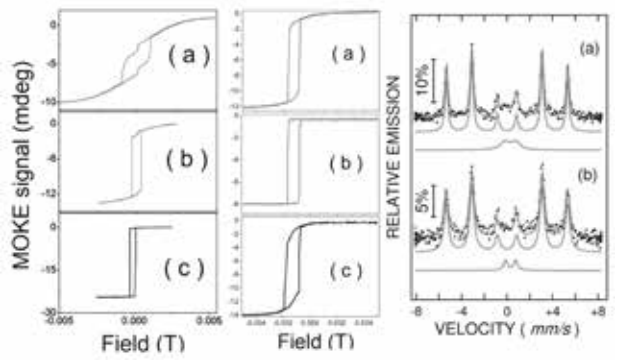

Fig. 1: Longitudinal MOKE loops, collected on the as deposited (left) and hydrogenated (middle) Si/Fe sample at different azimuthal angles: (a) θ = 90°, (b) θ = 45°, (c) θ = 0°. CEM spectra (right) of hydrogenated films: a) Si/Fe, b) Si/Fe-Cr-Al.

After the bilayer deposition, the XPS spectra (Fig.2) clearly evidence strong intermixing and oxidation, especially in the upper part of the films. Be is present in both neutral and oxidized states (BeO) at all investigated etching depths. The two W peaks, 4f7/2 and 4f5/2, are well resolved with a high spin-orbit splitting, showing neutral phases. The W concentration decreases drastically from 40 nm. The Fe peaks are in a reduced amount at etching depths between 1 and 27 nm. The Fe content increases considerably at 31 nm, and even more starting from 34 nm, correlated with the drastic decrease of W content, indicating a W/Fe interface with atomic intermixing.

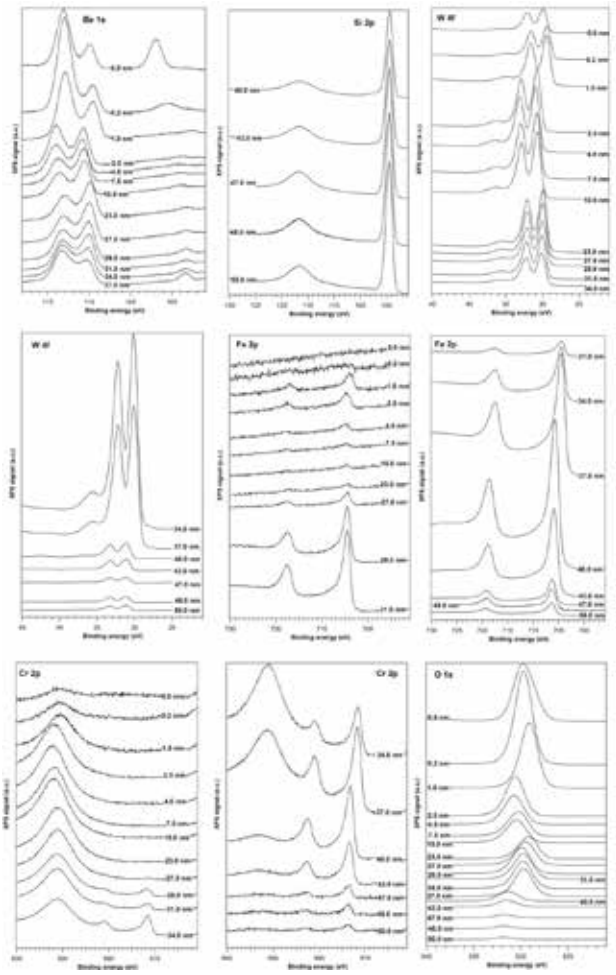

Fig. 2: XPS spectra of sample Fe0.89Cr0.11/Be/W_h.

The Cr peaks are seen starting from 29 nm and reveal the neutral phases in Cr 2p1/2 and 2p3/2 state. The Cr content decreases sharply at 47 nm, where Si signals are prevailing. As a consequence, it is observed that there is a relatively sharp Fe-Cr/Si interface, because both Fe and Cr signals decrease considerably at 47 nm, though Si is present even at 40 nm.

Most of the corresponding Mössbauer spectra (Fig.3) show clearly the presence of metallic a-Fe phase and superparamagnetic Fe oxides, as well as phases of Fe in the metallic structure with Si, Cr, W and Be neighbors and Fe-Si phases. No Fe-Be and Fe-W compounds are observed.

However, a higher amount of tungsten and oxygen atoms is provided by the XPS data also at the depth specific to the Fe layer. Only a few percents of Fe_2O_3 phases were evidenced from the Mössbauer spectra, whereas a ratio of O/Fe about 3 was derived from XPS data. Therefore, in addition to the Fe oxide phases, we may assume the formation of tungsten oxides in the Fe layer.

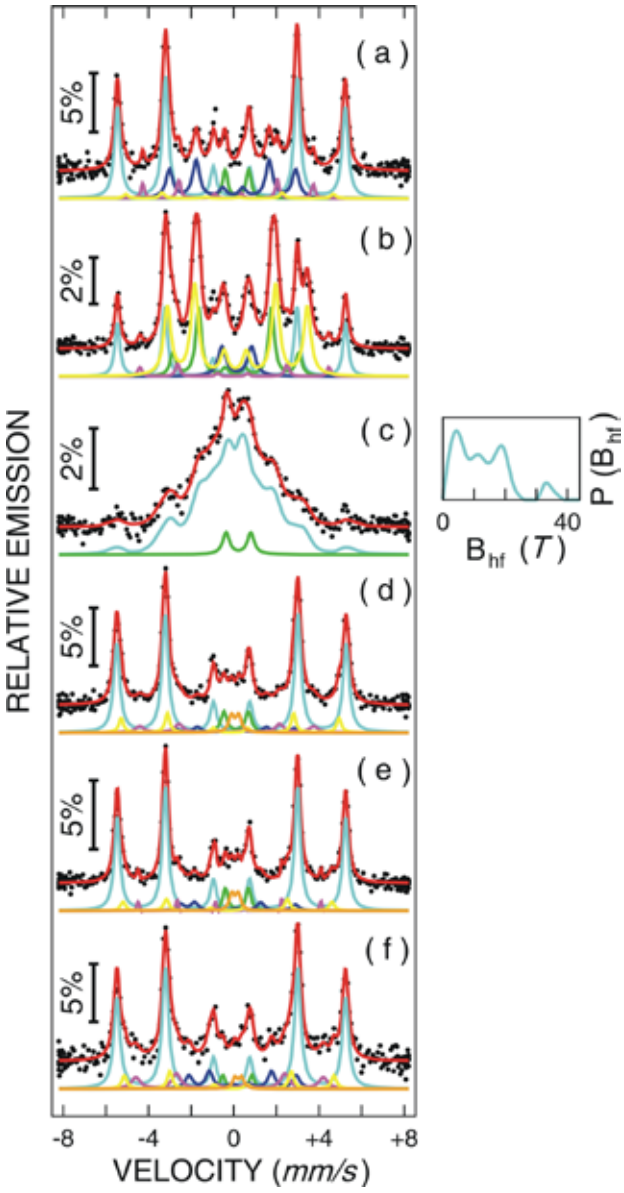

Fig. 3: CEM spectra of samples: (a) Si/Fe/Be/W, (b-d) Si/Fe/W/Be, $Fe_{0.89}Cr_{0.11}$/Be/W, $Fe_{0.89}Cr_{0.11}$/Be/W_h and (e-f) $Fe_{0.89}Cr_{0.11}$/W/Be_h and $Fe_{0.84}Cr_{0.11}Al_{0.05}$/Be/W_h.

The strong atomic intermixing in the top structures of W and Be layers (with a high amount of W overall in the effective structure, including the Be layer) is clearly supported by the XPS data.

References

[1] R.A. Pitts et al, J Nucl Mater 415 (2011) S957.

[2] J.B. Whitley, et al, J Nucl Mater 155 (1988) 82.

[3] S.Greculeasa, G.Schinteie, P.Palade, G.Filoti, I.Ghita, V.Kuncser, Rom Rep Phys 68 (2016) 249.

[4] S.Greculeasa, P.Palade, G.Schinteie, G.Lungu, C.Porosnicu, I.Jepu, C.Lungu, V.Kuncser, J Nucl Mater 481 (2016) 73.

[5] S.Greculeasa, G.Schinteie, P.Palade, G.Filoti, L.Trupina, G.Lungu, O.Crisan, V.Kuncser, Adv Alloy Compound 1 (2014) 30.

Critical-state related AC magnetic response of superconducting thin films

L. Miu, I. Ivan, A. M. Ionescu, and A. Crisan

National Institute of Materials Physics

The AC magnetic response of superconductors at usual frequencies f and amplitudes h_{AC} is not completely understood. The activation energy U_{AC} derived from the analysis of the temperature T variation of the critical-state related AC magnetic signal in terms of thermally activated vortex hopping takes surprisingly high values in the vicinity of the DC irreversibility line (IL) [1, 2]. At low external magnetic fields H_{DC}, U_{AC} attains 10^3–10^4 K ($k_B = 1$), and remains high even deeply in the vortex liquid phase. This is essentially different from the behavior of the vortex-creep activation energy U in the vortex diffusion process at long relaxation time t scales [3]. Around IL, associated with the vortex solid-liquid transition, the renormalization of the pinning potential by thermally induced vortex fluctuations leads to $U \sim T$. The existence of a "pinned" vortex liquid is usually explained as due to the viscosity of the vortex system, resulting from vortex entanglement, cutting and reconnection [3]. However, we obtained high U_{AC} values even for almost decoupled YBCO/PrBCO superlattices [4], with the thickness of the superconducting and non-superconducting blocks of four unit cells, where the vortex system is surely disentangled.

The widely accepted extension of the vortex diffusion (flux creep) at short t scales cannot explain the large differences between U_{AC} and U. We proposed a new approach for the AC magnetic response [4, 5], in which the large U_{AC} values in the vicinity of the IL are generated by a non-diffusive vortex motion during the AC cycle, with the mean vortex hopping length overcoming the average distance between the pinning centers. In these conditions, the thermal smearing of the pinning potential is weak, owing to a short pinning time, and U_{AC} results from the strong influence of the pinning enhanced viscosity to the vortex hopping process.

For a quantitative analysis, we registered (using a PPMS) the AC response of YBCO films with embedded BZO nanorods and Y_2O_3 nanoparticles [5], where the average spacing between the pinning centers of ~10 nm [6].

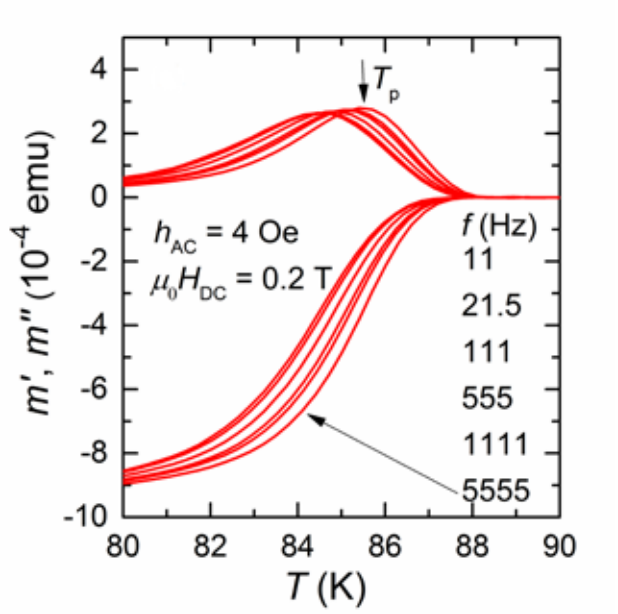

Fig. 1: Temperature dependence of the in-phase (m′) and out-of-phase (m″) components of the AC magnetic moment in increasing T (after the YBCO film was cooled from above T_c to 80 K) with the AC field amplitude h_{AC} = 4 Oe at various frequencies f ($\mu_0 H_{DC}$ = 0.2 T). The peak temperature T_p indicated in by an arrow shifts to lower values by decreasing f. The DC and AC fields where oriented perpendicular to the film surface.

The AC response of the investigated film (with the thickness d = 400 nm) is presented in Fig. 1, where $| m' |^{2/3} \propto J$, the screening current density at full critical state penetration, whereas m″ (the dissipative component) becomes maximum at the peak temperature T_p (first full critical state penetration starting from low T). As exemplified in the inset of Fig. 2, ln(f) vs. $1/T_p$ is linear, supporting a thermally activated vortex hopping process, according to the Arrhenius law $f = f_0 \exp[-U_{AC}(J_p, T_p)/T_p]$, with $U_{AC}(J_p, T) = U_0(J_p)(1 - T/T_c)$. A linear fit supplies the attempt frequency f_0 and U_0, the apparent U_{AC} at T = 0 and $J = J_p = 1.02 h_{AC}/d$. Concerning the U_{AC} value, for $m_0 H_{DC}$ = 0.2 T and h_{AC} = 4 Oe, as an example, one has $U_0 = 4.58 \times 10^4$ K, and $f_0 \sim 7 \times 10^{10}$ Hz. For the constant $J = J_p$ (h_{AC} = 4 Oe), it results $U_{AC}(T = 88.5\ K) \sim 1500$ K. This is unexpectedly high for a specimen close to the IL, as indicated by the DC magnetic hysteresis curve (not shown). By changing h_{AC}, one obtains a logarithmic J dependence of U_0 and U_{AC} (see the main panel of Fig. 2).

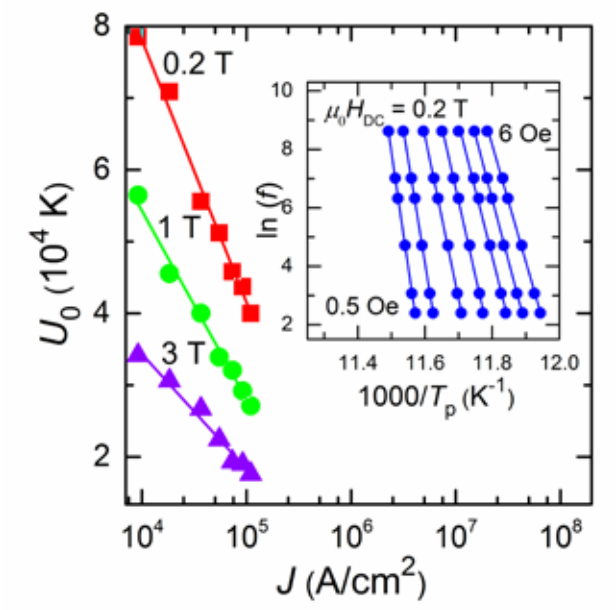

Fig. 2: Main panel: The apparent activation energy U_0 in the low-T limit vs. ln(J) (where J is the screening current density) at various external DC fields. The U_0 values where obtained from the linear fit in the Arrhenius plots such as those illustrated in the inset, and J(at T_p) = 1.02h_{AC}/d. The continuous lines represent the linear fit.

Thus, one can write $U_{AC}(J) = U_c \ln(J_d/J)$, where U_c represents a characteristic pinning energy, and J_d is the (true) dynamic critical current density, reached at $f = f_0$. Useful information about the vortex hopping process can be obtained from the m′(f) data, supplying J(t) and the electric field at the sample edge E(t) (resulting from dm′/dt) at short t = 1/f scales (Fig. 3). A linear extrapolation of J(1/f) towards $f = f_0$ leads $J_d \sim 4 \times 10^5$ A/cm^2, a value used below.

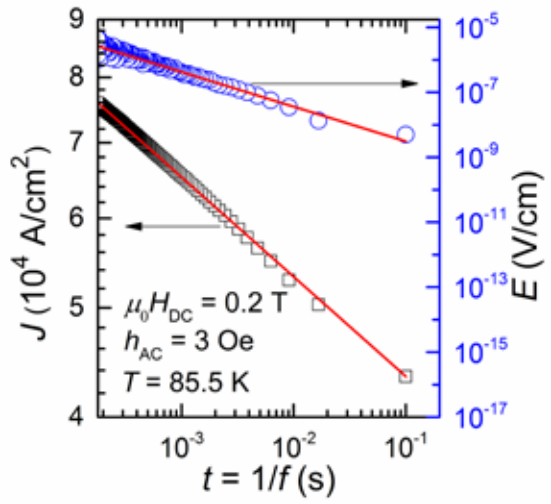

Fig. 3: Time $t = 1/f$ variation of the screening current density J and of the electric field at the sample edge E determined at T = 85.5 K, $\mu_0 H_{DC}$ = 0.2 T with h_{AC} = 3 Oe. The continuous lines represent a linear fit.

With the electric field E = 10^{-7} V/cm and an effective hopping time (towards the sample centre or in the opposite direction) $t_h = 1/(2f)$ of 2 ms, the vortex hopping length $l_h = Et_h/\mu_0 H_{DC} = 100 \pm 20$ nm. The important aspect here is that l_h overcomes the mean distance between the pinning centres.

Finally, the bare activation energy barrier has been addressed [4, 5] in the simplest way for isolated vortices (at low DC fields), by taking into account the work for dragging a vortex segment of length L_{eff} (in the conditions of a pinning enhanced viscosity) over a distance l_h with $J = J_d$. In terms of J_d (determined by us), this is $\Phi_0 L_{eff} l_h J_d$. With J in the specimen, in the above approximation, $U_{AC} = \Phi_0 L_{eff} l_h (J_d - J)$. The mean hopping distance l_h extracted above plays the role of the "interaction length", and is much larger than the radius of the pinning centres. It means that even at the relatively low frequencies used by many authors the contribution of thermally activated flux creep (if any) to U_{AC} is small. The effective length of the hopping vortex segment L_{eff} was taken as the averaged length of the straight portion of the BZO nanorods, which in YBCO films was found to be around 80 nm [6], and the presence of Y_2O_3 nanoparticles does not drastically reduce L_{eff}. With $J_d \sim 4 \times 10^5$ A/cm^2 and $J = J_p << J_d$, the above relation supplies $U_{AC} \sim 2 \times 10^3$ K. This accounts for the order of magnitude of U_{AC} just below IL at $\mu_0 H_{DC}$ = 0.2 T, supporting our new approach for the AC magnetic response of superconductors.

Funding from PNII PCCA 138/2012.

References

[1] E. Bartolomé et al., Phys. Rev. B 81, 184530 (2010).

[2] V. Ruoco et al., Supercond. Sci. Technol. 25, 122001 (2012).

[3] G. Blatter et al., Rev. Mod. Phys. 66, 1125 (1994), and references therein.

[4] L. Miu, I. Ivan, A. M. Ionescu, and D. Miu, AIP Advances 6, 065027 (2016)

[5] I. Ivan, A. M. Ionescu, D. Miu, P. Mele, and L. Miu, Supercond. Sci. Technol. 29, 095013 (2016)

[6] P. Mele et al., Supercond. Sci. Technol. 21, 032002 (2008).

Crystallization mechanism and luminescence properties of new rare-earth doped oxychloride nano-glass-ceramics

C. Secu, C. Bartha, E. Matei si M. Secu

National Institute of Materials Physics

New hybrid materials based on stabilized RE^{3+}-doped nanoscaled particles embedded in glassy matrix (so called nano-glass ceramics [1]) represents a high potential for applications in various fields (optical amplifiers, optical waveguides, etc.) since they allow the exploitation of the optical phenomena with the optical transparency due to lack of scattering.

Sol-gel route using metal alkoxides and trichloracetic acid as precursors has been used to prepare oxyfluoride glass-ceramic containing RE^{3+}-doped nanoscaled chloride nanoparticles (LaOCl and $BaCl_2$) embedded in a silica matrix through controlled crystallization at higher temperatures of the xerogel [2,3].

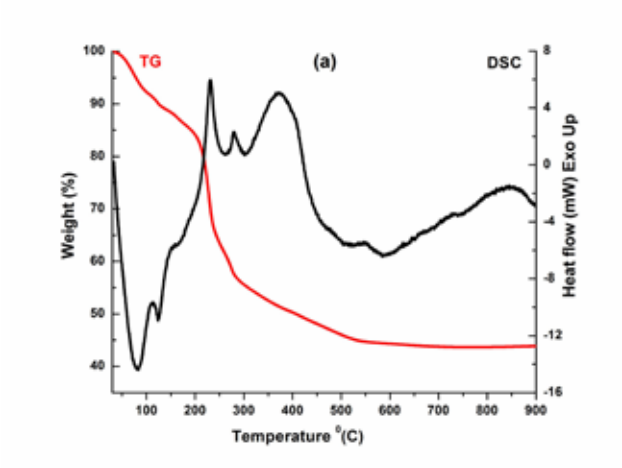

Fig. 1: DSC/TG curves of SiO_2-LaOCl xerogel

Thermal analysis and X-ray diffraction (Fig 1-2) have indicated that lanthanum oxychloride (LaOCl) nanocrystalline phase is the result of complex thermally decomposition and pyrolysis processes. The two DSC peaks at 230 and 280 °C were assigned to the lanthanum and europium trichloracetates decomposition: $2Ln(CCl_3COO)_3 \rightarrow 2LnCl_3 + 3CCl_3COCl + 3CO_2 + 3CO$, (Ln = La, Eu).

The temperature range above 450°C corresponds to the LaOCl formation by hydrolytic and oxidative reactions of the $LaCl_3$:

$LaCl_3 + H_2O \rightarrow LaOCl + 2\ HCl$

$LaCl_3 + O_2 \rightarrow LaOCl + Cl_2$

X-ray diffraction (XRD) pattern recorded on xerogel annealed above 450 °C showed LaOCl nano-crystalline phase precipitation in the glass matrix (Figure 2).

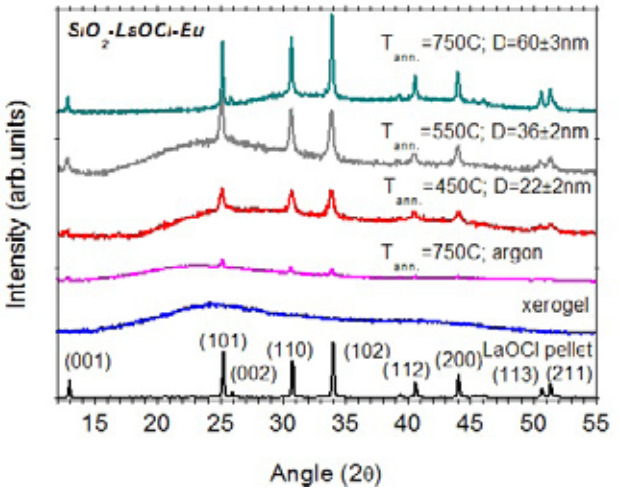

Fig. 2: XRD patterns of the annealed xerogel by comparison to the LaOCl pellet

SEM analysis of the a grain showed smooth surface of the grain and an uniform distribution of the La, Eu, Cl and O elements.

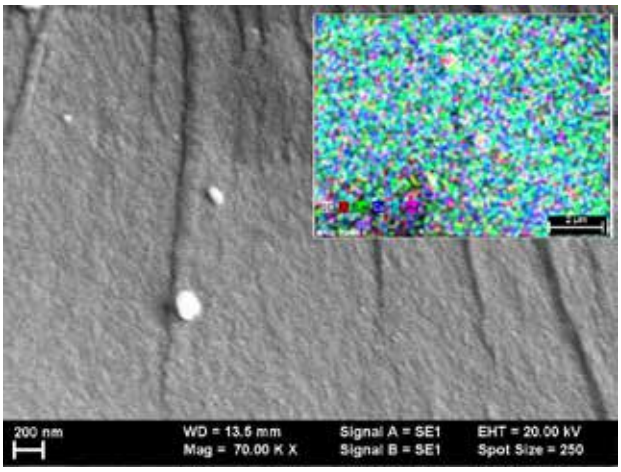

Fig. 3: Electron microscopy image (SEM) of a grain and the elemental analysis (EDX)

Photoluminescence (PL) spectra (Figure 4) evolution reflects the significant local modifications surrounding Eu^{3+} ions from a random one (in the xerogel) to a crystalline one (inside the LaOCl nanocrystals, with a (C_{4v}) local coordination symmetry). PL spectra analysis by using Judd-

Ofelt theory have shown an increase of the Eu^{3+} luminescence efficiency from about 5% in the xerogel to about 40% in the glass-ceramic assigned to lower phonon energy of the oxychloride matrix and dehydration that reduce the probability of non-radiative de-excitations.

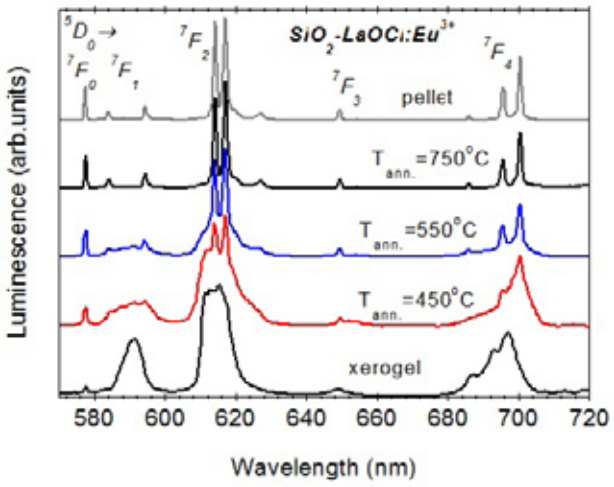

Fig. 4: Normalized PL spectra recorded on Eu^{3+}-doped SiO_2-LaOCl nano-glass ceramics by comparison to the LaOCl pellet.

Thermal analysis and X-ray diffraction (Figure 5) measurements of Er-doped SiO_2-$BaCl_2$ xerogel has shown that crystallization process is based on a homogenous crystallization mechanism with $BaCl_2$ nucleation centres resulted from thermal decomposition of Ba–trichloracetate at 314 °C according to the reaction:
$Ba(CCl_3COO)_2 \rightarrow BaCl_2 + CCl_3COCCl + CO + CO_2$ followed by subsequent growth into $BaCl_2$ nanocrystals after 745 °C anealing.

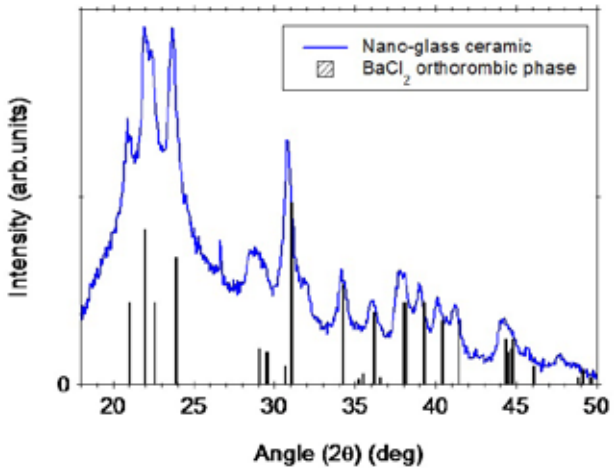

Fig. 5: The XRD pattern of the Er-doped SiO_2-$BaCl_2$ nano-glass ceramic annealed at 745 °C.

Under 810 nm laser light pumping it shows green (($^2H_{11/2}$, $^4S_{3/2}$) → $^4I_{15/2}$) and red ($^4F_{9/2}$ → $^4I_{15/2}$) up-conversion luminescences ascribed by a two-photon processes. The relative efficiency of the up-conversion is about 25-30 % compared to the β-$NaYF_4$:Er^{3+}(18%) up-converter due to the presence of residual hydroxyl ions and surface defects acting as luminescence quenching centres.

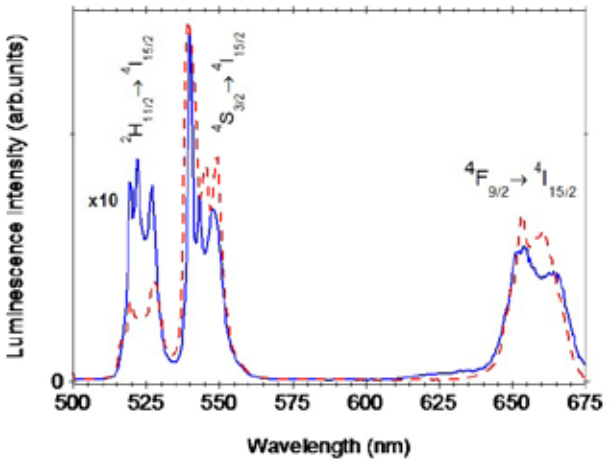

Fig. 6: Normalised UC luminescence spectra of Eu^{3+}-doped SiO_2-$BaCl_2$ nano-glass ceramics compared to the $NaYF_4$:Er^{3+} (18%).

Sol-gel route with has been successfully used for the synthesis of new oxychloride nano-glass ceramics having optical properties.The method is very well suited for the ***"spin-coating"*** deposition techniques of the glass-ceramics thin films in a waveguiding configuration for a wide range of photonic applications: integrated optical amplifiers, laser systems or integration with electronic devices for optoelectronics.

Funding from Nucleus Program PN16-4801 and IDEI 290/2011.

References

[1] M. Clara Gonçalves, L.F. Santos, R.M. Almeida: Rare-earth-doped transparent glass ceramics, C.R. Chim. 5,845 (2002)

[2] M. Secu, C. Secu, C. Bartha "Crystallization and luminescence properties of a new Eu3+-doped LaOCl nano-glass-ceramic", J. Eur. Ceram Soc. 36 (2016) 203–207

[3] M.Secu, C.E.Secu "Up-conversion luminescence of $BaCl_2$:Er^{3+}nanocrystals embedded in oxychloride nano-glass ceramic" J. Eur. Ceram Soc. 36 (2016) 1699–1703

Carbon monoxide adsorption on ferroelectric $Pb(Zr,Ti)O_3(001)$ surfaces

L.C. Tănase, N.G. Apostol, L.E. Abramiuc, C.A. Tache, L. Hrib, L. Trupină, L. Pintilie, C.M. Teodorescu

National Institute of Materials Physics

Ferroelectric materials are used in a wide category of applications, such as sensors, traductors, non-volatile memories. Ferroelectrics began during the last decade to be involved in the field on catalysis, due to their ability to provide charge carriers (electrons and holes), as well as electric fields at their surfaces, used to adsorb molecules on the surface [1], and these molecules can further undergo oxidation or reduction reactions.

Lead zirco-titanate ($PbZrTiO_3$, PZT), is one of the most studied materials, mainly due to its high out-of-plane remnant polarization, of about 1 C/m^2. In the present study, we use synchrotron radiation X-Ray photoelectron spectroscopy (XPS) to derive states and amounts of molecules adsorbed on surface, along with the investigation of the polarization state of the samples, derived from the band bending at the surface. 20 nm thick, atomically clean PZT(001) films were obtained by pulsed laser deposition, followed by a treatment in a well outgassed ultrahigh vacuum (UHV) environment implying annealing at about 700 K for 3–6 hours. Prior to the UHV cleaning procedure, all samples are routinely characterized by X-ray diffraction, atomic force microscopy (AFM) and piezoresponse force microscopy (PFM). After cleaning, PZT(001) samples exhibited good low energy electron diffraction (LEED) patterns (Fig. 1).

Atomically clean PZT layers present a well-defined $P^{(-)}$ polarization state, the sign of the band bending correspond to screening of the depolarization field by charges located inside the material (hole accumulation or missing cations) and only in this state the surface is able to adsorb CO, partly dissociating these molecules, at room temperature. The sticking of carbon and of CO on the surface is also found to be related to the non-vanishing out-of-plane polarization state.

The study reported in Ref. [2] discusses various aspects regarding the achievement of stable ferroelectric states by cleaning the samples in ultra-high vacuum, investigation of these states by XPS, correlating it with the stoichiometry and the carbon content on the surface (Fig. 1). A temperature dependent variation of the core level energies is used to extract information regarding the loss of the ferroelectric polarization with the increase of temperature.

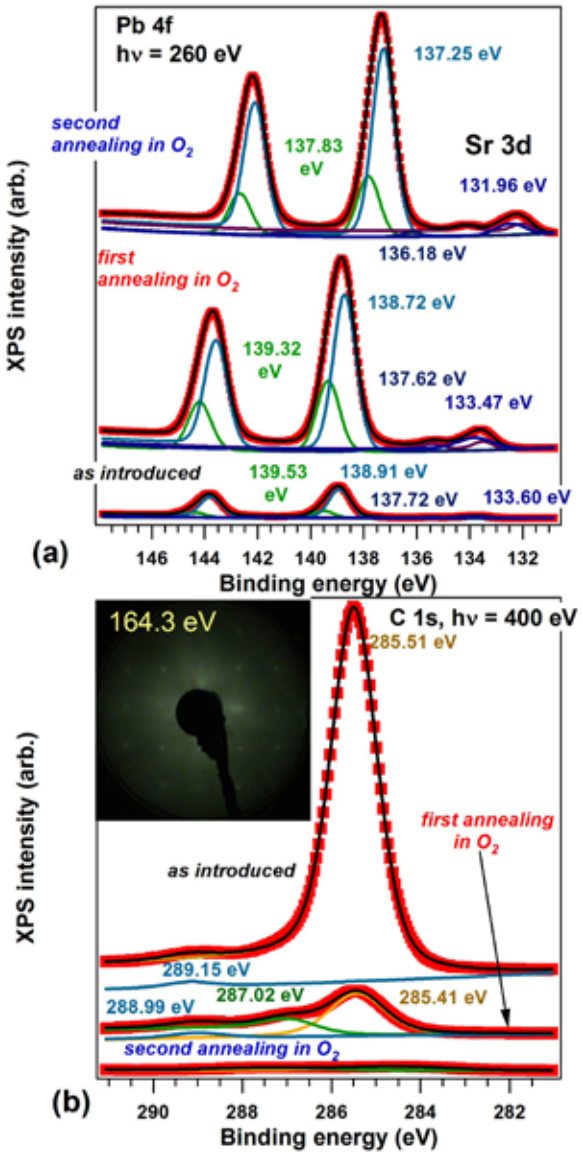

Fig. 1: The loss of carbon contamination, after the second annealing, results in a change in binding energy of Pb 4f core level towards lower values, which is interpreted as a stabilization of $P^{(-)}$ polarization state. Inserted in (b) is a LEED pattern obtained on clean PZT(001). Adapted from Ref. [2].

The attachment of CO molecules on PZT surfaces is investigated, as function of the initial state of the surface. No significant carbon signal is obtained when CO is dosed on samples exhibiting

$P^{(+)}$ or $P^{(0)}$ polarization, which can be interpreted either that CO does not adhere on these kind of surfaces, or that, considering that the orientation of the dipole moment of this molecule is oriented with the oxygen towards the surface, oxygen sticks on the surface, while the carbon is repelled. Fig. 2 illustrates both C 1s and Pb $4f_{7/2}$ XPS spectra, showing that, after CO dosing (6000 L) the amount of carbon increases only on the samples where the binding energy of the core levels are shifted towards lower values, which means that they describe an inwards polarization state, $P^{(-)}$. The C 1s spectrum exhibits two peaks, meaning that CO is adsorbed partly in a dissociated form.

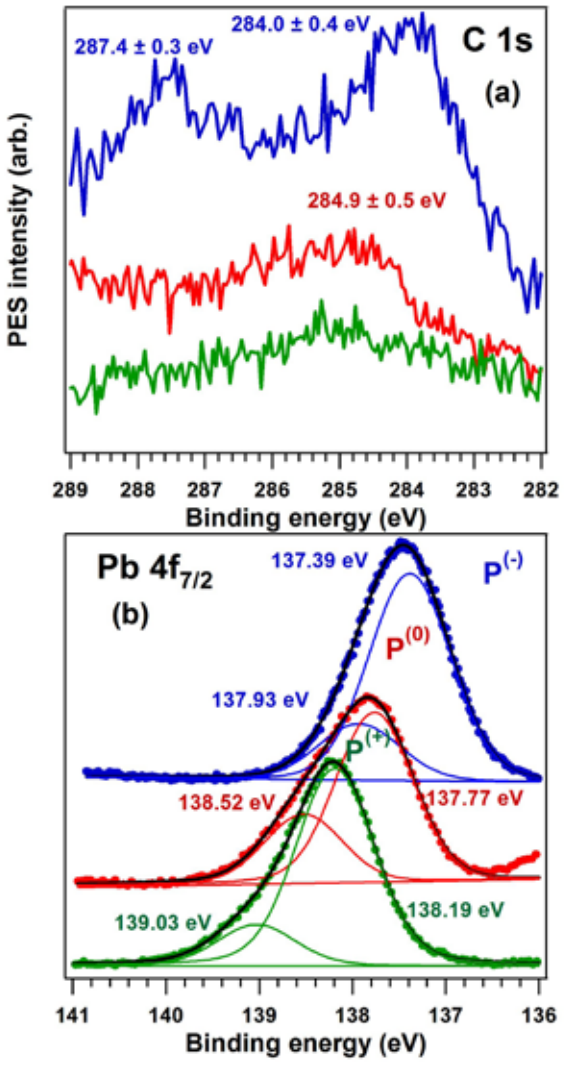

Fig. 2: Evidence by XPS of the fact that the CO molecules adhere mostly on $P^{(-)}$ surfaces. Adapted from Ref. [2].

The evolution of binding energies was followed during heating-cooling cycles, in order to investigate the interplay between polarization and the presence of carbon on the surface. Fig. 3 show the derived Pb $4f_{7/2}$ binding energy as function of C/Pb ratio. At elevated temperatures the $P^{(-)}$ polarization is lost, and the carbon coverages also decreases drastically. A Langmuir model allowed one to trace the carbon adsorption energy as being dependent on the PZT polarization state.

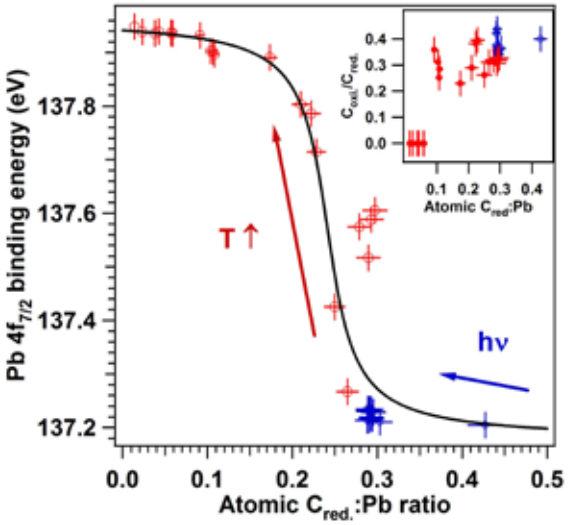

Fig. 3: Pf $4f_{7/2}$ binding energy evolution as function of the carbon coverage, during soft X-ray exposition after dosing and subsequent heating. Reproduced from Ref. [2].

The desorption of the dissociated carbon proceeds by uptaking oxygen from the PZT layer, and most probably carbon is desorbed in form of CO_2. When sufficient oxygen depletion is achieved, the samples return to the $P^{(+)}$ state. A direct conclusion may be that inwards polarized PZT surfaces are good candidates for both CO breakdown and subsequent oxidation, by using oxygen from the film, which may then be recovered by subsequent thermal treatment.

Funding from the Romanian Ministry of Education–Executive Unit for Funding High Education, Research, Development and Innovation (MEN-UEFISCDI) through Projects PN-II-RU-TE-2014-4-0456 and PN-II-ID-PCCE-2011-2-0006.

References

[1] L.E. Ştoflea, N.G. Apostol, L. Trupină, C.M. Teodorescu, Selective adsorption of contaminants on $Pb(Zr,Ti)O_3$ surfaces shown by X-ray photoelectron spectroscopy, J. Mater. Chem. A 2, 14386-14392 (2014).

[2] L.C. Tănase, N.G. Apostol, L.E. Abramiuc, C.A. Tache, L. Hrib, L. Trupină, L. Pintilie, C.M. Teodorescu, Ferroelectric triggering of carbon monoxide adsorption on lead zircon-titanate (001) surfaces. Sci. Rep. 6, 35301 (2016).

Structural, spectromicroscopic and magnetic investigations of Mn_xGe_{1-x}

L. C. Tanase, G.A. Lungu, L. E. Abramiuc, I. C. Bucur, N.G. Apostol,
R. M. Costescu, C.A. Tache, D. Macovei, C. M. Teodorescu
National Institute of Materials Physics
in collaboration with A. Barinov, Elettra Sincrotrone Trieste, SS 14, Km 163.5 Area Sci Pk, 34149 Trieste, Italy

In this study there were investigated structural, spectromicroscopic and magnetic properties of more samples of manganes deposited on Ge(001) samples, under different initial contiditions. The most techniques are designed for surface characterization, such as low energy electron diffraction (LEED), photoelectron spectroscopy (PES), magneto-optical Kerr effect (MOKE), while EXAFS (extended X-Ray absorbtion fine structure spectroscopy) is used to investigate the atomic ordering inside the samples. These results supplement the data previously reported by the same group on the same system. [1]

The EXAFS analysis (Fig. 1) shows that the Mn deposition at temperatures in the range 50–150 °C and with a relatively high growth rate brings about a very limited atomic diffusion of Mn in the Ge substrate, resulting in the metallic structure of the Mn overlayers. Increase of the substrate temperature (T_S) to 250–350 °C enables the Mn diffusion in Ge, followed by the nucleation of a Ge_3Mn_5-like structure, with the Mn atoms placed only on Mn1 sites. A further increase of T_S to 450 °C results in gathering of the Ge_3Mn_5 nuclei to clusters of a more coherent structure, with both Mn1, 2 sites occupied. However, this growing structure has still numerous Mn vacancies, probably preferentially placed on Mn2 sites.

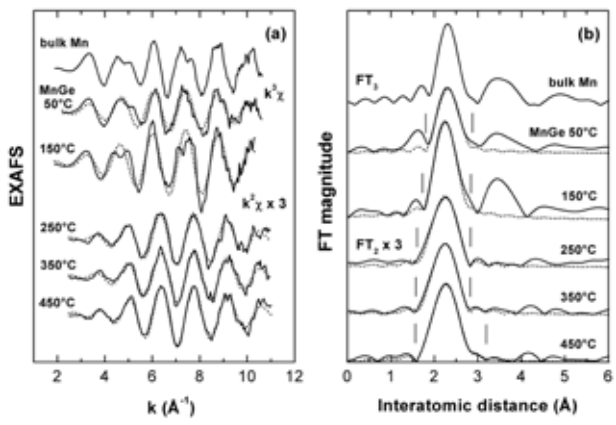

Fig. 1: EXAFS spectra recorded on Mn deposited on Ge(001) under different substrate temperatures. Reprinted from Ref. [2].

The spectromicroscopic investigations, performed at the Spectromicroscopy beamline at Elettra Sincrotrone Trieste reveal the low inhomogenity of the system, sign of a good dilution of manganese. Fig. 2 presents some relevant images [2]. Also, the Mn chemical state is unchanged over the areas scanned, and is also not changing in time. This is a sign that Mn is embedded in the Ge(001) crystal. The chemical composition determined by photoelectron microscopy is similar to Mn_5Ge_3.

The magnetic properties have been studied by MOKE magnetometry. Substrate temperatures below 200 °C gave rise to samples with Mn overlayers featuring metallic structure [1] and no magnetic signal, while substrate temperatures above 200 °C enabled Mn diffusion in Ge and formation of Mn_5Ge_3-like structure nucleation with hysteresis loops showing superimposed superparamagnetic and ferromagnetic components. Thus, It has been proven in the present paper that substrate temperature is a critical parameter that contribute to the stabilization of the magnetic ordering in Mn_xGe_{1-x} thin films.

While the MOKE ferromagnetic signal is achieved in conditions of T_S larger than 200 °C, EXAFS analysis reveals the formation of Mn_5Ge_3-like clusters. The magnetic ordering is additionally revealed, for the same samples, by spin-resolved photoemission [2].

Note also that we concluded in a previous paper [1] there that all the manganese diffuse under the first layer of Ge(001) surface, due to the preservation of the LEED (1 x 2) -(2 x 1) reconstruction and that the surface Ge dimers get to situate at larger distances once the manganese is immersed under the surface, giving rise to Mn_5Ge_3 clusters.

Also, we observed the relative insensitivity of the sample to contamination by the residual gas. This observation gets another argument by spectromicroscopy, where we observed high

stability of the chemical state of manganese.

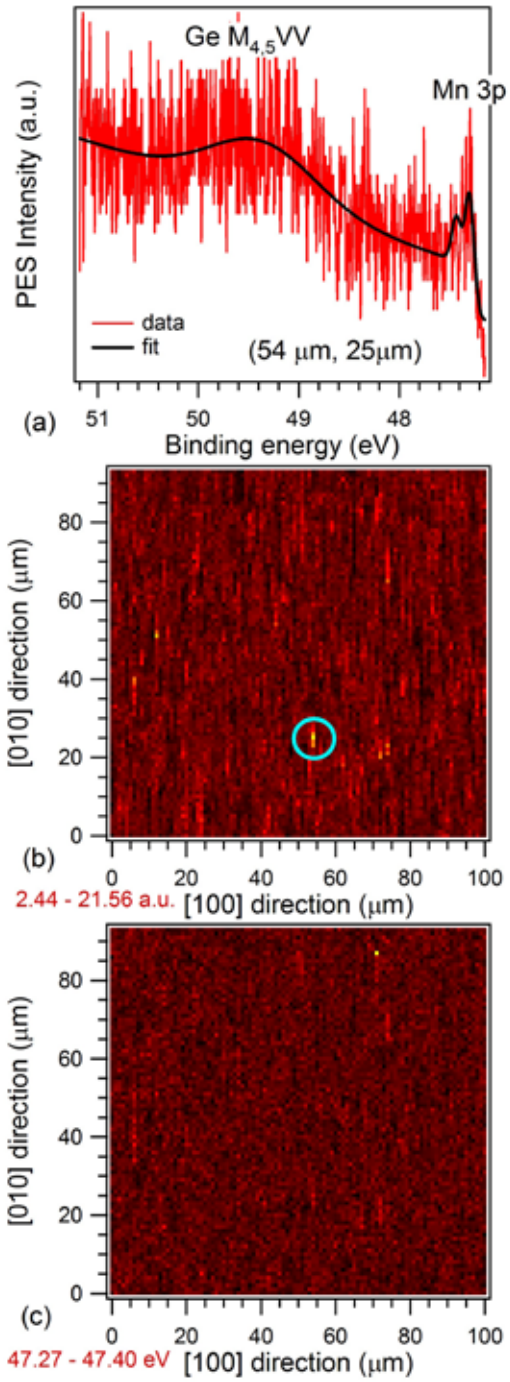

Fig. 2: Spectromiscopy images and individual spectrum on 10 nm Mn/Ge(001) deposited at 250 °C, reproduced from Ref. [2]. (a) represents typical micro-spectra, while (b) and (c) are maps of Mn 3p intensities and binding energies, respectively. Red numbers represent ranges for these maps. The spectra from (a) are taken from a small region denoted by the blue circle in (b).

This work [2] completes the information presented in the previous paper [1], revealing the importance of Mn_5Ge_3 phase regarding the magnetic ordering.

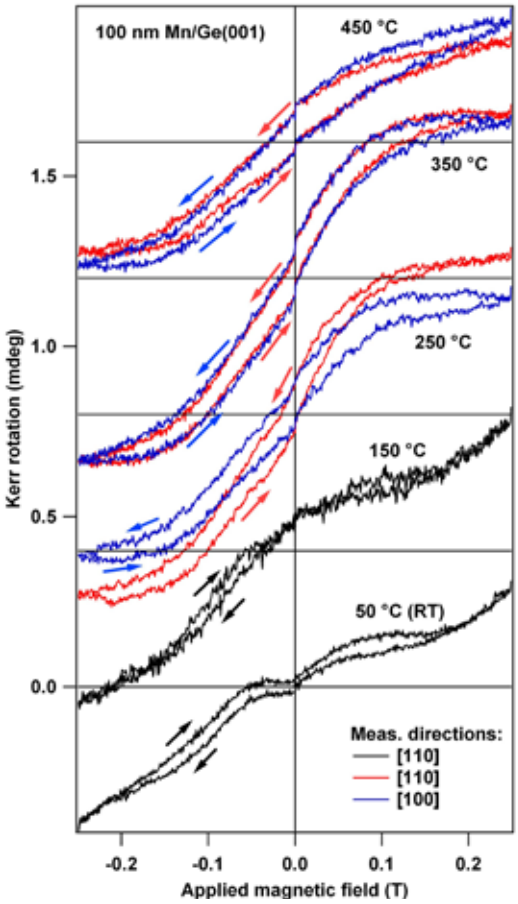

Fig. 3: MOKE hysteresis measured on different Mn/Ge samples, as function of the deposition temperature, revealing that the magnetic ordering is achieved at higher substrate temperatures. Reproduced from Ref. [2].

Funding from Core Program 2016-2017, Contract No. PN16-480101 and by the UEFSCDI Agency through the Project PN2-152/2012.

References

[1] G.A. Lungu, L.E. Stoflea, L.C. Tănase, I.C. Bucur, N. Răduțoiu, F. Vasiliu, I. Mercioniu, V. Kuncser, C.M. Teodorescu, Room temperature ferromagnetic Mn:Ge(001). Materials 7, 106-129 (2014).

[2] L.C. Tănase, G.A. Lungu, L.E. Abramiuc, I.C. Bucur, N.G. Apostol, R.M. Costescu, C.A. Tache, D. Macovei, A. Barinov, C.M. Teodorescu, Long range magnetic interaction in Mn_xGe_{1-x}: structural, spectro-microscopic and magnetic investigations, J. Mater. Sci. 52, 3309-3320 (2017).

Platinum alloying with germanium in Pt/Ge(001) results in low work function of the metal and non-rectifying interface

L.C. Tănase, A.E. Bocîrnea, A.B. Șerban, L.E. Abramiuc, I.C. Bucur, G.-A. Lungu, R.M. Costescu, C.M. Teodorescu

National Institute of Materials Physics

High conductive metals contacted with conventional semiconductors are good candidates for Schottky diodes or metal electrodes in p-n junctions and transistors. The two metals chosen for this study have different work functions: Cu (Φ_{Cu} ≈ 4.65 eV) and Pt (Φ_{Pt} ≈ 5.65 eV), compared to germanium (Φ_{Ge} ≈ 4.7–5.1 eV). According to the basic mechanism of Schottky barrier formation, a difference between the work functions of a metal and a semiconductor usually gives rise to a variance of the energy bands in the vicinity of the interface, visible by a downward or upward bending inside the semiconductor and the band bending should be equal to the difference between the metal work function and the one of Ge.

The aim of this study was to analyze the band bending occurring in two cases $\Phi_M > \Phi_S$ (Pt/Ge(001)) and $\Phi_M < \Phi_S$ (Cu/Ge(001)) by using photoelectron spectroscopy (XPS), when metals are deposited on atomically clean, well characterized Ge(001) surfaces. The inclusion of the LEED results together with XPS in the absence of contaminants is a first novelty of this study. It was proved that, in case of Cu/Ge(001) the band bending in the semiconductor takes place in the sense of the theoretical estimate for an ohmic contact with $\Phi_M < \Phi_S$, though the experimentally determined value (0.7–0.8 eV) is higher than $\Phi_M - \Phi_S \approx 0.35$ eV. This is consistent with a slight n doping near the interface due to the Cu deposition, which provides electrons and elevates the donor concentration.

The experiments started by confirming the surface crystallinity of clean Ge(001) surface through LEED (low energy electron diffraction), but, with metal deposition, the LEED patterns are strongly affected, for Cu on Ge substrate are preserved up to 4 Å of Cu deposited, whereas for 2 Å of Pt there was not possibe to obtain LEED pattern.

For the Cu/Ge(001) experiment, Cu 2p, Ge 2p and Ge 3d core level XPS spectra have been recorded on the sample gradually deposited with 2 Å, 4 Å, 8 Å, 16 Å, 24 Å, 40 Å, 100 Å of copper. Under small Cu coverage, Ge core levels feature a third component (atributed to Ge dimers at the surface), with lower binding energy (BE) with respect to the bulk. Cu $2p_{3/2}$ has a higher BE component ascribed to an interfacial state, while the other corresponds to the bulk. The evolution of the integral amplitude as function of the metal thickness reveals a deviation from the expected exponential shape at 16 Å which we explained by asuming a two-step alloy formation: we assume that up to 16 Å Cu thickness, no continuous layer-by-layer sheet is formed, but islands randomly distributed all over the Ge surface, embedded either in an intermixing of Cu–Ge, or into some thin Cu layers. In Fig. 1 one can notice the evolution of binding energies with respect to the Cu thickness for Ge 3d core level, so the band bending of 0.68 eV is downwards, as expected for a typical ohmic contact.

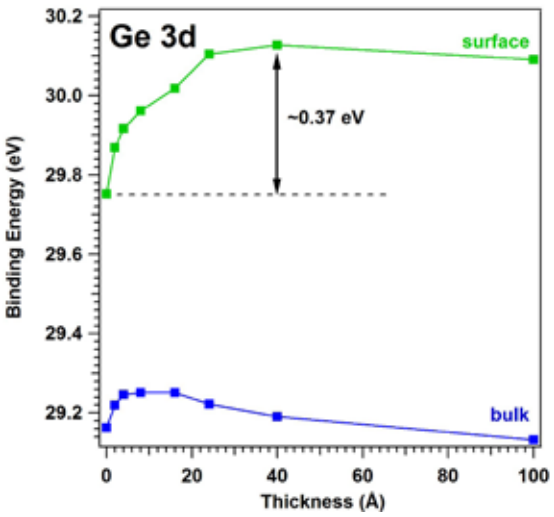

Fig. 1: The evolution of binding energies with respect to the Cu thickness for Ge 3d core level. Reprinted from Ref. [1].

In the case of Pt/Ge(001), we expected to build up a Schottky contact, by taking into account that $\Phi_M = \Phi_{Pt} = 5.7$ eV and $\Phi_S = \Phi_{Ge} = 5.0$ eV, but we observed a strong band bending in the same sense as in the Cu/Ge(001) case, even higher. We observed a variation of the BE of + 1.31 eV instead

of – 0.7 eV with Pt deposition. For the case of Pt/Ge(001), the behaviour is similar to Cu/Ge case, with Pt islands rising on the Ge surface, alongside with some stronger interdiffusion of Pt into first layers of Ge, evidenced by the high values of IMFP (inelastic mean free path) indicating a mixture of Pt-Ge. Due to a greater value of Pt density compared to Ge (and even Cu), these islands immerse into the Ge lattice conducting to some complexe alloys, but this process could happend only for smaller amounts of Pt (8-16 Å). This asumption is supported by the fact that the radiative heating of the substrate during metal deposition was higher in the case of Pt, and the energy variation of Ge 3d and the bulk component of Pt 4f. As shown in Fig. 2, the variation of BE for Pt 4f surface component is of 1.31 eV towards higher energies for both Ge 3d and Ge 2p.

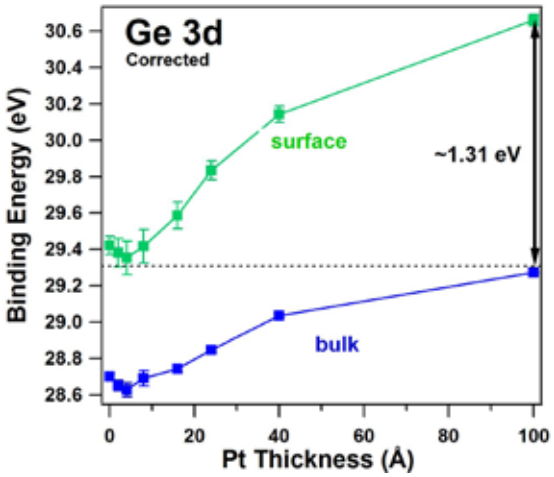

Fig. 2: The evolution of binding energies with respect to the Pt thickness for Ge 3d core level. Reprinted from Ref. [1].

We formulated a new hypothesis to explain the Pt/Ge(001) variations of BEs, given that Pt has a very high effective mass ($13m_e$) or, equivalently, a relatively narrow conduction band. Arguments for lowering the metal work function when intermixing with germanium occurs are discussed in the framework of the nearly free electron model (in terms of lowering the effective mass) or in terms of the tight binding model (in terms of increasing the conduction bandwidth). With Pt alloying (intermixing) with Ge it is expected that the effective mass of the alloy Ge_xPt_{1-x} decreases, or, equivalently, the bandwidth increases. Both models explain the increase of the Fermi kinetic energy upwards from the bottom of the conduction band (Fig. 3). The result is that the work function drops steeply from 5.7 eV to 3.7–3.8 eV in the case of Ge mixed with Pt. This hypothesis might be considered at least on the same footing as other explanations discussed in literature, such as traps at the interface, dislocations or tunneling.

Funding from the UEFISCDI Agency through Contract No. PN2-152/2011 and by the NIMP Core Programme PN16-4801 10N/2016.

References

[1] L.C. Tănase, A.E. Bocîrnea, A.B. Şerban, L.E. Abramiuc, I.C. Bucur, G.A. Lungu, R.M. Costescu, C.M. Teodorescu, Growth mechanisms and band bending studies in Cu and Pt on Ge(001) investigated by LEED and photoelectron spectroscopy, Surf. Sci. 653, 97-106 (2016).

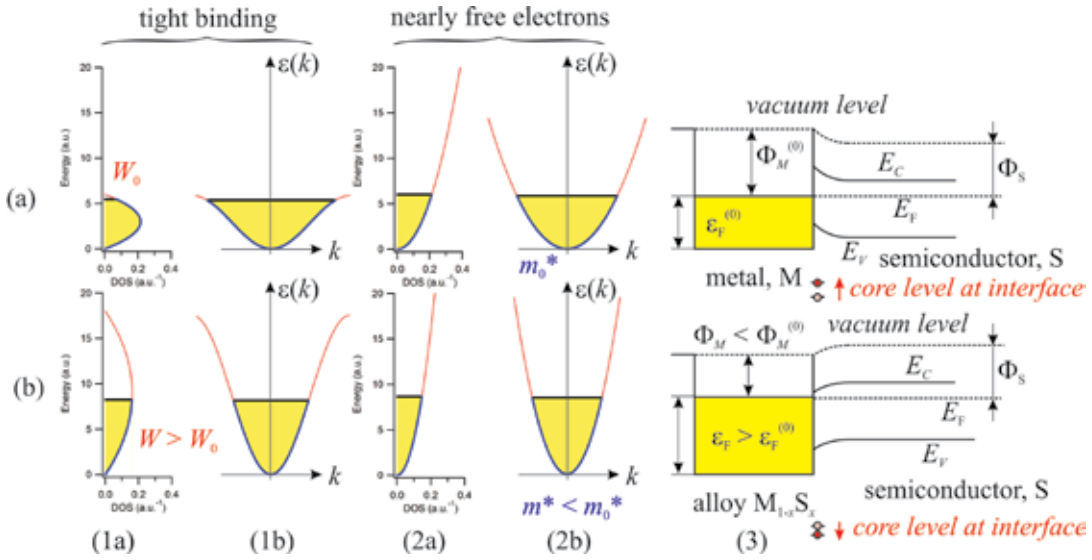

Fig. 3: Model proposed to explain the variation of the work function when platinum is intermixed with germanium. Reprinted from Ref. [2].

Structural and electrical properties of Al:ZnO thin films grown on *001* $SrTiO_3$ at different deposition temperatures

L.M. Trinca, A.C. Galca, G. Aldica, R. Radu, I. Mercioniu, L. Pintilie

National Institute of Materials Physics

Epitaxial growth is most of the time a key factor for achieving robust and long lasting optoelectronic devices. Aluminum doped zinc oxide, Al:ZnO (AZO), is a transparent conductive oxide that can be used as electrode in electronic devices, being considered for design and manufacture of emerging oxide electronics.

The growth of a conductive hexagonal phase (AZO) on cubic $SrTiO_3$ (001) single crystal (STO) is investigated. ZnO thin films deposited on (001) STO might exhibit two orientations: along ***a***-axis (ZnO grows with (110) plane parallel with the substrate) and along ***c***-axis (with 001 texture of the film) [1]. Assuming flat geometries, two possible arrangements at interface can be envisaged (Fig.1a).

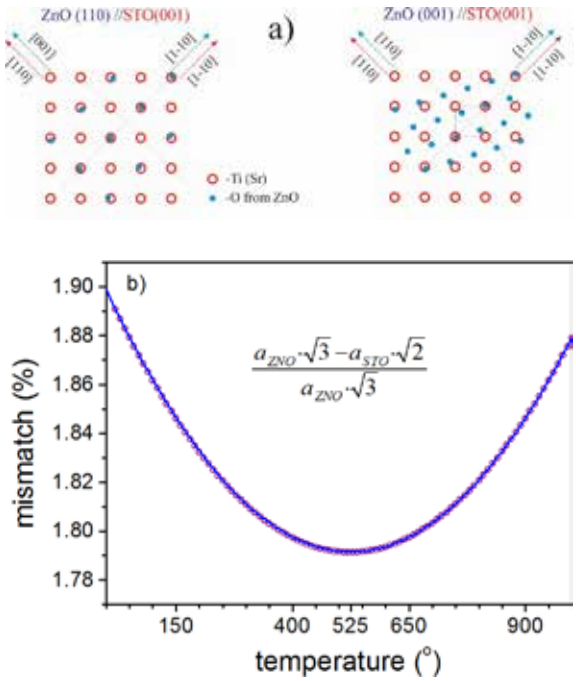

Fig. 1: a) possible arrangements of wurtzite planes on 001 plane of STO b) lattice mismatch as function of temperature.

A higher deposition temperature increases the adatoms mobility and could promote an epitaxial growth, while the lattice mismatch is dependent also on the temperature. Considering the thermal expansion of the two materials, the lattice mismatch between film and substrate can be calculated. Both (110)ZnO//(001)STO and (002) ZnO//(001)STO arrangements can be done by aligning the [1–10] direction of the wurtzite surface with the [1–10] direction of the cubic surface.

The mismatch as function of temperature is given in Fig.1b. In this case, the minimum lattice mismatch is at ~525°C (ε~1.79%). Along [110] direction, the lattice mismatch between the two arrangements are ε~6% for (110)ZnO//(001) STO and ε~70% for (001)ZnO//(001)STO. Hence, by assuming flat surfaces, the most favorable arrangement at substrate temperatures of about 525°C should be (110)ZnO//(001)STO.

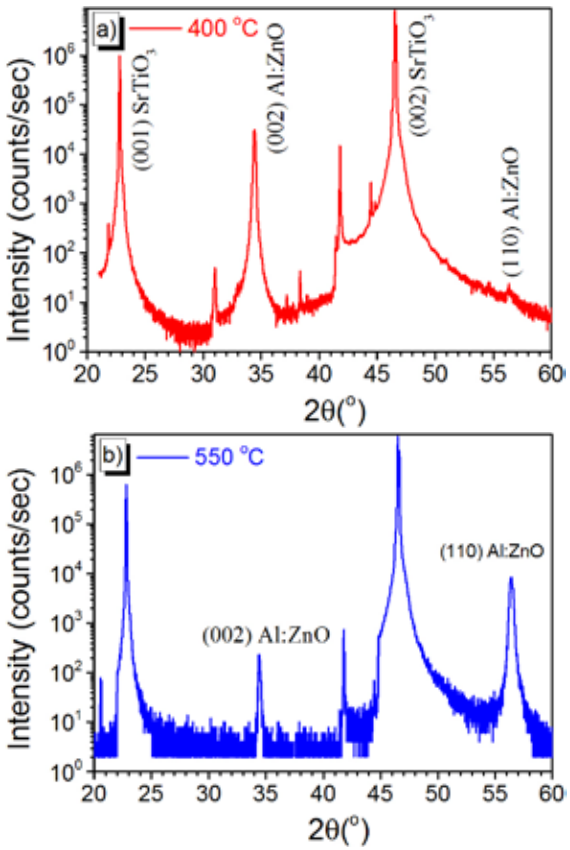

Fig. 2: 2θ–ω scans of AZO thin films deposited at 400°C (a) and at 550°C (b) on STO(001).

Selection of the 2θ–ω diffractograms recorded on AZO thin films grown on (001) STO are presented in Fig. 2. AZO layers deposited at low temperatures (300°C, 350°C) show only 002 orientation, while at higher deposition temperature both (001) and (110)

orientations coexist (Fig.3a). In all the cases, (110) is the secondary phase, except for the AZO thin film deposited at 550°C. This temperature is close to the one where the minimum lattice mismatch for (110)ZnO//(001)STO was calculated. It should be noted that 550°C is the temperature where the STO surface has an important Sr concentration, as discussed below.

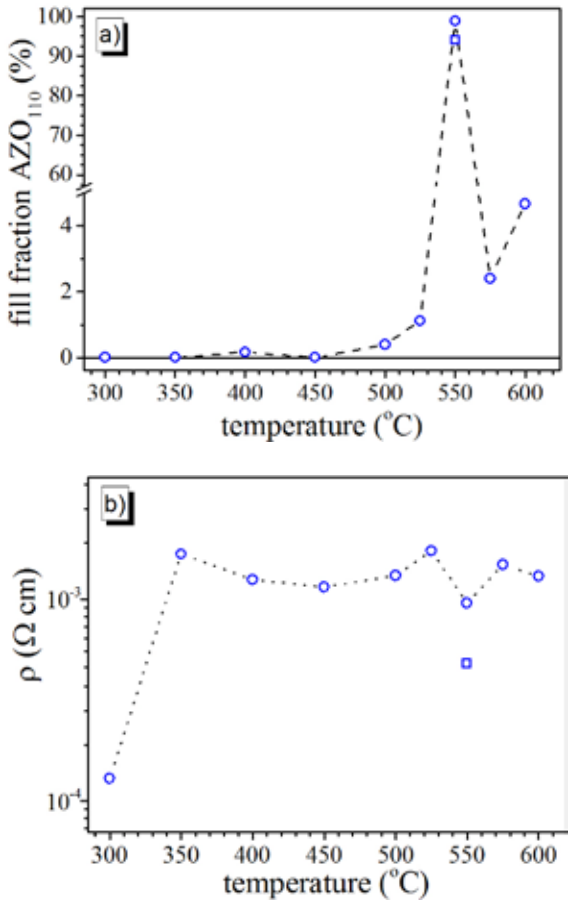

Fig. 3: a) the fill fraction of [110] oriented phase b) the electrical resistivities of AZO thin films.

The nucleation of crystallites at first stages of deposition takes place on certain sites on the substrate surface where the adatoms preferably land on or diffuse to. The STO surface changes as temperature increases, the most defective morphology occurs at 550°C where the content of Sr seems to be very high (with respect to TiO_2 terminations) [2]. Thus, the singularity at 550°C can be explained also by a high density of steps and islands of the STO surface (the morphology and composition are completely different than those at other temperatures) [2]. The orientation of AZO thin films is different on SrO- and TiO_2-terminations of STO surface, SrO- surface favoring the apolar ***110*** ZnO, while the TiO_2- surface promotes the growth of ***001*** ZnO.

The conductive character of AZO thin films was also investigated. The electrical resistivity of AZO layer grown at 550°C is the lowest from the entire 300-600°C series, except for the film deposited at 300°C which is completely ***002*** oriented (Fig 3b). To increase the concentration of the free carriers, the pulsed laser deposition took place in reactive oxygen atmosphere at low pressure (0.02 mbar O_2). Thus, the thin films will be degenerate semiconductors.

Concluding, we have shown that the texture of the AZO thin films is strongly affected by the substrate temperature and its morphology, while the substrate temperature dependence of each phase fill fraction can be discussed only by considering the morphological and compositional aspects of the STO substrate surface at each temperature. Selective growth of ***110*** AZO epitaxial film on ***001*** STO is a challenging task, most probably being required a full (ideal) SrO-terminated surface.

Funding from Romanian Ministry of Education (core programs PNII-09-45 and PN-III-16-48).

References

[1] L.M. Trinca, A.C. Galca, G. Aldica, R. Radu, I. Mercioniu, L. Pintilie, Appl. Surf. Sci. 364, 365–370 (2016).

[2] http://lippmaa.issp.u-tokyo.ac.jp/sto/anneal/

Optical glasses with tuned Faraday rotation

M. Valeanu, M.Sofronie, A.C. Galca, F.Tolea, A. Leca, V. Kuncser

National Institute of Materials Physics

in cooperation with M. Elisa[1], B. Sava[2], L. Boroica[2]

[1]National Institute of R & D for Optoelectronics INOE 2000

[2]National Institute for Laser, Plasma and Radiation Physics,

New glass materials presenting high magneto-optical effects are increasingly required due to their applications in spatial and time light modulators, non-reciprocal devices and integrated magneto-optics. However, some applications point to the need of optical materials with as low as possible magneto-optic effects. For example, the wide-field Kerr microscopy for the investigation of the magnetic domain structure requires optical lenses with almost null Verdet constant in order to be insensitive to any stray-fields emerging from the analyzed specimen.

The most known magneto-optic effect is the Faraday effect which consists in the nonreciprocal rotation of the polarization plane of light when passing through a transparent material, if an external magnetic field is applied along the wave-vector. The Faraday Rotation (FR) is defined as $\theta_F = VlH$ where l is the geometrical pathway of the light through the medium, H is the intensity of the magnetic field and V is the Verdet Constant (VC), which is dependent on the electronic properties of the material. The VC for a glass matrix doped with paramagnetic ions can be expressed as a sum of diamagnetic and paramagnetic contributions [1, 2]:

$$V_{dia} = -const_1 \cdot \chi_{dia} \frac{1}{(\frac{1}{\lambda} - \frac{\lambda}{\lambda_0^2})^2} \quad (1)$$

$$V_{para} = -const_2 \cdot \chi_{para} \frac{1}{/1 - \frac{\lambda^2}{\lambda_{eff}^2}/} \quad (2)$$

Each term has a different dispersion law and both terms are closely related to the magnetic behavior of the component ions. Depending upon whether the ions have filled or unfilled electronic configuration, the VC is positive for diamagnetic or respectively negative for paramagnetic materials.

Starting from an aluminophosphate glass matrix Li_2O-BaO-Al_2O_3- P_2O_5 five samples doped with 3 mol % La_2O_3, or with 3 mol% and 6 mol% Dy_2O_3 or Tb_2O_3 were prepared and characterized in respect to magnetic and magneto-optical properties by magnetometry and ellipsometry. The magnetic measurements reveal for the un-doped and La^{3+} doped glasses a diamagnetic behavior with temperature independent negative magnetic susceptibility. For the Tb^{3+} and Dy^{3+} doped glasses the magnetic susceptibility follows a pure Curie low attesting the paramagnetic behavior.

The VC for the prepared glasses was evaluated from FR measured over the entire visible spectrum, by transmission ellipsometry. The magnetic field assisted FR measurements were carried out via a toroidal permanent magnet, with the applied field parallel to the wave vector. In Fig 1 are shown the wavelength dispersions of the VC for the un-doped glass matrix and matrices doped with La^{3+} or with different concentration of Tb^{3+}. The curves are smooth except for some resonance wavelengths corresponding to some f-f transitions evidenced also in the transmittance spectra. For comparison there are shown the VC at λ=635nm measured on the same glasses by using a dedicated commercial equipment under the procedure described in [3]

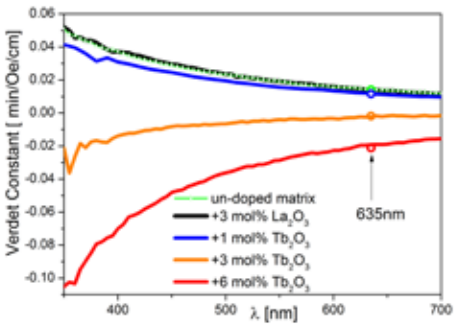

Fig. 1: The wavelength dependence of the VC, measured by ellipsometry for the un-doped glass and doped with 3 mol % La_2O_3 or with 1, 3 and 6 mol% Tb_2O_3.

Data in Fig.1 reveal that the VC of the matrix is positive and does not change by doping with other diamagnetic ions, but decreases and changes the sign as the paramagnetic contribution occurs. The wavelength dependence of the paramagnetic

and diamagnetic contributions to the VC were separated and quantitatively fitted according to (1) and (2). For the diamagnetic glasses the effective transition wavelength, causing the FR, λ_0 was found to be 108(4) nm in the range of values reported for other diamagnetic optical glasses. The wavelengths corresponding to $4f^n$-$4f^{n-1}5^d$ transitions responsible for the FR of rare earth doped matrix were evaluated from the representation of the inverse of the VC versus λ^2 (see insert Fig.2); for Dy^{3+} λ_{eff} was found to be 119 nm and 126 nm for Tb^{3+}, values somewhat higher than for free ions. This is related to the type of chemical bonds between the RE ion and surrounding matrix, stronger covalent bonds giving rise to stronger ligand fields and hence to a larger splitting of 5d levels which may superpose over the 4f ones. In concordance with the Van Vleck and Hebb assumption, the ratio between the paramagnetic contribution to the VC and the paramagnetic susceptibility was obtained independent of rare earth content (Fig.2).

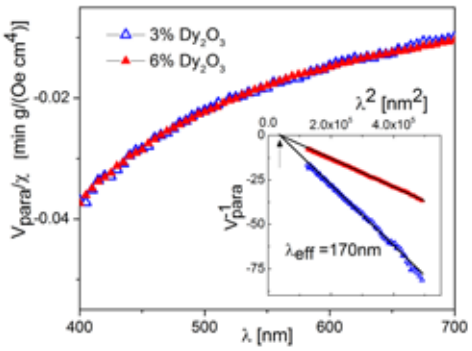

Fig. 2: Wavelength dependence of V_{para}/χ_{para} for 3 mol % and 6 mol % Dy_2O_3 samples. In the inset are shown the dependencies of inverse V_{para} versus the square wavelength for $\lambda>\lambda_{eff}$.

For applications of much practical interest would be the representation of a normalized VC per molar percent of RE. By choosing a suitable level of doping with paramagnetic rare earth elements one could design an optical glass with zero Faraday rotation. It is to note that both the diamagnetic and paramagnetic FR being wavelength dependent, a complete compensation can be achieved only over a very narrow wavelength range. For example, in the present case, the diamagnetic glasses introduce a positive rotation of about 0.018 min/Oe/cm at λ=600 nm. While the negative rotation introduced by 1mol% Tb_2O_3 is -0.007 min/Oe/cm, the positive rotation can be compensated in a glass containing about 2.5mol% Tb_2O_3. Fig 3 shows the VC for some aluminophosphates with different doping level of Tb_2O_3 designed to induce a zero FR at 405, 465, 580 or 635nm [4].

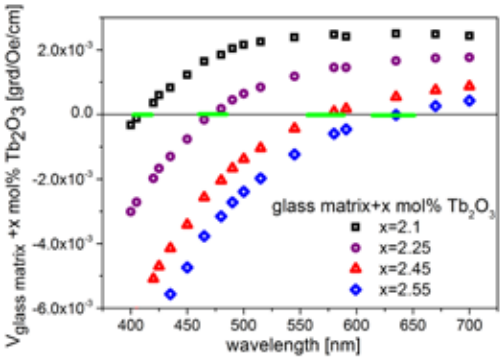

Fig. 3: Wavelength dependent compensation of FR in glasses doped with different mol% of Tb_2O_3

Funding from PCCA_186/2012 and Nucleus Program PN16-4801.

References

[1] Borrelli N F, J.Chemical Physics , 41(11), 3289 (1964)

[2] M. Valeanu, M. Sofronie, A.C. Galca, F. Tolea, M. Elisa, B. Sava, L. Boroica and V. Kuncser „Relationship between magnetism and magneto-optical effects in new aluminophosphate glasses" Journal of Physics: Condensed Matter 49, 075001, (2016)

[3] M. Sofronie, M. Elisa, B. A. Sava, L. Boroica, M. Valeanu, and V. Kuncser "Rapid determina-tion of Faraday rotation in optical glasses by means of secondary Faraday modulator" Review of Scientific Instruments 86, 053905 (2015);

[4] Patent: a/2016/00121 "A method of design for optical glasses with null Verdet constant" Authors: Aurel Leca, Mihaela Sofronie, Victor Kuncser, Mihaela Valeanu, Mihail Elisa, Bogdan Sava

NANOSCALE PHYSICS

SELECTED RESULTS

On the agent role of Mn^{2+} in redirecting the synthesis of $Zn(OH)_2$ towards nano-ZnO with variable morphology

D. Ghica, I.D. Vlaicu, M. Stefan, L.C. Nistor and S.V. Nistor

National Institute of Materials Physics

Doping nanocrystals, typically grown using colloidal synthesis, is still an experimental challenge and the progress in controlling and understanding the incorporation of impurities in semiconductor nanocrystals has been slow [1]. Thermally induced decomposition of doped precursors has proved to be an efficient alternative way to obtain doped nanocrystals. Zinc hydroxide - $Zn(OH)_2$ has attracted a lot of interest during the last years as a precursor in the synthesis of nano-ZnO with controlled size and morphology. Therefore doped $Zn(OH)_2$ was expected to be a valuable precursor for doped nano-ZnO. However, our attempts to prepare $Zn(OH)_2$ by coprecipitation in the presence of Mn^{2+} ions failed to produce the expected $Zn(OH)_2$:Mn [2], each sample resulting in nano-ZnO:Mn. To our knowledge, this is the first observation of a redirection of the $Zn(OH)_2$ synthesis towards nano-ZnO by doping instead of by modifying synthesis or post-synthesis parameters as temperature, pressure, stirring.

In an effort to understand the extent of the manganese effect on the reaction products and to determine the Mn^{2+} concentration threshold for the synthesis redirection to take place, we performed a systematic study of the samples prepared without and with a Mn^{2+} source, varying the nominal Mn^{2+} ions concentration. Structural and morphological studies were performed by X-ray diffraction (XRD), transmission electron microscopy (TEM) and Fourier transform infrared (FTIR) spectroscopy.

The localization and distribution of the Mn^{2+} ions in the $Zn(OH)_2$ and ZnO samples were determined by multifrequency electron paramagnetic resonance (EPR) spectroscopy in the Center for advanced ESR techniques (CetRESav - http://cetresav.infim.ro) from our institute. All samples were prepared by coprecipitation as described in refs. 2, 3.

The XRD investigation of the samples prepared without Mn^{2+} and with Mn^{2+} ions in a wide nominal concentrations range showed that the synthesis redirection takes place for a Mn^{2+} concentration as low as 1 ppm (Fig. 1) [3]. In the doped samples the synthesis product is ZnO with mean crystallite sizes slightly decreasing with the Mn concentration increase (from 38 nm – 1ppm Mn to 32 nm – 5000 ppm Mn). The morphology and size of the ZnO:Mn nano-particles vary, as evidenced in the TEM images [3], from mostly lamellar and rod shaped towards a rather uniform spherical shape with smaller sizes, due to the increase of the Mn concentration.

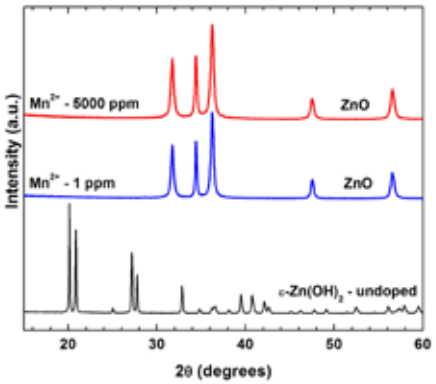

Fig. 1: XRD diffractograms of the undoped (bottom) and Mn^{2+} doped (upper) samples.

The Q-band EPR spectra of the undoped and doped samples (Fig. 2) consist of Mn^{2+} ions spectra with different hyperfine splitting, associated with the crystalline structure changes [3]. Fig. 3 gives an example of an EPR spectrum of a doped sample which is decomposed in components corresponding to the Mn^{2+} ions substitutionally localized in tetrahedrally coordinated Zn^{2+} sites in nanocrystalline ZnO - (c), disordered ZnO - (d) and isolated Mn^{2+} ions segregated in a disordered secondary phase (x) [3]. We showed by FTIR that this secondary phase could consist of remaining nitrate compounds from the precursors, in an amount below the detection limit of XRD. We also found out by quantitative EPR investigations that the percentage of segregated Mn^{2+} ions from the total concentration of Mn^{2+} ions incorporated in the samples decreases with the nominal concentration increase, while the percentage of Mn^{2+} ions localized in ZnO nanocrystals increases [3].

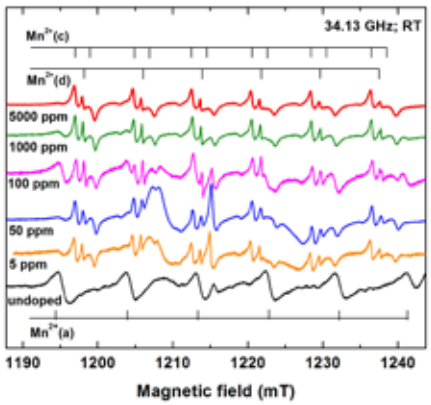

Fig. 2: Multiscan Q-band EPR spectra for the undoped (bottom) and Mn^{2+} doped (upper) samples. The six hyperfine lines / doublet-lines of the Mn^{2+} (a), Mn^{2+} (d) / Mn^{2+} (c) paramagnetic centers are marked with vertical bars.

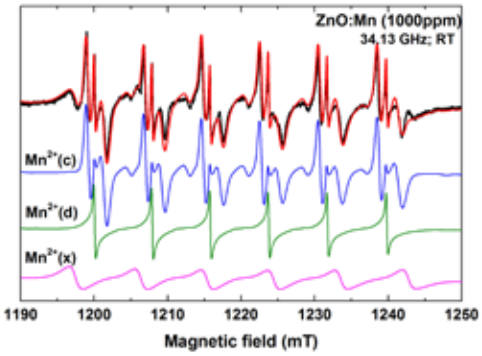

Fig. 3: Experimental (black) and simulated (red) Q-band EPR spectrum of the ZnO:Mn (1000 ppm) sample. Contributions to the simulated spectrum of the Mn^{2+} ions localized in crystalline (Mn^{2+}(c) - blue) and disordered (Mn^{2+}(d) - green) ZnO environment, and in the unknown disordered phase (Mn^{2+}(x) - magenta) are shown below.

To investigate the role of the Zn^{2+} ions in obtaining ZnO:Mn instead of $Zn(OH)_2$:Mn, other metal hydroxides such as $Mg(OH)_2$, $Ca(OH)_2$ and $Cd(OH)_2$ were synthesized by the same procedure in both pure and Mn^{2+} doped (1000 ppm) forms. We have found out by XRD [3] that this effect takes place only for $Zn(OH)_2$, while the synthesis of other M(II) hydroxides (M(II) = Ca^{2+}, Mg^{2+}, Cd^{2+}) by the same procedure is not affected by the presence of a Mn source in the starting material. A possible explanation for the synthesis redirection from $Zn(OH)_2$ towards nano-ZnO is based on the different coordination properties of the Mn^{2+} and Zn^{2+} ions, which could lead to a coordinative hindrance for the Mn^{2+} ions [3]. Indeed, while $Mn(OH)_2$, $Mg(OH)_2$, $Ca(OH)_2$, $Cd(OH)_2$ exhibit the same CdI_2 type crystal structure (hexagonal system), where each cation is surrounded by six anions forming a slightly compressed octahedron, in the case of $Zn(OH)_2$ the Zn^{2+} ion has a tetrahedral coordination, each cation being surrounded by four anions.

TEM and FTIR investigations evidenced morphological changes of the ZnO nanostructures associated with the Mn concentration increase [6]. This result points to an interesting possibility to control the morphology and size of the ZnO nanostructures by varying the doping concentration, which is important for designing ZnO nanoparticles with high surface area for specific applications, such as catalysis or gas sensing.

Funding from ANCS, Core Program project number PN16-480102 and from a grant of the Romanian National Authority for Scientific Research and Innovation, CNCS – UEFISCDI, project number PN-II-RU-TE-2014-4-0939.

References

[1] D. J. Norris, A. L. Efros, S. C. Erwin, Doped nanocrystals, Science 319, 1776 (2008).

[2] S. V. Nistor, D. Ghica, M. Stefan, I. Vlaicu, J. N. Barascu, C. Bartha, Magnetic defects in crystalline $Zn(OH)_2$ and nanocrystalline ZnO resulting from its thermal decomposition, J. Alloys Compd. 548, 222 (2013).

[3] D. Ghica, I. D. Vlaicu, M. Stefan, L. C. Nistor, S. V. Nistor, On the agent role of Mn^{2+} in redirecting the synthesis of $Zn(OH)_2$ towards nano-ZnO with variable morphology, RSC Advances 6, 106732 (2016).

Multitechnique characterization of iron oxide based MRI contrast agents in murine model

V. A. Maraloiu, V. S. Teodorescu, I. D. Vlaicu, M. Stefan, D. Ghica

National Institute of Materials Physics

in collaboration with A. Tamion; M. Hillenkamp; A. Hillion; H. Rositi; F. Chauveau; D. Le Guellec; M.-G. Blanchin; M. Wiart; V. Dupuis University of Lyon, France

F. Appaix, A. Broisat, C. Ghezzi, B. van der Sanden Grenoble Institute of Neuroscience, France

Magnetic particles of iron oxide are used in a wide range of biomedical applications. A promising application of Ultra small SuperParamagnetic Iron Oxide (USPIO) agents is MR lymphography. An important characteristic of any contrast agent is its elimination from the body.

We used a multitechnique approach to determine the fate of nanoparticles after administration in murine model. 8 nm crystalline maghemite (γ-Fe_2O_3) core nanoparticles coated with organic coverage derived from glucose and with a dye Texas Red Cadaverine covalently linked to the surface were administered in atherosclerotic $ApoE^{-/-}$ and control C57Bl6 mice. Ex vivo samples of aorta, kidneys, liver and spleen were taken at different times (between 1 to 419 days) after intravenous injection.

Two Photon Laser Scanning Microscopy (TPLSM) showed a heterogeneous distribution of nanoparticles, mostly localized in macrophages under the fibrous collagen cap (Figure 1) [1]. Transmission electron microscopy (TEM) techniques were employed to determine the biolocalization and biodegradation of USPIOs. At Day 20 after iv injection, USPIOs were sequestered in vesicles (CTEM view, Figure 2a). Electron diffraction patterns (Figure 2 c-e) recorded in different areas of a phagolysosome demonstrate that there are USPIOs remained crystallized in the maghemite structure, but also USPIOs transformed into ferritin, an iron storage protein. Quantifications of Electron Energy Loss Spectroscopy (EELS) spectra present the variations of atomic concentrations from [O]=61%, [Fe]=39% (characteristic to maghemite composition) to [O]=72%, [Fe]=28% (characteristic to ferritin) [2]. The biotransformation of USPIOs into ferritin was also confirmed by Electron Paramagnetic Resonance (EPR) measurements and zero-field-cooled (ZFC) / field cooled (FC) susceptibility measurements. Figure 3 shows that the obtained ZFC/FC curve is the superposition of USPIO and ferritin contributions [2].

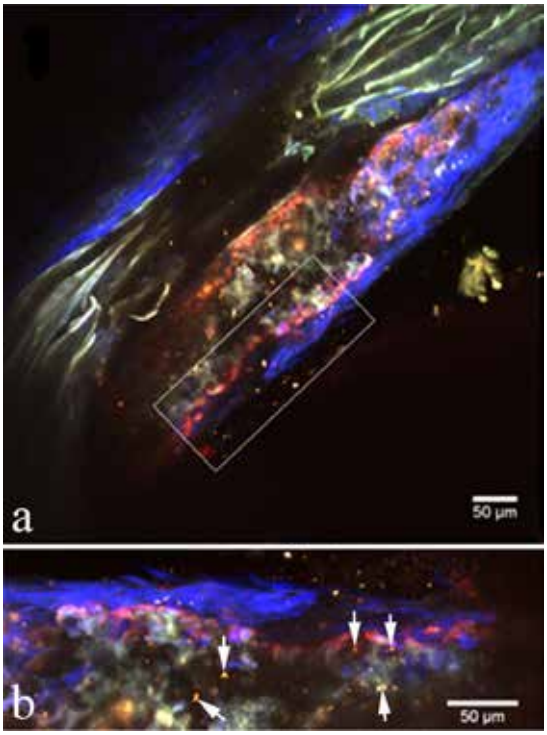

Figure 1: (a) Z-projections of 68 TPLSM images with 3 m slice spacing of atherosclerotic plaques in non-fixed aortic rings 20 days after USPIOs iv injection. (b) Zoom of (a) (white rectangle) showing that USPIO particles (arrows) were mostly detected under the collagen cap (blue, endogenous SHG signals).

Using a multitechnique approach, we determined the biolocalization and biotransformation of USPIOs and we showed for the first time that USPIOs biotransformation leads to excess ferritin in the spleen for more than one year post-injection.

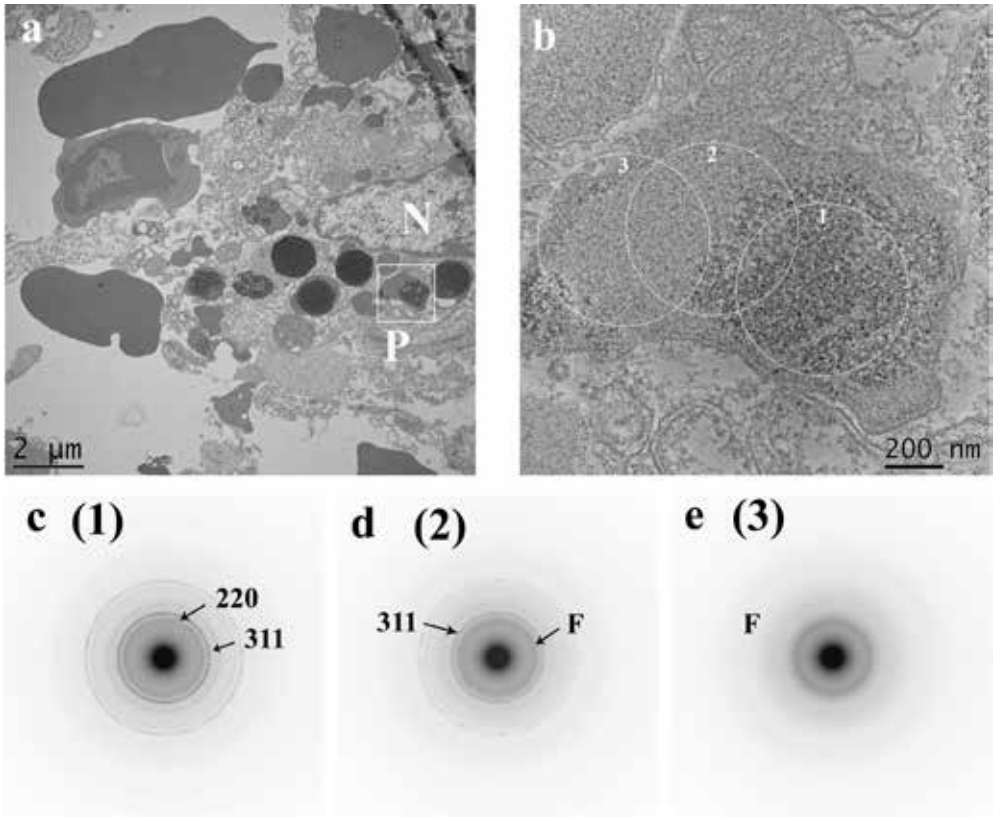

Figure 2: TEM study of the spleen at D20: (a) overview of a cell with nucleus (N) and several phagolysosomes; (b) enlargement of the phagolysosome P (framed area), exhibiting three different regions 1 to 3; (c-e) electron diffraction patterns corresponding to regions 1 to 3 respectively; 220 and 311 rings correspond to intense reflections from maghemite structure, F corresponds to the brightest 102 ring of ferrihydrite structure.

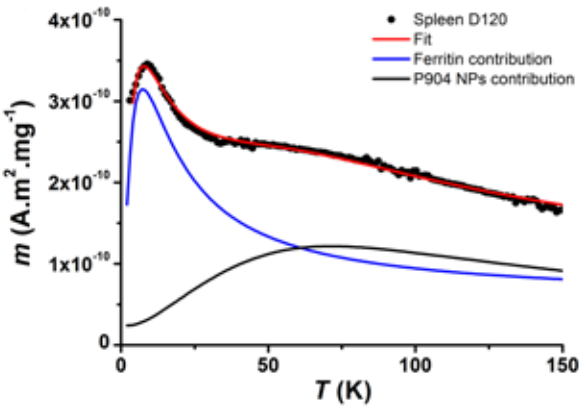

Figure 3: ZFC/FC curves at D120 for spleen. The fit was obtained using the P904 USPIO and ferritin contributions.

Financial support from ANCSI Romania, CORE project No. PN09-450102 and from Romanian National Authority for Scientific Research, CNCS – UEFISCDI, project number PN-II-RU-PD-2011-3-0067.

References

[1] V.A. Maraloiu, F. Appaix, A. Broisat, D. Le Guellec, V.S. Teodorescu, C. Ghezzi, B. van der Sanden, M.G. Blanchin; "Multiscale investigation of USPIO nanoparticles in atherosclerotic plaques and their catabolism and storage in vivo"; Nanomedicine: Nanotechnology, Biology and Medicine 12 (1), 191-200 (2016).

[2] A. Tamion; M. Hillenkamp; A. Hillion; V.A. Maraloiu; I.D. Vlaicu; M. Stefan; D. Ghica; H. Rositi; F. Chauveau; M.-G. Blanchin; M. Wiart; V. Dupuis; "Ferritin surplus in mouse spleen 14 months after intravenous injection of iron oxide nanoparticles at clinical dose"; Nano Research; 9(8), 2398-2410 (2016).

Ge nanocrystals embedded in oxides with memory and photosensing properties

A-M. Lepadatu, A. Slav, I. Stăvărache, C. Palade, A. Mărăloiu, C. Logofătu, S. Lazanu, T. Stoica, V. S. Teodorescu, M. L. Ciurea

National Institute of Materials Physics

in cooperation with D. Vasilache[1], A. Cismaru[1], M. Dragoman[1], M. Braic[2], A. Kiss[2], P. Prepelita[3]

[1]National Institute for Research and Development in Microtechnologies, Romania

[2]National Institute for Optoelectronics, Romania

[3]National Institute for Laser, Plasma and Radiation Physics, Romania

Ge nanocrystals (NCs) in oxides are great candidates as active materials in different structures / devices, the most important being trilayer memory capacitors and photosensitive sandwich structures. In the trilayer structures, the intermediate layer of Ge NCs plays the role of floating gate in which the NCs act as charge storage centers, while in the photosensitive structures, the film of Ge NCs embedded in oxides is photosensitive as photogenerated carries are trapped in Ge NCs. The morphology (NCs size, density, spatial distribution) of active layer controls the specific properties of structures / devices.

We prepared ***gate oxide/floating gate of Ge NCs in oxide/tunnel oxide/p-Si wafer*** trilayer capacitors with gate and tunnel layers of HfO_2 or SiO_2. The floating gate of Ge NCs in oxide was obtained in two approaches, by depositing either a continuous Ge or a Ge-oxide intermediate layer. All layers were deposited by magnetron sputtering, except tunnel SiO_2 that was thermally grown in the rapid thermal processor. The as-deposited structures are amorphous and a subsequent rapid thermal annealing (RTA) was performed for nanostructuring, i.e. Ge and HfO_2 NCs formation. Also, RTA controls the density and size of Ge NCs and also the separation of floating gate to Si substrate. The best memory structures are obtained for 600 °C and 7–8 min RTA in the case of using HfO_2 and 900 °C and 15 min RTA for SiO_2-based trilayers [1–4]. The capacitors are completed with top and bottom Al electrodes.

Photosensitive films of $GeSiO_2$ were deposited on heated n-Si wafers (300, 400 and 500 °C) using magnetron sputtering without subsequent annealing. ITO top electrode and Al bottom were used.

Aiming to obtain enhanced memory and photosensing properties, we focused our attention on manipulating the morphology of trilayers and photosensitive layers. We complexly characterized the structures by (HR) TEM, HAADF-STEM and EDX, XPS and Raman spectroscopies. The structures functionality was proven by specific measurements of ***C-V*** and ***C-t*** curves for capacitors, and photocurrent spectral distribution and photocurrent-voltage curves for photosensitive layers.

Fig. 1 reveals by HAADF-STEM and HRTEM images the ***gate HfO_2/Ge NCs in HfO_2/tunnel HfO_2/p-Si*** trilayer with as-deposited continuous Ge intermediate layer annealed at 600 °C. One can see that HfO_2 is crystallized, and in the intermediate layer a row of 5–7 nm Ge nanoparticles located in the initial position of as-deposited Ge layer is evidenced [1]. These nanoparticles are crystalline as shows Raman peak at 299.2 cm^{-1} in Fig. 2, corresponding to quantum confinement of phonons in 6.5 nm Ge NCs.

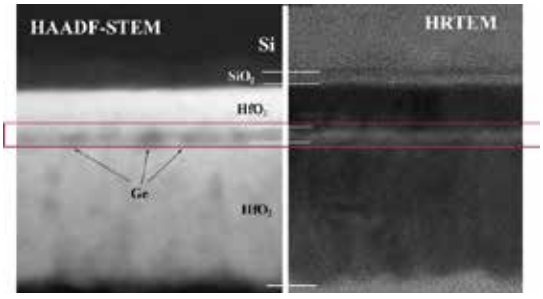

Fig. 1: HAADF-STEM and HRTEM images on a ***HfO_2/Ge/HfO_2/p-Si*** trilayer structure, 600 °C RTA.

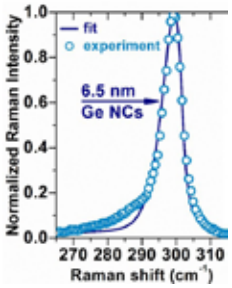

Fig. 2: Raman spectrum measured on a ***HfO_2/Ge/HfO_2/p-Si*** trilayer structure, 600 °C RTA.

The ***C-V*** characteristics recorded on these capacitors are presented in Fig. 3. They show a hysteresis loop with memory window ΔV = 1 V independent on the frequency showing the charge storage only in Ge NCs. The ***C-t*** curves show ~25% capacitance decay after first 4000 s followed by a very slow capacitance decrease (inset of Fig. 3).

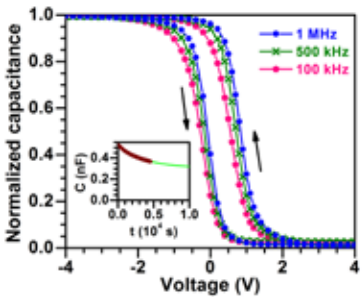

Fig. 3: Normalized ***C-V*** curves and ***C-t*** decay (1 MHz) taken on $HfO_2/Ge/HfO_2/p\text{-}Si$ trilayer, 600 °C RTA.

Based on the $HfO_2/Ge/HfO_2/p\text{-}Si$ trilayers, a matrix of discrete capacitors was fabricated showing good memory properties [5]. Also, a cross-bar memory structure based on Ge NCs in SiO_2 was fabricated, the best memory window being of 2 V [2].

By using $HfO_2/Ge\text{-}HfO_2/HfO_2/p\text{-}Si$ trilayers with co-sputtered intermediate layer instead of a continuous Ge one, an improvement of memory properties is achieved [3], e.g. memory window of ~1.8 V (Fig. 4).

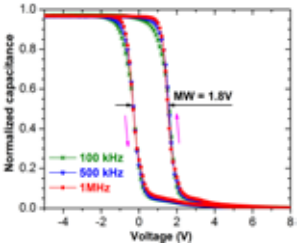

Fig. 4: Normalized ***C-V*** curves measured on $HfO_2/Ge\text{-}HfO_2/HfO_2/p\text{-}Si$ capacitor, 600 °C RTA.

In the case of photosensitive $GeSiO_2/n\text{-}Si$ ***wafer*** structures the photoelectric properties are enhanced by adjusting the substrate temperature during deposition (from 300 to 500 °C) also by tailoring the structure and morphology. Fig. 5 clearly shows by XRD measurements the modification of structure with the increase of substrate temperature. For 300 °C, the films are amorphous, while for 400 and 500 °C, the films are crystallized in cubic Ge NCs (~5 nm size).

The best photoresponse characteristics were obtained for films deposited at 500 °C, being ~10^3 photocurrent to dark current ratio and 7 A/W responsivity (Fig. 6) [6].

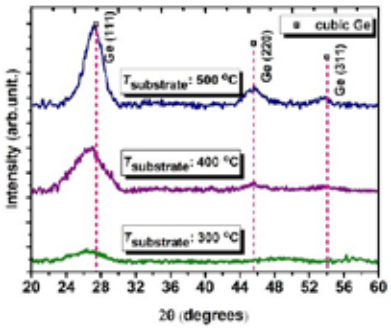

Fig. 5: XRD diffractograms measured on $GeSiO_2$ ***films*** deposited at different substrate temperatures.

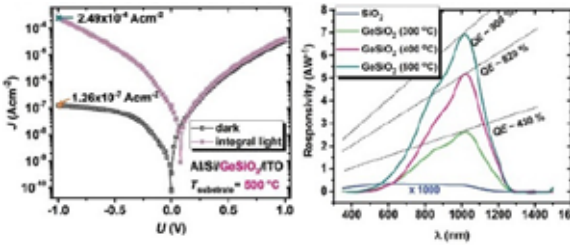

Fig. 6: $Al/Si/GeSiO_2/ITO$ structures with photosensitive film deposited at 500 °C: left, ***I-V*** curves measured in dark and integral light; right, spectral responsivity curve compared with the ones for 300 and 400 °C deposition and with the one obtained on a SiO_2 film.

We can conclude that the morphology of active layer, i.e. floating gate with charge storage centres of Ge NCs or photosensitive layer with Ge NCs embedded in oxide, is the key for enhancing the desired properties.

References

[1] A. Slav, C. Palade, A.M. Lepadatu, M.L. Ciurea, V.S. Teodorescu, S. Lazanu, A.V. Maraloiu C. Logofatu, M. Braic, A. Kiss, Scripta Mater. **113**, 135-138 (2016).

[2] D. Vasilache, A. Cismaru, M. Dragoman, I. Stavarache, C. Palade, A.-M. Lepadatu, M.L. Ciurea, Phys. Status Solidi A **213**, No. 2, 255-259 (2016).

[3] A.M. Lepadatu, Proc. Romanian Acad. A **17**, 322-327 (2016).

[4] C. Palade, A. Slav, A.-M. Lepadatu, A.V. Maraloiu, S. Lazanu, C. Logofatu, V.S. Teodorescu, M.L. Ciurea, CAS 2016 IEEE Proc. (2016 International Semiconductor Conference, Oct. 10-12, Sinaia, Romania), pp.163-166, New York (2016).

[5] A. Slav, C. Palade, A.-M. Lepadatu, S. Lazanu, M.L. Ciurea, D. Vasilache, M. Dragoman, patent application A/00723, OSIM (2016)

[6] I. Stavarache, V.A. Maraloiu, P. Prepelita, G. Iordache, Beilstein J. Nanotechnol. **7**, 1492-1500 (2016).

Optical signatures of magnetic impurities in self-assembled quantum dots

V. Moldoveanu, I. V. Dinu, R. Dragomir

National Institute of Materials Physics

The original motivation for studying magnetic quantum dots is to be found in the observation of six exchange-induced exciton photoluminescence emission lines for CdTe QDs doped with a single Mn atom [1]. In more recent papers [2] such magnetic impurities are called solitary dopants. Possible schemes for optical manipulation of their localized spin encourage the rather fancy name ”solotronics”. In most experiments the ground state exciton states are made of heavy holes (HH). However, the light-hole (LH)-HH mixing in optically active QDs cannot be always neglected. Recent experiments [3] revealed that the highest energy level in the valence band can be tuned from a HH-like character to LH-like character. This tuning can be achieved either by applying strain or by modifying the shape of the dot. In particular, if the height is larger than the radius, the dot becomes a nanopillar, its aspect ratio H/2R is large and induces a light-hole character. The starting point of our work was simply this: can we find traces of exchange-induced LH spin flip in the optical properties of such QDs? From the theoretical point of view we go beyond the two-band effective models borrowed from quantum optics. In these models the interaction effects are neglected and the geometry of the QD or the location of the magnetic impurity are not even discussed.

The single-particle states for electrons and holes are found via Kohn-Luttinger kP theory within the envelope function approximation. The electron-Mn and hole-Mn spin-spin interactions are short-ranged and depend explicitly on the position of the magnetic impurity in the dot. Also, it turns out that the strengths of the two exchange interactions are different, the hole-Mn interaction being four times larger than the electron-Mn coupling. The crucial point here is that by changing the Mn location one changes the exchange interaction strength and all the spectral properties. We take into account the Coulomb interaction and we calculated the corresponding many-body states (MBS) within the configuration interaction method. The contribution of the magnetic anisotropy is also included.

From Fig. 1 one notices that if the QD height H is larger than 9nm the weight of the LH state in the fundamental valence band state is about which makes the associated state mostly LH. It is then clear that for QD nanopillars the excitonic response is controlled by LH excitons.

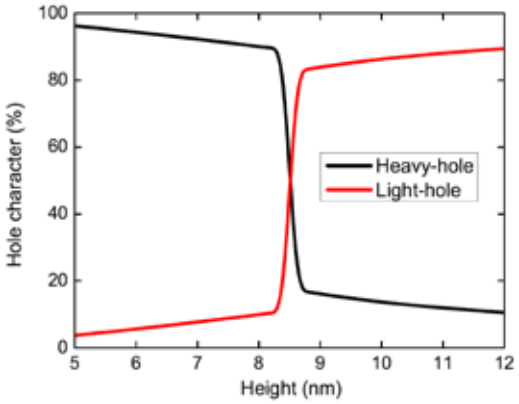

Fig. 1: The weights of the HH and LH character in the lowest energy valence-band state as a function of the QD height. The QD radius R=5 nm.

The exchange interaction induces simultaneous ”jumps” of the two interacting spins by exactly one spin quanta. In particular the LHs spin reversal from down to up can only happen if the Mn spin decreases by one, such that that the states involved in flip processes will ”mingle” in a superposition of states. Such a superposition contains both bright and dark excitons. It is precisely this coupling one can explore to detect dark excitons. In fact a large amount of bright excitons in a given mixture leads to a higher absorption peak in the exciton spectra.

The effects of these spectral properties on the optical response are shown in Fig. 2. Suppose we start from the ground state (i.e there are no conduction electrons, the valence states are fully occupied and the Mn spin is maximal (5/2). Then using the Fermi Golden Rule we can derive the absorption spectra corresponding to light pulses of circular left polarization σ_- or right polarization σ_+. The red peaks correspond to excitons activated by σ_- pulses while the blue peak corresponds to the single LH exciton activated by σ_+ pulse. This exciton cannot be mixed because flipping the electron spin would require the increase of the Mn spin which is

already maximal. Note that the blue peak is almost insensitive to the Mn location. On the contrary, for the σ_- pulse we observe a multiple peak structure. If the Mn is located at the center of the dot we get 4 absorption peaks. However, as the Mn atom is shifted towards the top edge of the dot only two peaks appear.When the Mn atom is located on the cylinder top edge the exchange interaction vanishes and one recovers the four exchange-free excitons. Clearly, at z_{Mn} = 5.14 nm we are left with only two optically active excitons that give rise to two photoluminescence peaks which are clearly associated with mixtures of bright and dark excitons. These qualitatively different PL spectra can serve to check the location of the Mn atom within the dot, and to estimate the strength of the h-Mn exchange interaction.

The dependence of the exchange interaction on the Mn position leaves its fingerprints on the exciton and biexciton dynamics. We illustrated this fact by studying the exchange-induced Rabi oscillations of the LH excitons and mixed biexcitons. Damping due to the intraband relaxation was also taken into account.

Our results were recently published in [4].

Funding: PNII-ID-PCE Grant No.103/2011, Core Programme Contract No. PN16-480101.

References

[1] L. Besombes et al., Phys. Rev. Lett. 93, 207403 (2004).

[2] J.Kobak et al., Nat.Comm. 5, 1 (2014).

[3] Huo et al. Na. Physics 10, 46 (2014).[4]V. Moldoveanu et al., Phys. Rev. B 93, 165421 (2016).

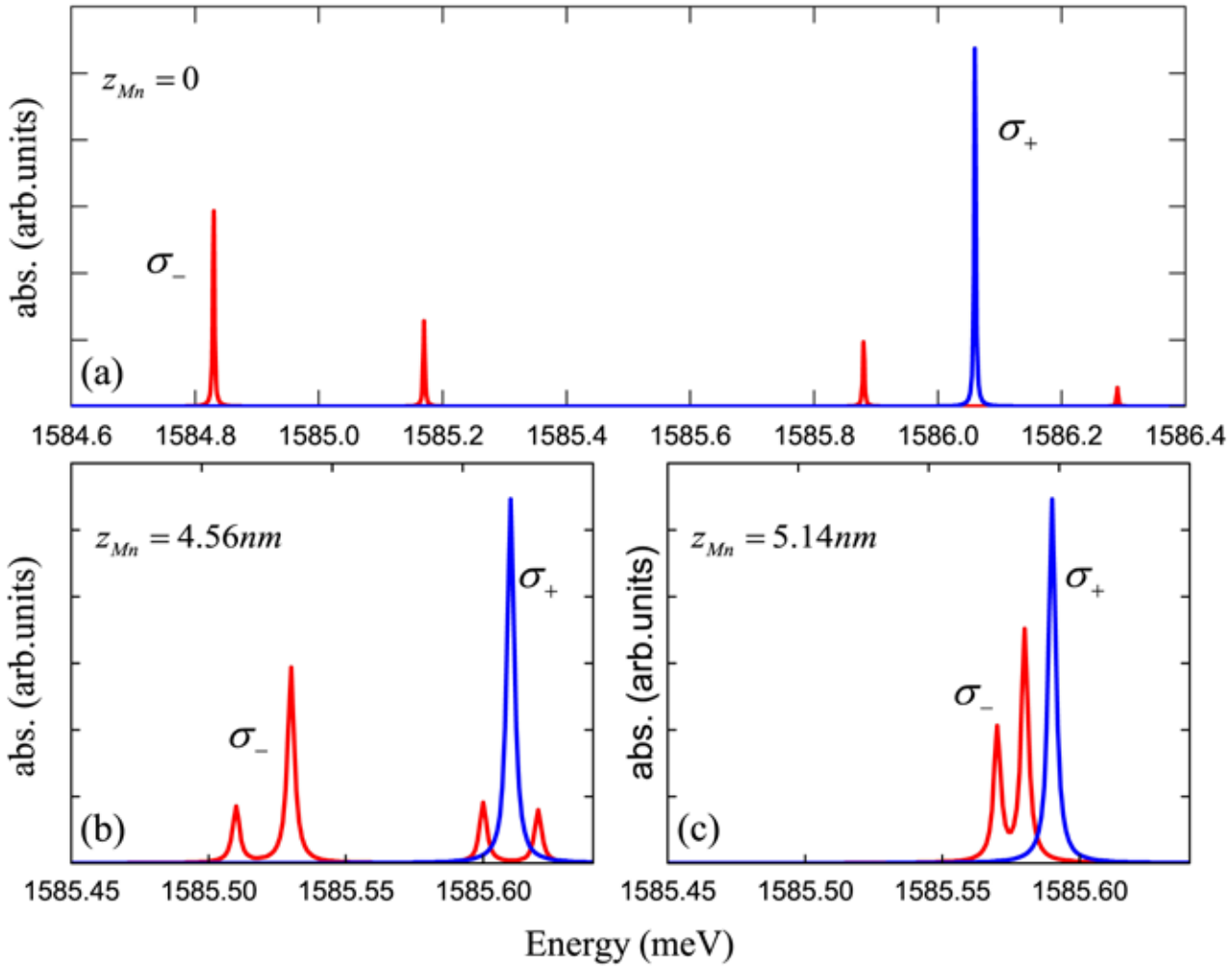

Fig. 2: Light-hole exciton absorption spectra associated to σ_- (red) and σ_+ (blue) pulses for several positions of the Mn atom on the z-axis. (a) z_{Mn} = 0, (b) z_{Mn} = 4.56nm ,(c) z_{Mn} = 5.14nm.

Phosphorene topological edge states and quantum transport

B. Ostahie, A. Aldea

National Institute of Materials Physics

The very recent revival of the black phosphorus physics comes from the technical possibility to obtain monolayers, known as phosphorene, with specific topological properties. Phosphorene is a quasi-two-dimensional structure organized as a puckered hexagonal lattice, the top and side views being shown in Figs. 1 (a) and 1 (b), respectively. One may think that, due to the structural similarity, the electron properties of phosphorene are resembling those of graphene. However, in contradistinction to graphene, the phosphorene is an anisotropic direct gap semiconductor, much more attractive for electronic devices. Aside from the monolayered structure, multilayers of black phosphorous are also studied, mainly in order to control the band gap, in the perspective of a potential application for field-effect transistors.

In the tight-binding model, the phosphorene lattice is described by five hopping integrals t_1, t_2, ..., t_5 [1], which induce the significant differences in the electron spectrum that are noticed when compared to graphene. The model points out also the anisotropy of the energy spectrum: both the top of the valence band and the bottom of the conduction band look quadratically as function of k_y, but nearly linear as function of k_x (Dirac-type) (see Fig. 2), a situation which is described in terms of hybrid Dirac spectrum [2]. The hopping integral t_4 plays a distinctive role as it connects sites of the same kind on the hexagonal lattice, breaking the bipartitism of the lattice, and, as a consequence, the electron-hole symmetry of the energy spectrum is also broken.

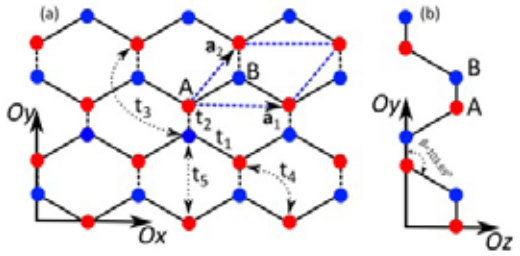

Fig. 1: (a) Schematic representation of phosphorene t_1, t_2, t_3 , t_4 , t_5 are the hopping amplitudes that connect the lattice sites; A (red) and B (blue) index the two types of atoms, and the dashed blue lines represent the unit cell with a_1 and a_2 as unit vectors. (b) The projection of the lattice on the *yz* plane.

The Hamiltonian of the phosphorene lattice describe in the Fig.1 can be write as:

$$H = H_0 + H_4 \qquad (1)$$

$$H_0 = \sum_{n,m} E_A a^{\dagger}_{n,m} a_{n,m} + E_B b^{\dagger}_{n,m} b_{n,m} +$$
$$t_1(e^{i\phi_1} a^{\dagger}_{n+1,m} + e^{-i\phi_1} a^{\dagger}_{n,m}) b_{n,m} + t_2 a^{\dagger}_{n,m+1} b_{n,m}$$
$$+t_3 e^{i\phi_3} a^{\dagger}_{n,m+2} + e^{-i\phi_3} a^{\dagger}_{n-1,m+2}) b_{n,m}$$
$$+t_5 a^{\dagger}_{n+1,m-1} b_{n,m} + H.c.$$

$$H_4 = \sum_{n,m} t_4(e^{i\phi_{4B}} b^{\dagger}_{n,m+1} + e^{-i\phi_{4B}} b^{\dagger}_{n-1,m+1}) b_{n,m}$$
$$+t_4(e^{i\phi_{4A}} a^{\dagger}_{n,m+1} + e^{-i\phi_{4A}} a^{\dagger}_{n-1,m+1}) a_{n,m} + H.c.$$

were E_A and E_B are the atomic energies at the sites A and B, respectively, and, according to [1], t_1 = - 1.22 eV, t_2 = - 3.655 eV , t_3 = - 0.205 eV, t_4 = - 0.105 eV, t_5 = - 0.055 eV. In the chosen gauge of the vector potential, only three hopping integrals acquire a Peierls phase in magnetic field, namely, t_1, t_3, and t_4. The spectral properties of the Hamiltonian (1) can be studied under different boundary conditions describing different geometries as the infinite sheet, the ribbon, or the finite plaquette. The phosphorene infinite sheet can be simulated assuming periodic boundary conditions along the both directions O_x and O_y.

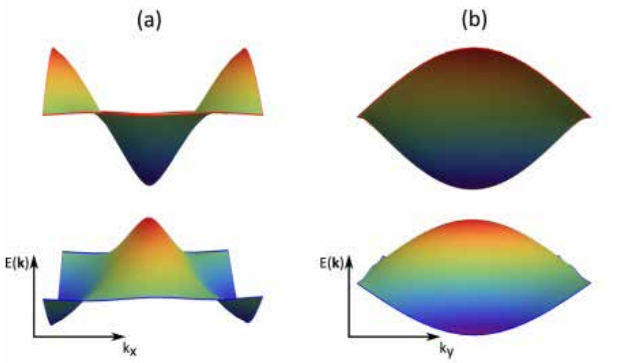

Fig. 2: The energy spectrum of the phosphorene lattice with periodic boundary conditions. The anisotropy of the spectrum around the point can be observed: (a) Dirac-type behavior, and (b) Schrodinger-type behavior.

The energy spectrum of the Hamiltonian (1) can be obtained analytically from the characteristic equation resulting a two-band spectrum of

semiconducting type. The eigenvalues are displayed in Fig. 2, where three aspects have to be noticed: the presence of the gap, the strong anisotropy, and the electron-hole asymmetry of the bands.

To investigate the transport properties in strong perpendicular magnetic field, we simulate the electronic Hall device by attaching four leads to a finite phosphorene plaquette [2].

In what concerns the Hall conductance in the quantum regime, there are significant new aspects in comparison with the graphene. First, one has to notice the large plateau $G_H = 0$ that corresponds to the central gap Fig.3. Next, one notices the lack of the valley degeneracy in the low-energy range, such that the quantum Hall plateaus are the conventional (spinless) plateaus n = 0, ±1, ±2, ... in units e^2/h, the same as for the twodimensional electron gas (2DEG) subject to a perpendicular magnetic field. As a specific feature, one may notice in Fig. 3 that the lengths of the plateaus in the positive and negative regions are slightly different, as a manifestation of the spectral asymmetry. The quantum plateaus are supported obviously by the chiral edge states existing in the Hofstadter spectrum of the finite-size plaquette, however, one should not forget that the central gap contains also topological edge states bunched in the quasiflat band. The value $G_H = 0$ everywhere in the gap confirms that these edge states are nonchiral, and do not support the QHE.

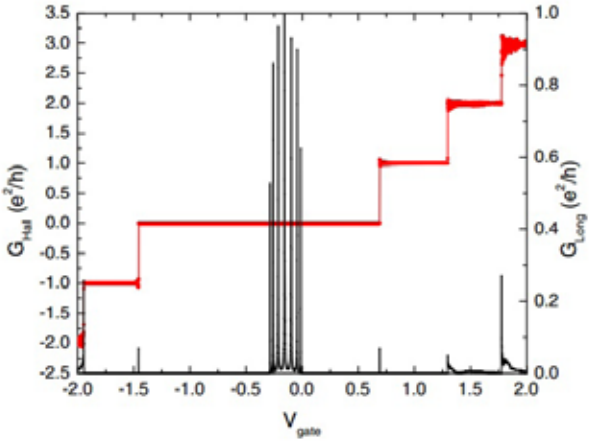

Fig. 3: Hall and longitudinal conductances in the quantum Hall regime as a function of the gate potential. The longitudinal conductance shows a series of peaks in the range of the quasiflat band.

In this paper we have studied the spectral and transport properties of phosphorene lattice, and we put in evidence the anisotropy of energy spectrum, and the non-chirality of the topological edge states by simulating a quantum Hall device.

We acknowledge the financial support from Romanian Core Research Programme PN16-480101.

References

[1] A. N. Rudenko and M. I. Katsnelson, Phys. Rev. B 89, 201408(R) (2014).

[2] B. Ostahie and A. Aldea Phys. Rev. B 93 075408 (2016).

Magnetite nanoparticles. Controlling magnetic properties by nucleation and inter-particle interactions

V. Sandu, S. Greculeasa, A. Kuncser, G. Schinteie, P. Papade, C. Bartha, V. Kuncser

National Institute of Materials Physics

in collaboration with N. Iacob[1] and L.Vekas[2]

[1]National Institute for Laser, Plasma and Radiation Physics

[2]Laboratory of Magnetic Fluids, Romanian Academy-Timisoara Division

Magnetite nanoparticles embedded in glassy matrices, i.e., magnetite-based glass-ceramics, display interesting magnetic properties which depends on the growth procedure. Glass-ceramics grown by controlled crystalliza-tion of iron-containing parent borosilicate glasses in the presence of P_2O_5 (1%wt) as nucleating agent were investigated. Their physics mirrors both the properties of the magnetically ordered grains/ crystallites of magnetite and the paramagnetism of the glassy matrix. All batches had a constant content of boron and sodium oxides (28.6 wt% B_2O_3 and 6.4 wt% Na_2O) but different amounts of Fe_2O_3. Specifically, 17.5 and 24.5 wt% Fe_2O_3 were used for the batches labelled as BSFP17 and BSFP24, respectively. The rest was SiO_2. A reference glass-ceramics, labelled BSF_{ref}, was made with 17.5 wt% Fe_2O_3 and 0.5. wt% Cr_2O_3 instead of P_2O_5. In all samples, XRD and Mössbauer spectroscopy data show that magnetite is the unique crystalline phase. Electron microscopy shows the presence of submicron crystallites and also of nanoparticles with a bimodal distribution of the grain size. On the other side, Mössbauer spectroscopy shows a non-uniform temperature dependence of the paramagnetic response which is also consistent with a bimodal size distribution. Consequently, to depict the magnetic response we have also to consider a bimodal distribution of the blocking temperatures.

The low-temperature magnetic behavior of magnetite-based glass-ceramics is strongly influenced by a few basic aspects: ***i***) a multimodal size distribution of the magnetite particles which imposes a peculiar response to the external fields, mainly, the bimodal size distribution of the tiny nanoparticles; ***ii***) the paramagnetic background of the glassy matrix; ***iii***) the intrinsic structure of the nanoparticles; ***iv***) the interparticle interactions.

According to size distribution, in real systems, there is a temperature range where a mixture of blocked and unblocked nanoparticles coexists. In other words, there is a distribution of the blocking temperatures T_B, $f(T_B)$, which was extracted from the temperature T dependence of the magnetization m [1] as:

$$f(T_B) \propto \frac{d(m_{ZFC}-m_{FC})}{dT},$$

where m_{ZFC} and m_{FC} are the zero field cooled and field cooled magnetizations, respectively. Accordingly, the low-T details of m_{zfc} vs. T plot are related to the main characteristics of $f(T_B)$. (Fig. 2).

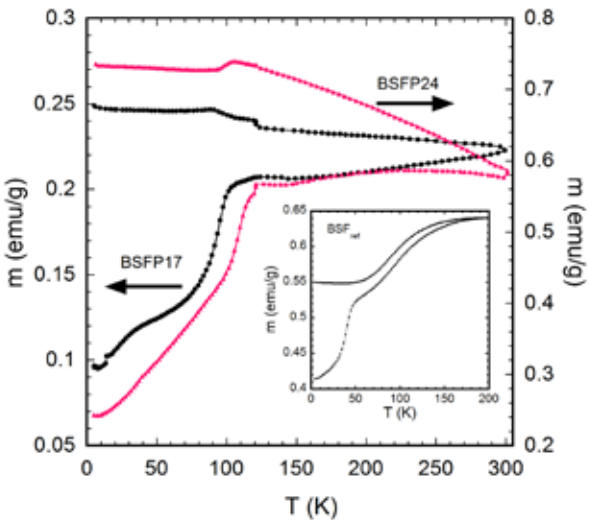

Fig. 1: Temperature dependence of the magnetization of magnetite-based glass-ceramics as measured at 50 Oe

The distribution functions of T_B are presented in the Fig. 2 together with the associated relaxation data. It is obvious that a well-defined mode is accompanied by one or more modes of much lower amplitude. Therefore, we have introduced a main blocking temperature, T_{Bm}, corresponding to the main peak of the distribution. The lowest temperature dip, $T_{dip} < T_{Bm}$, also proves to be important for the relaxation process.

The time dependence of the remanent magnetization $m_{rem}(t)$ shows that relaxation has specific features in the following T-ranges which are related to the distribution function $f(T_B)$: *i*) $T <$ 20 K, *ii*) 20 ≤ $T <$ 60 K, *iii*) 60 ≤ $T < T_p$, and *iv*) $T_p < T$.

Although the relaxation of the remanent magnetization is positive, $S > 0$, there is a T-range centered on T_{dip}, 20 K < T < 60 K, where the temperature dependence of the derivative dS/dT is negative. It is proposed that the determinant role in the relaxation process of the remanent magnetization m_{rem} is played by the inner spin structure of the nanoentities. This structure consists of a magnetically ordered core and a magnetically disordered shell. Consequently, the

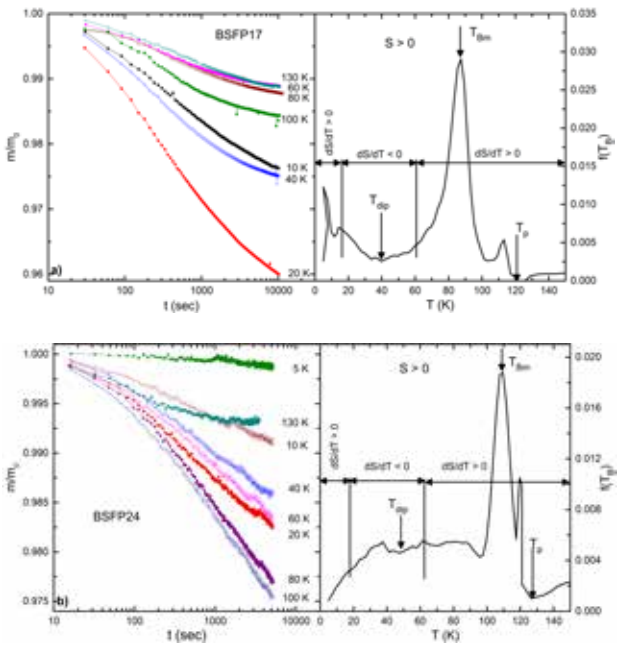

Fig. 2: Time dependence of the remanent magnetization for magnetite-based glass-ceramic at low temperatures. a) BSFP17; b) BSFP24. The right panels show the temperature dependence of the blocking distribution functions.

relaxation occurs either by the relaxation of the total magnetization, i.e., the superspin reversal, or the relaxation of a particular spin structure which is dominant, be it shell or core. The existence of a size distribution of the nanoparticles leads to a distribution of the relaxation times. Therefore, at a given T, we can have a "soup" of free superspins and blocked particles whose shell spins have a slower relaxation rate.

Another interesting feature related to the relaxation time of nanoparticulate systems is related to its dependence of the strength of the inter-particle interactions. This effect was carefully investigated in terms of a modified superparamagnetic (SPM) state, using experimental evaluations on ferrofluid samples based on coated magnetite nanoparticles, with volume fractions ranging from the very low value of the volume fraction of 0.005 (approaching the pure SPM regime of NPs) to a medium value of 0.16 (modified SPM regime of NPs) [3]. The influence of the modified SPM behavior of the specific absorption rate of the ferrofluid samples was investigated by calorimetric and magnetic measurements. It was proven that a direct effect of the interparticle interactions in the regime of the modified SPM resides, beside the usual increase of the anisotropy energy barier per nanoparticle, in the decrease of the specific time constant of the relaxation law, usually considered as a material constant (Fig.3).

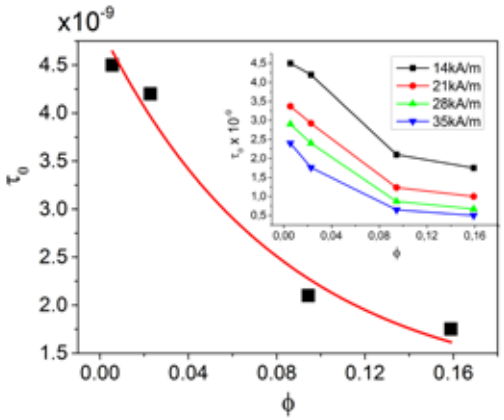

Fig. 3: Evolution of SPM time constant (in respect with volume fraction). Inset of the figure shows the same evolution coresponding to different magnetic field intensities

Work was supported by the Romanian Ministry of Education, Executive Unit for Funding High Education, Research, Development and Innovation under the Idea-Complex Research Grant PN-II-ID-PCCE-2011-2-0006 (contract #3/2012 and Core Program-2016.

References

[1] J. C. Denardin, et al., Phys. Rev. B 65 064422 (2002)

[2] V. Sandu, S. Greculeasa, A. Kuncser, V. Kuncser, J. Am. Ceram. Soc. 99 4013 (2016)

[3] N. Iacob, G. Schinteie, C. Bartha, P. Palade, L.Vekas, V. Kuncser, J. Phys. D: Appl. Phys. 49, 295001 (2016)

Aggregates of Mn^{2+} ions in mesoporous self-assembled cubic ZnS:Mn quantum dots: composition, localization, structure and magnetic properties.

S. V. Nistor, M. Stefan, L. C. Nistor, V. Kuncser, D. Ghica and I. D. Vlaicu

National Institute of Materials Physics

The magnetic properties of II-VI semiconductor nanocrystals (NCs) depend on the presence and localization of the incorporated transition metal ions (TMIs) [1]. For cubic $Zn_{1-x}Mn_xS$ NCs of a few nm diameter, called quantum dots (QDs), prepared by co-precipitation, collective magnetism was reported in some cases for $x \geq 0.015$ (c = 15000 ppm) and attributed to the incorporated TMIs [2]. Other authors reported paramagnetism, even at higher nominal concentrations [3].

The analysis of the electron paramagnetic resonance (EPR) spectra from the Mn^{2+} ions incorporated in cubic ZnS QDs self-assembled into a mesoporous structure revealed the presence of isolated Mn^{2+} ions localized at substitutional Zn^{2+} sites in the core and on the surface of the NCs, as well as in an aggregated phase [4]. Quantitative EPR investigations of such 2.9 nm size cZnS:Mn QDs have shown that, up to the highest c = 50000 ppm nominal concentration, the Mn^{2+} ions incorporated at isolated sites in the core and on the surface of QDs are in a diluted paramagnetic state characterized by magnetic dipole-dipole interactions and cannot be responsible for collective magnetism [5,6]. Therefore, the reported collective magnetism could originate only from the aggregated Mn^{2+}, a possibility not investigated so-far.

We examined by EPR, XRD, analytical high resolution transmission electron microscopy (HRTEM) and magnetometry the composition, localization, structure and magnetic properties of the aggregates of Mn^{2+} impurity ions responsible for the broad single Lorentzian component line in the EPR spectra of the cubic ZnS:Mn QDs prepared by co-precipitation with nominal Mn^{2+} ions concentration in the 200 to 50000 ppm range [7]. The presence of magnetic ordering in the aggregated phase was observed by EPR in the samples doped with c > 2000 ppm Mn^{2+}, as a sharp decrease in the derivative peak-to-peak line width ΔBpp. Moreover, while the EPR line intensity obtained by double integration of the experimental Lorentzian line, which is directly proportional to the magnetic susceptibility χ, exhibited for the sample with c = 2000 ppm a Curie law temperature dependence $I^{-1} \sim \chi^{-1} \sim T$, reflecting a dominant paramagnetic system, the sample with c = 20000 ppm exhibited a Curie-Weiss type $I(T) = C^*(c)\,[T - \theta(c)]^{-1}$ variation. The characteristic $\theta = (-75 \pm 10)$ K temperature points to an antiferromagnetic coupling ($\theta < 0$), typical for Mn^{2+} ions in II-VI semiconductors.

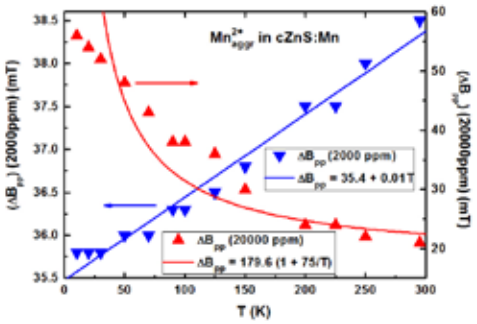

Figure 1: Variation of the peak-to-peak EPR line width vs T for the low (2000 ppm) and high (20000 ppm) Mn^{2+} nominal concentration samples [7].

Similarly, the T-variation of the ΔBpp (Fig. 1) shows for the c = 2000 ppm sample a linear dependence, typical for a paramagnetic system, while for the c = 20000 ppm sample it exhibits a non-linear dependence, typical for magnetic clusters of antiferromagnetically coupled ions.

Hysteresis loops collected at different temperatures, for the highly and lowly doped samples, revealed a coercive field of ~ 100 Oe at 2 K in the first case, while a much lower value (a few tenths of Oe) was observed in the last one. The magnetization at saturation ***vs.*** T data (Fig. 2) revealed, besides a magnetic ordered state present up to a relatively high temperature (300 K) in both samples, a strong increase of the saturation magnetization at T < 50 K (as well as of the coercive field) in the highly doped sample.

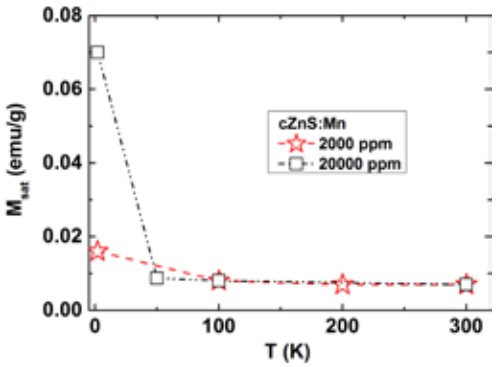

Figure 2: Magnetization at saturation vs T in the two analyzed samples, after subtraction of the diamag-netic and paramagnetic contributions [7].

One concludes that the magnetic ordered state, observed up to 300 K, responsible for the slowly varying saturation increase with T decrease, belongs to a magnetic phase involving exchange interactions over large volumes, specific for magnetic diluted systems. The strong increase in the saturation magnetization at T_B < 50 K in the highly doped sample is attributed to magnetic clusters in the frozen magnetic state, behaving as an assembly of Stoner-Wohlfarth magnetic monodomain nanoparticles, most probably consisting of Mn^{2+} ions [7]. If such magnetic clusters are large enough, they are super-paramagnetic at higher temperatures, and give rise at T < T_B to the observed increase of the saturation magnetization in the highly doped sample. A large size dispersion of such clusters is expected, which would result for the finest clusters in blocking temperatures below 2 K, contributing thus to the paramagnetic susceptibility. These results are in aggreement

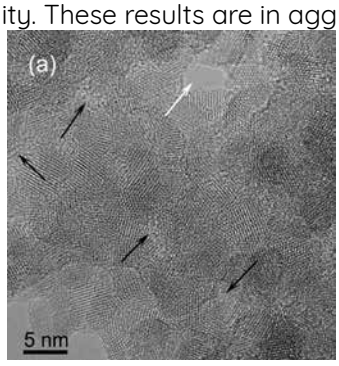

Figure 3: HRTEM image of mesopo- rous cubic ZnS:Mn with c = 20000 ppm. Some of the pores filled with an amorphous material are indicated by black arrows [7].

with the EPR data. From the spin concentration data of the isolated (core+surface) and aggregated Mn^{2+} ions obtained by EPR, magnetic susceptibility and magnetization at saturation quantitation one could determine the total concentrations of incorporated Mn^{2+} ions as 370/440 ppm and 3600/3350 ppm in the samples with c = 2000 ppm and 20000 ppm, respectively. These values compared well with the AA analysis of the same samples [7].

Analytical HRTEM/STEM investigations of the cubic ZnS:Mn (c = 20000/50000 ppm) samples evidenced an amorphous phase with a dominant Zn-Mn-O – type composition, localized in the pores and cZnS intergrain spaces (Fig. 3), very likely hosting the clusters of Mn^{2+} ions responsible for the observed collective magnetism properties.

Funding from the CNCSIS-UEFISCDI projects PNII-IDEI-74/2011, PNII-IDEI-75/2011 and Nucleus Program PN16-4801).

References

[1] R. Beaulac et al., Colloidal Transition-Metal –Doped Quantum Dots. In Nanocrystal Quantum Dots, V. I. Klimov Ed. CRC Press: New York, 397- 453, 2010.

[2] I. Sarkar et al., Ferromagnetism in ZnS Nanocrystals. Dependence on Manganese Concentration. Phys. Rev. B78, 224409 (2007)

[3] N. Tsujii et al., Magnetic Properties of Mn- and Eu-Doped ZnS Nanocrystals. J. Appl. Phys. 93, 6957-6959 (2003).

[4] S. V. Nistor, M. Stefan, L. C. Nistor, E. Goovaerts , G. Van Tendeloo, Incorporation and Localization of Substitutional Mn^{2+} Ions in Cubic ZnS Quantum Dots. Phys. Rev. B 81, 035336 (2010).

[5] S. V. Nistor, M. Stefan, L. C. Nistor, D. Ghica, I. D. Vlaicu, A. C, Joita, Doping Ultrasmall Cubic ZnS Nanocrystals with Mn^{2+} Ions over a Broad Nominal Conc. Range. J. Phys. Chem. C119, 23781-23789 (2015)

[6] S. V. Nistor, M. Stefan, L. C. Nistor, D. Ghica, I. D. Vlaicu, Distribution and Interaction of Mn^{2+} Ions Incorporated in Cubic ZnS Quantum Dots over a Broad Concentration Range. J. Alloys Compd. 662, 193-199 (2016).

[7] S. V. Nistor, M. Stefan, L. C. Nistor, V. Kuncser, D. Ghica, I. D. Vlaicu, Aggregates of Mn^{2+} Ions in Mesoporous Self-Assembled Cubic ZnS:Mn QDs. Composition, Localization, Struc-ture and Magnetic Properties. J. Phys. Chem. C120, 14454-14466 (2016).

Accurate spectral calculations for electrons in 2D systems with degenerate levels

M. Ţolea, M. Niţă

National Institute of Materials Physics

The presence of degenerate levels in the electronic spectrum raises the issue of spins alignment, an instance of particular relevance for nano-magnetism and for testing Hund-like rules. Such a system with degenerate levels placed at mid-spectrum is the Lieb lattice, i.e. the side centered square lattice (see Figs. 1 and 2), first proposed in [1] as a rigorous example of itinerant ferromagnetism in the presence of on-site Hubbard interactions and for the half-filling situation (i.e. the number of electrons equals the number of sites). Recently, the Lieb lattice received renewed attention in the context of 2D superconductivity, the possibility to be obtained as an optical lattice, or for its specific topological properties [2–5].

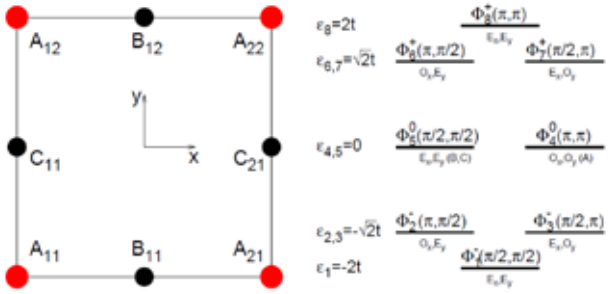

Fig. 1: One-cell Lieb lattice and its levels structure.

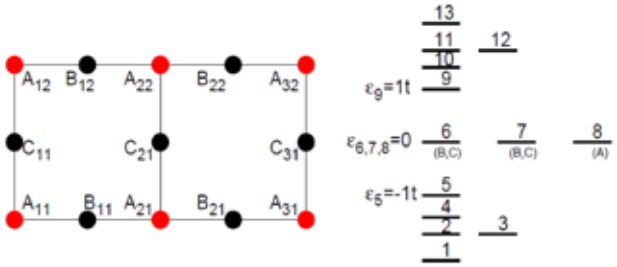

Fig. 2: Two-cell Lieb lattice and its levels structure.

In [6], we performed accurate spectral calculations for Lieb lattices with up to four cells. Supplementary from the mentioned motivation of calculating the spin of the ground state and testing Hund-like rules, we were also interesting of testing some known theorems of condensed matter physics in situations outside their strict range of applicability: the Lieb theorem [1] and the Milke theorem [7]. In particular the Lieb theorem states that a bipartite system (i.e. formed of sub-lattices A and B, and with hopping only between points from different sub-lattices; e.g. the Lieb lattice and the graphene are bipartite) with even number of sites in the presence of Hubbard on-site interaction, and half filled with electrons, has the ground state given by the mismatch between the number of sites in the two sub-lattices: S=1/2||A|-|B|| (where |A| is the number of sites from the sub-lattice A).

A particular attention was paid to the smallest one cell lattice - see Fig.1, which allows (having only eight sites) an analytical solution at small interactions, as well as numerical exact diagonalization for any value of the interactions. If only Hubbard interaction is considered we are in the frame of the Lieb theorem, which predicts S=0 for the situation of half-filling, i.e. the two electrons occupying the degenerate levels at mid-spectrum chose the singlet as ground state, instead of the triplet, of greater spin, as suggested by the Hund rule. However our alternative proof for this specific system allows for an insight on the role of the states spacial distributions and their symmetry properties. The energy difference between Singlet and Triplet was calculated to be:

$$\Delta E = -\frac{U_H^2}{16\sqrt{2}t} - \frac{U_H^2}{64t} \cong -0.059\frac{U_H^2}{t},$$

where U_H is the Hubbard energy and is the hopping between nearest neighbours.

Similar arguments are presented for two-cell Lieb lattice -depicted in Fig.2- with odd number of sites (outside of the Lieb theorem conditions). Again the “Hund” state (with maximum spin for the case of three electrons occupying the three degenerate levels at mid spectrum) is not the lowest in energy, the electrons preferring the state with one spin flipped (we called it “Lieb” state, and it is obtained from the maximum spin state -Hund- if a single spin is flipped). When the long range interaction () is turned on, again we fall outside the frame of the Lieb theorem (in which only Hubbard interaction is considered), however our calculations indicate that Lieb state remains favored as ground state instead of the Hund one. For the one cell lattice, $V_L/U_H$when the ratio exceeds a certain value, another singlet becomes

ground state and the excitation energy increases drastically, as seen in Fig.3, where a comparison with the Octagon configuration is also presented.

For lattices with three and four cells, another state of lower spin ("Para") is available for the electrons on the degenerate levels, and our numerical calculations indicate that this state indeed becomes ground state for a certain value of the long range interaction, as shown in Fig.4. For the bigger lattices (3x1 and 4x1), exact diagonlization is not feasible numerically, and we use a combination of Hertee Fock (for the lowest occupied levels) and Configuration -Interaction (for the levels at the mid-spectrum and immediately below/above).

Funding: PNII-ID-PCE Research Programme (Grant No. 0091/2011) and the Core Programme Contract No. PN16-480101.

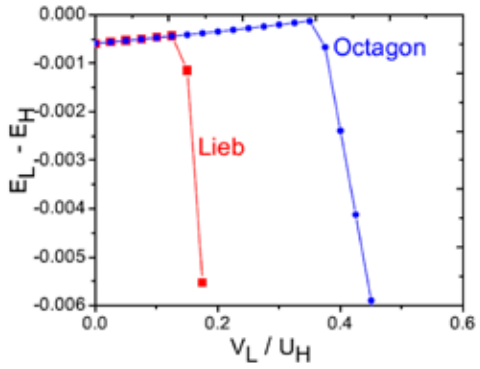

Fig. 3: Singlet (L) - Triplet (H) energy difference in the presence of both Hubbard and long range interaction, for the one-cell Lieb lattice and the Octagon, respectively.

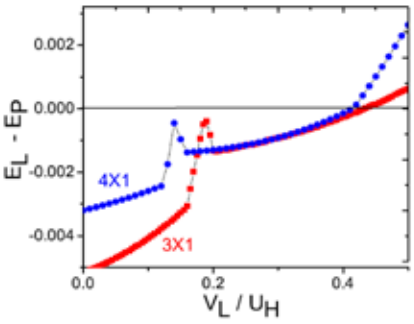

Fig. 4: Energy difference between the Lieb and the Para state, for the 3x1 and 4x1 Lieb lattices. When the ratio exceeds (approx) 0.4, the Para state becomes ground state instead of the Lieb state.

References

[1] E.H. Lieb, Phys. Rev. Lett. 62, 1201 (1989).

[2] V.Apaja, M.Hyrkas, and M.Manninen, Phys. Rev. A 82, 041402(R) (2010).

[3] R. Walters, G. Cotugno, T.H. Johnson, S.R. Clark, and D. Jaksch, Phys. Rev. B 87, 043613 (2013).

[4] M. Niță, B. Ostahie, A. Aldea, Phys. Rev. B 87, 125428 (2013).

[5] B.Jaworowski, A. Manolescu, and P. Potasz, Phys. Rev. B 92, 245119 (2015).

[6]M. Tolea, M. Nita, Phys. Rev. B 94, 165103 (2016).

[7] A. Mielke, Phys.Lett.A 174, 443 (1993).

POTENTIAL APPLICATIONS

SELECTED RESULTS

Effects of vanadium doping on sintering conditions and functional properties of Nb-Li co-doped PZT ceramics. Comments on Li location

L. Amarande, C. Miclea, M. Cioangher, M.N. Grecu, I. Pasuk

National Institute of Materials Physics

In this work [1], we investigated the effects of small amounts of vanadium additions on sintering conditions, structural, electro-mechanical, ferroelectric and dielectric properties of Nb-Li co-doped PZT ceramics, providing indirect information about lithium location in the lattice. The valence state and location of vanadium paramagnetic ions were also examined.

PZT ceramics were prepared by conventional sintering method, with the following compositions, assuming a B-site Li location: $Pb(Ti_{0.463}Zr_{0.51}Nb_{0.02}Li_{0.007})\ O_3$ denoted PZT-Nb, $Pb(Ti_{0.463}Zr_{0.51}Nb_{0.01}V_{0.01}Li_{0.007})\ O_3$ and $Pb(Ti_{0.463}Zr_{0.51}V_{0.02}Li_{0.007})\ O_3$ denoted, by their vanadium molar concentration, as PZT1 and PZT2, respectively. They were sintered for 2h, at temperatures ranging from 1000 °C to 1250 °C. PZT-Nb was sintered only at 1250 °C, (the optimal sintering temperature), as a reference for vanadium doping effect. As reported [2], vanadium promoted rapid densification of PZT, by liquid phase sintering, and reduced the sintering temperature with 100-150°C. The XRD diagrams of PZT1, represented in Fig.1, at different calcining and sintering temperatures, correspond to a perovskite structure with a mixture of tetragonal and rhombohedral phases and small amounts of unreacted oxides. Similar XRD diagrams were obtained for PZT2.

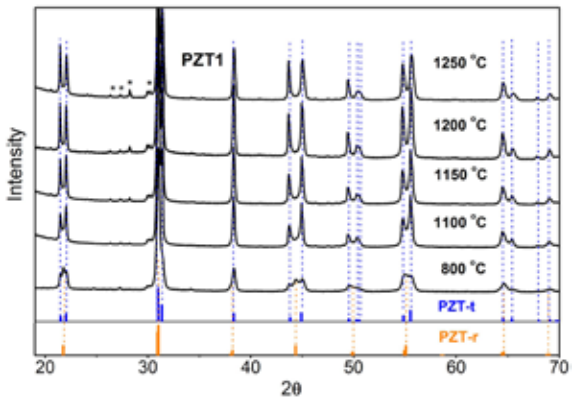

Fig. 1: XRD patterns of PZT1, calcined and sintered at different temperatures.

The amount of the rhombohedral phase decreased from 40 wt % to less than 9 wt %, with the increase of these temperatures. The presence of vanadium increased the lattice tetragonality and the grain size. It also decreased the dielectric constant with 25% and the dissipation factor with 50% in PZT2 compared to PZT1.

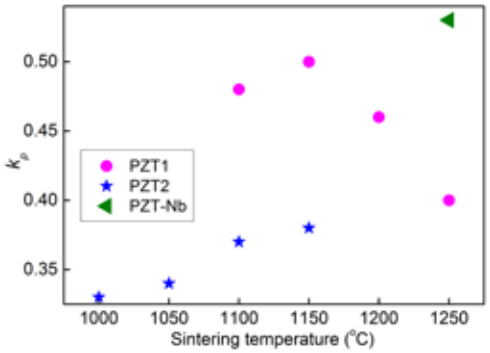

Fig. 2: k_p vs. sintering temperature

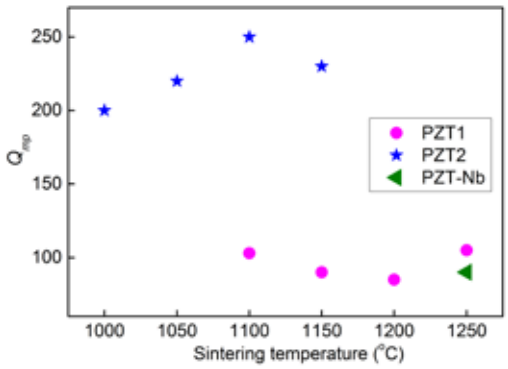

Fig. 3: Q_{mp} vs. sintering temperature

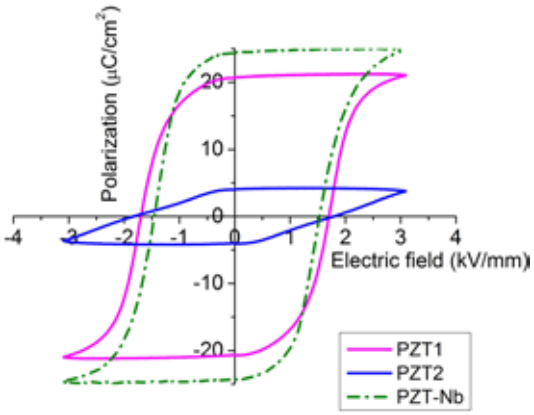

Fig. 4: Remanent hysteresis loops.

The electromechanical coupling factor k_p of PZT2 is by 20 % lower, while Q_{mp} is more than twice higher than for PZT1 (Figs. 2 and 3). PZT2 has a completely different remanent hysteresis loop, compared to PZT1 and PZT-Nb, with a significantly lower remanent polarization for all sintering temperatures, as shown in Figs. 4 and 5. The correlation of the dielectric, piezoelectric and ferroelectric measurements leads to the conclusion that PZT2 is piezoelectrically harder (i.e. lower dielectric constant, loss, electro-mechanical coupling factor and remanent polarization and increased mechanical quality factor and coercive field) than PZT1 and PZT-Nb.

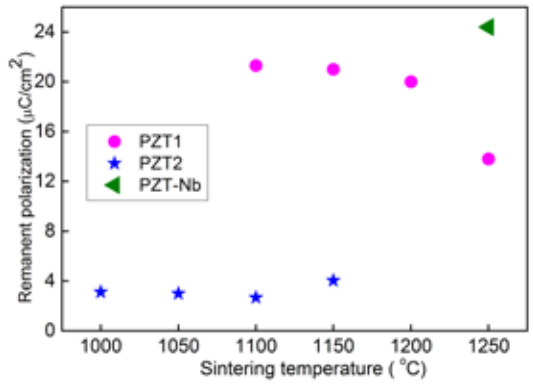

Fig. 5: Remanent polarization vs. sintering temperature.

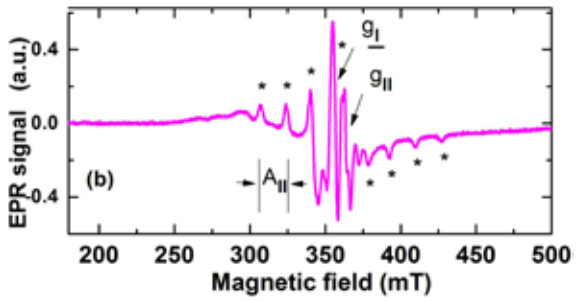

Fig. 6: Room temperature EPR spectrum of PZT1.

This behaviour could be due to a complex effect of Li location in the PZT lattice, the multivalence state of vanadium, and the presence of defects in the lattice. Li location in PZT is scarcely discussed in the literature. It was reported that Li^{1+} ion, can enter both A- and B-sites of a perovskite lattice [3-4]. If we assume the Li substitution on each of these two sites, the electrical neutrality will be maintained by lead vacancies and the reduction of a fraction of V^{5+} to V^{4+}, for A-site location, or by oxygen vacancies, for B-site location. The reduction of vanadium valence is possible due to its multivalence state and could be due to the presence of niobium donor co-dopant. Thereby, it is more likely that Li enters the A-site, in materials PZT1 and PZT-Nb, since the presence of lead vacancies and V^{4+} ions in the lattice (evidenced by EPR spectroscopy) are in agreement with the soft properties of these materials. The reduced V^{4+} ions were incorporated in the lattice, as vanadyl ions (VO^{2+}), in an octahedral location, as shown in Fig.6, where the eight hyperfine lines of vanadyl are evidenced in EPR spectrum of PZT1.

Instead, for PZT2, it is more reasonable to assume a B-site Li substitution, as the resulting charged oxygen vacancies defects, evidenced in EPR spectrum, are in agreement with the harder piezoelectric behaviour of this material. As reported in other works [4], lithium location was indirectly deduced from its derivative effects on the experimental results in correlation with the presence of other co-dopants. Thus, it was assumed that vanadium promotes the B-site, while niobium facilitates the A-site Li substitution in PZT.

Funding from Nucleus Program PN09-450103.

References

[1] L. Amarande, C. Miclea, M. Cioangher, M.N. Grecu, I. Pasuk, "Effects of vanadium doping on sintering conditions and functional properties of Nb-Li co-doped PZT ceramics. Comments on Li location." J. of Alloys and Comp. 685 (2016) 159-166.

[2] D.E. Wittmer, R.C. Buchanan, Low-temperature densification of lead zirconate-titanate with vanadium pentoxide additive, J. Am. Ceram. Soc. 64 (8) (1981) 485-490.

[3] Y.D. Hou, L.M. Chang, M.K. Zhu, X.M. Song, H. Yan, "Effect of Li_2CO_3 addition on the dielectric and piezoelectric responses in the low-temperature sintered 0.5PZN–0.5PZT systems", J. Appl. Phys. 102 (8) (2007) 084507.15.

[4] N. Lei, M. Zhu, P. Yang, L. Wang, L. Wang, Y. Hou, H. Yan Effect of lattice occupation behavior of Li+ cations on microstructure and electrical properties of $(Bi_{1/2}Na_{1/2})TiO_3$-based lead-free piezoceramics, J. Appl. Phys. 109, 054102 (2011) 054102.

Bulks and tapes of MgB_2 fabricated by Spark Plasma Sintering: technology, properties and additives

P. Badica*, G. Aldica, V. Sandu, L. Miu, S. Popa, M. Burdusel, A.M. Ionescu, I. Pasuk, M. Enculescu, A. Kuncser, M.A. Vlaicu, V.S. Teodorescu

National Institute of Materials Physics

in collaboration with 'Politehnica' University of Bucharest, University of Bucharest, Horia Hulubei National Inst. of Nuclear Physics and Engineering, Tohoku University, and National Institute of Materials Science

Development of MgB_2 for superconductivity applications is of much interest. MgB_2 is a superconductor with a relatively high critical temperature of 39 K. The low density of MgB_2 (2.63 g/cm^3) recommends it for different portable applications. Enhancement of the flux pinning can be realized by using additives. They can substitute into the crystal lattice of MgB_2 or they can produce a composite. Associated defects, residual strain and nano impurities can play the role of effective pinning centers improving functional characteristics of MgB_2 such as the critical current density J_c and the irreversibility magnetic field H_{irr}. It results that investigation of additives [1-7] (Figs. 1-6) and of the processing processes are important for controlling and enhancement of the MgB_2 quality. Irradiation with different particles can be useful, either [5] (Fig. 5).

In our works we have used spark plasma sintering (SPS) for MgB_2 processing.

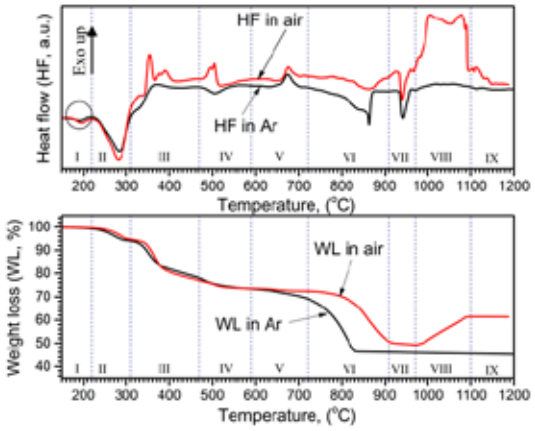

Fig. 1: DSC-TGA curves [1] of $C_6H_{10}G_2O_7$ in air and Ar. This additive was shown to promote strong enhancement of J_c [7].

Bulks [2-5] and powder-in-tube tapes [6] of MgB_2 in Fe-sheath were processed by SPS. Our results indicate that additives such as graphite does not improve J_c (Fig. 2), while c-BN, C60 and to some extent (cBN+C60) does it (Fig. 3). Processing by SPS in N_2 atmosphere can produce MgB_9N (Fig. 4) nano impurity leading to enhancement of J_c. Proton irradiation (Fig. 5) and addition of (SiC+Te) to MgB_2 tapes (Fig. 6) are shown to modify pinning and other aspects.

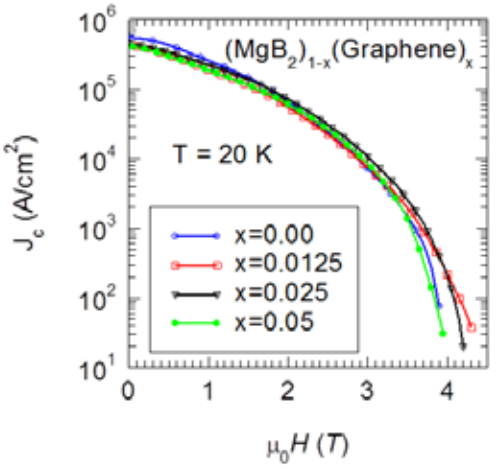

Fig. 2: Magnetic field dependence of the critical current density at 20 K for graphene added samples [2].

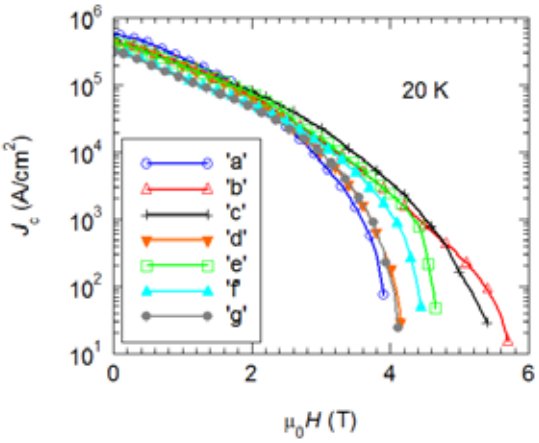

Fig. 3: Magnetic field dependence of the critical current density at 20 K for samples: a – MgB_2, b – $(MgB_2)(c\text{-}BN)_{0.01}$, c – $(MgB_2)_{0.95}(C)_{0.05}$, d – $(MgB_2)_{0.9875}(C)_{0.0125}(c\text{-}BN)_{0.01}$, e – $(MgB_2)_{0.975}(C)_{0.025}(c\text{-}BN)_{0.01}$, f – $(MgB_2)_{0.95}(C)_{0.05}(c\text{-}BN)_{0.01}$, g – $(MgB_2)_{0.925}(C)_{0.075}(c\text{-}BN)_{0.01}$ [3].

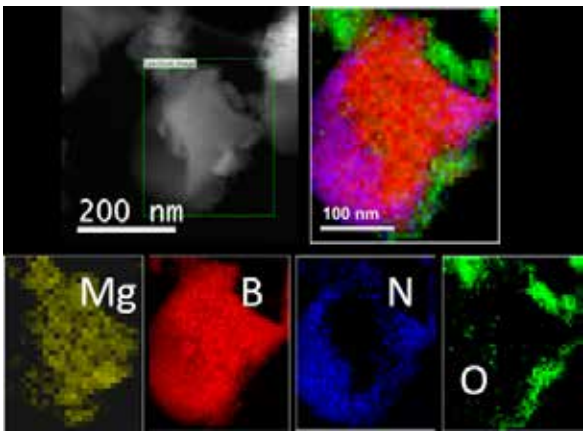

Fig. 4: Sample of MgB_2 processed by SPS in N_2 atmosphere for a heating rate of 100°C/min: TEM image and elemental maps based on energy loss spectra (EELS) around the peaks at 1305 eV (Mg), 188 eV (B), 401 eV (N) and 532 eV (O). [4]

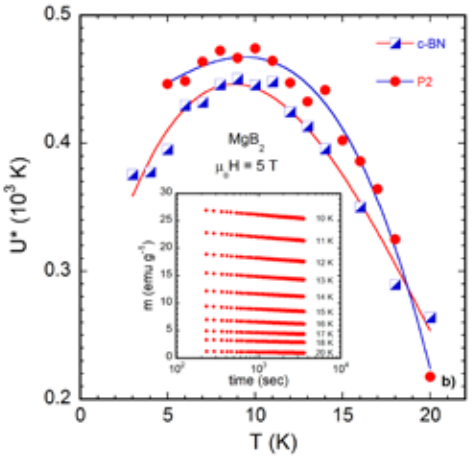

Fig. 5: Temperature dependence of the normalized vortex-creep activation energy ***U**** for $(MgB_2)(c\text{-}BN)_{0.01}$ and for irradiated MgB_2 (P2 – 11,3 MeV, 3.8 x 10^{17} protons/cm^2). ***U**** was evaluated based on the curves of time relaxation of the magnetic moment ***m*** (double logarithmic scale, see inset). [5]

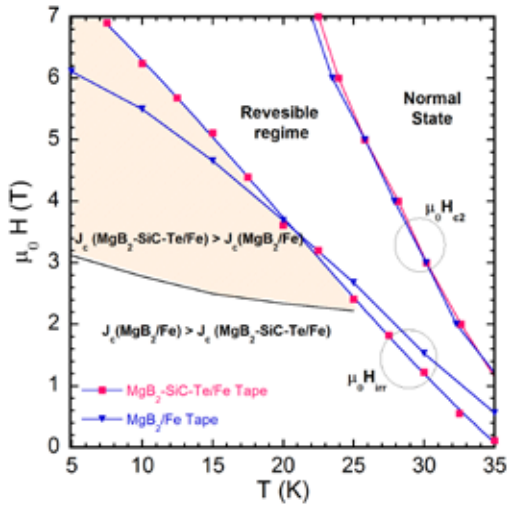

Fig. 6: Optimal regimes for current transport of the MgB_2-SiC-Te/Fe and MgB_2/Fe tapes. [6]

References

1. D. Batalu, A. Paun, M. Ferbinteanu, G. Aldica, A.M. Vlaicu, V.S. Teodorescu, P. Badica, Thermal analysis of repa-germanium (Ge-132), Thermochimica Acta 644 (2016) 20–27.

2. G. Aldica, M. Burdusel, S. Popa, Y. Hayasaka, P. Badica, Graphene addition to MgB_2 superconductor obtained by ex-situ spark plasma sintering technique, Materials Research Bulletin 77 (2016) 205–211.

3. A. M. Ionescu, G. Aldica, S. Popa, M. Enculescu, V. Sandu, I. Pasuk, A. Kuncser, L. Miu, P. Badica, Spark Plasma Sintered MgB_2 co-added with c-BN and C_{60}, Mater Chem. Phys. 170 (2016) 201-209.

4. P. Badica, M. Burdusel, S. Popa, I. Pasuk, I. Ivan, H. Borodianska, O. Vasylkiv, A. Kuncser, A. M. Ionescu, L. Miu and G. Aldica, Reactive spark plasma sintering of MgB_2 in nitrogen atmosphere for the enhancement of the high-field critical current density, Supercond. Sci. Technol. 29 (2016), 105020 (7 pp.).

5. V. Sandu, L. Craciun, A. M. Ionescu, G. Aldica, L. Miu, A. Kuncser, Superconductivity in MgB_2 irradiated with energetic protons, Physica C 528 (2016) 27-34.

6. V. Sandu, G. Aldica, S. Popa, M. Enculescu, P. Badica, Tellurium addition as a solution to improve compactness of ex-situ processed MgB_2-SiC superconducting tapes, Supercond. Sci. Technol. 29 (2016) 065012 (10 pp).

7. D. Batalu, G. Aldica, P. Badica, $Ge_2C_6H_{10}O_7$-added MgB_2 superconductor obtained by ex-situ spark plasma sintering, IEEE Trans. Appl. Supercond. 26 (2016) 7100104 (4 pp).

*Contact: badica2003@yahoo.com (P. Badica)

Electrochromic properties of polyaniline-coated fibre webs for tissue engineering applications

M. Beregoi, C. Busuioc, A. Evanghelidis, E. Matei, F. Iordache, M. Radu, A. Dinischiotu, I. Enculescu

National Institute of Materials Physics

1. Introduction

The development of artificial muscles with similar properties to natural muscles is important for a variety of technical fields ranging from reconstruction medicine to robotics and is a great challenge for the researchers worldwide. [1] "Artificial muscles" is a term which defines all structures that can reversibly modify their shape and/or volume by applying various external stimuli (electric current or voltage, temperature, pH, etc.). The main materials used for fabricating artificial muscles can be divided in three categories: electroactive polymers, shape memory alloys and piezoelectric ceramics. The most intensively used are electroactive polymers due to their fast response time, good mechanical properties, low applied voltage response and low cost. Polyaniline (PANI) is a conducting polymer which presents both electroactivity and electrochromism. Its' three oxidation states (leucoemeraldine-fully reduced, emeraldine-half oxidized and pernigraniline-fully oxidized), present each a characteristic colour. Moreover, PANI is a biocompatible material and it was used for study ***in vitro*** and ***in vivo*** systems.[2] The volume changes which occur at a certain potential when PANI is put in contact with an ions source, can be attributed to the insertion/removal of ions in and out of the polymers' chain and to the consequent conformational changes of the macromolecules. Further, the modification of PANI colour takes place due to the protonation/deprotonation processes and allows the fabrication of electroactive devices which can move simultaneously with the colour change.[3]

The electrospinning technique is widely used in the field of regenerative medicine due to the possibility of obtaining fibres with submicronic diameters which are comparable with different biofibers.[4,5] It consists of spinning a thin polymer fiber from a solution by applying an intense electric field to a droplet. Usual dimensions are submicronic which makes the method rather unique.

2. Electrochromic devices fabrication

A main characteristic of PANI based artificial muscles is the fact that the reversible dimensional changes can be correlated with the modification of colour.

For fabricating materials with complex features the preparation techniques should be combined. In this case, the electrospinning method was used for obtaining poly(methyl methacrylate) (PMMA) fibres, DC magnetron sputtering was employed to cover the electrospun fibre meshes with a thin gold layer in order to make them conductive, and electrochemical deposition of PANI represented the last step in the algorithm. In **Fig. 1** is presented the schematic procedure of electrochromic fibres preparation. PMMA fibres meshes were obtained starting from 10% (w/v) polymer solution. The fibres were collected on copper frames and were coated with 200 nm gold layer. The fibre networks were then thermally attached on a gold covered stainless steel holder in order to perform the electrochemical deposition of PANI. In the end, PANI was deposited on the gold covered PMMA fibres by using 0.05 M aniline and 1 M H_2SO_4 aqueous solution, applying consecutive pulses with 0 V the inferior limit and 1 V the upper limit, with a delay time of 0.5 s. The gold covered webs were used as working electrode, a platinum plate as counter electrode and commercial saturated calomel electrode as reference. The polymerization time was varied from 150 to 550 s, with an increment of 100 s.

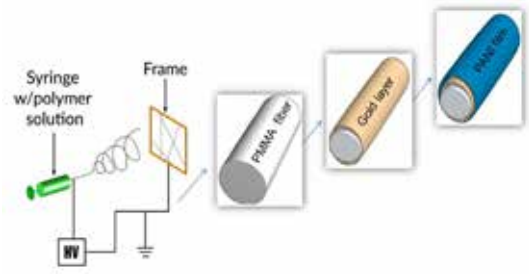

Fig. 1: Schematic representation of electrochromic fibres preparation.

3. Results and discussions

Firstly, the prepared fibres morphology was characterized as a function of the deposition time. In **Fig. 2** the digital photographs and Scanning Electron Microscopy (SEM) images at different magnifications are shown for the gold coated PMMA fibres and for those covered with a PANI film (with a deposition time of 550 s). As one can see, the gold layer fully covers the PMMA fibres, and is smooth and homogenous. The average diameter of gold coated PMMA fibres is around 0.9 m. The thickness of the PANI layer depends on the deposition time, for 550 s an approximate diameter of about 5 m being obtained.

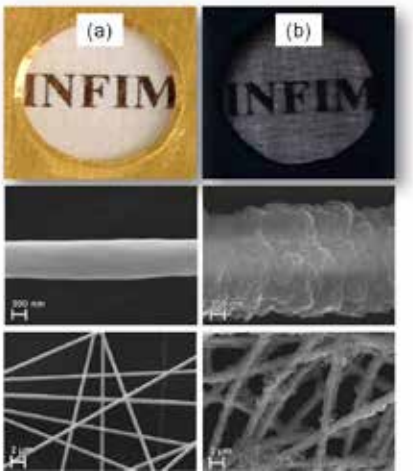

Fig. 2: Digital photos and SEM images of (a) metalized and (b) PANI coated fibres with the deposition time of 550 s.

The optical properties of the gold coated electrospun fibre meshes can be correlated with the transmittance spectra which depend on the fibre density. The samples used exhibited a transmission of around 70 %. In order to use such PANI coated fibres in tissue reconstruction applications, preliminary cells assays were made using human amniotic fluid stem cells and CCD-1070Sk (ATCC-CRL-2091), isolated from human skin. All analyzes were performed for as electrospun PMMA fibres, gold coated PMMA fibres and PANI coated meshes. Therefore, **Fig. 3** presents the fluorescent microscopy images for (a) PMMA and (b) PANI coated fibres with 450 s deposition time after 5 days of incubation, measured at the absorbance of 570 nm. These images and other complementary test (such biochemical assay and flow cytometry) revealed that the PANI coated fibres have a good compatibility with eukaryotic cells. Likewise, the cells show a normal metabolism, they grow and proliferate in the presence of PANI, while PMMA fibres present the lowest degree of attachment. The same results were registered when fibroblast cells were used, after 48 h of incubation.

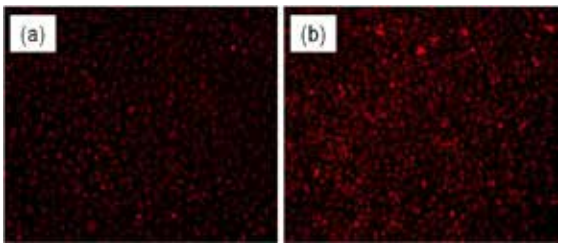

Fig. 3: Cell viability assay (CMTPX) on human amniotic fluid stem cells of (a) PMMA and (b) PANI coated fibres with 450 s deposition time.

4. Conclusions

The reported technique can be used for preparing smart materials with potential applications in tissue engineering field due to the high cells adhesion degree and stability.

Acknowledgments

All authors acknowledge UEFISCDI (project 159/2012HEFFES) and Nucleus Program PN16-4801 for the financial support.

References

[1] J. Li, S. Connell, R. Shi, "Biomimetics learning from nature, Biomimetic architectures for tissue engineering", InTech 487–505 (Chapter 24) (2010).

[2] M. Beregoi, C. Busuioc, A. Evanghelidis, E. Matei, F. Iordache, M. Radu, A. Dinischiotu, I. Enculescu, "Electrochromic properties of polyaniline-coated fiber webs for tissue engineering applications", Int. J. Pharm. 510, 465-473 (2016).

[3] E. Detsi, P.R. Onck, J.T.M. De Hosson, "Electrochromic artificial muscles based on nanoporous metal-polymer composites", Appl. Phys. Lett. 103, 193101 (2013).

[4] W. Lu, J. Sun, X. Jiang, "Recent advances in electrospinning technology and biomedical applications of electrospun fibers", J. Mater. Chem. B 2, 2369–2380 (2014).

[5] X. Wang, B. Ding, B. Li, "Biomimetic electrospun nanofibrous structures for tissue engineering", Mater. Today 16, 229–241 (2013).

Transparent field-effect transistors based on AlN-gate dielectric and IGZO-channel semiconductor

C. Besleaga, G.E. Stan, I. Pintilie

National Institute of Materials Physics

in cooperation with P. Barquinha, E. Fortunato and R. Martins, Department of Materials Science, Faculty of Sciences and Technology, New University of Lisbon and CEMOP-UNINOVA, Quinta da Torre, P 2829-516 Caparica, Portugal

Nowadays, the thin film transistors based on a-Si:H or polycrystalline Si dominate the large scale electronics. a-Si:H can be obtained with low costs and good uniformity on large area substrates. The low production cost of this material, derived from the maturity of the silicon industry, is however accompanied by a major shortcoming: its low field effect mobility (~1 cm^2/Vs). In the last years, studies were performed in the search of alternative semiconductor materials able to exceed the technological shortcomings of a-Si:H. The transistors based on amorphous In-Ga-Zn oxide (IGZO) have mobility values larger than 10 cm^2/Vs. Another important advantage of IGZO based transistors, with respect to Si based transistors, is the transparency in visible range, which facilitates a good transmission of the light through each pixel and therefore, more efficient and bright displays. Consequently, due to their high channel mobility, the thin film transparent transistors (TTFT) will give rise to a new generation of devices with shorter response time and higher calculus capacity, and to displays with higher refresh rates. The TTFT technology implies the exclusion of the SiO_2 grown by thermal oxidation on Si substrate. The SiO_2 films deposited by alternative methods (magnetron sputtering or plasma enhanced chemical vapor deposition) are often less pure and more defective, and therefore, have inferior dielectric properties with respect to the ones synthesized by thermal oxidation. This problematic context generated the need of developing new materials, superior to SiO_2, which can be integrated in TTFT devices. In the last years, Y_2O_3, La_2O_3, HfO_2, ZrO_2, SiN_x, TiO_2 and Ta_2O_5 were used as gate dielectric in thin film transistors.

To the best of our knowledge, this paper [1] is the first published study regarding the use of aluminium nitride (AlN) as gate insulator, in combination with the IGZO (an established high-quality channel semiconductor), for the development of fully transparent transistors. Aluminium is an abundant natural resource and requires simple purification procedures, which makes it cheaper than Y, La, Hf or Zr. Furthermore, in the case of TiO_2, Ta_2O_5, HfO_2, ZrO_2 and SiN_x, the small conduction band (CB) offset can give rise to leakage currents in the dielectric/IGZO structure. Besides, an appropriate CB to IGZO, AlN additionally possesses a very good stability in corrosive atmospheres and high temperatures environments. Its thermal conductivity of ~17 $Wm^{-1}K^{-1}$, is ten times higher that of SiO_2 (~1,3 $Wm^{-1}K^{-1}$), and thus, can overcome the self-heating issues reported in the case of SiO_2. Moreover, the coefficient of thermal expansion (CTE) of AlN matches well that of IGZO (CTE_{AlN}≈5.3 x 10^{-6} K^{-1} vs. CTE_{IGZO}≈5.23 x 10^{-6} K^{-1}). Thus, due to the compatibility of the CTEs, the AlN based devices will not be affected by the delamination of the thin films.

AlN thin films of different thicknesses were fabricated by a low temperature reactive radio-frequency magnetron sputtering process, using a low cost, metallic Al target. Their electrical properties have been thoroughly assessed. Subsequently, the 200 nm and 500 nm thick AlN layers have been integrated as gate-dielectric in transparent TFTs with IGZO as channel semiconductor.

A clear clockwise C-V hysteresis with magnitudes of 7 V (Figure 1) and 4 V is observed for AlN/IGZO MIS devices, showing 10^{12} cm^{-2} near interface traps density. The fixed charge density values, of ~-3x$10^{12}$$cm^{-2}$ are similar with those of other dielectrics used in TFTs, such as thermally grown SiO_2 and Al_2O_3 deposited by atomic layer deposition.

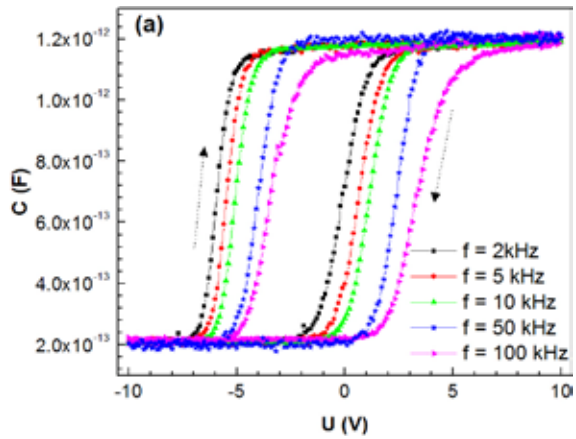

Figure 1: Typical results recorded for AlN/IGZO MIS device: capacitance vs. voltage at different frequencies: 2 kHz -black square, 5 kHz - red circle, 10 kHz - green up triangle, 50 kHz - blue star and 100 kHz - magenta diamond.

The best devices, with AlN thickness of 500 nm, showed a field effect mobility of 1.5 cm^2/Vs, an I_{ON}/I_{OFF} of $2.5 \cdot 10^6$, a subthreshold swing of 0.44 V/dec and gate-source currents of 10^{-13}A (Figure 2).

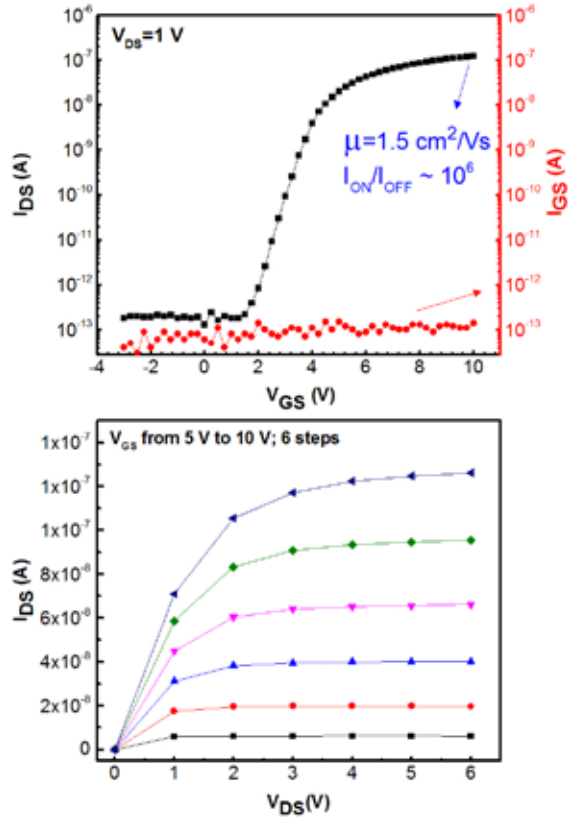

Figure 2: Linear and output characteristics of typical AlN/IGZO TFT.

Figure 3 shows the evolution with time of the transfer curves, undergoing bias stress with a constant gate voltage (V_{BIAS}) of +20 V for a total time of 6 min, while keeping the source and drain electrodes grounded. The main effect of keeping the structure in accumulation is the large positive shift (with more than 10 V) of the transfer curves, phenomenon connected to the negative charge trapped at or close to the dielectric/ semiconductor interface.

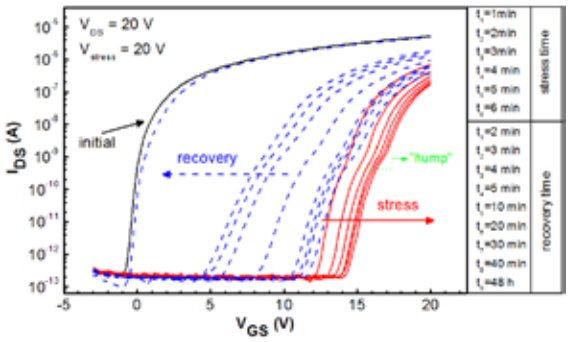

Figure 3: Evolution of the transfer characteristic during constant bias stress and its recovering.

The difference between the initial state of the device and the present state is visibly reduced with the increasing of the recovery time up to 48 h, where the I-V curves showed an almost complete recovery of the device.

This study brings into the light the use of AlN in transparent field effect transistors, as a highly promising gate dielectric alternative.

The electrical measurements performed on both MIS and TFT structures revealed that the dielectric/semiconductor interface still needs to be improved, as a relatively large effect (although recoverable) of bias stress is still visible in the devices. On the other hand, no degradation of AlN gate-dielectric layer was observed during the device stress testing.

Funding was received from CNCS-UEFISCDI PN-II-RU-TE-2014-4-1122 and PN-II-PT-PCCA-2013-4-0677.

References

[1] C. Besleaga, G.E. Stan, I. Pintilie, P. Barquinha, E. Fortunato, and R. Martins, "Transparent Field-effect Transistors based on AlN-gate Dielectric and IGZO-channel Semiconductor", Applied Surface Science 379, 270–276 (2016).

Dielectric and magnetic characterization of ferrites ceramics fabricated by various methods

M. Cernea, L. Diamandescu, G. Aldica, V. Mihalache and R. F. Negrea

National Institute of Materials Physics

in collaboration with R. Trusca, University POLITEHNICA of Bucharest, 060042, Romania

The ferrites are considered as important materials for modern electronic industry like as: magnetic audio and video tapes, high density digital recording media, magnetic fluids, etc [1].

Most of the ferrites exhibit high temperature ferromagnetism, high resistivity, low eddy current, and low-loss dielectric properties. Among the different oxide materials, the cubic spinel-type cobalt ferrite ($CoFe_2O_4$) exhibits large magnetostriction, at room temperature, due to the high positive magnetocrystalline anisotropy governed by the presence of Co^{2+} ion in the octahedral sites of the spinel lattice [2]. Other metal oxides as $MFe_{12}O_{19}$ (M=Ba, Sr) ferrites are characterized by good chemical and thermal stability, high saturation magnetization and high theoretical maximum coercivityand have applications in capacitors, microelectronics and microwave devices (cell mobile phones). The magnetic and dielectric properties of ferrites are highly sensitive to their preparation conditions, sintering temperature, and compositions. Based on these reported data, we studied $CoFe_2O_4$ and $Ba_xSr_{1-x}Fe_{12}O_{19}$ (x=0.05-0.35) ceramics, prepared by various methods [3,4]. The powders of these ferites were prepared by sol-gel and solid state reaction methods and, the ceramics were sintered by spark plasma sintering (SPS) methods and also, by classical technique. We investigated and compared the dielectric and magnetic characteristics of these ferittes fabricated by different methods.

The dielectric properties of the sintered $Ba_xSr_{1-x}Fe_{12}O_{19}$ hexaferrites derived from sol-gel and mixed oxides methods and classical sintered are listed in Tab.1, [4].

Table 1.

Dielectric permittivity (ε) and dielectric loss (tan δ) at room temperature, for sintered $Ba_xSr_{1-x}Fe_{12}O_{19}$ hexaferrites derived from sol-gel and mixed oxides methods.

Sample	100 Hz		1 kHz		1 MHz	
	ε	tan δ	ε	tan δ	ε	tan δ
$BSFO_{0.05}$, (s-g)	463	1.79	160	0.96	23	0.012
$BSFO_{0.15}$, (s-g)	388	1.45	136	0.82	21.5	0.008
$BSFO_{0.25}$, (s-g)	82	0.43	37	0.13	19.5	0.003
$BSFO_{0.35}$, (s-g)	52	0.15	32	0.06	18.8	0.005
$BSFO_{0.05}$, (ox)	389	1.85	132	1.25	30	0.14
$BSFO_{0.15}$, (ox)	345	0.73	118	1.23	29	0.12
$BSFO_{0.25}$, (ox)	75	0.59	46	0.39	20	0.09
$BSFO_{0.35}$, (ox)	37	0.57	26	0.42	17	0.02
$BSFO_{0.15}$, (ox)	470	3.60	217	1.12	39.2	0.51, [5]
$BSFO_{0.30}$, (ox)	439	3.12	225	0.95	37.9	0.50, [5]

As can be seen in Tab.1, the sol-gel method leads to $BSFO_x$ ceramics with higher permittivity and smaller dielectric losses compared to $BSFO_x$ ceramics derived from the mixed oxides method.

$CoFe_2O_4$ nanosized powder (~70 nm) was prepared by sol-gel method and dense ceramic was obtained by spark plasma sintering. The evolution with frequency (***f***) of the real part of the permittivity (ε') and losses (tan δ) for the $CoFe_2O_4$ ceramic, at room temperature, are presented in the Fig.1(a),(b).

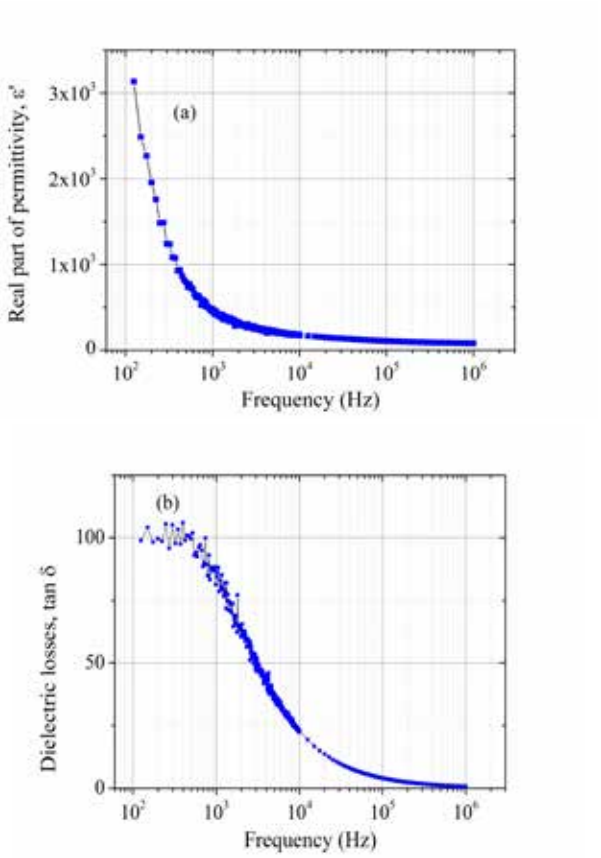

Fig. 1: Frequency dependence of (a) real part and (b) imaginary part of the permittivity for $CoFe_2O_4$ ceramic sintered by SPS method

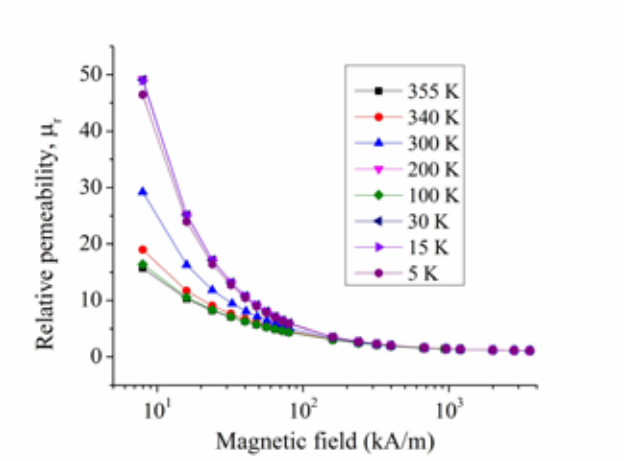

Fig. 2: shows relative permeability vs. ***H*** curves for different temperatures of SPS sintered sample

The relative permeability (μ_r) of $CoFe_2O_4$ sintered pellet decreases with increase of the magnetic field (***H***), at constant temperature. Relative permeability is almost independent of temperature for magnetic field ***H*** > 8 kA/m and, decreases with increasing field and temperature (Fig.3).

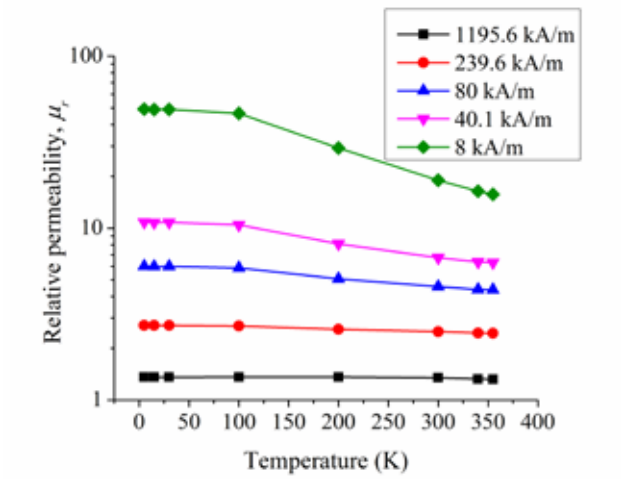

Fig. 3: Temperature dependence of the relative permeability (μ_r) for $CoFe_2O_4$ ceramic, at different ***H*** values.

Dielectric and magnetic properties of these ceramics recommend them for applications in the microwave or radio frequency range.

Funding from the COST Action MP0904, for financial support to STSM of M. Cernea at ISTEC; and from the EU(ERDF) and Romanian Government under POS-CCE project CEUREMAVSU Nr. 01/01.03.2009 allowing the acquisition of the research infrastructure.

References

[1] Vasundhara et al., J. Appl. Phys. 113, 194101 (2013

[2] Slonczewski J. C., J. Appl. Phys. 32 (1961) 253S–263SM.

[3] Cernea, P. Galizia, I. V. Ciuchi, A. Gheorghe, V. Mihalache, L. Diamandescu, C. Galassi, J. Alloy Compd. 656, 854-862 (2016).

[4] M. Cernea, R. F. Negrea, I. V. Ciuchi, C. Baldisserri, R. Trusca, C. Galassi, Ceram. Int. 42, 1050-1056 (2016).

[5] F. M. M. Pereira et al., J. Mater. Sci.: Mater. Electron. 20, 408–417 (2009).

Aspects of native oxides etching on n-GaSb(100) surface

C. Cotirlan, R.V. Ghita, C.C. Negrila, C. Logofatu, F. Frumosu, G.A. Lungu
National Institute of Materials Physics

The implementation of GaSb-based alloys in thermophotovoltaic (TPV) devices is affected by the problems of reproducible control of their surface properties. It is worth to mention that the chemical reactivity of antimonides is a distinct characteristic of these materials. This paper presents data regarding the evolution of surface native oxides on n-GaSb(100) before and after Ar^+ ion sputtering, respectively chemical etching with $HCl:H_2O_2:C_6H_8O_7$ at room temperature in order to obtain uniform and stable contacts [1]. The composition of native oxides was put into evidence qualitatively by an Energy-Dispersive X-ray Spectroscopy (EDS) analysis and Angle Resolved X-ray Photoelectron Spectroscopy (ARXPS).

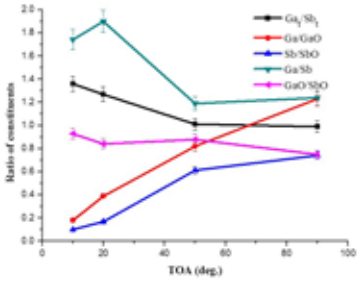

Fig. 1: Review of ARXPS results for native GaSb surface [2]

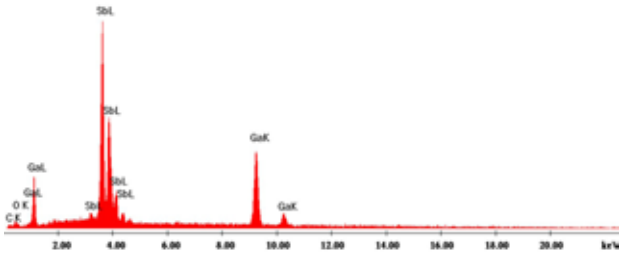

Fig. 2: EDS spectrum of native n-GaSb(100) surface [2]

Maximum analysis depth for ARXPS is three orders of magnitude less than in EDS. EDS is only for elemental analysis, while ARXPS gives chemical state information. Then, the samples were examined morphological by Scanning Electron Microscopy (SEM), and Atomic Force Microscopy (AFM).

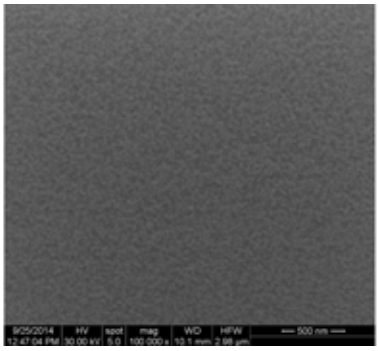

Fig. 3: SEM image of native n-GaSb(100) surface [2]

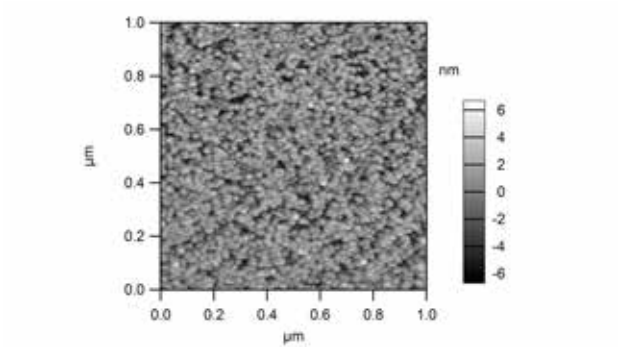

Fig. 4: AFM image of native n-GaSb(100) surface [2]

Each etching step was analyzed in connection with the evolution of surface stoichiometry for a contact aluminium epitaxial deposition, and a passivation treatment of a photosensitive surface. The final thermal annealing for oxide desorption on 100÷450 °C range in high vacuum SPECS installation was applied on native GaSb surfaces [2] in a similar manner to those of Si, Ge, GaAs. The reconstruction of semiconductor surface was investigated by low-energy electron diffraction (LEED). The degree of novelty for this work is represented by a technology based on a new chemical etchant, Ar^+ ion sputtering, and thermal annealing used for removing the native oxides in order to prepare rapidly the n-GaSb surface required in a TPV device manufacturing process. The impurities can affect the adherence of ohmic and Schottky contacts, and due to the thermal decomposition of native oxides from GaSb surface the interface metal/semiconductor is also affected. The practical experience reveals that the simple preparation of a surface is a non-realistic expectation, i.e. surface preparation is a

result of combined treatments. In this view, the surface preparation with ion beam sputtering is an efficient technique that removes rapidly and ***in situ*** the native oxides.

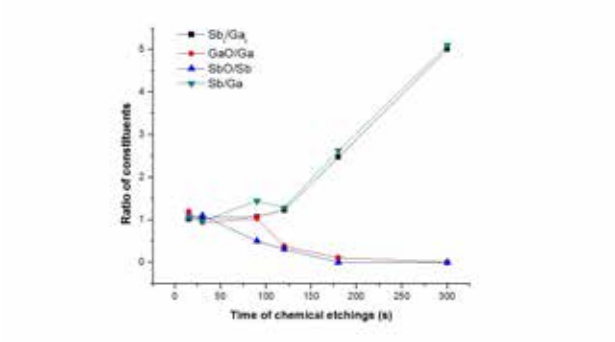

(a)

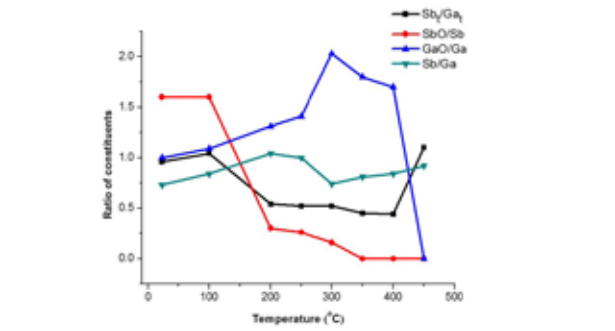

(b)

Fig. 5: (a) Chemical etchings and (b) controlled thermal treatments for cleaning the GaSb surface [2]

However, the major cleaning effect of semiconductor surface is always accompanied by surface damaging. The removal of surface damage is obtained by cycles of thermal annealing at a relative high temperature. It is worth to mention that the ion beam etching leaves a surface enriched in Ga atoms. This fact means a non-stoichiometric characteristic.

In the case of chemical etching preparation, the specific etchants for semiconductor are selective in respect to the crystallographic plane (***i.e.*** the etch rate is different).

The chemical etching is an effective and rapid ***ex situ*** preparation technique that leave a slightly non-stoichiometric surface (there exists a surface depletion in Ga atoms). Also, the chemical etching leaves traces of native oxide. Then the preparation includes thermal treatments, but the annealing implies a temperature lower that in case of ion beam sputtering.

In conclusion, the efficient technology for III-V compounds surface preparation is considered to be the combination between chemical etching and controlled thermal treatment.

Fig. 6: The LEED image of clean GaSb surface for 80.3 eV electron energy at normal incidence [2]

The effect of surface preparation can be observed by XPS for the surface chemical quality, by AFM for surface morphology, and by LEED for the structural characteristics.

This work was funded by Executive Agency for Higher Education, Research, Development and Innovation, under PCCA Contracts no. 68/2014 and no. 277/2014.

References

[1] C. Cotirlan, R.V. Ghita, C.C. Negrila, C. Logofatu, Applied Physics A: 117, 1359-1365 (2014).

[2] C. Cotirlan, R.V. Ghita, C.C. Negrila, C. Logofatu, F. Frumosu, G.A. Lungu, Appl. Surf. Sci 363, 83–90 (2016).

Direct and contactless electrical control of temperature of paper and textile foldable substrates using electrospun metallic-web transparent electrodes

C. Busuioc, A. Evanghelidis, A. Galatanu, I. Enculescu
National Institute of Materials Physics

In the present report, the surface temperature control of different types of materials, including paper and textiles, was demonstrated by Joule heating of metallic-web transparent electrodes both by direct current and by RF induced eddy currents. Polymeric submicronic fiber webs were prepared by electrospinning, and metal sputtering was subsequently performed to transform them into flexible transparent electrodes. These electrodes were thermally attached to different substrates, including paper, textiles and glass. Using thermochromic inks, we demonstrated a high degree of control of the substrates' surface temperature by means of the Joule effect. Moreover, contactless heating with induced currents is a premiere for transparent electrodes and opens up a score of new application fields.

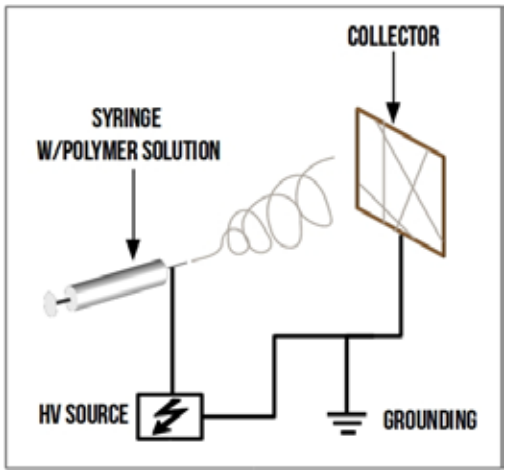

Figure 1: Electrospinning setup used to create transferable metallic webs.

Electrospinning is a technique that allows the fabrication of continuous, uniform, submicronic polymer fibers by applying a high-intensity electric field to a polymer solution or melt droplet. The resulting thin polymer fiber mats have found numerous applications, ranging from biological tissue scaffolds to filtration devices. Recently, such metal-covered mats were employed as transparent electrodes that could be easily attached to almost any type of substrate. The fiber density was controlled via the preparation step and was the parameter that further determined both the electrode's degree of transparence and its electrical conductivity. As is the case for the classical transparent metal oxide electrodes, there is a direct relation between conductivity and optical transmission.

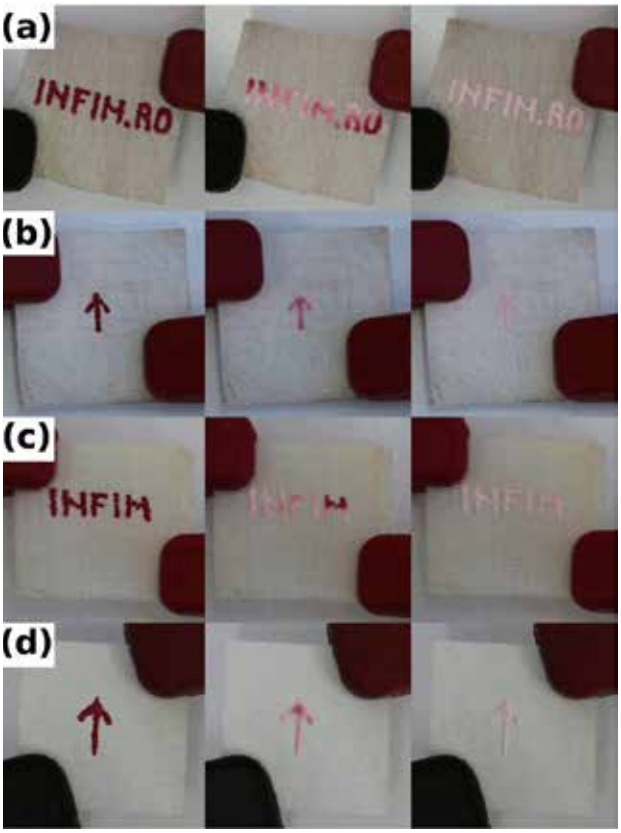

Figure 2: Images of gold- and silver-covered polymer fiber networks attached to different substrates; these images show the temperature transition of the thermochromic ink for (a) gold on fabric, (b) gold on paper, (c) silver on fabric, and (d) silver on paper

After the electrospinning process, the copper frames with the collected polymer fiber webs were covered with a metallic layer of either gold or silver using DC or RF magnetron sputtering, respectively. The thickness of the metallic layers was estimated through SEM measurements as the difference between the coated and uncoated fibers to be approximately 200 nm. The metalized fiber meshes were subsequently transferred onto glass, textile or paper substrates. Appropriately

sized pieces of glass substrates were placed on a heating plate set to 250 °C, and the frames were laid directly over them and left for 10 min. This step led to the polymer fibers melting and acting as an adhesive of the metallic webs to the substrate. Commercially available reversible thermochromic ink as purchased from Colour Changing was then applied to the samples with a fine paintbrush, as letters, patterns or as an arrow. The thermochromic transition temperature of the paint is 47 °C, from red to white.

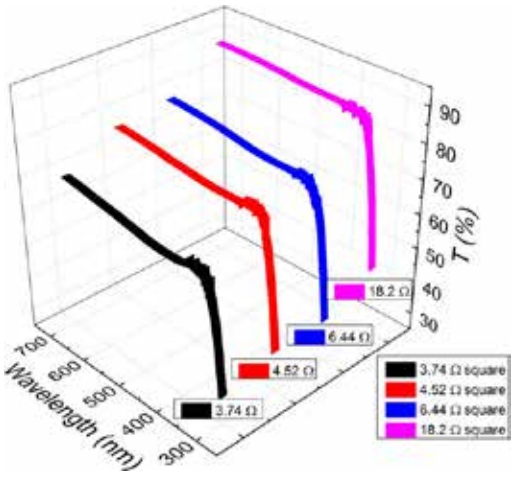

Figure 3: Transmission spectra of four polymer fiber webs attached to glass substrates and the correlation between transmission and resistance (inset figure).

The transmission spectra of a four-sample set, displayed in Fig. 3, indicate that increasing the electrospinning time leads, as expected, to a decrease in transmission in the visible range, which is a direct consequence of a thicker and denser layer of fibers. The fiber density also influences the conductivity of the metalized fiber layers, with denser networks being more conductive. The sheet resistance on a device scale was derived from the current-voltage curves of the glass-substrate-attached samples (2.5 × 2.5 cm^2) and is correlated with their optical transparency.

Figure 4: Thermochromic transition contactless induced on a gold web electrode covered paper substrate.

An induction heater setup working at 232 kHz was employed for producing a similar effect without a direct contact to the sample. During the simple on-off test conducted with the induction heater, the samples showed the same behavior as with direct contact based Joule heating – the results being visible in Fig. 4. Full transition of the dye was achieved, which implies that a temperature of at least 47 °C was obtained at the surface of the fibers. As it was the case with the direct contact the sample was able to support multiple on/off cycles without any apparent damage.

Such fiber-based systems could be easily integrated into novel applications that require transparency, flexibility, low power consumption and low processing costs. Contactless heating of common materials through transparent electrodes is a premiere which opens up numerous paths for new applications.

Funding from project 159/2012 HEFFES. Author Cristina Busuioc acknowledges the Sectorial Operational Programme Human Resources Development 2007–2013 of the Ministry of European Funds (Financial Agreement POSDRU/159/1.5/S/132397).

References

[1] C. Busuioc, A. Evanghelidis, A. Gălățanu, I. Enculescu, "Direct and contactless electrical control of temperature of paper and textile foldable substrates using electrospun metallic-web transparent electrodes", Scientific Reports 6, 34584 (2016)

Wicking/wetting properties of porous media/films with surface structure by images processing

L. Frunza, V.F. Cotorobai, I. Zgura, C.P. Ganea, S. Frunza, M. Enculescu, C. Florica
National Institute of Materials Physics

Wicking is a well-known phenomenon of the spontaneous liquid flow in a porous substrate, driven by capillary forces. These forces are in turn related to the wetting. The physical basis of wetting and wicking are thus molecular interactions within a solid or liquid or across the interface between liquid and solid. Much research was done on wetting of solid surfaces (see some classical reviews [1, 2]), related to contact angle, contact line, liquid/solid adhesion, wetting transition and spreading dynamics.

Wicking and wetting are also common phenomena in the processing and use of textile materials, in evaluating comfort and performance of clothing fabrics, hygiene products, etc.

We described then the liquid transport behavior of fabrics [3] by simultaneously processing the images of the wet spot during the radial outward wicking and the weight decrease of the liquid reservoir (considered infinite) due to liquid transport through the horizontal tissue (Fig.1).
The images were recorded with a webcam giving advantages in data processing. Afterward, the resulting image series were processed with routines especially developed in LabVIEW to determine the area of the wet spot. The programs were adapted to textile specific inhomogeneous and anisotropic structure.

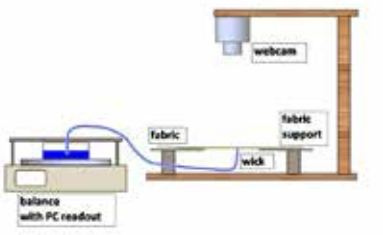

Fig. 1: Setup of simultaneous measurement of the mass of wicking liquid and acquirement of the image of the wet spot on the fabric sample [3].

The time dependence of the wet area leads to information about the wicking kinetics and further, by modeling the data (Fig. 2), to the possible mechanism. The experiments were performed using diluted solutions of dyes (rhodamin 6B or brilliant blue). The data allow an easy comparison of the textile behavior. Determination of the mass loss of the test liquid might be useful especially for the colored fabrics.

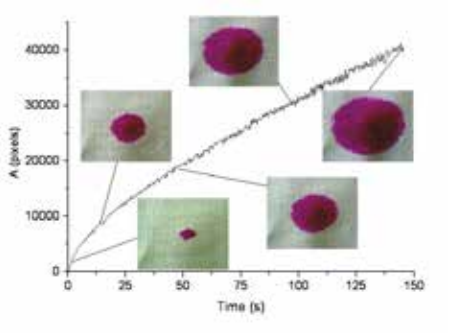

Fig. 2: Spreading of the wet spot obtained from continuous fed with R6B solution of the LINV18 fabric sample. The images were taken at different times: 5, 10, 50, 100 and 150s. The graph shows the area variation in time [3].

The equations and their parameters for the best fit of the graphs representing the time variation of the wet spot area and of the mass of liquid obtained for the studied samples are as follows:

$$A = b \cdot t + c \quad (1)$$

$$A = b' \cdot t \quad (1')$$

$$A = d \cdot t^{f} \quad (2)$$

where ***A*** is the measured area of the wet spot, ***t*** is the time, ***b*** (***b'***), ***c***, ***d*** and ***f*** are parameters. The last equation can be seen as answering to the well known model of Lucas-Washburn expressed as

$$l^2 = (\frac{\gamma}{\eta}\frac{\cos\theta}{2})rt \quad (3)$$

where ***l*** is the capillary length where the liquid arrived and ***t*** is the wicking time, γ – the surface tension of the liquid, θ – the contact angle between the liquid and the sorbent, η - the viscosity of the liquid..

The wicking rate calculated at a specified time (e.g. 20s from the beginning) can be used

for comparing the wicking properties of the fabrics. These might be of interest in practical applications of textiles especially when liquid transport is concerning. The fit characteristics get indirect information on contact angle, surface properties and effective mean pore radii of the material.

Another way to study the wicking/wetting of the fabrics is the classical method of static sessile droplet deposition (with a DSA100 Drop Shape Analysis System from Kruss). In the case of some polyester (PES) samples deposited by TiO_2 by two methods (sol-gel and sputtering) we could estimate the existence of a difference in interaction between the water drop and the fabric from the difference in the contact angle values [4]. In addition, wetting properties were conversely changed under alternate darkness/illumination conditions and differences in the photoinduced hydrophilicity was also observed.

Optical microscopy investigations were performed with a set-up adapted for fabrics and sketched in Fig. 3a. The voids were thus observed and compared.

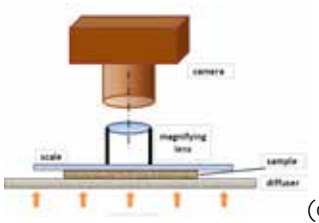

(a)

(b)

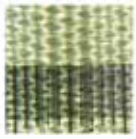

(c)

Fig. 3: (a) Experimental set-up for taking optical images: the light passes through a diffuser, the sample, the scale, a magnifying lens and enters the photo camera. (b) and (c) show the obtained opyical images for two polyester samples [4].

The behaviour might be approximated by the Cassie-Baxter equation in the form:

$$\cos\theta_c = f\cos\theta_0 - (1-f) \qquad (4)$$

where θ_C is the contact angle formed on the treated fabric and θ_0 is the contact angle formed on untreated fabric. The ***f*** parameter is the fraction of the surface contacting the water droplet. Some values are given in Table 1 [4].

Table 1

Sample	CA/degree	$f = \frac{1+\cos\theta_c}{1+\cos\theta_0}$
PES2	136.9	0.24457
PES3	138.1	0.23188
TiO_2 SG/PES2	169.3	0.01782
TiO_2 SG/PES3	169.7	0.01683
TiO_2 SP4/PES2	133.8	0.20981
TiO_2 SP4/PES3	166.0	0.02044

The values of contact angle mostly increases in the case of polyester samples by the TiO_2 deposition. The samples coated by sol gel have a few degrees, more than those coated by sputtering. In addition, there is a photoinduced superhydrophilicity for the coated samples. The layer prepared by the sol–gel exhibited lower hydrophilicity after illumination, compared to TiO_2 films prepared by sputtering.

The authors thank the Romanian National Research Council for the financial support under the Project ID281.

References

(Endnotes)

[1] P.G. de Gennes, Wetting: statics and dynamics, Rev. Modern Phys. 57 (1985) 827-863.

[2] R.J. Good, Contact angle, Wetting and adhesion – a critical review, J. Adhesion Sci. Technol. 6 (1992) 1269-1302.

[3] V. F. Cotorobai, I. Zgura, M. Birzu, S. Frunza, L. Frunza, Wicking behavior of fabrics described by simultaneous acquiring the images of the wet region and monitoring the liquid weight, Colloids Surf. A: Physicochem. Eng. Aspects 497 (2016) 146–153.

[4] I. Zgura, S. Frunza, L. Frunza, M. Enculescu, C. Florica, V.F. Cotorobai, C.P. Ganea, Polyester fabrics covered with amorphous titanium dioxide layers: combining wettability measurements and photoinduced hydrophilicity to asses their surface properties, Rom. Rep. Phys., 68 (2016) 259-269.

Iodine Migration and Degradation of Perovskite Solar Cells Enhanced by Metallic Electrodes

C. Besleaga, L.E. Abramiuc, V. Stancu, A.G. Tomulescu, M. Sima, L. Trinca, N. Plugaru, L. Pintilie, I. Pintilie

National Institute of Materials Physics

in collaboration with G.A. Nemnes University of Bucharest, Faculty of Physics, 077125, Magurele, Ilfov, Romania
M. Iliescu OPTOELECTRONICA - 2001 S.A., 077125, Magurele, Ilfov, Romania
H. G. Svavarsson, A. Manolescu Reykjavik University, Menntavegur 1, IS-101 Reykjavik, Iceland

The hybrid organic-inorganic perovskite solar cells (PSC) based on halide perovskites are the newest class of photovoltaic devices showing an unprecedented fast development in terms of power conversion efficiency (PCE), reaching values over 20% in as-prepared samples. However, while the high PCE values and potentially low production costs are important advantages, challenges to overcome are related to stability in time and overall reliability. Our study focuses on possible intrinsic degradation mechanisms in standard mixt PSC based on FTO/TiO_2/$CH_3NH_3PbI_{2.6}Cl_{0.4}$, in the absence of pinholes, moisture, overheating, and with limited exposure to UV and oxygen. For this, the performance of these PSC, in terms of PCE values, was monitored over a long storage time (more than 120 days) in N_2 atmosphere, dark, and humidity below 10%. We followed the different degradation behavior of pinhole-free PSC, with and without spiro-OMeTAD as holes transporter material (HTM), with and without Ag, Mo/Ag and Au counter electrodes [1]. Fig. 1 shows the PCE values versus time for samples without pinholes. The given PCE values are the average values determined from the forward and reverse photocurrent-voltage (J-V) scans. In order to suppress the relaxation induced currents, generated by the over-polarization of the samples or of the use of a too high scan rate, which inherently add to the photocurrent [2], all the J-V measurements were performed with 20 mV/s bias scan rate, starting from -0.1 V to a voltage slightly over V_{oc} and back. While all the devices show a small, slow degradation in time, an additional very sever and fast burn-in period at the beginning of aging occurs in solar cells with Mo/Ag electrodes (PSC-Mo/Ag).

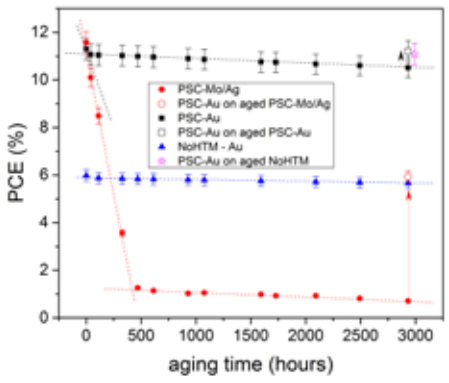

Figure 1: Changes in the PCE during aging. The black and red arrows show the recovering of PCE when fresh Au electrodes are deposited on aged PSC.

The PSC-Ag without Mo buffer layer degrades even faster than PSC-Mo/Ag (not shown here). The partial PCE recovering of the aged PSC-Mo/Ag sample when new Au electrodes are used indicates that, compared with Au, the use of Ag produces more damage in the cell. We found that in the absence of counter electrodes no degradation occurs in any of the perovskite solar cell layers during the aging for 3 months at 24°C in controlled atmosphere [1]. With fresh deposited Au electrodes on aged cells, PCEs similar to completely new devices are obtained. This result encouraged us to investigate in more detail the role of the electrodes in the degradation process. For this, Mo/Ag and Au electrodes were sputtered on the same sample (see Fig. 2). These cells were further analyzed by High Resolution X-ray Photoelectron Spectroscopy (HRXPS) in multiple regions, depicted as areas 1 to 7 in Fig. 3. The iodine is detected only on and in the vicinity of electrodes and considerably more on Mo/Ag than on Au.

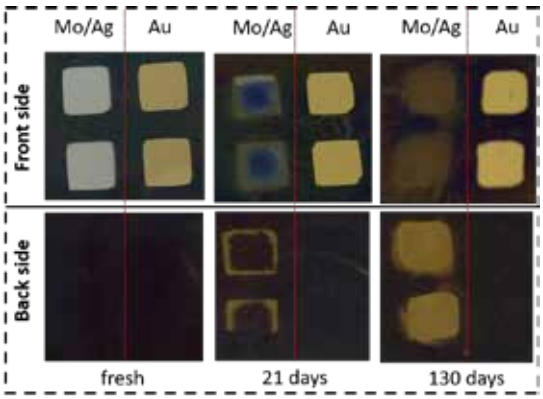

Figure 2: Photographs of the front- and back-side of a PSC sample at different aging times at 24°C.

The amount of I 3d detected on and near the Ag electrode increases with aging time while at and near the Au electrode remains almost constant even after overheating the samples at 70°C.

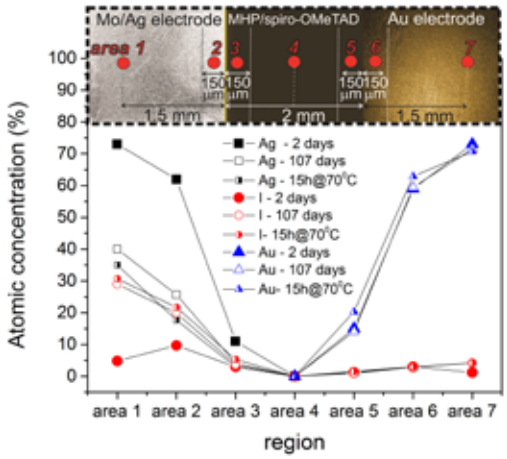

Figure 3: Atomic concentration of Ag, I and Au in different regions on and in between Ag and Au electrodes of PSC samples.

The reason for the continuous increase of iodine on Ag electrodes is the formation of stable AgI compound, observable also visually as a yellow color on the initially white Mo/Ag electrodes in Fig. 2. At the same time, the XRD patterns show a decomposition increasing in time of the $CH_3NH_3PbI_3$ (MAPI) phase of the $CH_3NH_3PbI_{2.6}Cl_{0.4}$ mixt perovskite only for structures with Ag electrodes, accompanied by the formation of crystalline PbI_2 [1], a yellow compound that can be seen when looking to the back-side of the cell (see Fig. 2). Below the Au electrodes, none of the phases of the halide perovskite decompose and the dark-brown color is preserved. Such different behaviors could be explained assuming that during the initial stage of electro-migration the negatively charged iodide ions drifting towards the Au electrode accumulate in the vicinity of Au and create an electric field blocking the further migration of I^-. Although a similar internal electric field occurs during electro-migration of iodide towards the Ag electrodes, the formation of AgI diminishes the negative charge accumulating at the electrode and weakens the electric field, allowing thus a further drift of I^-. This process continues in time leading to more and more iodine leaving the perovskite, passing the HTM and reaching the Ag electrode, causing the fast and irreversible degradation of the solar cell. The decomposition of MAPI phase in samples with Ag electrodes occurs also when no bias is applied on the cells, pointing to a continuous electro-migration of iodine from the halide perovskite even in the absence of any external bias. This is due to the difference in the work function of FTO (~ 5 eV) and Ag electrodes (~ 4.4 eV). Thus, these results indicate that the electro-migration of iodine through the solar cell, is triggered by the presence of metallic contacts with significantly different workfunction compared to front electrode and/ or high chemical reactivity with the compounds of the layers in proximity, although other factors like the exposure to air, humidity, UV, electrical stress may constitute important prerequisites.

Funding from EEA Financial Mechanism 2009-2014 under the project contract no 8SEE/30.06.2014

References

[1] C. Besleaga et al. "Iodine Migration and Degradation of Perovskite Solar Cells Enhanced by Metallic Electrodes", J. Phys. Chem. Lett. 7, 5168–5175 (2016).

[2] G.A. Nemnes et al. "Dynamic Electrical Behavior of Halide Perovskite Based Solar Cells", Sol. Energ. Mater. Sol. C 159, 197–203 (2017).

ZnO nanowires prepared by low-cost methods for superhydrophobic surfaces and field effect transistors

C. Florica, A. Costas, N. Preda, E. Matei, I. Zgura, A. Kuncser, M. Enculescu, I. Pintilie, L. Pintilie, I. Enculescu

National Institute of Materials Physics

In the last years, due to the wide range of potential applications of ZnO nanowires (NWs) e.g. superhydrophobic surfaces, electronic devices (especially field effect transistors - FETs), bio- or chemo- sensors, a considerable effort has been made for preparing such nanostructures by low-cost, scalable methods which use naturally abundant raw materials. In our studies, the ZnO NWs were prepared by wet methods (aqueous solution growth - ASG [1] and electrodeposition on interdigitated patterned electrodes - ED-IPE [2]) and dry techniques (thermal oxidation in air - THOX [1, 3]).

The SEM images of the synthesized ZnO NWs (Fig. 1) reveal the influence of the preparation approach on the NWs sizes (diameter-D and length-L), the following values being estimated: ASG (20 nm, 10 m), ED-IPE (100 nm, 5 m) and THOX (30 nm, 30 m).

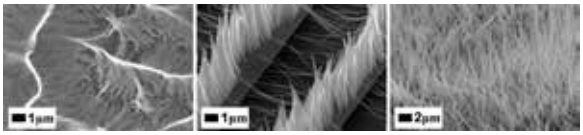

Fig. 1: SEM images of ZnO NWs prepared by ASG (left), ED-IPE (center) and THOX (right).

In the case of ZnO NWs-ASG and ZnO NWs-THOX, both have similar values for the energy band-gap, ~3.3 eV, (insets, Fig. 2), while the emission data are quite different: ZnO NWs-ASG (Fig. 2 left) reveals a broad emission band, centered at ~2.2 eV and ZnO NWs-THOX (Fig. 2 right) exhibits two emission bands: one intense, sharp, centered at ~3.3 eV due to the band-edge emission and another, weak, broad, centered at ~2.3 eV originating from different types of point defects. The HRTEM images (insets Fig. 2) confirm the good structural quality of ZnO NWs-ASG, with a slightly rough surface and the high quality crystalline structure of the ZnO NWs-THOX, with a smooth surface.

ZnO NWs-ED-IPE are self-contacted allowing their electrical characterization without other additionally contacting steps.

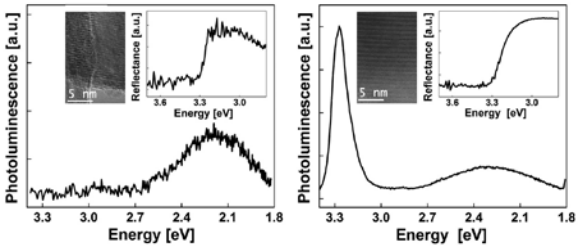

Fig. 2: Photoluminescence and reflectance spectra and HRTEM images of ZnO NWs synthesized by ASG (left) and THOX (right).

The optical results obtained for samples deposited at three working electrode potentials (Fig. 3a and Fig. 3b) were correlated with the electronic transport data (Fig. 3c).

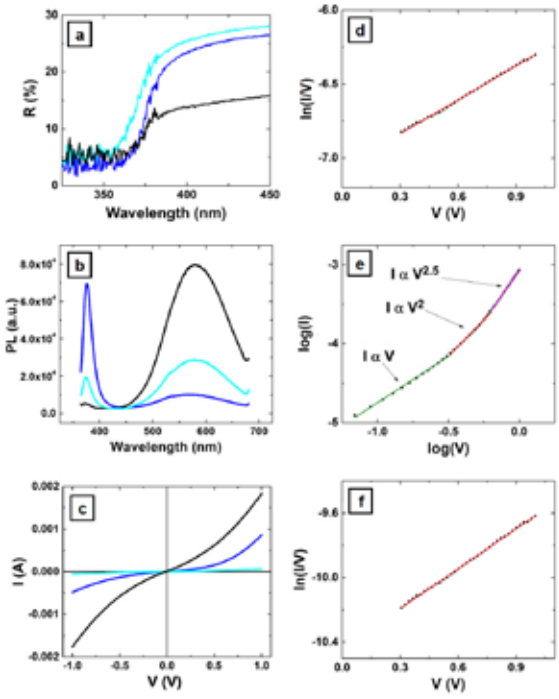

Fig. 3: Reflection (a) and photoluminescence (b) spectra and I-V characteristics (c) of ZnO NWs arrays obtained by ED-IPE at: -800 mV (black), -1000 mV (blue) and -1100 mV (cyan). Representation of ln (I/V) vs. V and log (I) vs. log (V) for ZnO NWs deposited at -800 mV (d), -1000 mV (e) and -1100 mV (f).

I-V characteristics can be explained based on the space charge limited current (SCLC) mechanism. For ZnO NWs (deposited at -800 mV and -1100 mV) where high defect emission was observed, we

deal with SCLC with uniform trap distribution (Fig. 3d and Fig. 3f). For ZnO NWs (deposited at -1000 mV) where low defect emission was observed, we deal with an ohmic region I~V, a SCLC with shallow levels traps distribution $I \sim V^2$ and a SCLC with exponential traps distribution $I \sim V^{2.5}$ (Fig. 3e).

For exploiting the properties of the easily synthesized ZnO NWs, they were used as channels in back-gate FETs configuration. In the SEM images (Fig. 4a and Fig. 4b) can be seen single ZnO NWs with Ti/Au contacts.

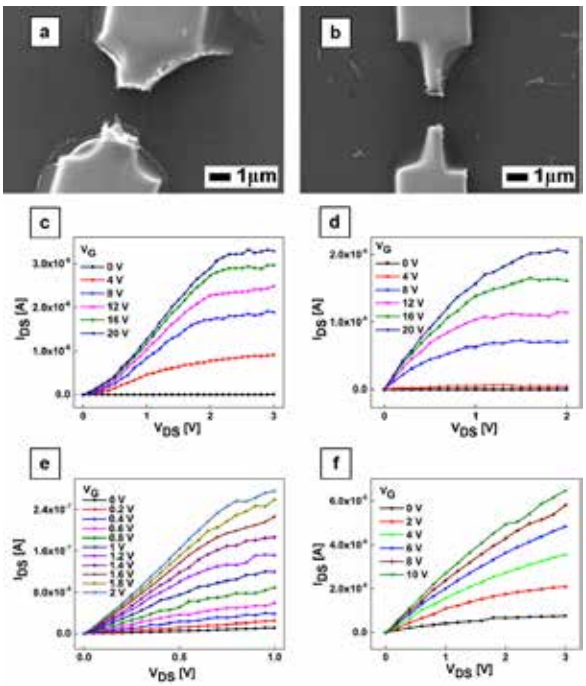

Fig. 4: SEM images (a, b) of single contacted ZnO NWs and the output characteristics of the back-gated FETs before (c, d) and after passivation with PMMA (e, f). The ZnO NWs were prepared by ASG (left) and THOX (right).

A comparison of the FETs' parameters was made taking into account the NWs' preparation method and the NWs' surface states i.e. in air (Fig. 4c and Fig. 4d) or passivated with a PMMA layer (Fig. 4e and Fig. 4f). Thus, the crystalline structure quality and the surface roughness of the ZnO NWs have a direct impact on the electrical characteristics of the transistors.

After the passivation with PMMA, the FETs' parameters are changed due to both limiting the interaction between the single ZnO NWs and the environment and enhancing the gate coupling effect. The fabricated FET's devices have excellent performances working in low power operation mode, with on-off ratios of about 10^4-10^5, high mobilities (up to 167 cm^2/Vs) and better switching behaviour (269 mV/decade).

Another functionality of the ZnO NWs-THOX was evidenced by their wetting properties (Fig. 5). Thus, a transformation (useful for very effective corrosion-resistant coating for the Zn) takes places: from a hydrophilic behavior with high water droplet adhesion (Zn foil) to a superhydrophobic one with low water droplet adhesion (Zn foil covered with ZnO NWs).

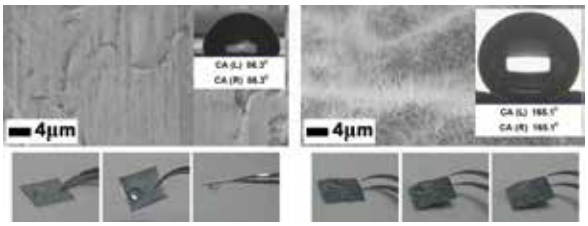

Fig. 5: SEM images, wetting and water adhesion properties of Zn foil (left) and of ZnO NWs arrays grown on Zn foil by THOX (right).

ZnO NWs synthesized by cost efficient techniques can be easily employed as building blocks for novel electronic devices or for the development of self-cleaning surfaces.

Funding from Core Program, contract no. PN16-480102; TE 12/2013; IDEI 24/2013; PD 18/2013 and PCCE 3/2012.

References

[1] C. Florica, A. Costas, A. Kuncser, N. Preda, I. Enculescu, "High performance FETs based on ZnO nanowires synthesized by low cost methods", Nanotechnology 27, 475303 (2016).

[2] E. Matei, A Costas, C. Florica, M. Enculescu, I. Pintilie, L. Pintilie, I. Enculescu, "Electrical properties of templateless electrodeposited ZnO nanowires", Mat. Sci. Semicon. Proc. 42, 364 (2016).

[3] C. Florica, N. Preda, A. Costas, I. Zgura, I. Enculescu, "ZnO nanowires grown directly on zinc foils by thermal oxidation in air: Wetting and water adhesion properties", Mater. Lett. 170, 156 (2016).

Sub-micrometre hollow bioglass cones deposited by radio-frequency magnetron sputtering: Formation mechanism, properties and prospective biomedical applications

A.C. Popa, G.E. Stan, C. Besleaga, V.A. Maraloiu

National Institute of Materials Physics

in cooperation with L. Ion University of Bucharest, Faculty of Physics, 077125 Magurele–Ilfov, Romania
D.U. Tulyaganov Turin, Polytechnic University in Tashkent, 100174 Tashkent, Uzbekistan
J.M.F. Ferreira, Department of Materials and Ceramics Engineering, CICECO, University of Aveiro, 3810-193 Aveiro, Portugal

Microneedles constitute one of the hottest topics of biomedical research [1]. They allow painless transdermal delivery of vaccines and drugs and avoid the emotional trauma of multiple injections of large doses of active substances with potential irritating or even toxic outcomes [1]. Our work [2] reports on the unprecedented magnetron sputtering deposition of sub-micrometric hollow cones objects of bio-glass (BG) at low temperature in the absence of any template or catalyst (Fig. 1).

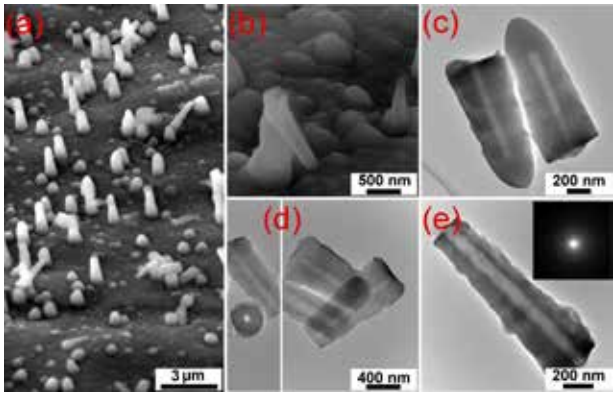

Figure 1: (a,b) SEM and (c–e) TEM images of (a) arrays and (b–e) individual BG submicrometer cones grown by radio-frequency magnetron sputtering at a working pressure of 0.4 Pa argon onto Ti substrates. Inset (e): Typical SAED pattern of a BG cone.

The influence of the sputtering conditions on the formation and development of BG cones was surveyed and the phenomenological trends were thoroughly depicted and discussed [2]. A model of BG hollow cones growth is proposed, with the self-shadowing as the prominent underlying mechanism for the formation of the sub-micrometre BG cones. Thereby, it is suggested the possibility of conceptualizing magnetron sputtering as an alternative approach for the fabrication of resorbable BG needles for challenging medical applications. The origin of the tubular channel inside of the cones having a roughly constant diameter of ~50 nm (Fig. 1-c–e), is another unique aspect. Its formation has been associated with an asymmetric oxidation with strongly oxidized regions on Ti substrate peaks, and incomplete oxidation in valleys and flatter areas. The incomplete oxidized regions can attract and bind more easily other ad-atoms (Si, Ca, Mg, etc.) than the strongly oxidized peak areas. Thereby, the peaked surface cannot be easily wetted by the ad-atoms, creating a gap that shall be transmitted upwards, giving rise to the birth of the inner channel. Following our microscopic observations we have noticed that obturation of inner channel occurred systematically at a critical cone diameter of ~300–350 nm. This suggests that capillary condensation of gaseous species takes place when diameter becomes narrower, allowing the newly arrived atoms to form the occlusion dome.

One envisaged application of BG cones refers to the treatment of cancer and other neurodegenerative disorders. A local and reversible permeabilization of the blood brain barrier (with an average thickness of ~200 nm) in an area of interest could be realized by the injection of soluble submicrometer-needles (conical frustums), derived from the BG cones, in the artery that is supplying blood for the desired zone. The hollow submicrometer-needles by their dimension can pierce the blood brain barrier, allowing drugs to pass through the central channel until their dissolution, whilst providing focused treatment (Fig. 2).

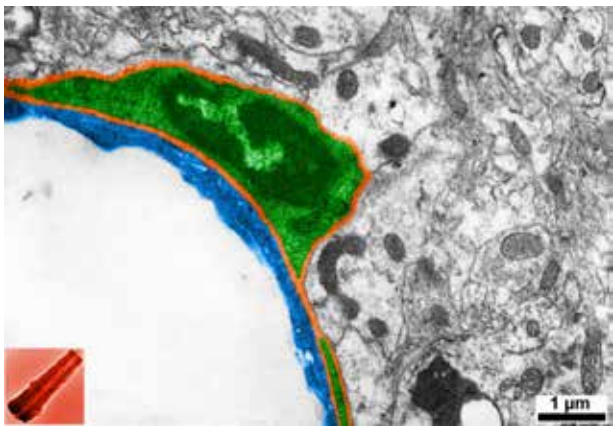

Figure 2: TEM image of normal rat brain: bottom left the lumen of capillary, the BBB (pseudo-coloured in blue), the basal membrane of the capillary (pseudo-coloured in orange), a pericyte in a pouch of the basal membrane (pseudo-coloured in green), and the brain tissue with fragments of neuronal, glial cells and the intercellular space (native grey scale). Inset: placed on the area of the capillary a TEM image of a sub-micrometre hollow cone pseudo-coloured in red) at the same magnification (hence using the same dimensional scale) as the brain tissue.

The new possible application of these BG objects is backed by highly promising results of degradation tests (Fig. 3) and cytocompatibility assays in a relevant cell culture model, i.e., of endothelial phenotype (Fig. 4) [2].

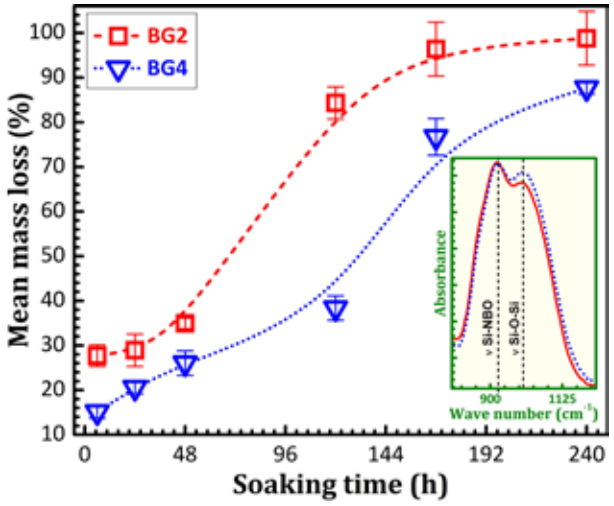

Figure 3: Weight loss profiles experienced along the degradation tests ((ISO 10993-14) by two BG materials with different structural arrangements (depolymerization degrees), derived by magnetron sputtering from the SiO_2–45.45, CaO–30.3, MgO–12.99, P_2O_5–2.6, CaF_2–4.33, and Na_2O–4.33 (mol.%) compositional system. Inset: Corresponding FTIR spectra of the BG sputtered materials.

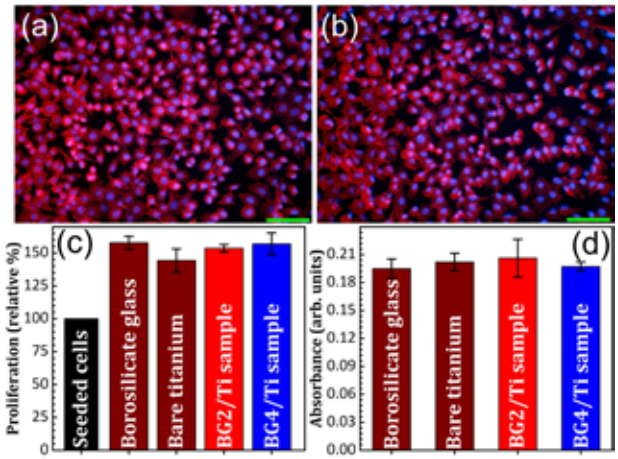

Figure 4: (a,b) Morphology of endothelial cells grown on (a) BG2 and (b) BG4 sputtered materials. (c) Cell proliferation – MTS assay. Values are normalized as percentages relative to the seeding cell number. (d) Cytotoxicity assays – LDH assay. Values are displayed in arbitrary absorption units showing good cytocompatibility of the BG coatings.

Our study could be of fundamental importance for applied physics and biomaterials science, as well as from technological point of view, opening new paths towards the fabrication of resorbable needles for controlled drug release.

Funding was received from CNCS-UEFISCDI in the framework of PN-II-RU-TE-2011-4-0164 (contact no. 49/2011) and PN-II-RU-TE-2014-4-0180 (contract no. 73/2015) projects.

References

[1] S. Indermun, R. Luttge, Y.E. Choonara, P. Kumar, L.C. du Toit, G. Modi, and V. Pillay, "Current Advances in the Fabrication of Microneedles for Transdermal Delivery", J. Controlled Release 185, 130–138 (2014).

[2] A.C. Popa, G.E. Stan, C. Besleaga, L. Ion, V.A. Maraloiu, D.U. Tulyaganov, and J.M.F. Ferreira, "Submicrometer Hollow Bioglass Cones Deposited by Radio Frequency Magnetron Sputtering: Formation Mechanism, Properties, and Prospective Biomedical Applications", ACS Appl. Mater. Interfaces 8, 4357–4367 (2016).

Organic blends for photovoltaic and non linear optic applications

A. Stanculescu, M. Socol, O. Rasoga, C. Breazu, N. Preda, I. Stavarache

National Institute of Materials Physics

in cooperation with F. Stanculescu University of Bucharest, Faculty of Physics, Magurele, Romania
L. Vacareanu "P. Poni" Institute of Macromolecular Chemistry, Iasi, Romania
G. Socol, National Institute for Laser, Plasma and Radiation Physics, Magurele, Romania
M. Girtan University Angers, Lab. LPHIA Angers, France

Organic materials are interesting for many applications, from energy conversion to photonics. Organic solar cells (OSC) offer an alternative to inorganic ones because can be manufactured on rigid/flexible substrates using low cost materials and processes [1]. Organic materials are promising for applications in information processing, telecommunication and integrated optics because the molecular structure can be modified/optimised to increase the optical nonlinear (ONL) response [2].

A way for improving the OSC parameters can be the identification of new materials. The mixture (blend) donor:acceptor as active layer assures an increased contact area and an improved charge transport surpassing the limitation of the bi-layer OSC. The absorption of the sunlight, implied in the generation of excitons, is enhanced by the use of donor with band gap, E_g~2 eV. The selected arylenevinylene oligomers having electron donating groups situated at the ends of the chain, of triphenylamine in 1,4-bis [4-(N,N'-diphenylaminolamino)phenylvinyl]benzene/ L78 and N-alkylcarbazole in 3,3'-bis(N-hexyl carbazole) vinylbenzene/ L13 show E_g=1.86 eV and 2.19 eV respectively [1].

So far, fullerene (C_{60}) with high electronic affinity and mobility, and optical absorption matching the solar spectrum, is an adequate acceptor. This combination donor/acceptor also satisfies the criteria related to the energy offset between LUMO of the components and HOMO of donor and LUMO of acceptor.

L78(L13):C60 mixed layers with weight ratio 1:1, 1:2 and 1:3, were prepared by Matrix Asssited Pulsed Laser Evaporation (MAPLE) at low fluences. The morphology characterized by grains/granules and clusters of grains randomly distributed in the layer evidenced by SEM images was correlated with the surface topography obtained by AFM (Fig.1) [1].

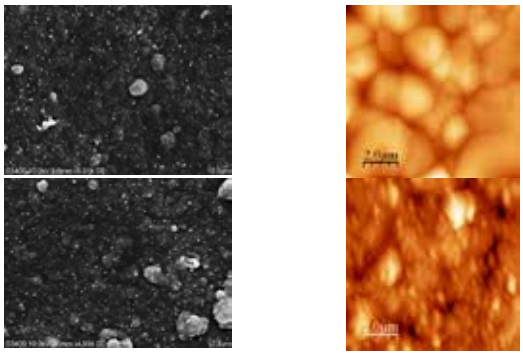

Fig. 1: SEM/AFM images of (a)/(b) L78:C60 and (c)/(d) L13:C60 (1:3) layer on glass [1]

The layers are disordered showing a large extension of the Urbach region (~ 2 eV) and high values of the Urbach energy, situated between 0.570 and 0.673 eV.

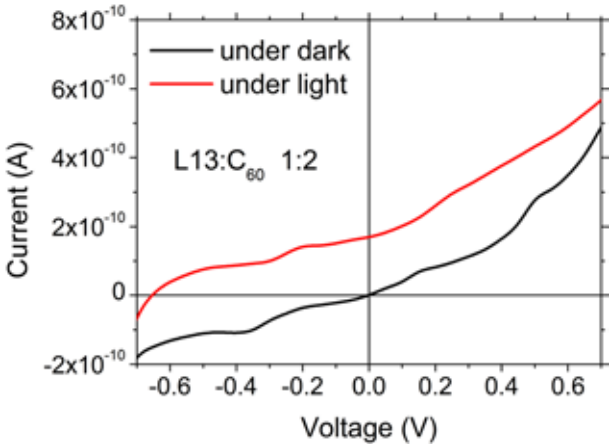

Fig. 2: I-V characteristics for glass/ITO/L13:C60 (1:2)/Al solar cell structure [1].

The solar cell structure realized with a L13:C_{60} (1:2) mixed layer (Fig.2) has shown the best V_{OC} (0.66 V) and FF (0.37) parameters [1], being promising as active medium in solar cells.

There have also been investigated the mixed layers prepared by MAPLE with a small molecule phthalocyanine donor (MgPc, ZnPc) and a non-

metallic phorphyrine acceptor (5,10,15,20-tetra(4-pyrydil)21H,23H-porphyne

(TPyP). The properties of the heterostructures with this mixed active layer were compared with those of the heterostructure realised in a stacked layers configuration. The transmission spectra (Fig.3) contain the characteristic B (Soret) and Q bands of the constituent materials [2].

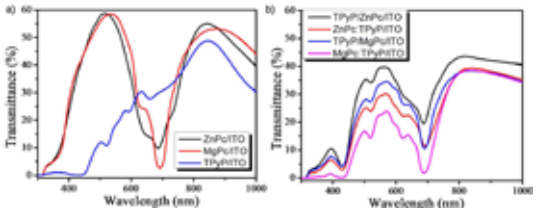

Fig. 3: UV–vis spectra of: (a) single layers and (b) structures obtained on ITO substrate [2].

The heterostructure glass/ITO/ZnPc:TPyP/Al shows a photogeneration process (Fig.4a) and the following parameters: V_{OC}= 0.77 V and FF = 0.28 [2]. The heterostructure with MgPc:TPyP active layershows a higher current compared to heterostructure with stacked layers (Fig.4b) [2].

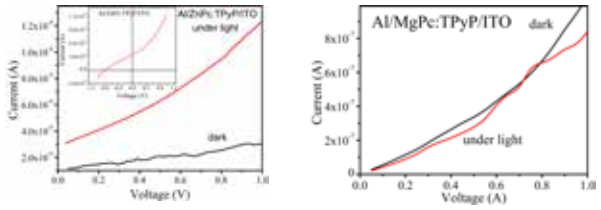

Fig.4: I–V: (a) Al/ZnPc:TPyP/ITO, (b) Al/MgPc:TPyP/ITO.

Organic:organic blends have been used to prepare, by spin coating, films containing inclusions of amidic monomers (M) in a matrix of polycarbonate of bisphenol A. The main advantages of using these blends in ONL applications are related to the properties of monomer inclusions and very good transparency of the polycarbonate matrix. In addition, the films can be easy processed from solution on large area, including flexible substrates, and the properties of the blend can be tailored by the concentration of monomer. The monomers synthesised from maleic anhydride and some aniline derivatives contain -NH- or -NH-NH- intercalated groups and COOH (M1), $-NO_2$ (M2), $-N(C_2H_5)_2$ (M4), two $-NO_2$ (M7) groups substituted to the aromatic nucleus [3].

The correlation between SEM and AFM measurements has shown different morphology of the film characterised by inclusions with size between hundreds of nm and few μm: smaller inclusions and lower roughness in polycarbonate:M1(M4) and wider and higher inclusions and higher roughness in polycarbonate:M2(M7). The strongest SH signal was evidenced in polycarbonate:M1 blend film (Fig.5a) showing very good transmission and low roughness [3]. The polycarbonate:M7 layer shows a saturation of the SH signal (Fig. 5b), associated with molecular conformational changes determined by the laser thermal effect involving the reorientation of the dipoles and changes in the polarizability of the sample [3].

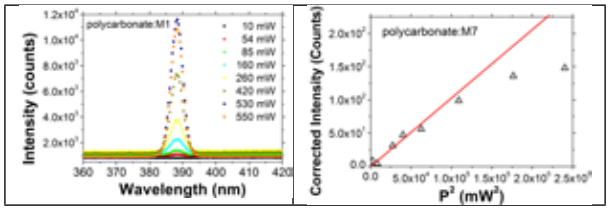

Fig. 5: (a) Second harmonic (SH) for different laser power; (b) SH versus square of laser average power.

Funding from National Core Founding Program, Contract No: 45N/2009, CEX-05-D11-63, Bilateral cooperation Romania-France project 783/2014, PN-II-PT-PCCA-2013-4-1439, UEFISCDI contracts no 649/2009 and 148/2011, POSDRU/187/1.5/S/155559, ANCS STARROSA 65/2013.

References

[1] A.Stanculescu, G. Socol, L. Vacareanu, M. Socol, O. Rasoga, C. Breazu, M. Girtan, F. Stanculescu, MAPLE preparation and characterization of mixed arylenevinylene based oligomers:C60 layers, Appl. Surf. Sci. 374, 278-289 (2016).

[2] M. Socol, N. Preda, O. Rasoga, C. Breazu, I. Stavarache, F. Stanculescu, G. Socol, F. Gherendi, V. Grumezescu, G. Popescu-Pekin, M. Girtan, N. Stefan, Flexible heterostructures based on metal phthalocyanine thin films obtained by MAPLE, , Appl. Surf. Sci. 374, 403-410 (2016).

[3] F. Stanculescu, A. Stanculescu, Polycarbonate-based blends for optical non-linear applications, Nanoscale Research Letters 2016, 11:87, doi: 10.1186/s11671-016-1256-5.

Low level NO_2 detection under humid background and associated sensing mechanism for mesoporous SnO_2

A. Stănoiu, C.E. Simion, V.S. Teodorescu, O.G. Florea

National Institute of Materials Physics

in cooperation with S. Somacescu[1], J.M. Calderon-Moreno[1], A. Sackmann[2]

[1]"Ilie Murgulescu" Institute of Physical Chemistry, Romanian Academy, Bucharest, Romania

[2]AG Weimar, Institute of Physical Chemistry, University of Tübingen, Germany

In this report, thick films of mesoporous SnO_2 have been prepared via hydrothermal treatment using Cetyltrimethyl-ammonium bromide (CTAB) as ionic surfactant [1]. The as-obtained sensitive materials were deposited onto Al_2O_3 substrates provided with interdigitated Pt electrodes and heater, via screen-printing technique. Insights about the gas sensing performances were acquired by means of simultaneous electrical resistance and work function changes measurements. The measured surface specific area was 127m^2/g whereas the pore size mean value was 4 nm.

The morphological aspects (size and shape) have been highlighted through Scanning Electron Microscopy (SEM) and High Resolution Transmission Electron Microscopy (HRTEM) (Figure1).

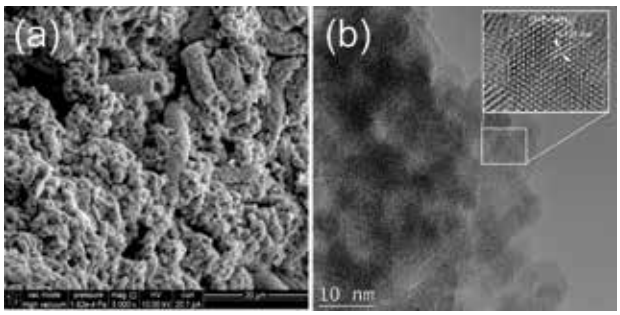

Fig. 1: SEM (a) and HRTEM (b) images of SnO_2 as-prepared materials.

Crystallites show good uniformity with spheroidal like aspect, exhibiting a diameter of 4-5 nm. A comparison between, the sensitivity towards NO_2 in dry and 50% relative humidity (RH) is represented in Figure 2. The associated sensor signal was calculated according to the formula: $S = R_{NO2}/R_{air}$. As can be seen the maximum in sensitivity is attained for 150°C as operating temperature.

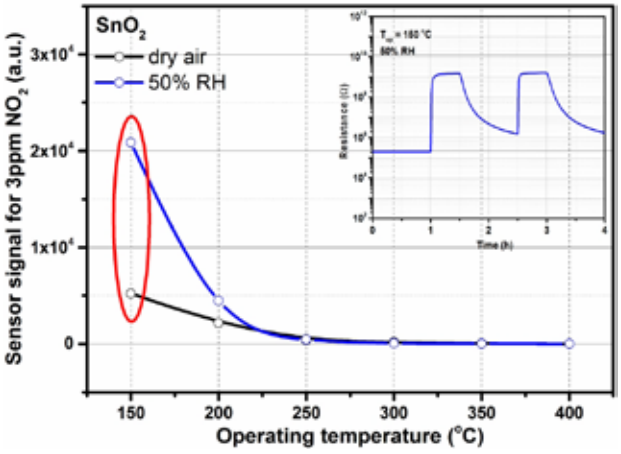

Fig. 2: The effect of operating temperature on SnO_2 sensitivity towards 3 ppm NO_2 under dry and 50% RH background.

Most striking is the high NO_2 sensitivity under the presence of RH, since an opposite effect is recorded for most of the semiconducting metal oxide gas sensors. As such, the complementary work function investigations have been involved in order to address a possible interaction mechanism. From simultaneous evaluation of the electrical resistance and work function changes under dry air background (Figure 3) one can see that the work function variations $\Delta\theta$ are solely related to the band bending changes $q\Delta V_s$.

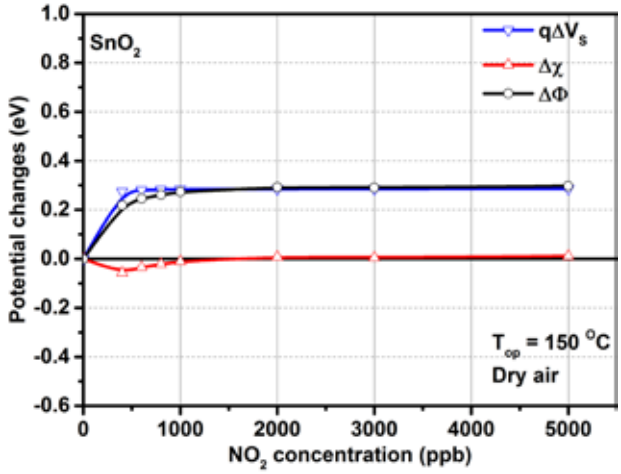

Fig. 3: The effect of NO_2 over potential changes under dry air background.

Such effect can be associated with the direct adsorption of at the SnO2 surface which induces subsequent withdraw of free charge carriers from the conduction band (increase in the surface band bending) [2].

Under 50% RH background, the NO_2 exposure induces an increase of both work function and band bending beside the decrease of the electronic

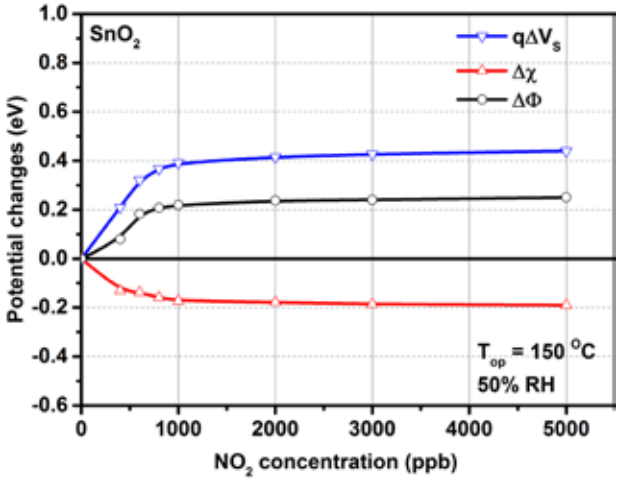

Fig. 4: The effect of NO_2 over potential changes under 50% RH background.

The most relevant difference between Figure 3 and Figure 4 is the electronic affinity pattern behaviour. The changes in Δχ can be associated with dipolar surface species. As such, under 50% RH one should take into account the NO_2 interaction with the dipolar complex:. Consequently, the coverage in net dipolar species decreases, reflected through a decrease in the overall electronic affinity. The proposed gas surface interaction pathway is described by the following quasi-chemical equation:

The long-term stability of the SnO_2 sensitive material was randomly evaluated through 110 days and by repetitive measurements over 169-185 days (Fig. 5).

For the first set of experiments, the data were acquired by exposing the sensor to 3 ppm NO_2 under 50% RH, keeping constant the operating temperature (150 °C). Repetitive measurements have been performed over 16 days.

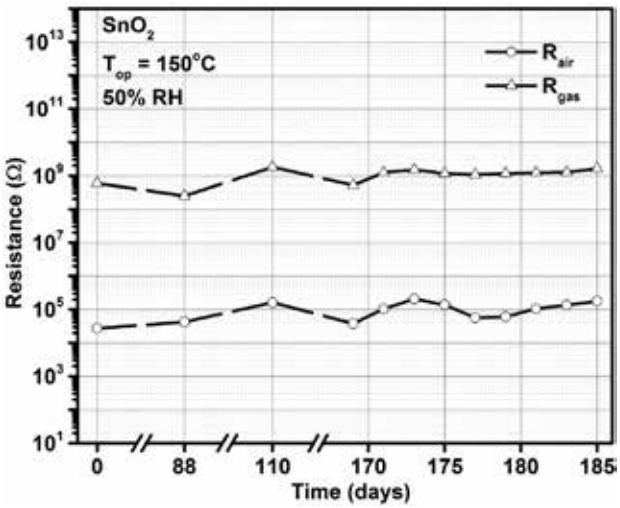

Fig. 5: Long term electrical resistance evaluation over 185 days.

The associated statistics for the electrical resistance behaviour are: and .

The selective-sensitivity to NO_2 has been evaluated (Fig. 6) towards commonly explored reducing gases: CO, CH_4, NH_3, SO_2 and H_2S.

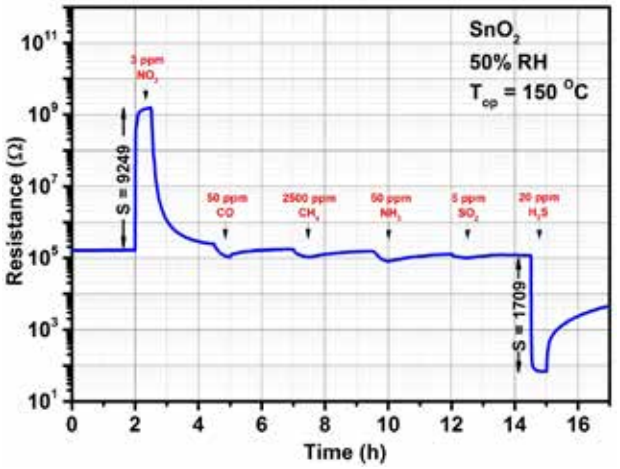

Fig. 6: Selective-sensitivity evaluation of SnO_2 under 50% RH background.

The only interfering effect towards NO_2 detection is with H_2S under the same operating conditions.

We demonstrated the high selective-sensitivity potential of SnO_2 towards NO_2 detection and its associated gas sensing mechanism.

Funding from Core Program PN16-4801 and PN09-450102/2015

References

[1] A. Stanoiu, S. Somacescu, J.M. Calderon-Moreno, V.S. Teodorescu, O.G. Florea, A. Sackmann, C.E. Simion, Sens. Actuators B Chem. 231, 166-174, (2016).

[2] M. Ivanovskaya, A. Gurlo, P. Bogdanov, Sens. Actuators B Chem. 3869, 1-4, (2001).

Ferroelectric varactors for microwave compact tunable antennas

L. Trupina, L. Nedelcu, M. Cernea, M. G. Banciu

National Institute of Materials Physics

in cooperation with L. Huitema[1], A. Crunteanu[1], M. Rammal[1], A. Ghalem[1], V. Madrangeas[1], D. Passerieux[1], P. Dutheil[2], F. Dumas-Bouchiat[2], P. Marchet[2], and C. Champeaux[2]

[1]XLIM UMR 7252 CNRS/Universite de Limoges, 87060 Limoges, France

[2]SPCTS UMR 7315 CNRS/Universite de Limoges, 87068 Limoges, France

Planar inter - digitated capacitors (IDC) and out of-plane metal - insulator - metal (MIM) electrically tunable microwave components of $0.92(Bi_{0.5}Na_{0.5})TiO_3$-$0.08BaTiO_3$ (BNT-BT) and $Ba_{2/3}Sr_{1/3}TiO_3$ (BST) ferroelectric thin films were developed for integration in frequency agile compact antennas. The varactors have been designed and simulated for integration within an antenna that allows the tuning of its operating frequency on the whole ISM band, with efficiencies higher than 70%.

The parameters of the MIM structures strongly depend on the quality of the thin films used as bottom electrode. For instance, the Ir layer directly deposited on SiO_2/Si substrate presents (111) and (200) mixed orientation while the film grown on Ti layer exhibits a strong preferred (111) orientation. The structural match between iridium (111) and titanium (001) planes clearly promotes the preferred orientation of iridium layer, demonstrating the decisive impact of lattice match on the oriented growth of Ir film on the highly oriented Ti layer [1]. The thermal stability of the Ir/Ti electrode was also analysed. The stability of iridium thin film at high temperature in oxygen atmosphere is highly dependent on growth condition and its thickness. The surface morphology of the thin iridium layers deposited at 400 °C (Fig.1 a) changes during annealing process due to titanium diffusion and its oxidation (Fig.1 b).

The 60-nm-thick iridium layer grown at 700 °C (Fig.1 c) shows good thermal stability with only a slight modification of the surface morphology (Fig. 1 d) and could be successfully used as electrode in devices based on oxide thin films. Within the limits of experimental error, there is no change on the electrical resistivity before and after thermal annealing ($12{\cdot}10^{-8}\,\Omega{\cdot}m$).

The microwave properties of the BNT-BT ferroelectric films and their potential to be integrated in tunable components for RF applications were investigated [2].

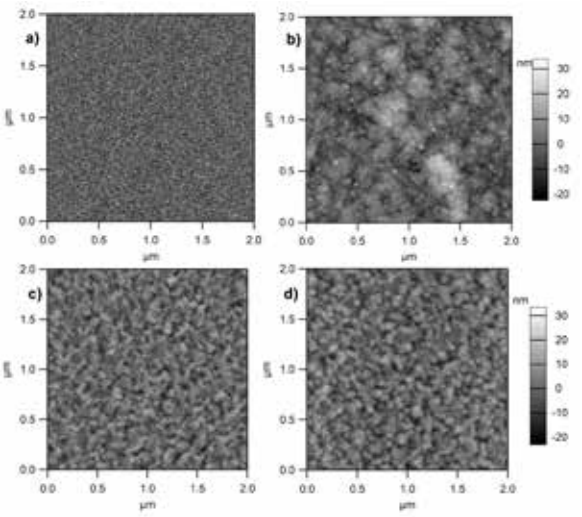

Fig. 1: AFM images of as grown 20-nm-thick (a) and 60-nm-thick (c) Ir film on Ti(10 nm)/SiO_2/Si substrates and after annealing (b) and (d) at 700°C in oxygen atmosphere [1].

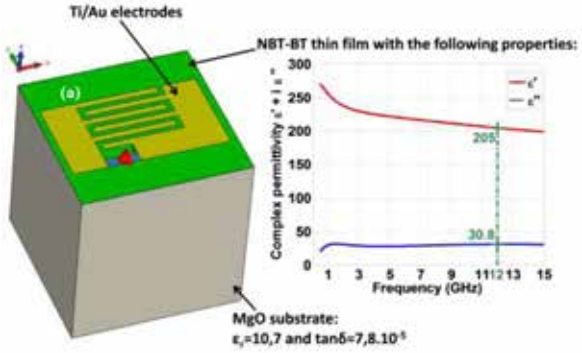

Fig. 2: BNT-BT-based IDC 3D design along with the frequency evolution of the complex permittivity parameters integrated in the 3D electromagnetic simulation [2].

3D electromagnetic simulations (Fig. 2) integrating the BNT-BT thin film properties given by the cavity method have been compared with the measured device prototype. The very good agreement between the measurements and the simulations confirms the layer dielectric properties in the 100 MHz–15 GHz frequency range.

However, the low tunability under high bias voltage makes these IDCs components incompatible with autonomous devices integrating WiFi applications. To solve this issue, we studied BNT-BT-based MIM capacitors. By reaching 30% of tunability for DC-bias voltages lower than 10 V (Fig. 3), microwave applications could foresee the integration of BNT-BT films. As these results are the first ones presented for such a material, fabricated components based on BNT-BT seem very promising for microwave applications.

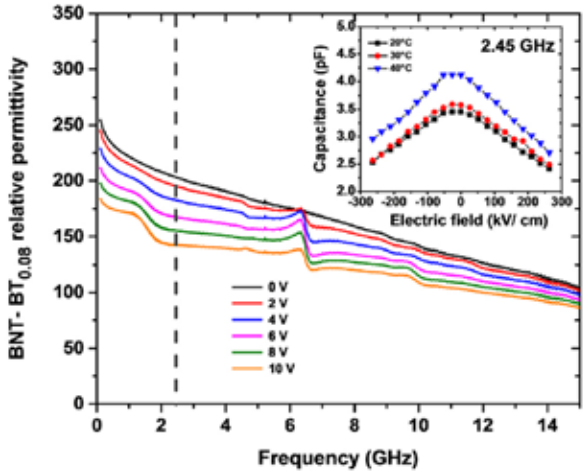

Fig. 3: Frequency dependence of the relative permittivity for the BNT-BT film integrating the MIM device. Inset: MIM capacitance value variation with the temperature and the applied voltage at 2.45 GHz [2].

As shown in Fig. 4a, the MIM varactors of BST exhibit a tunability up to 82% under applied voltages as low as 10V and low resitive losses. [3]. However, MIM devices show acoustic resonances (Fig. 4b) associated with the electrostrictive behaviour of BST layer. The analysis of these resonances indicates the existence of an interface layer at the BST / Ir boundary with acoustic and dielectric properties different from those of the BST layer [4].

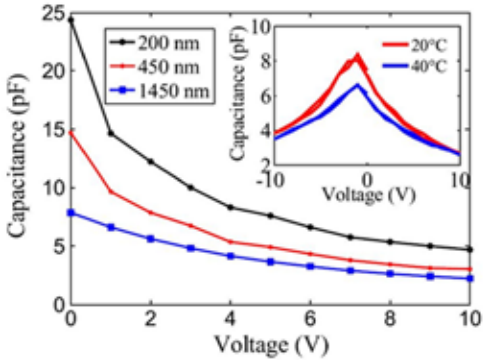

(a)

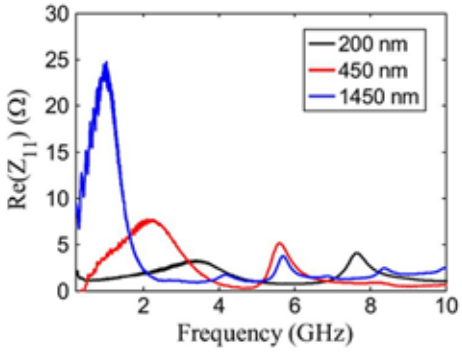

(b)

Fig. 4: (a) Capacitance at 2.45 GHz. Inset: Capacitance for the 1450-nm thick BST film. (b) Real part of the input impedance at 10 V [3].

Funding: This work was financially supported by the National Authority for Scientific Research (ANCS)-Romania and the "Agence Nationale de la Recherche" (ANR)-France, under the MAESTRO project (PN-II-ID-JRP-RO-FR-2012-0160) and Nucleus Program PN16-4801.

References

[1] L. Trupina, L. Nedelcu, C.C. Negrila, M.G. Banciu, L. Huitema, A. Crunteanu, M. Rammal, A. Ghalem, J. Mater. Sci. 51(18):8711-8717, 2016.

[2] L. Huitema, M. Cernea, A. Crunteanu, L. Trupina, L. Nedelcu, M.G. Banciu, A. Ghalem, M. Rammal, V. Madrangeas, D. Passerieux et al., J.Appl.Phys.119(14), 2016.

[3] A. Ghalem, M. Rammal, L. Huitema, A. Crunteanu, V. Madrangeas, P. Dutheil, F. Dumas-Bouchiat, P. Marchet, C. Champeaux, L. Trupina et al., IEEE Microw. Wireless Comp. Lett. 26(7):504-506, 2016.

[4] A. Ghalem, L. Huitema, A. Crunteanu, M. Rammal, L. Trupina, L. Nedelcu, M.G. Banciu, P. Dutheil, C. Constantinescu, P. Marchet et al., J. Appl. Phys. 120(18), 2016.

PATENTS AND PATENT REQUESTS

PATENT AWARDED

1. Popescu Mihai, Niciu Gheorghe Horatiu, Radu Vasile Dorel, Niciu Daniela Ortensia, Stroescu Hermine Maria, Sava Florinel, Lőrinczi Adam, Velea Alin.
Method for synthesis of high purity As_2S_3, for optical applications
Patent awarded by decision no. 123654 / 26.02.2016

2. Popescu Mihai, Niciu Gheorghe Horatiu, Niciu Daniela Ortensia, Manea Adrian, Lőrinczi Adam, Velea Alin, Simandan Daniel - Iosif, Sava Florinel
Method for obtaining materials from chalcogenid systems As_2S_3-Eu_2S_3 and As_2S_3-Er_2S_3
Patent awarded by decision no. 3/ 207/ 30.09.2016.

PATENT REQUESTS

Poloșan Silviu, Păcală Ovidiu, Păcală Mirela
Method to obtain a ceramic glass of bismuth germanate with scintillator properties
A00995/2010, published in BOPI on 26.02.2016

Banciu Marian Gabriel, Nedelcu Liviu, Geambașu Cezar Dragoș, Lucian Trupină, Militaru Nicolae Gheorghe, Nicolaescu Ioan
Microwave antenna with resonators from different dielectric materials
A00873/2016

Ghiță Rodica, Logofătu Constantin, Negrilă Constantin-Cătălin, Frumosu Florica, Predoi Daniela
Method of obtaining oxide compounds on n-GaSb surface
A00677/2016

Cotîrlan-Simionuc Costel, Rizea Adrian, Ursu Dănuț Vasile
Optoelectronic devices with electrically configurable metasurface for light polarization control and obtaining optical resolution below the classical limit of diffraction
A00186/2016

Leca Aurel, Sofronie Mihaela-Iuliana, Kuncser Victor Eugen, Văleanu Mihaela Cristina, Elisa Mihail, Sava Bogdan Alexandru, Beldiceanu Anca
Method of designing optical glasses with null Verdet constant
A00121/2016

Aldica Gheorghe Virgil, Burdușel Mihail, Bădică Petre
Method of processing and superconductor band in metallic sheet with MgB2-based core
A00150/2016

Florica Camelia-Florina, Preda Nicoleta-Roxana, Costas Liliana-Andreea, Evanghelidis Alexandru Ionuț, Oancea Mihaela, Enculescu Maria-Monica, Matei Elena, Enculescu Ionuț-Marius
Method of obtaining of some unidimensional nanostructures of ZnO by thermal oxidation in air of a Zn foil
A00302/2016

Predoi Daniela, Ciobanu Steluța Carmen, Popa Cristina-Liana, Iconaru Simona-Liliana
Method of obtaining Zn doped hydroxiapatite in collagen matrix for biomedical applications
A00483/2016

PATENT REQUESTS

Slav Adrian, Palade Cătălin, Lepădatu Ana-Maria, Lazanu Sorina, Ciurea Lidia Magdalena, Vasilache Dan, Dragoman Mircea
Capacitive matrix for non-volatile memory based on Ge nanocrystals embedded in HfO_2 and method of manufacturing this
A00723/2016

Stan George, Pintilie Ioana, Beşleagă Stan Cristina, Botea Mihaela, Dobrescu Gabriel, Cioca Mihai, Culea Liviu, Soare Petre, Pintilie Lucian
Pyroelectric detection element for working at elevated temperatures
A00747/2016

Pintilie Lucian, Pintilie Ioana, Ianculescu Carmen Adelina
Ferroelectric bulk ceramic with enhanced properties for pyroelectric detection through concentration gradient
A00284/2016

EVENTS

National Institute of Materials Physics
Atomistilor Str. 405A, PO Box MG7, Magurele, 077125 Ilfov, Romania, Telephone : +40213690185
Fax: +40213690177, E-mail : director@infim.ro, www.infim.ro

Advanced Thermal Analysis and Applications

October 13, 2016
National Institute of Materials Physics
405A, Atomistilor Str., Magurele

PARTNERS:

SARTOROM

NETZSCH

Advanced Thermal Analysis and Applications

Program

10:00 am	**Registration and Welcome Coffee**	
10:10 am	Welcome and Intro to INCDFM	CS. I Dr. Ionut Marius Enculescu
10:15 am	Introduction to SARTOROM	Gabriela Ionita
10:20 am	Introduction to NETZSCH Analyzing&Testing	Dr. Markus Meyer
10:30 am	**DSC - Differential Scanning Calorimetry**	Dr. Markus Meyer
11:00 am	**DSC - Temperature memory effect in Ni-Fe-Ga alloys**	Dr. Felicia Tolea
11:15 am	TGA - Thermogravimetric analysis	Dr. Markus Meyer
11:45 am	STA - Simultaneous Analysis	Dr. Markus Meyer
12:15 pm	Lunch Break	
01:00 pm	DMA - Dynamic Mechanical Analysis	Dr. Markus Meyer
01:30 pm	DMA - Using DMA for SMAs characterization: Temperature scans vs. strain sweeps	Dr. Bogdan Pricop
01:45 pm	LFA - Light Flash Apparatus	Dr. Markus Meyer
02:15 pm	LFA-Thermo-physical properties of metal-ceramic composites	MSc. Magdalena Galatanu
02:30 pm	SBA-Simultaneous Determination of Seebeck **Coefficient and Electrical Conductivity**	Dr. Markus Meyer
02:45 pm	**SBA- Why is Seebeck effect important beyond** classical thermo-electricity applications	Dr. Andrei Galatanu
03:00 pm	Visit the National Institute of Materials Physics	

International Workshop of Materials Physics

Dates: **May 23-25 2016**
Venue: **NIMP Conference Hall, 405A Atomistilor Str., Magurele**

The **National Institute of Materials Physics (NIMP)** is a lead scientific institution in Romania, determined to become an excellence research center at European level. Its current research topics are related to solid state physics and materials science, with special focus on oxide materials, organic-inorganic composites and hybrid structures, dedicated for applications ranging from electronics and life sciences to green energy or nuclear fusion reactors. The Institute has a modern infrastructure, covering various preparation/deposition methods and a wide number of characterization techniques, highly qualified personnel and a significant number of collaborations with research institution from abroad.

The **International Workshop of Materials Physics** organized by NIMP aims at becoming a periodic forum in the exchange of ideas between the local researchers and distinguished members of the international research community in the field. Presentations will be both related to scientific breakthroughs and success stories of applications of research results in industry.

Accordingly, the extra - scientific topics of the workshop for its first edition will be covering the following aspects:

- **Connecting NIMP to new hot research topics** with the aim to develop new collaborations of high potential success for EU project applications (with special emphasis on novel materials and interface with life sciences)
- **Increasing attractiveness for foreign researchers** to come and work at NIMP (with the possibility to apply for ERA-Chair projects or ERC grants)
- **Increasing the performance and improving the image of NIMP's researchers** in order to successfully apply for ERC grants (learning from the experience of ERC grantees)
- **Learning good practices for improving excellence in research**, with special emphasis on the innovative aspects and the general relation with the industry (including discussions regarding application for TEAMING and TWINNING projects)

PROGRAM

23RD OF MAY	**2016**
08:30 - 09:00	***REGISTRATION***
09:00 - 09:15	***OPENING (GENERAL DIRECTOR OF NIMP)***
CHAIR : IONUT ENCULESCU	***ELECTRONICS***
09:15 - 09:45	**Rodrigo MARTINS** *"Exploiting Paper as Active Component in Novel Transistor Architectures"*
09:45 - 10:15	**Elvira FORTUNATO** *"Why metal oxide nanoparticles are so interesting?"*
10:15 - 10:30	**Radu DRAGOMIR** *"Selective exchange effects in single-Mn doped quantum dots"*
10:30 - 10:45	**Camelia FLORICA** *"High performance field effect transistors based on single ZnO nanowires"*
10:45 - 11:00	***COFFEE BREAK***
CHAIR : Cristian Mihail TEODORESCU	***ULTRA-THIN and 2D***
11:00 - 11:30	**Nick BARRETT** *"Electron spectromicroscopy of ferroelectric oxides"*
11:30 - 12:00	**Marin ALEXE** *"Topological structures and torroidal ferroelectricity in ultra-thin films and devices"*
12:00 - 12:30	**Silvano LIZZIT** *"Synchrotron radiation photoemission and photoelectron diffraction: the 2D materials case"*
12:30 - 12:55	**Angelo AGOSTINO** *"Synchrotron light for material characterization and modification in the frameworks of international projects"*
12:55 - 13:10	**Laura ABRAMIUC** *"Photoelectron spectromicroscopy of $Pb(Zr,Ti)O_3$(001) and (111) surfaces"*
13:10 - 14:30	***LUNCH***
CHAIR : Ioana PINTILIE	***ENERGY***
14:30 - 15:00	**Thomas RATH** *"Research on Emerging Materials for Hybrid Photovoltaics at Graz University of Technology"*
15:00 - 15:30	**Alexandru NEMNES** *"Ab initio calculations of the band alignment in halide perovskite solar cells"*
15:30 - 16:00	**Daniel VIZMAN** *"New trends in directional solidification of multicrystalline silicon for photovoltaic applications"*
16:00 - 16:15	**Cristina BESLEAGA-STAN** *"Stability in perovskite solar cells"*
16:15 - 16:30	**Neculai PLUGARU** *"Atomistic simulations of methylammonium lead halide layers on $PbTiO_3$ (001) surfaces"*

16:30 - 16:45	***COFFEE BREAK***
16:45 - 18:00	**ROUND TABLE** *EU priorities in materials research (co-chairs Rodrigo Martins, Elvira Fortunato)*
19:00 - 22:00	***DINNER***

24TH OF MAY 2016

CHAIR : Aurelian-Catalin GALCA	***FUNCTIONALITIES***
09:00 - 09:30	**Guus RIJNDERS** *"Long range symmetry propagation initiated at heterostructure interfaces"*
09:30 - 10:00	**Viorel POP** *"Hard Magnetic Materials with Reduced Rare-Earth Content"*
10:00 - 10:15	**Andra-Georgia BONI** *"Influence of interlayer type on ferroelectric/dielectric characteristics of multilayered structures"*
10:15 - 10:30	**Ion IVAN** *"AC driven magnetic flux quanta in YBCO composite thin films with complex pinning structures"*
10:30 - 11:00	***COFFEE BREAK***
CHAIR : Mariana STEFAN	***LARGE INFRASTRUCTURES***
11:00 - 11:30	**Jana KOLAR** *"CERIC-ERIC - European Research Infrastructure Consortia and Materials Science in Central East Europe"*
11:30 - 12:00	**Primož ŠKET** *"SLONMR: From small organic compounds to macromolecules"*
12:00 - 12:30	**Marek STANKIEWICZ** *"SOLARIS - new synchrotron light source in Europe"*
12:30 - 12:45	**Nicoleta APOSTOL** *"Chemistry of carbon and carbon monoxide on $Pb(Zr,Ti)O_3$(001) surfaces"*
12:45 - 13:00	**Raluca NEGREA** *"Electron microscopy at NIMP: capabilities and collaboration opportunities"*
13:00 - 13:20	*Presentation from Carl-Zeiss*
13:20 - 14:45	***LUNCH***
CHAIR : Victor KUNCSER	***MATERIALS FOR LIFE SCIENCES, CATALYSIS***
14:45 - 15:15	**Mangala SRINIVAS** *"Nanoparticles for multimodal clinical and preclinical in vivo imaging"*
15:15 - 15:45	**Nicoleta LUPU** *"Low T_c Glassy Magnetic Alloys for Medical Applications"*
15:45 - 16:15	**Vladimír MATOLÍN** *"Thin film catalysts for fuel cell technology"*

16:15 - 16:30	**George STAN** *"Dental implant fixtures bio-functionalized with mechanically resistant and cytocompatible bioglass coatings by magnetron sputtering technique"*
16:30 - 16:45	**Ovidiu CRISAN** *"Nanoparticles and nanoclusters versatile synthesis methods: pathway towards integrated devices for nanosensing and biomedical applications"*
16:45 - 17:00	***COFFEE BREAK***
17:00 - 17:45	*How to write a successful application (ERC, Horizon 2020)?*
19:00 - 22:00	*Dinner sponsored by Carl-Zeiss*

25TH OF MAY 2016

CHAIR : Mihaela BAIBARAC ***CARBON AND NANO***

09:00 - 09:30	**Mircea DRAGOMAN** *"Beyond graphene: hundreds of atomically thin materials"*
09:30 - 10:00	**Magdalena TITIRICI** *"Sustainable Carbon Materials and Chemicals from Biomass Hydrothermal Processes"*
10:00 - 10:15	**Adelina MATEA** *"Anti-Stokes Raman spectroscopy as a method to identify metallic and mixed metallic/semiconducting configurations of multi-walled carbon nanotubes"*
10:15 - 10:30	**Ana Maria LEPADATU** *"Morphology-driven charge storage properties of trilayer structures with Ge nanocrystals in HfO_2"*
10:30 - 11:00	**Russell BINIONS** *"Functional metal oxide thin films from electric field assisted aerosol assisted chemical vapour deposition"*
11:00 - 11:30	***COFFEE BREAK***

CHAIR : Lucian PINTILIE ***FUNCTIONALITIES***

11:30 - 12:00	**Steve DUNN** *"Photoinduced carrier dynamics – the ferroelectric dipole's influence on recombination"*
12:00 - 12:30	**Mihai GIRTU** *"Research in Materials Physics at Ovidius University of Constanta"*
12:30 - 12:55	**Augusto Claudio MARCELLI** *"Nanoscale phase separations in quantum materials"*
12:55 - 13:10	**Iosif-Daniel SIMANDAN** *"Photoexpansion in a-As_2S_3: a possible new mechanism"*
13:10 - 13:25	**Cristian SIMION** *"Transducing mechanism of ammonia detection using $BaSrTiO_3$"*
13:25 - 13:30	***CLOSING***
13:30 - 15:00	***LUNCH***

"ALD FOR NOVEL SENSORS AND BIOSENSORS" WORKSHOP

Dates: **11 May 2016 to 12 May 2016**

Venue: **NIMP Conference Hall, 405A Atomistilor Str., Magurele, Romania**

PROPOSED TOPICS:

- Modelling growth chemistry of novel sensorial interfaces based on oxides, nitrides, sulphides (W, V, Se-based) and graphene-like layers
- Technological processes and physical-chemical characterization of nucleation and growth of layers/structures
- New up-scalable methods for synthesis of chemical precursors
- Hybrid organic/inorganic thin films for biosensors

COST MP1402 SCIENTIFIC WORKSHOP

"ALD FOR NOVEL SENSORS AND BIOSENSORS"

11-12 May 2016

Place: National Institute of Materials Physics, Magurele

Programme

Day 1: 11 May 2016

09:00 – 10:00	**Registration**
10:00 – 10:10	Welcome (Director of NIMP and members of organizing committee)
10:10 – 10:40	On modeling fluctuation kinetics and fluctuation dynamics in adsorption-based sensors, Olga Jakšić, University of Belgrade **- Invited talk**
10:40 – 11:10	Hybrid ALD-CVD Processes for the Development of Optical Coatings, Naoufal Bahlawane, Luxembourg Institute of Science and Technology (LIST) **- Invited talk**
11:10 – 11:40	**Coffee break**
11:40 – 12:10	Laser printing of organic/inorganic composites for sensors fabrication, Maria Dinescu, NILPRP, Magurele, **- Invited talk**
12:10 – 13:10	**Oral presentations**
12:10 – 12:30	DNA-Electrochemical Biosensors for In Situ Sensing of DNA Damage, Victor Diculescu, NIMP, Magurele
12:30 – 12:50	Hybrid $CoCl_2$/polyimide materials for moisture sensing, Mariana Dana Damaceanu, "Petru Poni" Institute of Macromolecular Chemistry", Iasi
12:50 – 13:10	Laccase biosensor based on graphene quantum dots and MoS_2, Antonio Radoi, IMT-Bucharest
13:10 – 14:30	**Lunch at Restaurant**

14:30 – 15:00	Thin films made from heterocyclic polymers for high performance applications, Maria Bruma, "Petru Poni" Institute of Macromolecular Chemistry", Iasi - **Invited talk**
15:00 – 16:00	**Oral presentations**
15:00 – 15:20	Chemoresistive Gas Sensing Materials, Rachel Wilson, University College London
15:20 – 15:40	Bi-Based Graphene- like Nanostructures Produced by Laser Ablation and Their Functional Properties, Valentin Serban Teodorescu, NIMP, Magurele
15:40 – 16:00	A highly sensitive chemosensors for Zn^{2+} and its coordination complexes based on podants with azaheterocycles skeleton, Violeta Vasilache, "Alexandru Ioan Cuza" University, Iasi

Day 2: 12 May 2016

09:00 – 09:30	**Registration**
09:30 – 10:00	Hydrothermal-electrochemical deposition process: An attractive technique to fabricate nanostructured hybrid organic-inorganic thin films based biosensors, Roxana Mioara Piticescu, National R&D Institute for Non-ferrous and Rare Metals, Pantelimon, Romania - **Invited talk**
10:00 – 11:20	**Oral presentations**
10:00 – 10:20	Plasmonic metasurfaces with deep subwavelength details for chemical sensing, Zoran Jakšić, University of Belgrade
10:20 – 10:40	Formation of bioglass hollow sub-micron cones by magnetron sputtering and their prospective biomedical applications, George Stan, NIMP, Magurele
10:40 – 11:00	Improving the performance of Ge NCs-based nonvolatile memory capacitors by manipulating/controlling the lateral separation between NCs, Ana-Maria Lepadatu, NIMP, Magurele
11:00 – 11:20	Core-shell polymer/GaN nanofibers towards flexible gas sensors, Seda Kizir, Bilkent University, Ankara
11:20 – 11:40	**Conclusions and closing of the workshop**
11:40 – 13:15	**Visit of NIMP facilities**
	Lunch at Restaurant

INTERNATIONAL COOPERATION

INTERNATIONAL COOPERATION PROJECTS

LARGE COOPERATIONS
CERN RD50 "Radiation hard semiconductor devices for very high luminosity colliders" Pintilie I (http://rd50.web.cern.ch/rd50/): 48 research institutions from 27 countries around the world Scientific coordonator of the workpackage "Defect/Material Characterization"
NORWAY FUNDS Pintilie I Project funds SEE (EEA Grants) "Perovskites for Photovoltaic Efficient Conversion Technology" (PERPHECT) Partners: NIMP (INCDFM), Physics Faculty U. Bucharest, Optoelectronics 2000 SA (Romania); U. Iceland, U. Reykjavík (Iceland); U. Oslo (Norway) 2014-2017
FP 7 PROJECT Mercioniu I Development of a sintering centre and know-how exchange for non-equilibrium sintering methods of advanced ceramic composite materials (SINTERCER) FP7 EU-Research Potential – Capacities – REGPOT-CT-2013-316232-SINTERCER Coordinator: The Institute of Advanced Manufacturing Technology, Krakow, Poland Partners: Politecnico di Torino (POLITO), Torino, Italy, Institute of Ceramics and Glass (ICV- CSIC), Madrid, Spain, University of Rostock (UR), Rostock, Germany, National Institute of Materials Physics (NIMP), Bucharest – Magurele, Romania, Aalto University School of Chemical Technology, Espoo, Finland, RHP-Technology GmbH & Co. KG (RHP), Seibersdorf, Austria, Universidade de Aveiro(UA), Aveiro, Portugal, University of Science and Technology (AGH), Cracow, Poland, Institute of Metallurgy and Materials Science of Polish Academy of Sciences (IMIM), Cracow, Poland, (http://www.ios.krakow.pl/sintercer)
EURATOM Galatanu A EUROfusion Consortium, Grant agreement No. 633053 2014-2018
COST project Pintilie L COST actiunea MP1308 "Towards Oxide-Based Electronics (TO-BE)" (http://www.cost.eu/COST_Actions/mpns/Actions/MP1308) Coordinator: Dr Fabio Miletto Granozio (IT) 2014-2018

COST project
Ciurea ML
COST action HERALD (MP1402) "Hooking together European research in Atomic Layer Deposition (HERALD)" (http://www.cost.eu/COST_Actions/mpns/MP1402)
Coordonator: Dr. Simon Elliott, Ireland
2014-2018

COST project
Crisan A
COST action MP 1201 "Nanoscale SuperConductivity: Novel Functionalities through Optimized Confinement of Condensate and Fields "
2015-2016.

ERA-NET project
Mercioniu IF
Project M-ERA NET 9/2015
Integrated sensors with microfluidic characteristics using the LTCC technology (INTCERSEN)
Coordinator: TU Iasi, Romania
Partners: NIMP, Magurele, Romania; SC INTELECTRO SRL, Iasi, Romania; „J. Stefan" Institute Slovenia; HIPOT Slovenia; Dropsens, Spain; NAMASTE, Slovenia.
2015-2017

ERA-NET project
Trupina L
Integration of new and improved materials for smart millimeter-wave sensors
Project M-ERA.NET
French partner: Universitatea din Limoges, AirMems (SME)
2016 – 2019

ERA-NET project
Ciurea ML
Project M-ERA NET Call 2014
PhotoNanoP (High photoconductive oxide films functionalized with GeSi nanoparticles for environmental applications)
Partners from Romania (IMT, OPTOELECTRONICA- 2001 S.A) and Iceland (Reykjavik University (School of Science and Engineering) - RU-SSE, Pi Technology)
2016-2018

ERA-NET project
Stoica TS
Project M-ERA NET Call 2015
GESNAPHOTO (Nano-structured GeSn coatings for photonics)
Partners from Romania (INOE-2000, OPTOELECTRONICA- 2001 S.A) and Germany (Forschungszentrum Jülich, Peter Grünberg Institute PGI-9, nanoplus Nanosystems and Technologies GmbH)
2016-2019

ERA-NET project
Vlaicu ID
Project M-ERA NET
Innovative nano-materials and architectures for integrated piezoelectric energy harvesting applications (HarvEnPiez)
Coordonator: Iosef Stefan Institute din Ljubljana, Slovenia
Partners: Institute of Solid State Physics, University of Latvia (ISSP UL), Latvia; National Institute of Materials Physics (NIMP), Romania; Faculty of Electrical Engineering, Power Engineering and Information Technology, (Intelectro Iasi SRL), Romania; Technical University Iasi (TU Iasi), Romania
2016-2019

C-ERIC
Ghica C
Graphene for Water in Life Science,
CERIC Grant
Coordinator: Elettra Sincrotrone Trieste
Partners: Technical University Graz (Austria), Charles University Prague (Czech Republic), NIMP (Romania)

ELETTRA (Trieste) Synchrotron projects
Apostol NG
Adsorption, desorption and molecular reactions at ferroelectric surfaces,
Project Nr. 20155416,
2016.

OTHER INTERNATIONAL PROJECTS

Project IFA-CEA
Predoi D
New bioceramic nanocomposite with antibacterian activity for medical applications
French partner: Laboratory of Chemistry and Biology of Metals (LCBM) Grenoble.
2014-2016

Project PICS
Predoi D
Nanoparticles for remedy of contaminated soils
French partner: Institut des Sciences de la Terre d'Orléans.

Project IFA-CEA
Chirila C
Optimised pyroelectric elements on Si wafers for sensing and energy harvesting
French partner: CEA Grenoble Laboratorul de Componente pentru Micro-Actuatori
2016-2019

Project IFA-CEA
Pintilie L
Proelectricity in PZT thin films and multilayers
French partner: CEA Grenoble Laboratorul de Componente pentru Micro-Actuatori
2014-2016

PROJECT ANR-ANCS (RO-FR) PN-II-ID-JRP-RO-FR-2012-0160
Nedelcu L
Compact and integrated agile antennas based on tunable ferroelectric materials
Coordinator: XLIM UMR 7252 CNRS, University of Limoges
Partners: SPCTS UMR 7315 CNRS, University of Limoges; National Institute of Materials Physics, Romania
2014 – 2016

Programme Hubert Curien PHC Brancusi
Baibarac M
Optical properties of SWNTs highly separated in metallic (98%) and semiconducting (99%) functionalized with conjugated polymers
Partner: Institut des Materiaux Jean Rouxell, Nantes, France 2015-2016

Programme Hubert Curien PHC Brancusi
Socol M
Metallic electrode with 2D photonic crystal architecture for multilayer (bio) organic structures
Partner: University Angers, France 2015-2016

Programme Hubert Curien PHC Brancusi
Crisan O
Surface-functionalized nanostructures for applications in photonics and spin manipulation technologies
Partner: Laboratoire Léon Brillouin UMR12 CEA-CNRS, Commissariat à l'Énergie Atomique et aux Énergies Alternatives CEA Saclay, France: Prof. A. Filoramo
2016-2018

BILATERAL COOPERATION PROJECTS (AGREEMENTS)

Cernea M
Joint Research Project CNR Italy– Romanian Academy
Study and Development of Single-Phase Multiferroic Perovskite Ceramic and Thin Films for Multifunctional Devices
2014-2016

Ghica C
Departamnt Surfaces-Interfaces,Institut of Materials Physics and Chemistry, Strasbourg, France
Effet de la réduction de taille, de la forme et des caractéristiques des interfaces sur la structure et les propriétes des matériaux nanostructurés
2012-2016

Stan GE
University of Aveiro, Portugal
Development of a new generation of highly biocompatible dental titanium implants functionalized by sputtering techniques with novel bioactive glass materials
2016 – 2020

A. Stanculescu
University of Angers- Photonics Laboratory, France
Accord de coopération scientifique dans le domaine des films minces notamment sur les thématiques suivantes: structures multicouches organiques à basse dimension et composantes or oganiques et hybrides.
University of Western Cape, Departament of Chemistry, SensoLab, Soth Africa
Polymeric single/multylayer heterostructures for photovoltaic and electronic applications; polymeric field effect transistors for sensing applications; organic and hybrid devices (realisation, characterization)

Badica P
Tohoku University, Japonia
Joints of superconducting tapes: fabrication and characterization
Proiect: ICC-IMR Visiting Prof. collaboration and exchange of researchers/students INCDFM-HFSLM-Tohoku University

M. Baibarac
Institut des Materiaux Jean Rouxel, Nantes, France
Surface plasmons enhancement of optical properties of SWNTs, highly separated in metallic and semiconducting components, electrochemically functionalized with conjugated polymers.

COOPERATION PROJECTS WITH FOREIGN INSTITUTES AND UNIVERSITIES

Ciurea ML
Department of Physics and Astronomy, University of Catania, CNR-IMM, Catania, Italy
Ge-based nanostructures for applications as photodetectors or transparent electrodes for photovoltaic cells

Ciurea ML, Lepadatu AM
Istituto Nazionale di Fisica Nucleare-Laboratori Nazionali di Frascati, Frascati, Italy
Nanostructures based on Ge nanoparticles immersed in oxidic matrices for optical sensors applications

Ciurea ML, Lepadatu AM
National Academy of Sciences of Ukraine, V. Lashkaryov Institute of Semiconductor Physics, Kiev, Ukraine
Study of electrical and optical properties correlated with morphology and structure of films based on Ge nanoparticles immersed in oxidic matrices

Crisan O
Swiss Federal Laboratory for Materials Research & Technology, EMPA, Thun, Switzerland
Prof. Patrik Hoffman

Crisan O
John Dalton Institute, Manchester Metropolitan University, Manchester, UK
Prof. John Colligon

Crisan O **Institut des Materiaux et Molecules du Mans I3M, Fac. Des Sciences, Universite du Maine, Le Mans, France** Prof. N. Randrianantoandro
Crisan O **Department of Renewable Energy, University of Sharjah, United Arab Emirates** Prof. Hamid al-Naimyi
Maraloiu VA / Teodorescu VS **Institut Lumière Matière – Université Claude Bernard, Lyon, France** Biolocalisation et biotransformation de nanoparticules à coeur d'oxydes magnétiques. Fonctionnalisation des substrats par irradiation laser à faible fluence Convention Bilatérale de Coopération et Echange 2013-2014
Miclea CF **Los Alamos National Laboratory, Los Alamos, NM. USA.** Measurements, co-publication, specimen exchange
Miclea CF **Max Planck Institute for Chemical Physics of Solids, Dresden, Germany** Measurements, co-publication, specimen exchange
Nedelcu L **Research Center for Development of Far-Infrared Region, University of Fukui, Japan** Measurements, specimen exchange
Nistor SV **Institute of Physics, Czech Academy, Prague** Investigation by magnetic electronic resonance techniques and optical spectroscopy of the semiconducting II-VI materials optically activated with transitional ions
Nistor SV **Physics Department, Antwerp University, Belgium** Development of new advanced multifunctional materials containing defects
Pintilie L **UMP CNRS-Thales, Palaiseau, France and Université Paris-Sud** Measurements, specimen exchange
Pintilie L, Pintilie I **University of Oulu, Finland** Ferroelectric measurements
Pintilie L **Universitatea Tehnica Darmstadt, Germany** Specimen exchange, co-publication
Pintilie I **Universitatea din Oslo, Norway** Specimen exchange, working stages
Pintilie L **UMP CNRS-Thales, 1 Av. Fresnel, Palaiseau, 91767, France and Université Paris-Sud** Specimen exchange, common measurements

Preda N **Yildiz Technical University, Turkey** Learning Agreement for Traineeships within the ERASMUS Program
Predoi D **Institut de Chimie de la Matière Condensée de Bordeaux CNRS-UPR 9048 France** Elemental analysis, hydrogen storage
Predoi D **Universite Bordeaux, EA 4592 Géoressources&Environnement, ENSEGID, France** Collaboration project IFA CEA C2-06, TEM, environment tests
Predoi D **Marcoule Institute for Separative Chemistry, France**
Predoi D **Technical University Ostrava, Cehia**
Predoi D **Institute of Life Sciences Research and Technologies: Laboratory of Chemistry and Biology of Metals (LCBM) Grenoble, France** Collaboration project IFA CEA C4-05- biological tests
Predoi D **Institut des Sciences de la Terre d'Orléans, France** Raman, ICP, magnetic measurements
Predoi D **Université du Havre, France** Ultrasound studies
Predoi D **Horiba Jobin Yvon S.A., France** Zeta potential, DLS, photoluminescence
Predoi D **University of Dayton, Research Institute, USA** Carbon nanotubes
Stoica T **Peter Grünberg Institute, Forschungszentrum Jülich, Germany** 2D materials based on chalcogenides of transition metals, 2D-TMD
Teodorescu CM **Elettra Trieste (Italia)** CoSMoS -Combined Spectroscopy and Microscopy operating at SuperESCA
Teodorescu CM **IRAMIS CEA Saclay (France)** Chemical switching of ferroelectric surface topology (proiect RO-FR PN-II-ID-JRP-2011-2)

NIMP FUNDING

Core Programme	5.177.266 Euro
Ideas	1.252.624 Euro
Partnerships	1.023.714 Euro
International Projects	547.604 Euro
Human Ressources	521.184 Euro
Complex Ideas	216.577 Euro
ROSA	58.763 Euro
Euratom	204.208 Euro
Economic Contracts	37.913 Euro
POC	113.425 Euro
TOTAL	**9.150.278 Euro**

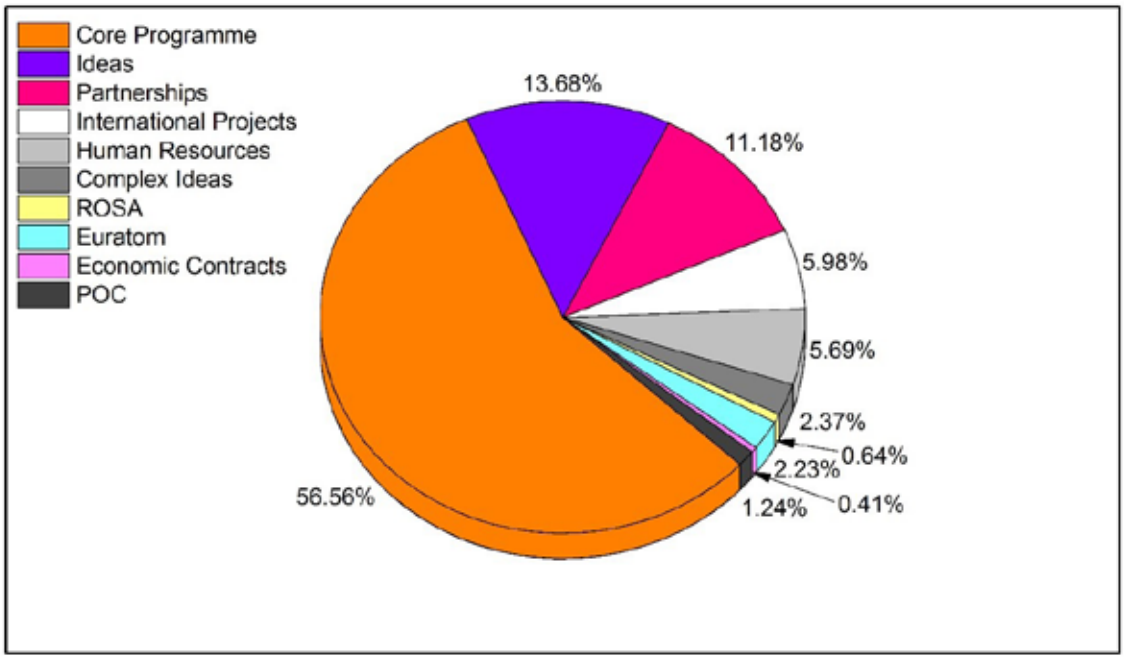

Scan the QR code, for electronic version

National Institute of Materials Physiscs

405A Atomistilor Street, 077125, P. O. Box: MG 7 Magurele, Ilfov, Romania

Phone: +4021 369 01 85, Fax: +4021 369 01 77, e-mail: director@infim.ro, www.infim.ro